Ion exchange membranes in seawater applications
Processes and characteristics

A.H. Galama

Thesis committee

Promotor
Prof. Dr H.H.M. Rijnaarts
Professor of Environmental Technology
Wageningen University

Co-promotors
Dr J.W. Post
Scientific Program manager
Wetsus, European Centre of Excellence for Sustainable Water Technology, Leeuwarden
Dr P.M. Biesheuvel
Scientific Project manager
Wetsus, European Centre of Excellence for Sustainable Water Technology, Leeuwarden

Other members
Prof. Dr J. van der Gucht, Wageningen University
Prof. Dr K. Bouzek, Institute of Chemical Technology Prague, Czech Republic
Prof. Dr N.E. Benes, University of Twente, Enschede
Prof. Dr A. van der Padt, Wageningen University

This research was conducted under the auspices of the Graduate School for Socio-Economic and Natural Sciences of the Environment (SENSE)

Ion exchange membranes in seawater applications

Processes and characteristics

A.H. Galama

Take only what you need and leave the land as you found it
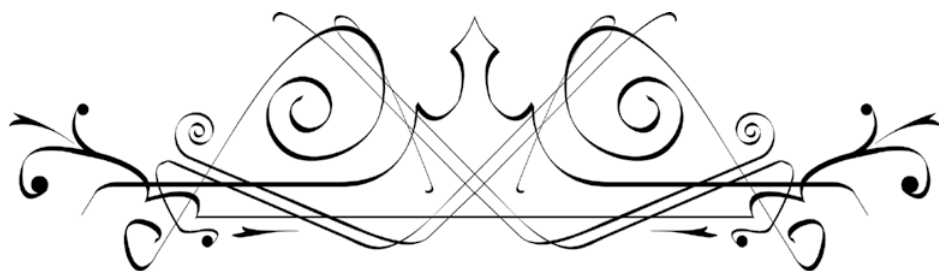
Arapaho proverb

Table of Contents

x

Chapter 1

Introduction

1.1 The need for desalination

Without water there would be no life. All over the world scientists believe that the first life started in water. Whether this is true or not, fact is that all organisms in one way or another rely on water. About 71% of the earth surface is covered with water, at most places water is all around and as such water is not a scarce resource. The problem is that most of this water is salty or not readily available to humankind and other life depending on fresh water. As shown in Figure 1, the (available) amount of fresh water is only a fraction of the total water on earth.
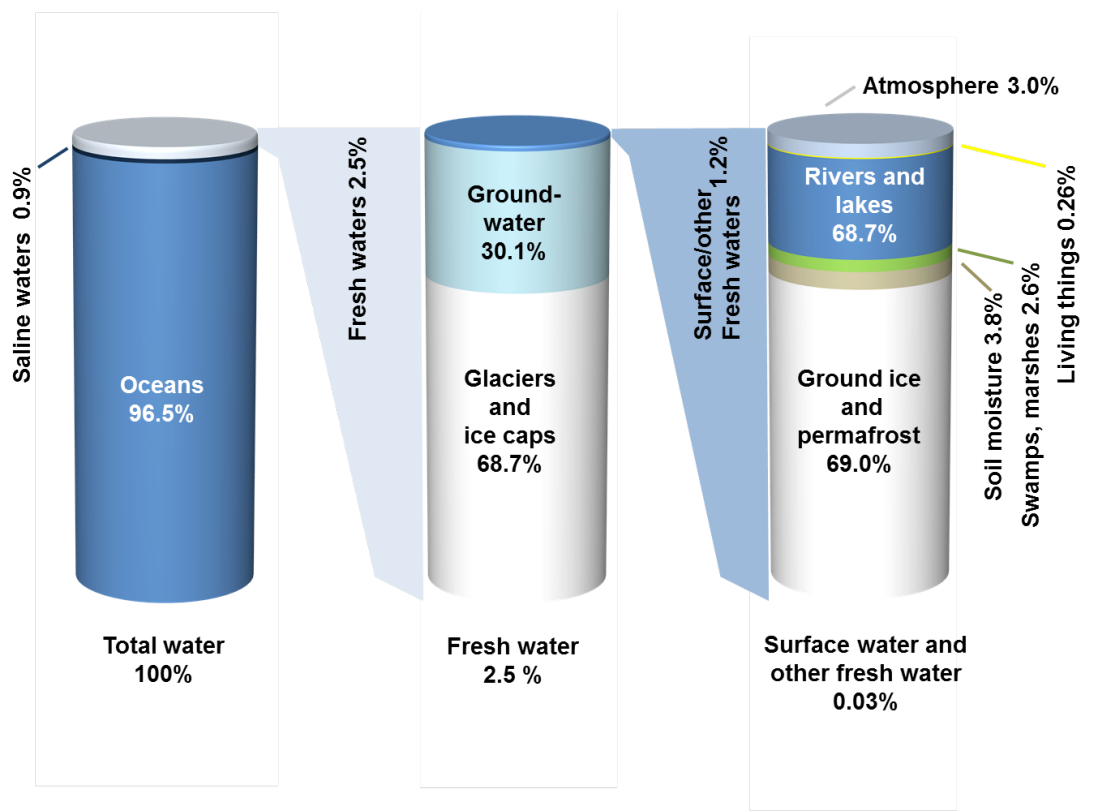
Figure 1. Distribution of the water on earth, data from [1].

With Figure 1 in mind, it is understandable that water scarcity does occur, especially in a world with increasing population and where freshwater sources are unevenly distributed. Economic growth leads to higher water demand and the quantity and quality of existing water resources is negatively affected by human activity. Occurrence of worldwide climate change can negatively affect water shortage, especially in densely populated areas located in regions that are becoming more arid, while freshwater demand continuous to increase. According to the United Nations and the World Health

Organization 0.7-1.2 billion people suffer from water scarcity, and another 500 million people approach this situation [2]. With the present climate change scenario, it is estimated that in 2030 about half of the world population will be living in severely water stressed areas [2].

Fresh surface water is in some regions not or only limited available or is unsuitable for drinking water due to pollution. Especially in these regions, groundwater is often used as primary water source as it is most accessible, cheap and reliable in quality [3]. However there are limits to ground water extraction as the situation of overexploitation can easily be reached, which leads to a negative impact on the environment [3]. For ensuring future water availability inclusion of renewable water resources in sustainable water management is very important [4-7]. Water conservation, improved catchment, storage, distribution, and adequate water infrastructure are important to improve the use of natural existing freshwater resources [8]. The only two feasible ways to enlarge the volume of available fresh water resources, beyond these natural resources, are desalination and water reuse [9, 10].

As water tends to end up in the ocean, seawater is an apparently unlimited water source, which can be used without impairing natural freshwater ecosystems [11]. However, to avoid negative side effects of desalination, seawater intake and discharge of brines should be carefully implemented [8, 11, 12]. Desalination techniques can supply fresh water wherever salt or brackish water sources are available. By converting only a small fraction of the salty water sources into fresh water, already a significant contribution to solving the problem of water scarcity could be achieved [9]. Therefore desalination is often thought of as a good way to counteract or mitigate water scarcity.

According to the International Desalination Association (IDA) in 2013 already 300 million people were relying on desalinated water for some, or all, their daily needs [13]. In that same year the estimated number of installed desalination plants worldwide exceeded 17.000, were spread over 150 different countries, and had a total capacity of about 80 million m^3/d [13]. As shown in Figure 2, a rapid growth of the desalination market is expected in the near future. It is estimated that the global desalination capacity will be about 180 million m^3/d in 2024, and a further increase to 280 million m^3/d in 2030 is expected [14].

Figure 3 shows the different fractions of the feed waters that were used in desalination facilities. It is expected that the fraction seawater will increase due to the growth in the seawater desalination market.
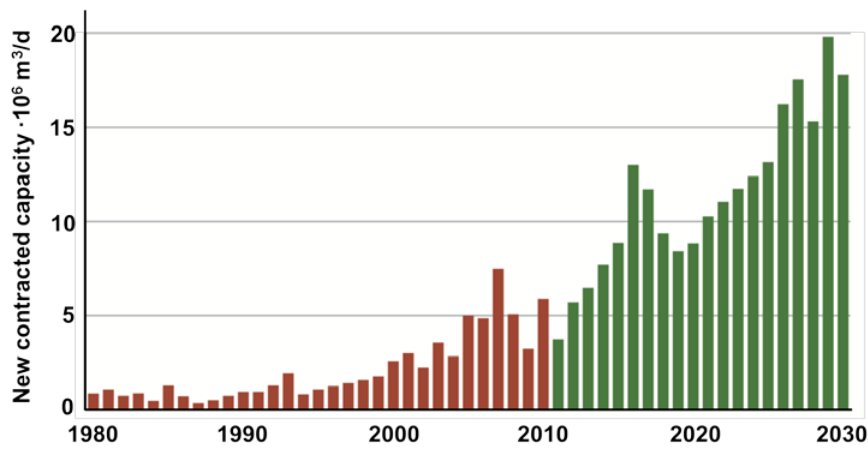
Figure 2. Past and expected annual growth of the desalination market [15].
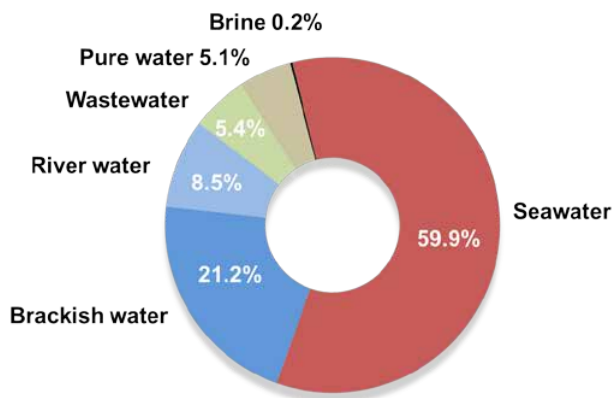
Figure 3. Feed water source of the desalinated water in 2011 [15].

1.2 Desalination

Desalination (a.k.a. desalinization, demineralization, or desalting) can be defined as the process that is used to lower or completely remove the salt content of a solvent. Technologically spoken, in an ideal desalination technology a pure salt fraction and a pure solvent (i.e. water) fraction are obtained after the desalination process, while the energy consumption does not exceed the thermodynamically minimum required amount of energy. In real life however, a complete separation of salt and water is often not required and desalinated waters need remineralization or potabilization [16, 17]. Furthermore, not energy requirements (kWh/m³), but the desalination costs (€, $, ¥ / m³) determines which technology is used. In practice an ideal technology is capable of

meeting the demanded process requirements for the lowest possible price and secondly at the lowest energy demand.

In many desalination technologies a water stream with certain concentration of salt is split into a concentrate or brine stream and a diluate or desalinated stream. Existence of a brine stream implies a loss of water and is for that reason undesirable. However, a higher water recovery unavoidably leads to an increase in energy consumption, and as such to higher desalination costs [18, 19]. Brine streams are also from an environmental point of view highly undesirable and must be considered as a serious threat to marine and terrestrial ecology [11, 17, 20, 21]. To treat brine streams, so called zero liquid discharge (ZLD) technologies are in development [22, 23]. ZLD technologies can also be used in combination with mineral and metal extraction from desalination concentrate [23-27].

Sustainability of processes gained a lot of interest in the past decade. Seawater desalination is an energy intensive process, therefore it is not surprising that many investigations are done in combining desalination and renewable energy [28-33] or desalination and energy production [33, 34]. For a future perspective it is important that desalination technology, and thus fresh water availability, is not relying on an unsustainable source as fossil fuels. Reducing energy consumption on one hand and using sustainable energy on the other hand is therefore an absolute must for sustainable desalination.

1.3 Desalination technologies

When speaking of desalination, often distillation techniques and pressure driven membrane techniques are considered, therefore, desalination technologies are generally separated into phase-change/thermal technologies and membrane technologies [17, 28]. This is understandable as these technologies have by far the biggest share in the current desalination market as shown in Figure 4.

Distillation technology to produce freshwater from saline water was known and used already centuries before our calendar started [35]. Large scale desalination however started in the 19th century [35]. Roughly from the 2nd half of the 19th century till the 2nd half of the 20th century multiple-effect distillation (MED) was the main desalination technique. Subsequently, the thermal multi-stage flash (MSF) became the most common technology [36, 37]. Especially in the Middle East, distillation technologies were, and still are, applied on large scale. Membrane technologies are much younger than the distillation. In the 1950s ion selective membranes, with low electrical resistance were developed and applied in demineralization with electrodialysis (ED) [38-40]. Large

scale reverse osmosis (RO) was used for brackish water in the late 1960s [36]. Due to development of pressure membranes with higher permeability, RO could also be applied for seawater desalination and in the 1980s, RO was developed into a technology that was proven competitive with the thermal technologies [36]. Development of membrane technology continued and is presently outcompeting distillation technology with respect to desalination costs and energy consumption. Figure 5 shows how the capacity of the annually new installed membrane desalination technologies became much larger than the capacity of the annually new installed thermal desalination technologies.
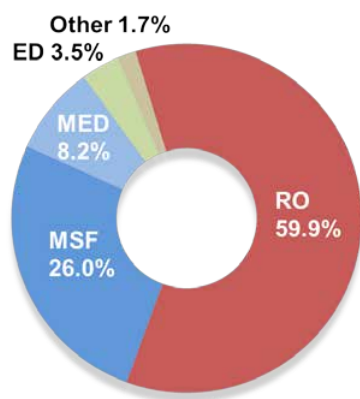
Figure 4. Market shares of the main desalination technologies; reverse osmosis (RO), multi-stage flash distillation (MSF), multiple-effect distillation (MED), electrodialysis (ED), and other [15].
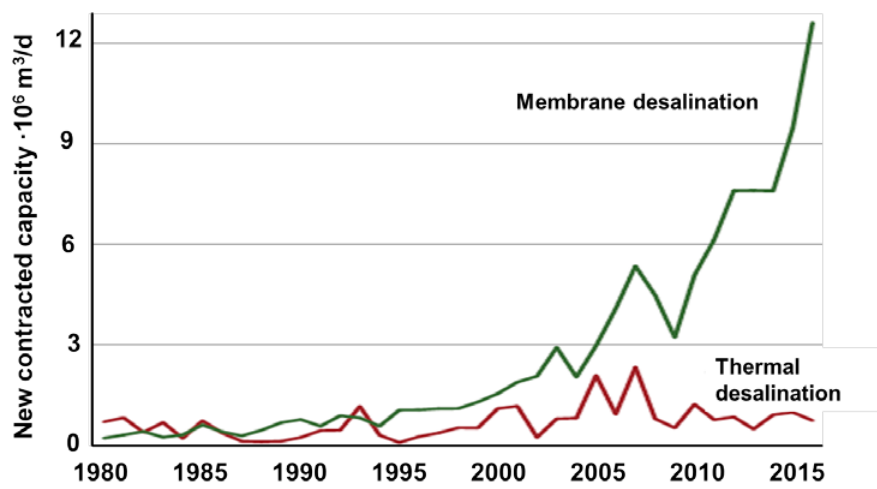
Figure 5. Past and expected annual growth of the desalination market with respect to membrane and thermal desalination technologies (Source: Global Water Intelligence / International Desalination Association 2010).

Although membrane based desalination has many advantages over thermal desalination, distillation remains popular in the Middle East, the region where the largest share of desalination technology is installed. In this region, water of extreme high salinity, high temperature, and with high membrane fouling potential is present, which limits the RO efficiency [10]. Moreover, in this area fossil fuels are readily available and relatively cheap, moreover, rest heat of e.g. oil refineries can be often used as energy source for the distillation process. In the rest of the world, however, RO is the preferred desalination technology [15]. Capacity of new seawater desalination plants is increasing and the largest seawater desalination plant (thermal) is capable of producing an amount of $1.025 \cdot 10^6$ m^3/d (Ras Al-Khair, Saudi Arabia 2014), while the largest seawater RO plant has a capacity of producing $0.624 \cdot 10^6$ m^3/d (Sorek, Israel 2013).
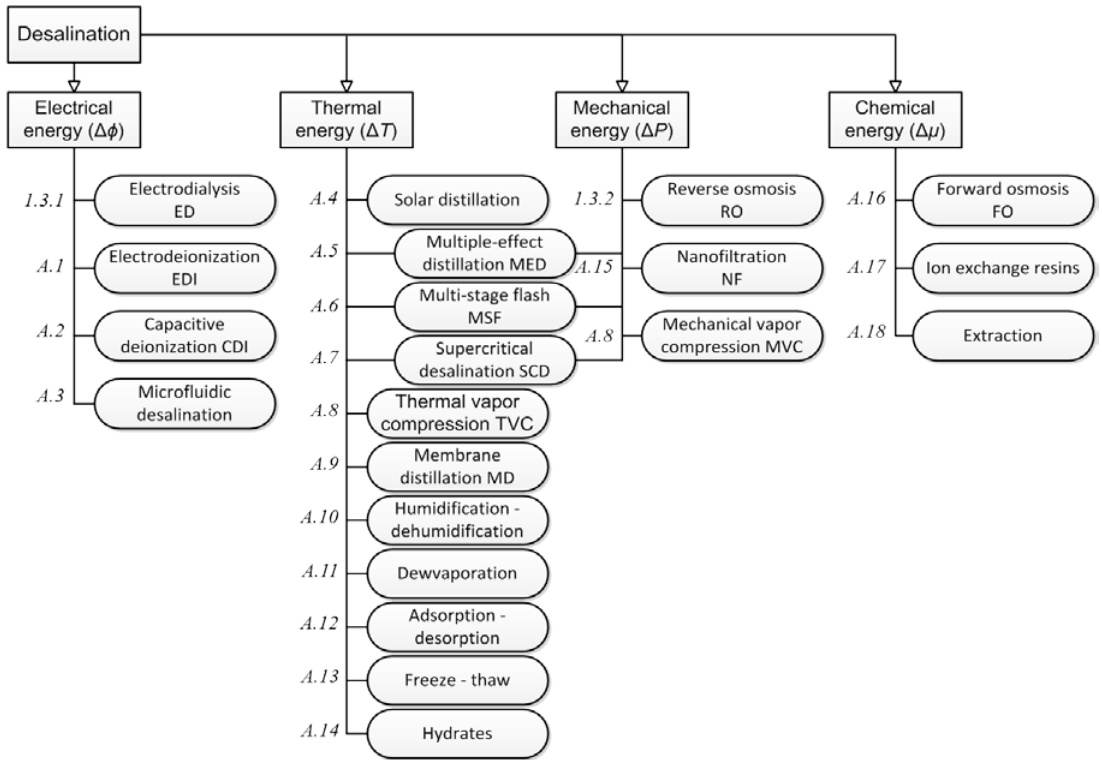
Figure 6. Desalination scheme of currently established, emerging or developing desalination technologies grouped by their (main) driving force. Cursive numbers indicate the paragraph with the description of the technology, where A. refers to Appendix A.

Besides the desalination technologies already mentioned, there are more technologies available, in development, or in conceptual stage (Figure 6). Aim of these technologies is to make the desalination process energetically and economically more attractive, and to increase sustainability of the desalination process. In this section an overview

of currently established, emerging and developing technologies is provided in Figure 6 and a description of the ED and RO process is given. In Figure 6, the desalination technologies are divided based on of their main driving force which is either a difference in; electrical potential ($\Delta \phi$), temperature (ΔT), pressure (ΔP), or chemical potential ($\Delta \mu$). The paragraph numbers with a description of the technology are indicated left of each technology, where A. refers to Appendix A.

1.3.1 Electrodialysis (ED)

The ED technology utilizes ion exchange membranes (IEMs) and an electrical field. These IEMs allow passage of ions, with minimum transport of water. A membrane stack is constructed from membrane cells that are formed by placing alternatingly a cation exchange membrane, a concentrate stream compartment (concentrate channel), an anion exchange membrane, and a diluate stream compartment (diluate channel). The last membrane cell of the stack is closed by an additional cation exchange membrane. On either side of the membrane stack an electrode compartment is created, which contains either the anode or the cathode. On these electrodes a current or a voltage is applied, which causes ion migration through the IEMs. Since IEMs are selective and mainly transport ions of specific charge sign, a concentrate and a diluate stream are created. Effectively the current is transported by ion movement through the stack, but an individual ion 'migrates' only half a cell. ED is mainly used for brackish water desalination, but it was recently shown to have potential as predesalination technique in high salinity waters [18, 41]. In practical applications ED is usually operated as EDR (electrodialysis reversal), by periodically switching polarity of the electrodes scaling and fouling issues are largely avoided [42].
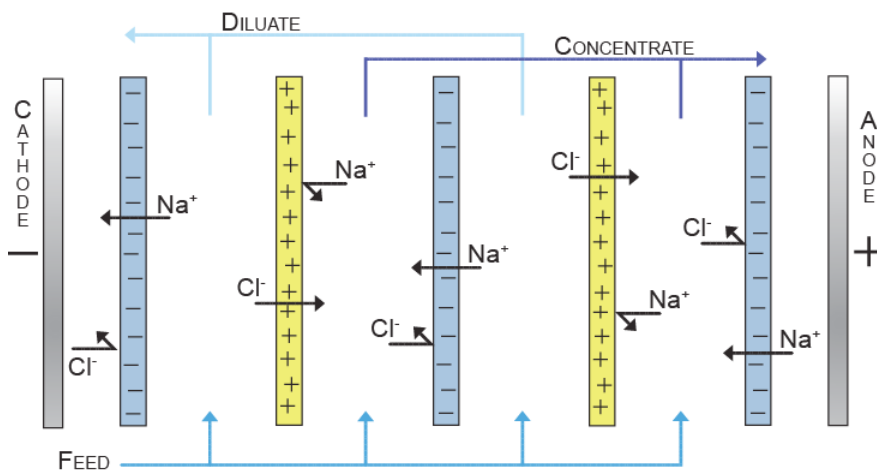
Figure 7. Schematic representation of the electrodialysis process.

Membrane desalination techniques are currently very popular in desalination. But of course, as any material, membranes have their limitations. Inspired by these limitations many researchers work on the development and improvement of membranes. Key properties for IEMs are: i) good ionic conductivity, ii) high selectivity, and iii) high thermal/chemical/mechanical stability. At present there is a large difference between the membranes used in ED stacks 'in the field' and the membranes that are developed in the lab. Highly conductive and selective membranes are already produced on small scale and are still very expensive, while low cost of such membranes is very important in determining the process feasibility of e.g. ED and fuel cell technology [43]. Nevertheless, through the development of these high quality membranes the potential application of desalination technologies that utilize IEMs is increasing.

A recent development in (reversed) electrodialysis is the use of profiled IEMs [44, 45]. Due to the use of these membranes, desalination energy consumption can be lowered and due to better mixing of boundary layers, further demineralization can be achieved. However, any membrane can in principle be profiled and as such this development should be considered as an improvement of the membrane stack flow channel design as it does not lead to better membrane properties. It might be even more interesting to have a glance on the developments of the membranes themselves. With increasing technological possibilities to produce and analyze membrane materials, the scientific and application interest in the nanostructure of membranes increased.

1.3.2 Reverse osmosis (RO)

Since 1995, RO is the most installed and by now the most widespread desalination technology [17]. RO is a pressure driven membrane technology that is based on the semi-permeability of the membranes. RO membranes are designed to allow relative large water flux (high water permeability) and at the same time retain as much colloids, ions and other charged particles as possible (low solute permeability). Good RO membranes can have NaCl rejection of 99.7% [46]. To generate a water flux through the membrane, a pressure difference across the membrane should be applied which exceeds the osmotic pressure. In seawater desalination the applied pressure is generally in the range of 55-68 bar [17] and spiral wound membranes are used [47]. Modern seawater RO systems are usually equipped with energy recovery devices, to reclaim great part of the energy used to create the required pressure difference and with high flux membranes [10, 47]. Energy consumption in such systems can be well below 2 kWh/m^3 of freshwater [17, 47]. RO is mostly used in seawater desalination, but also in brackish water desalination and water purification systems [10, 17]. For a brackish water reverse osmosis (BWRO), typically different membranes than in seawater reverse

osmosis (SWRO) are used. BWRO membranes have a higher water permeability and lower solute retention, which reduces the pressure (and energy) needed.
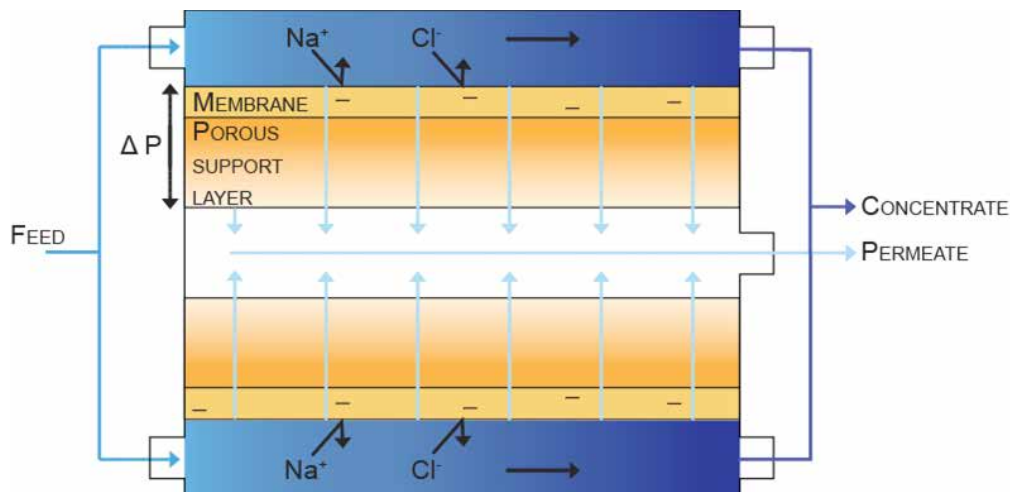
Figure 8. Schematic representation of the reverse osmosis process.

Membranes for pressure driven desalination processes require characteristics that allow a high water permeability, to obtain a larger water flux at similar membrane area, and a high salt rejection, to avoid impurities in the permeate. RO membranes possess in general high salt rejection and membrane development mainly focusses on increased water permeability. Nanostructured ceramic membranes, mixed matrix membranes, block copolymer membranes, and thin film nanocomposite membranes are some examples of membranes in development [48]. Two developments that look very promising for the field of pressure driven membrane desalination are aquaporins and nanoporous graphene. Aquaporin membranes are interesting for processes based on water transport, nanoporous graphene membranes also can be applied in cation exchange processes.

Aquaporins are pore forming proteins that are omnipresent in living cell membranes [49]. These protein pores allow great water transport rates and still show excellent solute retention for small solutes [50]. These proteins could be built into artificial membranes (biomimetic membranes) to largely enhance water permeability of e.g. RO, NF and FO membranes and as such less energy or membrane area is required for the desalination process [50, 51]. Water permeability may be 2 orders of magnitude larger compared to commercially available RO membranes [50, 51]. Membranes with aquaporins are still an object of study in research laboratory and have many technological challenges to overcome, but with developments in the membrane production strategy

[51] it is a technology with great potential [48].

Nanoporous carbon membranes also called carbon nanotubes [48, 52] are carbon pore forming structures with a diameter of ~1 nm which are, just like aquaporins, very permeable for water but not for solutes. A process efficiency gain of 5-1000 times compared to existing desalination technology was reported when the diameter is for 99% of the tubes smaller than 1 nm [52]. These carbon nanotubes can be built into polymer membranes, which can be attached on a porous support layer [48, 52]. Very efficient water transport through the nonpolar interior of the carbon nanotubes is possible due to the stability of the remaining hydrogen bonds after entering the pore [52].

Nanoporous graphene is even one step further. Graphene is a single atom thick layer of carbon atoms which form a strict two-dimensional material and exhibits exceptionally high crystal and electronic quality [53, 54]. Two dimensional materials like graphene have many future applications and hold the key to next generation products [55]. Therefore, it is not surprising that this material is also under investigation for desalination purposes. Research shows the possibility to create nanopores in the graphene with reactive characteristics, e.g. with hydrogenated or hydroxylated properties [56]. It was also shown that, compared to seawater RO membranes the water permeability can be enhanced with about 3 orders of magnitude while maintaining comparable salt rejection [56]. Desalination performance is sensitive to the pore size (~0.5 nm) and the pore chemistry (type of bonding on the pore edge). Graphene synthesis [57] is a rapidly advancing field, but nevertheless large scale application is still far from market. Due to its strength and because it is a monolayer that can be casted on a smooth support layer, instead of something that needs to be structured into a membrane, the potential for the use in desalination is likely to be even larger than the potential of aquaporins. Graphene oxide (GO) can be used in cation exchange membranes, either as composite (with polymer) or as freestanding films [58, 59]. It was revealed that graphene with a high oxidation level show high ionic conductance of the GO [59]. Addition of GO to a polymer membrane was shown to have a positive effect on current efficiency and induced lower energetic losses [58].

1.3.3 Hybrid desalination schemes

As illustrated by the scheme represented in Figure 6 and the description of the desalination technologies, there are many desalination processes and strategies available. Variability of the intake water due to e.g. salinity, scaling potential, fouling potential, and temperature, but also demanded specifications of the product water determine which technology is most suitable. Often a desalination scheme of multiple technologies is more beneficial than a stand-alone technology. A combination of two or several

technologies is referred to as a hybrid desalination process.

Combinations of membrane and thermal desalination plants in a hybrid desalination scheme can improve the desalination efficiency [17, 34, 60]. Hybrid desalination schemes can combine thermal and membrane technologies like MSF and RO [60, 61], but also two thermal technologies e.g. vapor compression with MSF or MED [62-64], or several different membrane desalination technologies like NF and RO [17]. The combination of FO and RO [65] could potentially lead to lower energy consumption as the first part of the desalination process takes place 'without' energy input. Maybe even more interesting hybrid desalination schemes than FO-RO combine a predesalination and an energy producing step in the form of reversed electrodialysis (RED) [66] or pressure retarded osmosis (PRO) [67] with RO. For the FO/PRO/RED-RO hybrid schemes is, however, always an impaired water stream required. Therefore, as a predesalination technology they should not be directly compared with e.g. ED.

Often thermal desalination process are combined with energy production plants, but combination of these technologies are not so much true hybrid desalination schemes as only the rest heat of the energy production plants is used. No real desalination efficiency is gained from such a hybrid system, although proper management of both systems, i.e. desalinating when there is power surplus and stop desalinating at the peak power consumption hours, can of course lead to increased overall energy efficiency [34].

Recently a promising hybrid desalination scheme involving ED and RO was discussed [18, 41, 68]. ED is used as a predesalination step, requiring minimum feed water pretreatment efforts and (brackish water) RO is used in a second step to produce water of superior quality at low energy demands and relative high water recovery. It was estimated that with this desalination scheme costs can be reduced by ~14% compared to RO as a stand-alone technology [41]. It was also suggested to use a hybrid desalination scheme of RO and ED [23, 69, 70], in which ED is used to enhance water recovery by further desalination of the concentrate. Here it is argued that such a scheme, would have higher capital expenses as high pressure equipment is more costly than low pressure equipment, furthermore is expected that irreversible losses of the RO-ED process are higher than in the ED-RO process as irreversible losses are larger in high pressure systems than in low pressure systems. Moreover, irreversible losses in the ED part are increased at large concentration gradients and lower required diluate concentration [18].

ED is generally regarded as unsuitable for treating waters of high salinity, as it is often stated that the energy consumption is proportional to the amount of salt that has to be

removed and as such high energy consumption is expected [18]. Undebatable, there is some truth in this statement, especially when considering ED as a stand-alone process. However, at high salinity stack resistances and internal gradients are smaller and the first half of the amount of salt can be removed with much lower losses than the second half [18, 71]. Therefore partial desalination of seawater can be done at relative low costs [72].

Development of the ED costs is schematically shown in Figure 9. This figure shows that cheaper membranes (of same quality) leads to lower overall costs and allows lower current densities to be applied, resulting also in lower energy consumption. Pumping and maintenance costs are not taking into account in this figure, but will increase when the membrane area is enlarged, only the scale of these costs is usually smaller.
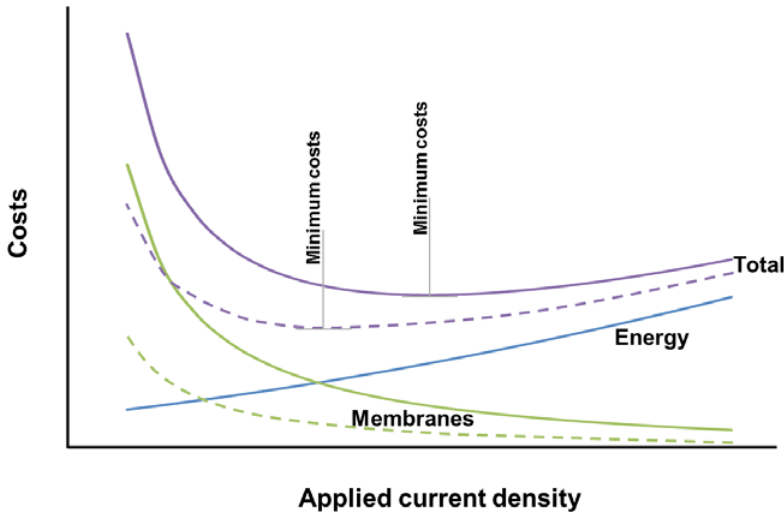
Figure 9. Schematic graph of the total desalination costs with electrodialysis as a result of the energy and membrane costs. The dotted line shows the desalination costs at reduced membrane price.

The graphs shown in Figure 9 indicate costs for the complete desalination of seawater. When there is only partial desalination of e.g. seawater, the graph representing the energy will be lowered and the minimum total costs are reached at higher applied current density. In contrary, when ED is used in brackish water desalination, energy consumption will be higher than the currently shown graph and the minimum total costs are reached at lower applied current density, where membrane costs and as such total costs are higher. As experimentally shown at low applied current densities the energy consumption can be decreased drastically [18]. Application of large membrane area

makes ED as a stand-alone process, however, economically unfeasible.

The success of ED and many other membrane based desalination technologies depends on the development of low cost, high quality (ion exchange) membranes. Ever since the idea of membrane water treatment arose, membranes are under development and performance is enhanced tremendously. At the present state, membranes are highly efficient in separation processes, providing a relatively environmental friendly and energy efficient process [73].

1.4 This thesis

As shown in Figure 5, currently, most newly installed desalination plants use membrane based technology. For the desalination of seawater most of the newly installed plants are SWRO plants, as it is currently the most cost effective of all the desalination technologies (shown in paragraph 1.3) at large scale. Most of the mentioned technologies can be more suitable than RO in certain niches of application. It is, however, not likely that in close future one of these technologies will out compete RO in the market of large scale seawater desalination. RO is already applied and continuously developed for many years, therefore, other (emerging) technologies on the desalination market might have more room for improvement than RO. Nevertheless, use of for example membrane with aquaporins or nanoporous graphene might also further enhance RO performance. Some limitations of present RO systems will, however, also occur with these 'super membranes'. Water recovery will not increase to a great extent since the process will still be limited by the osmotic pressure difference over the membrane. Also scaling, clogging, and fouling issues with SWRO will persist. The benefits of improved RO membranes will be much larger for water in the low salt concentration range (up to a few g/L), where large fluxes and high recovery can be obtained, than for treatment of for example seawater. When the flux through these new membranes can be increased, the RO footprint (in terms of size of facilities) can be substantially lowered, what may lower the investment costs.

All desalination technologies have their limitations what makes them preferred suitable in specific salinity ranges and which will determine their place in the desalination scheme. It is likely that in the near future, hybrid desalination schemes that combine multiple desalination technologies, using the strong points of each, will become more feasible than stand-alone (one process based) technologies. In this thesis the focus is on the hybrid desalination scheme of ED and BWRO that was presented by Post *et al.* [41]. Although ED and RO are used for over 60 years, the combination is only recently introduced. What is interesting in the combination of these two desalination

technologies is that ED is used in the high concentration range. This is interesting as ED is nowadays considered to be a brackish water treatment technology. The main application where IEMs are still used in seawater application can be found mostly in Japan, where ED is used for the production of table salt from seawater [74-76]. In addition, ED is recognized as technique for further concentrating brine solutions [77, 78], which is not possible with pressure driven membrane techniques due to the earlier mentioned constrains. It was shown that EDR can be operated under oversaturated $CaSO_4$ concentrations without formation of scaling [79]. So, ED is recognized in seawater application as a salt concentrating technology, but not as a desalination technology with high water recovery. That is remarkable, as fundamentally speaking these two applications are the same.
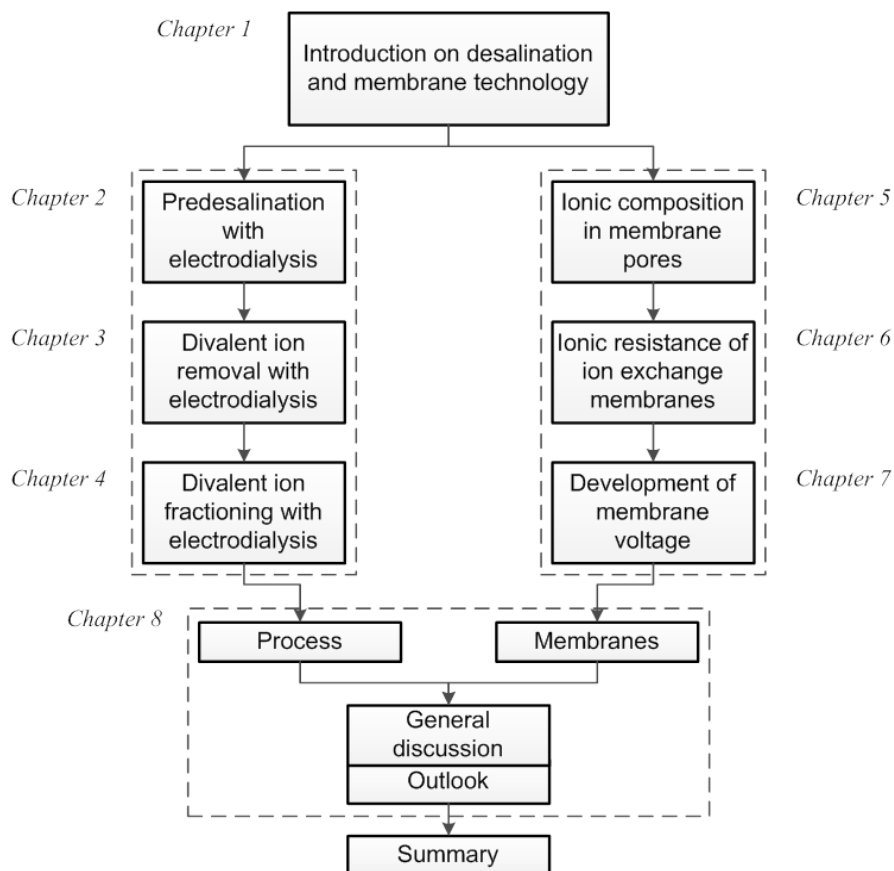

Figure 10. Structure of this thesis.

In this thesis, application of the ED process and IEMs for treatment of water at seawater salinity is investigated and discussed, Figure 10 provides an structure overview. The **aim** of this thesis is to investigate, and as such increase the knowledge about, the

use of ED and ion exchange membranes in applications with highly saline solutions, up to concentrations typical for seawater desalination. More specifically, it is the objective to identify and quantify the limitations of the ED process at high salinities, and has the goal to reach a better understanding of the processes involved in ED of feed waters with high salinity. The body of this thesis can be roughly divided into two sections with research chapters. In the first section (Chapters 2-4) the actual ED process and occurring phenomena when applied to seawater are discussed and thoroughly investigated. The second section (Chapters 5-7) is focusing specifically on the behavior of IEMs when applied to solutions of varying salinity. Findings in this second section are not ED specific, but are of interest for all IEM processes.

In **Chapter 2** the use of ED for predesalination of seawater is further discussed. The seawater ED process was experimentally investigated and is thoroughly analyzed. Energy losses are quantified for several applied current densities. The energy consumption of the ED-BWRO combination is compared with SWRO.

Divalent ions are responsible for scaling of RO membranes. It would therefore be beneficial to lower the scaling potential of the water during the predesalination step. In **Chapter 3** the effect on the diluate composition of different applied current densities in an ED stack is studied. As feed water ternary mixtures with monovalent/divalent ion concentrations comparable to those found in seawater, and artificial seawater are used. The effect of the applied current density on the transport rate of monovalent and divalent ions is elucidated. Shown effects are analyzed with a transport model and are related to concentration polarization.

Chapter 4 focusses on the removal of multivalent ions from seawater by a current induced ion exchange process or fractioning ED. In the presented ED processes, two options were experimentally investigated; i) an anion fractioning stack, where the ED stack consists of monovalent selective anion exchange membranes and standard grade anion exchange membranes, and ii) a cation fractioning stack, where the ED stack consists of monovalent selective cation exchange membranes and standard grade cation exchange membranes. A proof of principle is presented and the experimental results of artificial seawater fractioning are analyzed and discussed.

The principle of ED is based on membrane selectivity. Fixed charges on the polymer backbones of the IEMs act as an immobile ion phase and as such play a role in the formation of the electrical and chemical potential gradients. Equilibrium of the electrochemical potential in all present phases (i.e. liquid 1, membrane, liquid 2) is described by the Donnan equilibrium. In **Chapter 5** it was experimentally investigated in what quantities counterions and co-ions are present in a specific cation exchange membrane. The investigation was done in the concentration range of 0.01-3.0 M NaCl, concentra-

tions that can typically be found in applications of the ED process. The experimental results are compared with the theoretical results obtained with the classical Boltzmann equation. Discrepancy between theory and experimental data at low external salt concentrations are reported for over half a century in scientific literature. These findings were confirmed in this study and possible new explanations for these discrepancies are being discussed. In **Chapter 6** it is shown for the first time how resistance of an IEM is influenced by the external salt concentrations, when these external salt concentrations are different (i.e. a concentration gradient is present). The NaCl concentration in the external solutions were varied between 0.01-1.1 M. Experimental results are discussed, as well as the implications on the conceptual interpretations of IEMs and their structure. Results of membrane resistances when the external concentrations are equal are compared with results from earlier investigations. A qualitative model is presented that helps to further understand the obtained results. **Chapter 7** is about the (reversible) membrane potential that arises over an IEM when it is used to separate two solutions of varying salt concentration. Theory on the membrane potential is critically reviewed. The focus of this chapter is on the widely applied Theorell-Meyer-Sievers (TMS) theory and on the justness of its assumptions for the case of IEMs in a broad range of NaCl concentrations. Theory and experimental values are compared and discussed.

In **Chapter 8** all the results and conclusions from the research chapters are further discussed and a perspective on the use of ED and IEMs with high salinity feed waters is given. An outlook with respect to remaining research questions is also provided. In the final paragraph of Chapter 8 (8.7) an economical perspective of the hybrid ED-BWRO desalination scheme and a comparison with SWRO, is provided. After this chapter the work is summarized in an extensive **Summary** that includes all highlights and core findings of this thesis.

An overview of the used literature sources is provided individually at the end of each chapter.

1.5 Literature

[1] I.A. Shiklomanov, World water resources, in: P.H. Gleick (Ed.) Water in Crisis. New York, Oxford, 1993.

[2] U.N. UN, International Decade for Action 'Water for Life', in: Water scarcity, 2005-2015.

[3] E. Custodio, Aquifer overexploitation: what does it mean?, Hydrogeology Journal, 10 (2002) 254-277.

[4] R.B. Jackson, S.R. Carpenter, C.N. Dahm, D.M. McKnight, R.J. Naiman, S.L. Postel, S.W. Running, Water in a changing world, Ecological applications, 11 (2001) 1027-1045.

[5] J. Rockström, M. Falkenmark, L. Karlberg, H. Hoff, S. Rost, D. Gerten, Future water availability for global food production: the potential of green water for increasing resilience to global change, Water Resources Research, 45 (2009).

[6] C. Giupponi, Sustainable management of water resources: an integrated approach, Edward Elgar Publishing, 2006.

[7] P.H. Gleick, Water in crisis: paths to sustainable water use, Ecological applications, 8 (1998) 571-579.

[8] M. Elimelech, W.A. Phillip, The future of seawater desalination: energy, technology, and the environment, Science, 333 (2011) 712-717.

[9] M.A. Shannon, P.W. Bohn, M. Elimelech, J.G. Georgiadis, B.J. Marĩas, A.M. Mayes, Science and technology for water purification in the coming decades, Nature, 452 (2008) 301-310.

[10] L.F. Greenlee, D.F. Lawler, B.D. Freeman, B. Marrot, P. Moulin, Reverse osmosis desalination: Water sources, technology, and today's challenges, Water Research, 43 (2009) 2317-2348.

[11] S. Lattemann, T. Höpner, Environmental impact and impact assessment of seawater desalination, Desalination, 220 (2008) 1-15.

[12] S. Lattemann, M.D. Kennedy, J.C. Schippers, G. Amy, Global Desalination Situation, in: I. Escobar, A. Schäfer (Eds.) Sustainable Water for the Future – Water Recycling versus Desalination, Elsevier B.V., Amsterdam, Netherlands, 2010.

[13] IDA, International Desalination Association, in, Desalination by the numbers 2013.

[14] N. Misdan, W.J. Lau, A.F. Ismail, Seawater Reverse Osmosis (SWRO) desalination by thin-film composite membrane—Current development, challenges and future prospects, Desalination, 287 (2012) 228-237.

[15] L. Henthorne, T. Pankratz, S. Murphy, IDA world congress, The State of Desalination, in: Desalination: Sustainable Solutions for a Thirsty Planet, Perth, 2011, September 4-9.

[16] A.D. Khawaji, I.K. Kutubkhanah, J.M. Wie, Advances in seawater desalination technologies, Desalination, 221 (2008) 47-69.

[17] C. Fritzmann, J. Löwenberg, T. Wintgens, T. Melin, State-of-the-art of reverse osmosis desalination, Desalination, 216 (2007) 1-76.

[18] A.H. Galama, M. Saakes, H. Bruning, H.H.M. Rijnaarts, J.W. Post, Seawater Predesalination with Electrodialysis, Desalination, 342 (2013) 61-69.

[19] A.H. Galama, G. Daubaras, O.S. Burheim, H.H.M. Rijnaarts, J.W. Post, Fractioning electrodialysis: a current induced ion exchange process, Electrochimica Acta, 136 (2014) 257-265.

[20] D.A. Roberts, E.L. Johnston, N.A. Knott, Impacts of desalination plant discharges on the marine environment: A critical review of published studies, Water Research, 44 (2010) 5117-5128.

[21] T. Mezher, H. Fath, Z. Abbas, A. Khaled, Techno-economic assessment and environmental impacts of desalination technologies, Desalination, 266 (2011) 263-273.

[22] S. Heijman, H. Guo, S. Li, J. van Dijk, L. Wessels, Zero liquid discharge: Heading for 99% recovery in nanofiltration and reverse osmosis, Desalination, 236 (2009) 357-362.

[23] Y. Oren, E. Korngold, N. Daltrophe, R. Messalem, Y. Volkman, L. Aronov, M. Weismann, N. Bouriakov, P. Glueckstern, J. Gilron, Pilot studies on high recovery BWRO-EDR for near zero liquid discharge approach, Desalination, 261 (2010) 321-330.

[24] M. Turek, Dual-purpose desalination-salt production electrodialysis, Desalination, 153 (2003) 377-381.

[25] Y. Tanaka, R. Ehara, S. Itoi, T. Goto, Ion-exchange membrane electrodialytic salt production using brine discharged from a reverse osmosis seawater desalination plant, Journal of Membrane Science, 222 (2003) 71-86.

[26] T. Jeppesen, L. Shu, G. Keir, V. Jegatheesan, Metal recovery from reverse osmosis concentrate,

Journal of Cleaner Production, 17 (2009) 703-707.

[27] M. Petersková, C. Valderrama, O. Gibert, J.L. Cortina, Extraction of valuable metal ions (Cs, Rb, Li, U) from reverse osmosis concentrate using selective sorbents, Desalination, 286 (2012) 316-323.

[28] C. Charcosset, A review of membrane processes and renewable energies for desalination, Desalination, 245 (2009) 214-231.

[29] A. Al-Karaghouli, D. Renne, L.L. Kazmerski, Technical and economic assessment of photovoltaic-driven desalination systems, Renewable Energy, 35 (2010) 323-328.

[30] S.A. Kalogirou, Seawater desalination using renewable energy sources, Progress in Energy and Combustion Science, 31 (2005) 242-281.

[31] A. Subramani, M. Badruzzaman, J. Oppenheimer, J.G. Jacangelo, Energy minimization strategies and renewable energy utilization for desalination: A review, Water Research, 45 (2011) 1907-1920.

[32] M. Shatat, M. Worall, S. Riffat, Opportunities for solar water desalination worldwide: Review, Sustainable Cities and Society, 9 (2013) 67-80.

[33] V.G. Gude, N. Nirmalakhandan, S. Deng, Renewable and sustainable approaches for desalination, Renewable and Sustainable Energy Reviews, 14 (2010) 2641-2654.

[34] A. Helal, Hybridization—a new trend in desalination, Desalination and Water Treatment, 3 (2009) 120-135.

[35] J.D. Birkett, A brief illustrated history of desalination. From the bible to 1940, Desalination, 50 (1984) 17-52.

[36] B. Van der Bruggen, C. Vandecasteele, Distillation vs. membrane filtration: overview of process evolutions in seawater desalination, Desalination, 143 (2002) 207-218.

[37] M. Al-Shammiri, M. Safar, Multi-effect distillation plants: State of the art, Desalination, 126 (1999) 45-59.

[38] J.R. Wilson, Demineralization by electrodialysis, in, Butterworths Scientific Publications, London (UK), 1960.

[39] W. Juda, W.A. McRae, Coherent ion-exchange gels and membranes, Journal of the American Chemical Society, 72 (1950) 1044-1044.

[40] T. Kressman, Ion exchange resin membranes and resin-impregnated filter paper, Nature, 165 (1950) 568.

[41] J.W. Post, H. Huiting, E.R. Cornelissen, H.V.M. Hamelers, Pre-desalination with electro-membranes for SWRO, Desalination and Water Treatment, 31 (2011) 296-304.

[42] B. Pilat, Practice of water desalination by electrodialysis, Desalination, 139 (2001) 385-392.

[43] R. Yee, R. Rozendal, K. Zhang, B. Ladewig, Cost effective cation exchange membranes: A review, Chemical Engineering Research and Design, 90 (2012) 950-959.

[44] H. Strathmann, A. Grabowski, G. Eigenberger, Ion-exchange membranes in the chemical process industry, Industrial & Engineering Chemistry Research, 52 (2013) 10364-10379.

[45] D. Vermaas, M. Saakes, K. Nijmeijer, Power generation using profiled membranes in reverse electrodialysis, Journal of Membrane Science, 385-386 (2011) 234-242.

[46] R.H. Perry, D.W. Green, J.O. Malony, Perry's Chemical Engineers' Handbook., in, McGraw Hill, New York, 1997.

[47] B. Peñate, L. García-Rodríguez, Current trends and future prospects in the design of seawater reverse osmosis desalination technology, Desalination, 284 (2012) 1-8.

[48] M.M. Pendergast, E.M. Hoek, A review of water treatment membrane nanotechnologies, Energy & Environmental Science, 4 (2011) 1946-1971.

[49] P. Agre, S. Sasaki, M. Chrispeels, Aquaporins: a family of water channel proteins, American Journal of Physiology-Renal Physiology, 265 (1993) F461-F461.

[50] M. Kumar, M. Grzelakowski, J. Zilles, M. Clark, W. Meier, Highly permeable polymeric membranes based on the incorporation of the functional water channel protein Aquaporin Z, Proceedings of the National Academy of Sciences, 104 (2007) 20719-20724.

[51] C. Tang, Y. Zhao, R. Wang, C. Hélix-Nielsen, A. Fane, Desalination by biomimetic aquaporin membranes: Review of status and prospects, Desalination, 308 (2013) 34-40.

[52] B. Corry, Designing carbon nanotube membranes for efficient water desalination, The Journal of Physical Chemistry B, 112 (2008) 1427-1434.

[53] A.K. Geim, K.S. Novoselov, The rise of graphene, Nature materials, 6 (2007) 183-191.

[54] K.S. Novoselov, A.K. Geim, S. Morozov, D. Jiang, Y. Zhang, S. Dubonos, I. Grigorieva, A. Firsov, Electric field effect in atomically thin carbon films, Science, 306 (2004) 666-669.

[55] A. Neto, K. Novoselov, Two-dimensional crystals: Beyond graphene, Materials Express, 1 (2011) 10-17.

[56] D. Cohen-Tanugi, J.C. Grossman, Water desalination across nanoporous graphene, Nano letters, 12 (2012) 3602-3608.

[57] K. Celebi, J. Buchheim, R.M. Wyss, A. Droudian, P. Gasser, I. Shorubalko, J.-I Kye, C. Lee, H.G. Park, Ultimate Permeation Across Atomically Thin Porous Graphene, Science, 344 (2014) 289-292.

[58] S. Gahlot, P.P. Sharma, H. Gupta, V. KULSHRESTHA, P.K. Jha, Preparation of Graphene Oxide Nano-composite Ion-exchange Membranes for Desalination Application, RSC Advances, (2014).

[59] W. Gao, G. Wu, M.T. Janicke, D.A. Cullen, R. Mukundan, J.K. Baldwin, E.L. Brosha, C. Galande, P.M. Ajayan, K.L. More, Ozonated Graphene Oxide Film as a Proton‐Exchange Membrane, Angewandte Chemie International Edition, 53 (2014) 3588-3593.

[60] Y. Ghalavand, M.S. Hatamipour, A. Rahimi, A review on energy consumption of desalination processes, Desalination and Water Treatment, (2014) 1-16.

[61] O.A. Hamed, Overview of hybrid desalination systems—current status and future prospects, Desalination, 186 (2005) 207-214.

[62] M. Darwish, Thermal analysis of vapor compression desalination system, Desalination, 69 (1988) 275-295.

[63] A.S. Hassan, M.A. Darwish, Performance of thermal vapor compression, Desalination, 335 (2014) 41-46.

[64] H. El-Dessouky, H. Ettouney, F. Al-Juwayhel, Multiple effect evaporation—vapour compression desalination processes, Chemical Engineering Research and Design, 78 (2000) 662-676.

[65] T.Y. Cath, J.E. Drewes, C.D. Lundin, A novel hybrid forward osmosis process for drinking water augmentation using impaired water and saline water sources, in, Water research foundation, Denver, CO (USA), 2009.

[66] W. Li, W.B. Krantz, E.R. Cornelissen, J.W. Post, A.R. Verliefde, C.Y. Tang, A novel hybrid process of reverse electrodialysis and reverse osmosis for low energy seawater desalination and brine management, Applied Energy, 104 (2013) 592-602.

[67] V.S. Sim, Q. She, T.H. Chong, C.Y. Tang, A.G. Fane, W.B. Krantz, Strategic co-location in a hybrid process involving desalination and Pressure Retarded Osmosis (PRO), Membranes, 3 (2013) 98-125.

[68] S. Thampy, G.R. Desale, V.K. Shahi, B.S. Makwana, P.K. Ghosh, Development of hybrid electrodialysis-reverse osmosis domestic desalination unit for high recovery of product water, Desalination, 282 (2011) 104-108.

[69] E. Korngold, L. Aronov, N. Daltrophe, Electrodialysis of brine solutions discharged from an RO plant, Desalination, 242 (2009) 215-227.

[70] A. Pérez-González, A. Urtiaga, R. Ibáñez, I. Ortiz, State of the art and review on the treatment technologies of water reverse osmosis concentrates, Water Research, 46 (2012) 267-283.

[71] A.H. Galama, D.A. Vermaas, J. Veerman, M. Saakes, H.H.M. Rijnaarts, J.W. Post, K. Nijmeijer, Membrane resistance: The effect of salinity gradients over a cation exchange membrane, Journal of Membrane Science, 467 (2014) 279-291.

[72] R.K. McGovern, S.M. Zubair, J.H. Lienhard V, The cost effectiveness of electrodialysis for diverse salinity applications, Desalination, 348 (2014) 57-65.

[73] T. Xu, Ion exchange membranes: State of their development and perspective, Journal of Membrane Science, 263 (2005) 1-29.

[74] Y. Tanaka, Ion-exchange membrane electrodialysis for saline water desalination and its application to seawater concentration, Industrial and Engineering Chemistry Research, 50 (2011) 7494-7503.

[75] T. Sata, Ion Exchange Membranes; Preparation, Characterization, Modification and Application, The Royal Society of Chemistry, Cambridge UK, 2004.

[76] H. Strathmann, Ion-exchange membrane separation processes, Elsevier, Amsterdam NL, 2004.

[77] B. Van der Bruggen, L. Lejon, C. Vandecasteele, Reuse, treatment, and discharge of the concentrate of pressure-driven membrane processes, Environmental science & technology, 37 (2003) 3733-3738.

[78] M. Turek, K. Mitko, M. Chorzewska, P. Dydo, Use of the desalination brines in the saturation of membrane electrolysis feed, Desalination and Water Treatment, 51 (2013) 2749-2754.

[79] M. Turek, P. Dydo, J. Waś, Electrodialysis reversal in high CaSO4 supersaturation mode, Desalination, 198 (2006) 288-294.

[80] J. Wood, J. Gifford, J. Arba, M. Shaw, Production of ultrapure water by continuous electrodeionization, Desalination, 250 (2010) 973-976.

[81] A.H. Galama, G. Daubaras, O.S. Burheim, H.H.M. Rijnaarts, J.W. Post, Seawater electrodialysis with preferential removal of divalent ions, Journal of Membrane Science, 452 (2014) 219-228.

[82] E.J. Parsi, Removal of weakly basic substances from solution by electrodeionization, Patent US3291713A in, Google Patents, 1966.

[83] G.C. Ganzi, A.J. Giuffrida, A.D. Jha, Electrodeionization apparatus, Patent US4632745 A, in, Google Patents, 1986.

[84] S. Porada, R. Zhao, A. Van Der Wal, V. Presser, P.M. Biesheuvel, Review on the Science and Technology of Water Desalination by Capacitive Deionization, Progress in Materials Science 58 (2013) 1388-1442.

[85] S.J. Kim, S.H. Ko, K.H. Kang, J. Han, Direct seawater desalination by ion concentration polarization, Nature Nanotechnology, 5 (2010) 297-301.

[86] S.J. Kim, C.H. Seow, J. Han, Small-scale approach to big water problem, The international Desalination & Water Reuse quarterly, 20 (2010) 21-24.

[87] K.N. Knust, D. Hlushkou, R.K. Anand, U. Tallarek, R.M. Crooks, Electrochemically mediated seawater desalination, Angewandte Chemie International Edition, 52 (2013) 8107-8110.

[88] K.N. Knust, D. Hlushkou, U. Tallarek, R.M. Crooks, Electrochemical Desalination for a Sustainable Water Future, ChemElectroChem, (2014).

[89] S.O. Odu, A.G.J. van der Ham, S. Metz, S.R.A. Kersten, Design of a process for supercritical water desalination, in: 14th European Meeting on Supercritical Fluids Marseille (France), 2014.

[90] A. Alkhudhiri, N. Darwish, N. Hilal, Membrane distillation: A comprehensive review, Desalination, 287 (2012) 2-18.

[91] K. Bourouni, M. Chaibi, L. Tadrist, Water desalination by humidification and dehumidification of air: state of the art, Desalination, 137 (2001) 167-176.

[92] G. Prakash Narayan, M.G. St John, S.M. Zubair, J.H. Lienhard V, Thermal design of the humidification dehumidification desalination system: An experimental investigation, International Journal of Heat and Mass Transfer, 58 (2013) 740-748.

[93] K.C. Ng, K. Thu, Y. Kim, A. Chakraborty, G. Amy, Adsorption desalination: an emerging low-cost thermal desalination method, Desalination, 308 (2013) 161-179.

[94] K. Thu, K.C. Ng, B.B. Saha, A. Chakraborty, S. Koyama, Operational strategy of adsorption desalination systems, International Journal of Heat and Mass Transfer, 52 (2009) 1811-1816.

[95] G. Stepakoff, D. Siegelman, R. Johnson, W. Gibson, Development of a eutectic freezing process for brine disposal, Desalination, 15 (1974) 25-38.

[96] F. Van der Ham, G. Witkamp, J. De Graauw, G. Van Rosmalen, Eutectic freeze crystallization simultaneous formation and separation of two solid phases, Journal of crystal growth, 198 (1999) 744-748.

[97] T. Mtombeni, J. Maree, C. Zvinowanda, J. Asante, F. Oosthuizen, W. Louw, Evaluation of the performance of a new freeze desalination technology, International Journal of Environmental Science and Technology, 10 (2013) 545-550.

[98] J. Javanmardi, M. Moshfeghian, Energy consumption and economic evaluation of water desalination by hydrate phenomenon, Applied thermal engineering, 23 (2003) 845-857.

[99] W.G. Knox, M. Hess, G. Jones, H. Smith, The hydrate process, Chem. Eng. Prog, 57 (1961) 66-71.

[100] N. Hilal, H. Al-Zoubi, N.A. Darwish, A.W. Mohammad, Performance of nanofiltration membranes in the treatment of synthetic and real seawater, Separation Science and Technology, 42 (2007) 493-515.

[101] B. Van Der Bruggen, A. Koninckx, C. Vandecasteele, Separation of monovalent and divalent ions from aqueous solution by electrodialysis and nanofiltration, Water Research, 38 (2004) 1347-1353.

[102] N. Hilal, H. Al-Zoubi, N. Darwish, A. Mohamma, M. Abu Arabi, A comprehensive review of nanofiltration membranes: Treatment, pretreatment, modelling, and atomic force microscopy, Desalination, 170 (2004) 281-308.

[103] T.Y. Cath, A.E. Childress, M. Elimelech, Forward osmosis: principles, applications, and recent developments, Journal of Membrane Science, 281 (2006) 70-87.

[104] G.W. Batchelder, Process for the Demineralization of Water, US Patent: 3,171,799, in: United States Patent Office, 1965.

[105] J.R. McCutcheon, R.L. McGinnis, M. Elimelech, A novel ammonia—carbon dioxide forward (direct) osmosis desalination process, Desalination, 174 (2005) 1-11.

[106] M. Elimelech, Yale constructs forward osmosis desalination pilot plant, Membrane Technology,

2007 (2007) 7-8.

[107] F.G. Helfferich, Ion Exchange, McGraw-Hill, New York, (1962).

[108] A. Chapotot, G. Pourcelly, C. Gavach, Transport competition between monovalent and divalent cations through cation-exchange membranes. Exchange isotherms and kinetic concepts, Journal of Membrane Science, 96 (1994) 167-181.

[109] G. Pourcelly, P. Sistat, A. Chapotot, C. Gavach, V. Nikonenko, Self diffusion and conductivity in NafionR membranes in contact with NaCl+CaCl2 solutions, Journal of Membrane Science, 110 (1996) 69-78.

[110] M. Higa, A. Tanioka, K. Miyasaka, An experimental study of ion permeation in multicomponent ion systems as a function of membrane charge density, Journal of Membrane Science, 64 (1991) 255-262.

[111] A. Chapotot, G. Pourcelly, C. Gavach, F. Lebon, Electrotransport of proton and divalent cations through modified cation-exchange membranes, Journal of Electroanalytical Chemistry, 386 (1995) 25-37.

[112] S. Rengaraj, K.H. Yeon, S.H. Moon, Removal of chromium from water and wastewater by ion exchange resins, Journal of Hazardous Materials, 87 (2001) 273-287.

[113] S.D. Alexandratos, Ion-Exchange resins: A retrospective from industrial and engineering chemistry research, Industrial and Engineering Chemistry Research, 48 (2009) 388-398.

[114] N. Kabay, S. Sarp, M. Yuksel, M. Kitis, H. Koseoğlu, Ö. Arar, M. Bryjak, R. Semiat, Removal of boron from SWRO permeate by boron selective ion exchange resins containing< i> N</i>-methyl glucamine groups, Desalination, 223 (2008) 49-56.

[115] R. Davidson, W. Smith Jr, D.W. Hood, Structure and Amine-Water Solubility in Desalination by Solvent Extraction, Journal of Chemical and Engineering Data, 5 (1960) 420-423.

[116] A. Bajpayee, T. Luo, A. Muto, G. Chen, Very low temperature membrane-free desalination by directional solvent extraction, Energy Environ. Sci., 4 (2011) 1672-1675.

[117] G. De Souza, Water pretreatment unit using a fluorinated liquid, in, Organisation Mondiale de la Propriété Intellectuelle, France, 2010.

[118] C.H. Janssen, M.C. Kroon, S.J. Metz, J. van Spronsen, G.-J. Witkamp, Extraction of Sodium Chloride from Water and Solubility of Water in Hydrophobic Trialkylammonium Alkanoate-Based Ionic Liquids, Journal of Chemical & Engineering Data, 55 (2010) 3391-3394.

[119] D. Parmentier, S.J. Metz, M.C. Kroon, Tetraalkylammonium oleate and linoleate based ionic liquids: promising extractants for metal salts, Green Chemistry, 15 (2013) 205-209.

Appendix A

Figure 6 shows a scheme of currently established, emerging, and developing desalination technologies. A description of ED and RO was given in the main text. Descriptions of the other technologies shown in Figure 6 are given in this appendix.

A.1 Electrodeionization (EDI)

EDI is closely related with the ED process, but in the case of EDI the diluate channels and sometimes also the concentrate channels are filled with ion exchange resins [76, 80]. These resins are used to collect and discharge ions or to facilitate the transport of ions continuously by ionic or electronic substitution mechanisms [80]. In this way, high resistivity of the diluate channel, which leads to high energy consumption in ED, is avoided. EDI can be used batch wise, with a regeneration step of the media, but by far the most used application is the continuous electrodeionization (CEDI). In CEDI the applied current induces splitting of water molecules into hydrogen (H^+) and hydroxyl (OH^-) ions in the depletion layer (due to concentration polarization [81]) close to the IEMs and ion exchange resin surface [80, 82, 83]. These ions continuously regenerate the ion exchange resins, bringing them back from e.g. Na^+/Cl^- form, into the H^+/OH^- form. Ions leaving the resins are transported through the IEMs . Different CEDI modes are in use, in the standard design cation and anion exchange resins are present together in the diluate channel. Designs with separate anion or cation exchange channels are in use as well, and also bipolar membranes may be applied [76]. CEDI is used to produce water of extreme low salt concentration and is often applied as a post treatment to e.g. RO or ED products or as stand-alone technology to purify streams of low salinity.
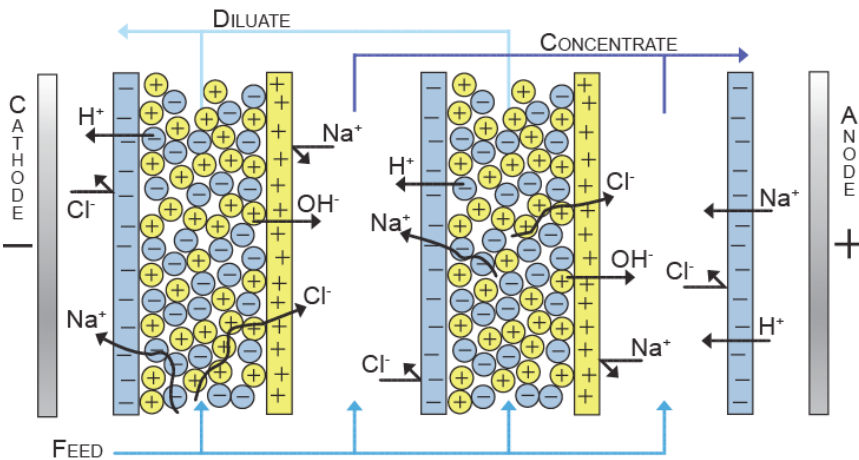
Figure A 1. Schematic representation of the electrodeionization process.

A.2 Capacitive deionization (CDI)

CDI is another electrically driven desalination technology [84]. The basic principle is that an electric field is applied on two porous electrodes, adjacent a flow channel, which causes ion migration from the feed water towards the electrodes. Ions are temporary adsorbed in an electrical double layer that forms on the surface of these porous electrodes. A negatively charged electrode (cathode) is present for the cations and a positively charged electrode (anode) for the anions. These porous electrodes are typically of very porous carbon and can be covered by an IEM to enhance selectivity of the process. In that case the process is referred to as membrane capacitive deionization (MCDI). When water flows along the electrodes, ions are removed and a diluate stream is produced. After certain time of applying current on the electrodes no more ions can be adsorbed by the electrode material. Now the ion release step takes place. The current is switched off and ions move back into the solution between the electrodes, forming a concentrate stream. So, with these two steps intermittingly a diluate and concentrate are produced. In theory part of the applied current can be reclaimed in the discharge step.
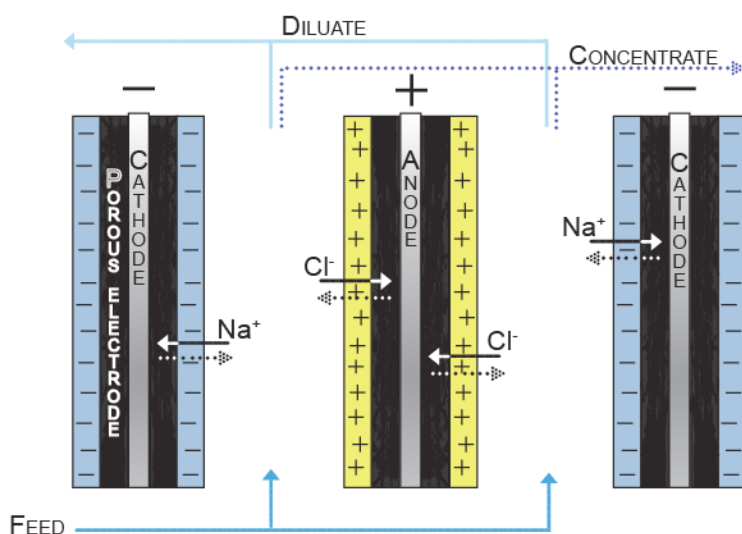
Figure A 2. Schematic representation of the capacitive deionization process.

A.3 Microfluidic desalination technologies

Electrochemically mediated desalination (EMD) is based on a desalination technique that uses ion concentration polarization (ICP) for desalination [85]. In the ICP desalination technique an over limiting current is generated over a 'nanojunction' (usually an ion selective membrane) to create polarization layers. This membrane is located

at a point where the channel splits in two channels. In the case of a cation exchange membrane ions (and other charges species) are depleted at the anode side and enriched at the cathode side. The ion depletion zone is generated around the entrance one of the two channels (or branches) after splitting the feed channel. This leads to formation of a desalination channel and a brine channel. The flow channels are small and have a typical size in the order of 100-1000 μm to avoid turbulence flow and to avoid mixing of the ion depletion layer [86]. In EMD the same branched channel can be used as with the ICP desalination but now instead of a nanojunction an (bipolar) electrode is used to create a depletion zone [87, 88]. When an anode is used at the splitting point of the feed channel and de 'fluid reservoirs' are grounded an ion depletion zone can be created around the fresh water branch entrance. Around the anode Cl$^-$ is oxidized to Cl$_2$, what leads to a reduced number of charge carriers and induces formation of a depletion zone. Benefit of this system over the ICP system is that no membranes or required. Both microfluidic desalination techniques showed promising results with respect to desalination performance and energy consumption [85-88] but are still under development.
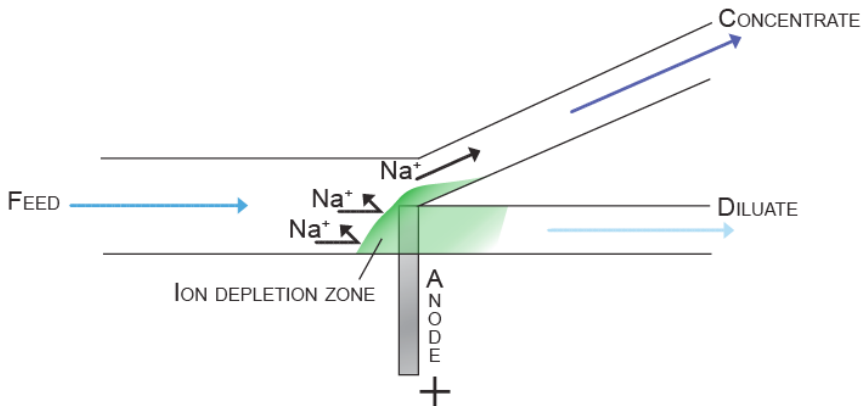
Figure A 3. Schematic representation of the microfluidic desalination process.

A.4 Solar *distillation*

Distillation of e.g. seawater is an easy and robust way to separate water and salts. The only requirements are a basin for the feed water, a heat source and a condensate collection point (e.g. a sponge [35] or glass plate). Most solar distils are constructed with a transparent cover (glass or plastic) on top of a feed water basin with a black or reflecting bottom. When exposed to the sun such a closed system heats up, and due to the black or reflecting bottom, as much energy as possible is used to increase the water temperature. After certain exposure time water will evaporate and forms a condensate layer on the inside of the cover. This cover is arced or placed under an arc, so that

condense is transported at the surface to the lowest point. At that point water drops are formed, which are collected in a basin. Application of these systems is generally small scale desalination, like the emergency solar stills on live boats.
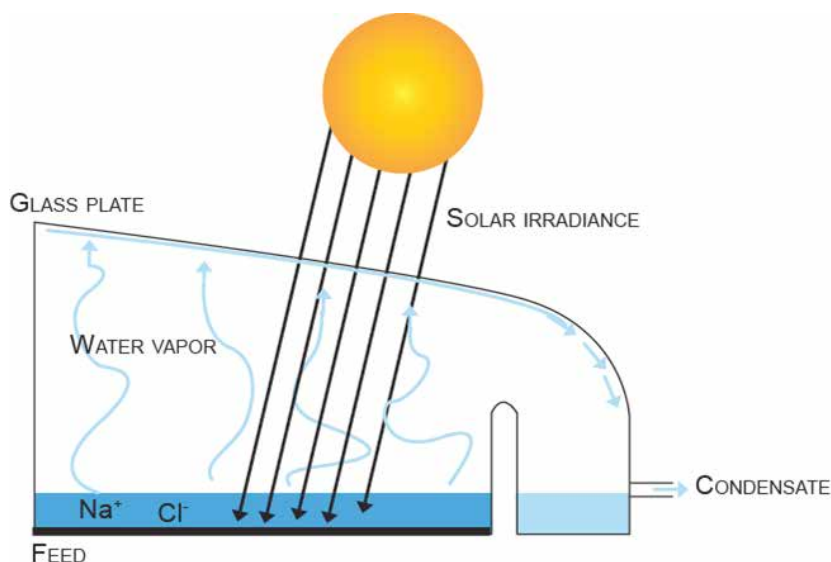
Figure A 4. Schematic representation of the solar distillation process.

A.5 *Multiple-effect distillation (MED)*

MED is a distillation technique that works with a series of evaporators called effects, and uses the principle of reducing the ambient pressure in the various effects [16]. These effects are usually large vessels that contain an evaporator and a spray device. This evaporator or heat exchanger is actually a tube (or multiple tubes) in which steam is supplied from a boiler and that heats up the tube. Preheated feed water is sprayed in a thin film onto the outer surface of the tube to promote rapid evaporation. The steam in the evaporator is decreasing in temperature as it flows through the effect and when it leaves the effect it is condensed into pure water. The condensate of the first effect is returned to a boiler. The evaporated feed water (steam) is forced into the evaporator of the second effect, where the exact same process takes place, but if now the vapor condenses in the end of the evaporator it is the product instead of boiler water. Many effects (typically 8-16) can be placed in array, in every effect the temperature and pressure is decreased. Non evaporated but, heated feed water from one effect can be supplied with the feed water to the following effect, where it may flash into steam as the pressure is reduced. Typically for seawater desalination the first effect is operated at 70 ˚C to avoid scaling. Each effect reuses the energy from the previous effect, making it an energy efficient process, especially when a source of waste heat is available

from e.g. a power plant [16, 37]. Steam of the last effect can be used to preheat the feed solution in a condenser. There are many ways how an MED plant can be constructed, but generally effects are horizontally arranged and are of the thin falling film type [37]. Application of MED plants is mostly in seawater desalination in the Middle East.
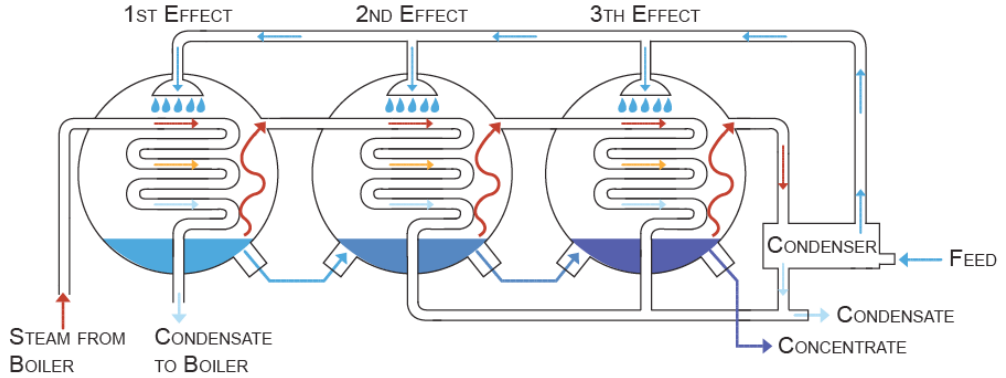
Figure A 5. Schematic representation of the multiple-effect distillation process.

A.6 *Multi-stage flash (MSF)*

When water is pressurized the boiling point shifts to a higher temperature. When water is heated till just under the boiling point at the ambient pressure and the heating is stopped nothing happens. However, when the ambient pressure is instantly decreased the water immediately starts boiling. This boiling process is known as flashing. Generally, only a small part of the water flashes to steam, as the phase transition from liquid to gas phase cools down the liquid. However when the pressure is decreased even further, the water will again start to boil. This is exactly the process that is used in MSF. Steam is forced along a heat exchanger system where it comes into thermal contact with the cooler feed water stream. The steam therefore condenses on the heat exchanger tube, and can be collected as fresh water. The heat generated by the condensation process is absorbed by the feed water stream which is heated up in return and as such carries away the latent heat and the low temperature of the stage can be maintained. In a continues process, the pressure in the chamber is unchanged, as equal amount of steam is produced from the entering brine and removed as condensate. When the feed water is preheated by all the heat exchangers of the different stages it is collected in the brine heater. Here only little additional heat is added to increase the water temperature to its maximum, which is the temperature setting for stage 1. The maximum temperature is usually between 90-120 ˚C to avoid scaling of e.g. bicarbonate [16]. In the final stage the brine and condensate have a temperature close to the incoming feed water, but the pressure is much lower than the atmospheric pressure. Large MSF plants typically contain 19-28 stages [16]. Just as with the MED plants the MSF plants are

very suitable to combine with power plants which produce a lot of waste heat. From a thermodynamic and heat transfer point of view MED is more efficient than the MSF distillation process [16].
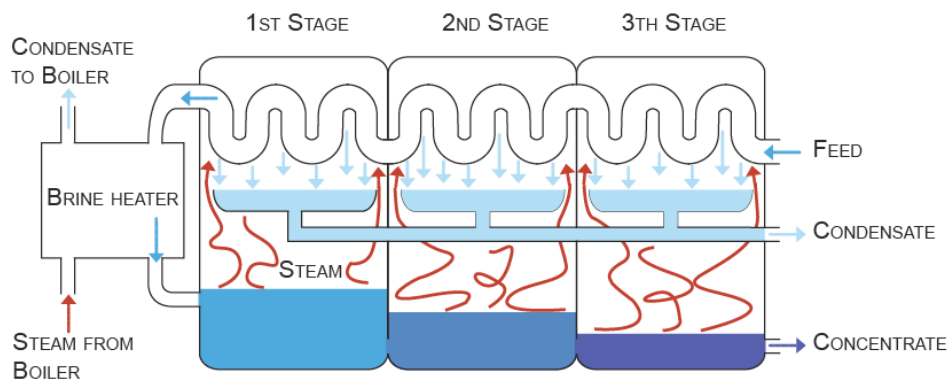
Figure A 6. Schematic representation of the multi-stage flash process.

A.7 Supercritical desalination (SCD)

SCD is based on the changing properties of water at supercritical conditions. Super-critical (SC) conditions are reached at very high pressure and temperature (T_c = 647 K, P_c = 22.1·10⁶ Pa). Under SC conditions, salts have very low solubility and therefore precipitate. In theory a pure water phase and a pure salt phase can be generated and therefore, no concentrate (brine) treatment step is required. In a typical SCD scheme the feed water is pressurized, preheated and further heated in the separator till the SC conditions are reached.
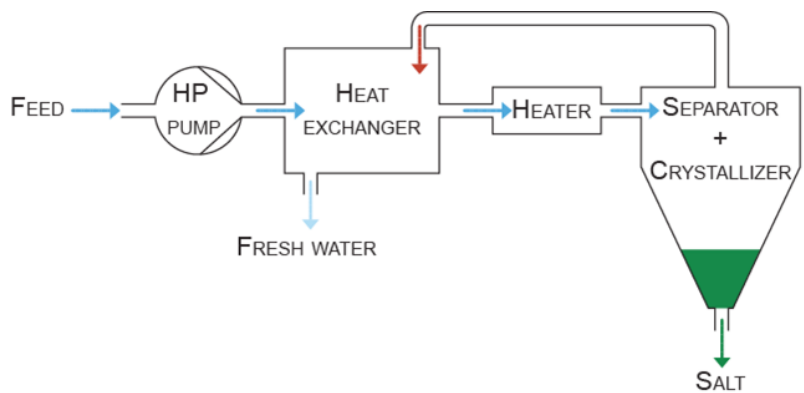
Figure A 7. Schematic representation of the supercritical desalination process.

At the SC conditions the stream is separated in a supercritical vapor phase and a con-centrated brine phase. The supercritical phase contains about 750 ppm salt, while the

brine has a concentration of approximately 50 wt.% NaCl [89]. The brine stream is fed into a crystallizer, where the pressure is lowered to atmospheric conditions, as a result the brine flashes to steam and salt. Heat from the steam can be reused and the condensate can be added to the product stream, lowering the salt content to about 720 ppm. With good heat integration and pressure reclamation the process can be used for desalination with relatively low energy consumption and zero liquid discharge. The supercritical conditions create a very corrosive environment and therefore high demands for the reactor material.

A.8 Vapor compression (VC)

VC is a distillation process that involves boiling of feed water and condensing the vapor to product water. The distillation is driven by heat from compressed vapor. Compressing a vapor increases not only the vapor pressure but also the vapor temperature. Compressing of vapor can be done by either a steam jet (thermo energy) [63] or by a mechanical compressor [62]. Mechanical vapor compression (MVC) can make use of normal vapor compression or vacuum vapor compression. The pressurized and superheated gas is led into a heat exchanger system in the boiling chamber (evaporator), where it transfers its latent heat of vaporization to the water in the boiling chamber. The steam inside the tubes cools down and condenses, just like in the MED system [62], but is still warm enough to preheat the incoming feed water stream, after which it forms the product water. The non-evaporated feed forms the concentrate, which can also be used for preheating the feed water before it is discharged. The VC process is generally used for small-scale desalination units (< 3000 m^3/day) [16].
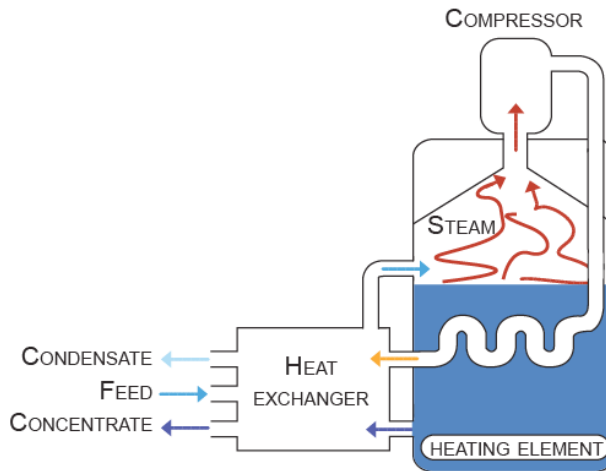
Figure A 8. Schematic representation of the vapor compression process.

A.9 Membrane distillation (MD)

MD is thermal driven membrane process [90]. A porous hydrophobic membrane only permeable for vapor molecules separates two phases with a difference in vapor pressure. On one side of the membrane there is a warm feed stream (not necessarily boiling), from which water evaporates on the other side there is a cold water stream, on which the vapor condenses. The temperature gradient over the membrane is typically 30-50 °C. Different configuration of MD are possible and are described [90]. There can be direct contact of the warm and hot water with the membrane, and as it is a hydrophobic membrane, only water vapor can pass the membrane. It can also be that there is a gap of stagnant air between the cold water and the membrane to limit heat conductance, by allowing an additional transport resistance. The cold water stream or air gap can also be replaced by a sweeping gas or on the permeate side of the membrane a vacuum can be applied. In these cases condensation is done in an external condenser. MD is a promising technology for desalination of highly saline waters [90].
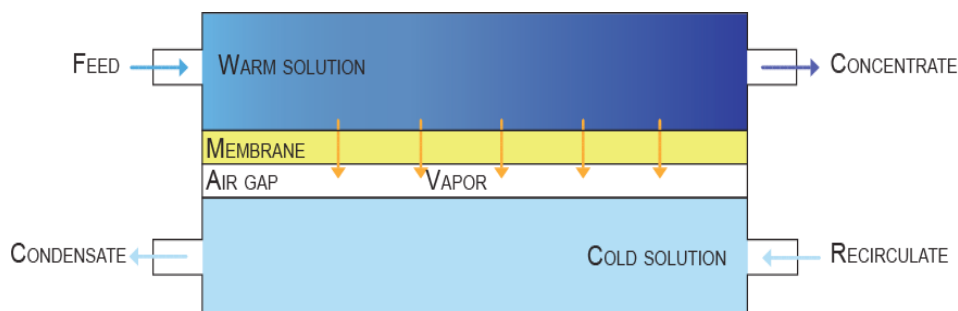
Figure A 9. Schematic representation of the membrane distillation process.

A.10 *Humidification-Dehumidification*

The humidification-dehumidification (HD) process makes use of the increasing vapor containing capacity of air at elevated temperature [91]. When saline feed water is in contact with flowing hot air, this air extracts some water vapor. To utilize this phenomenon, HD systems contain an evaporator, where water the feed water is brought in contact with a heated air stream, and a condenser (a cold surface) where the distilled water is collected after condensation. The condenser can be a heat exchanger, where feed water is preheated. Just like in other distillation processes an external heat or heating source is required to compensate for heat losses in the process. Air temperature in a HD process is typically 50-90 °C [60] and the process takes places under atmospheric pressure. Because low temperature energy can be used in this system it is very suitable to connect with e.g. solar or geothermal energy sources [60, 91]. Different system designs are developed on the HD principle [60]. HD is found mainly applicable for small

scale (few m³/d) decentralized water desalination [60, 91, 92].
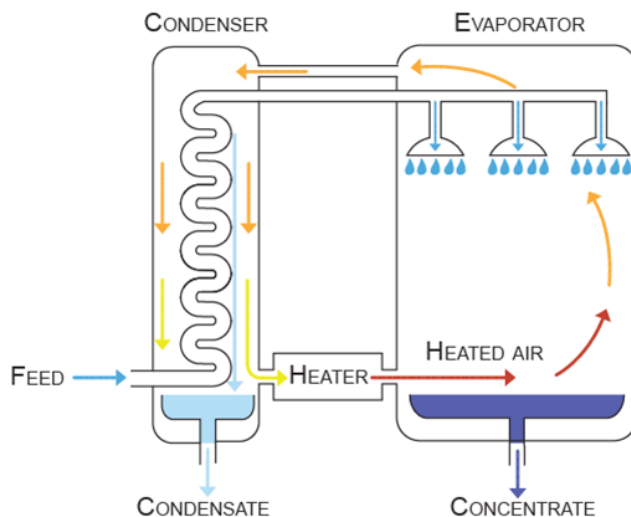
Figure A 10. Schematic representation of the humidification-dehumidification process.

A.11 *Dewvaporation*

A special case of the HD process is a process called dewvaporation [60, 91] . In the dewvaporation process the evaporator and condenser are merged in one vertical heat transfer plate. Feed water runs down on one side of the plate, where a warm air stream is present so water will evaporate from the water film. On the other side water vapor condenses from the cooled air on the vertical plate. The heat coming from the condensation process is used to warm up the feed water.

A.12 *Adsorption-Desorption*

Adsorption-desorption (AD) desalination [93, 94] is an evaporation process that uses the high affinity for vapor of very porous silica gel. AD is operated batch wise and is typically done in several reactor beds or sorption elements in which the adsorbing material is packed in tubular heat exchangers. In the first step of the process, feed water enters an evaporator that contains spray nozzles in order to promote evaporation at relative low temperatures (typically <35 ˚C [94]). Heat in this evaporator comes from an external source, but is also recovered from the system itself by a heat exchanger. The evaporator is connected with the adsorption beds, in which the vapor is adsorbed on to the silica gel at low pressure and temperature. After certain time heat is added to the system (typically <85 ˚C [94]) and the adsorbed vapor is released from the vapor saturated gel. This vapor is transported to a condenser where it condenses on the tube surface and the heat is reclaimed. The condensate is collected from the condenser. The

brine is discharged from the evaporator. The AD process is under research in pilot scale and the first installations are planned to build for practical application. Benefit over applied thermal technologies is that the energy consumption of the system is rather low as the distillation takes place at relative low temperatures. Although energy consumption is higher than with state -of-the-art membrane technologies it is a promising technique for situations where waste heat is present. Also is the technology suitable for coupling with solar or geothermal heating.
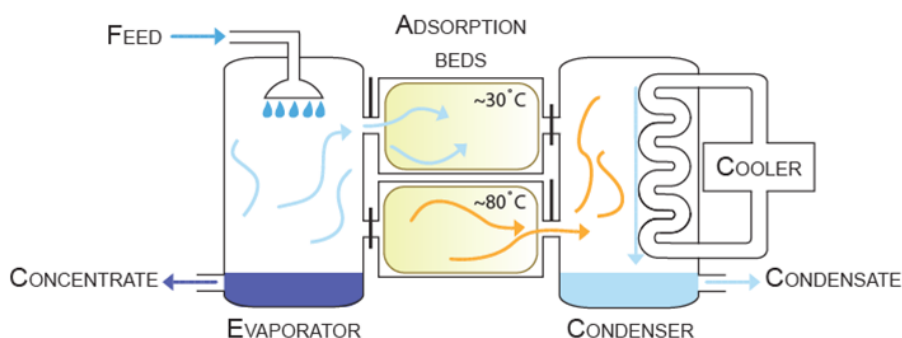
Figure A 11. Schematic representation of the adsorption-desorption process.

A.13 *Freeze-thaw*

When water freezes a crystalline ice structure that excludes impurities, like salt ions, is formed. A thermodynamic benefit of freeze-thaw desalination over distillation technologies is that the phase shift from liquid to solid (334 kJ/kg -6.01 kJ/mol) requires less energy than the phase shift from liquid to gas (2326 kJ/kg – 10.65 kJ/mol). However, this also means that the latent heat of freezing is lower than the latent heat of evaporation. Compared to the multiple stage evaporation processes, the recovery of latent heat in the often single stage freezing process is usually less efficient. Beneficial of the freeze-thaw process is that corrosion, scaling and precipitation issues are minimized at low water temperature. The process of freeze-thaw desalination is usually not a single-step separation but contains several steps of cooling the feed water, partial crystallization and separation, rinsing the ice to remove adhering concentrate and melting the ice to produce fresh water [16]. Different freeze technologies have been developed in the past 50-60 years. With vacuum freezing desalination (VFD) pre-cooled water is spray into a vacuum chamber, where part of the solution flashes into the vapor phase. This phase change cools down the liquid, which is than partially crystalized. In the secondary refrigerant freeze (SFR) method this flashing is done with a refrigerant (e.g. propane or butane), which can be reused. A third process is known as the eutectic freeze crystallisation (EFC) technology [95, 96]. Eutectic freezing takes place at the eutectic temperature, at which simultaneously ice crystals and solidified solutes are

formed. 'Location' of the eutectic freezing point in water depends on concentration and ion types present. Application of freeze-thaw technology can be in various fields [97], in desalination the technology is regarded as a good way to treat concentrates from other desalination technologies (zero liquid discharge) rather than a stand-alone desalination technology [70, 95-97].
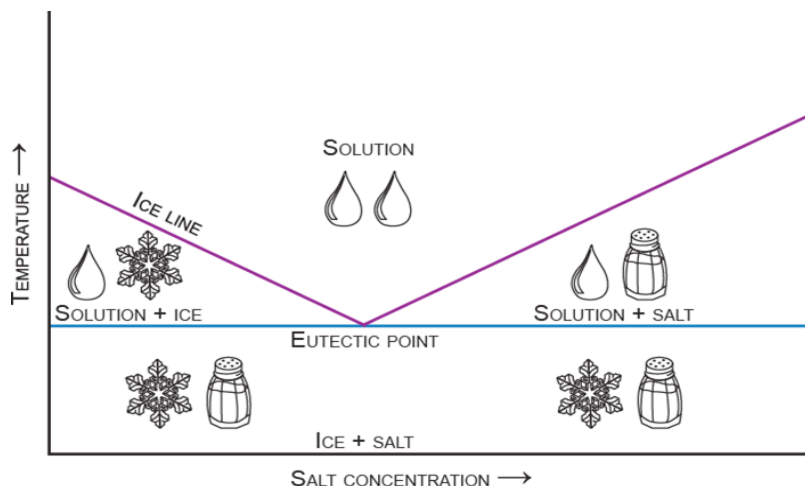
Figure A 12. Schematic representation of the eutectic point.

A.14 *Hydrates formation*

In the desalination process with hydrates formation, saline feed water is mixed with small hydrate (clathrate) forming hydrocarbon molecules [98, 99]. Solid hydrates form due to water molecules that form a cage-like structure around the hydrocarbon molecules [60, 98]. Within the icy hydrates no salts are present. Ambient reactor pressure and temperature and the type of hydrocarbon (refrigerator) are important for the formation of hydrate crystals [98]. A typical scheme for the hydration process includes cooling of the feed water, mixing with the hydrocarbon (e.g. propane [98]), separation and washing of the crystals and decomposition of the crystals. Decomposing is done by pressurizing the hydrates which leads to formation of hydrocarbon gas and fresh product water. Heat energy released during crystal formation can be used in the decomposition step to increase the process efficiency. Gas hydrate technologies are in use for the removal of water hardness [60], for desalination purposes this technology of hydrates formation is still under development. In order to drop the desalination costs by this technology, and to make it at least compatible with current mainstream desalination technologies, it is crucial to find an effective hydrate formation promoter [98].
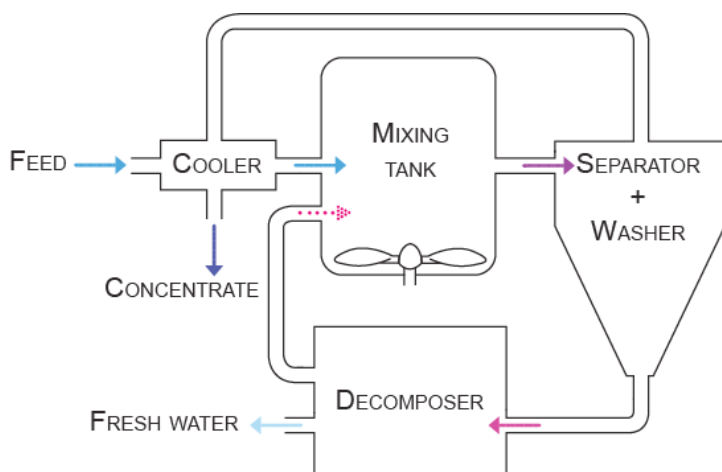
Figure A 13. Schematic representation of the hydrates formation process.

A.15 Nanofiltration (NF)

NF is based on the same principle as RO, however NF membranes have somewhat larger pore size (if it is appropriate to speak of pores) or at least have a higher molecular weight cut off compared to RO membranes [10]. RO membranes are assumed to have a pore size in the range of 0.1-1 nm and NF membranes in the range of 1-10 nm [10, 46]. These differences in pore size affect the performance of a membrane system. NF membranes typically have larger water and ion fluxes compared to RO membranes, which allows NF to operate under lower applied pressure. The applied pressure in a NF system is typically between 5 and 25 bar [100-102]. RO membranes show extreme high rejection towards all salt ions and a close to 100% rejection can be achieved. NF membranes however do not possess such large rejection qualities. Typical rejection values for multivalent ions are 60-95%, while typical rejection values for monovalent ions are between 30-70% [100-102]. NF is mainly applied in freshwater treatment for drinking water and in wastewater treatment [102]. As a stand-alone technology NF is not suitable for desalination, but as a pretreatment for e.g. RO the technology it can be applied. With NF membranes besides some salts also microorganisms and turbidity are removed, what leads to a better treatable stream for the RO process [102]. Just as with RO, fouling of the membranes remains an issue.

A.16 *Forward osmosis* (FO)

Osmosis is defined as the net movement of water across a semi-permeable membrane which is driven by the osmotic pressure difference across the membrane. If the osmosis process is used for e.g. desalination, it is often referred to as forward osmosis (FO) to stress that it is the opposite process as the much wider known RO technology. The

term direct osmosis is also used [103]. Just as with RO the FO membranes allow passage of water but reject ions and solutes. The principle of the FO is that a draw solution of higher concentration than the feed solution (preferable $c_{draw} >> c_{feed}$) is present and that a semi-permeable membrane separates the two streams. This concentration difference results in an osmotic pressure difference across the membrane and when there is no pressure or temperature difference across the membrane this leads to water transport from the feed solution towards the draw solution. Effectively the feed solution is concentrated and the draw solution is diluted. At some point the osmotic pressure is equal at both sides of the membrane and no further water transport takes place. Fresh water is not directly produced, but the initial product is a mixture of the draw solution and the fresh water. Key in this process is that a high osmotic pressure is generated by the solutes in the draw solution and that these solutes can easily be separated from the fresh water. The draw solution can contain e.g. a volatile solute [104]. Recent research shows a promising desalination process with a draw solution containing ammonia (NH_3) and carbon dioxide (CO_2) [105, 106].

Another way to use FO in desalination is to use an impaired fresh water stream and e.g. a seawater stream as feed water. Water from the impaired fresh water is transported through the FO membrane to the seawater. As such dilution of the seawater takes place. In such application of FO no draw solution and recovery step are required.
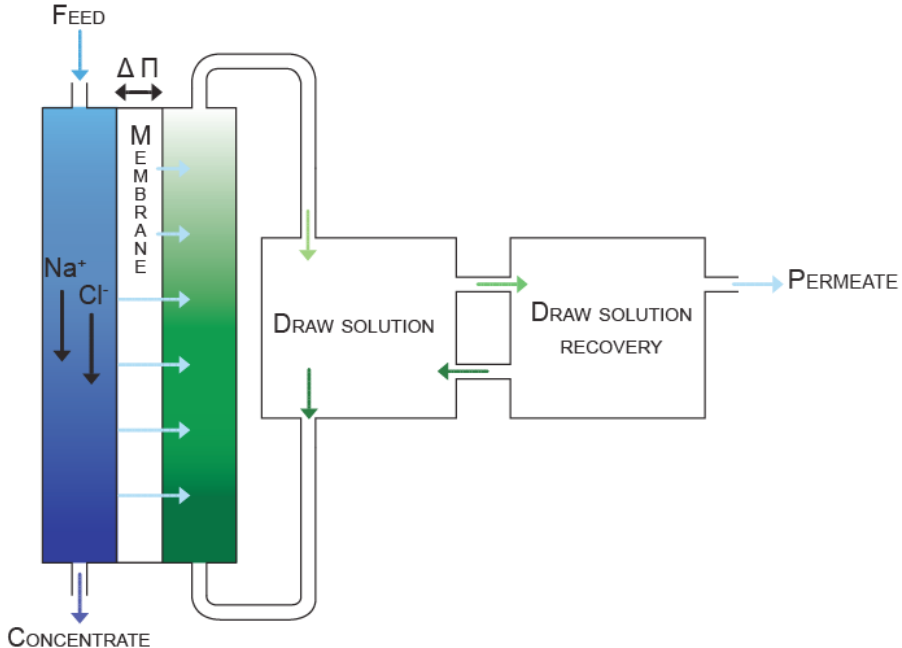
Figure A 14. Schematic representation of the forward osmosis process.

A.17 Ion exchange resins

Ion exchange resins are polymer beads that have a charged molecules linked to the polymer backbone. This charged molecule can be for instance a sulfonic acid group (cation exchanger) or a quaternary ammonium group (anion exchanger). Ions of opposite charge (counterions) than the fixed charge are present in the ion exchange resin. When put in a saline solution these counterions (e.g. H^+ or OH^-) are exchanged for salt ions, this exchange is driven by the difference in chemical potential of the resins internal solution and the outer solution. A drawback of using ion exchange resins is that you need to regenerate the resins in a highly concentrated solution. Moreover, as the capacity is limited, ion exchange is more suitable for low concentrated solutions. Ion exchange is not used for seawater desalination. As known from literature divalent ions have a higher affinity to the ion exchange resin than the monovalent ions [107-111]. This makes ion exchange resins suitable for e.g. water softening or water purification where harmful components are exchanged with harmless ions [112, 113]. For desalination purposes it could be interesting to use ion exchange resins to remove e.g. boron from RO permeate [114].
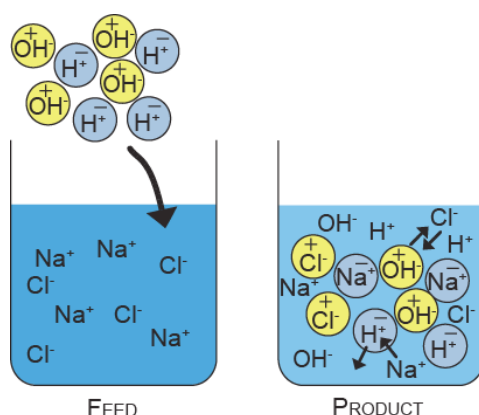
Figure A 15. Schematic representation of the ion exchange process.

A.18 Desalination by extraction

Desalination by extraction is a process in which a solvent is added to the water phase. There are two ways in which desalination can take place, either the water phase is extracted from the saline water mixture [115, 116], or the ions are extracted from the saline water [117-119]. Both processes include an extraction step and a separation step where water or ions are separated from the solvent. Extraction of water can be done with certain oils and medium chain fatty acids, which have the ability to dissolve water while rejecting the solutes (like ions) in water. It is important that the solvent does not

dissolve in water, but only water in the solvent, this is what happens with a so called directional solvent. The water solubility can be increased at higher temperature [115, 116]. Recent research shows that the process works at water temperature as low as 40-50 ˚C, but the efficiency is increased at higher water temperature [116]. When the two phases (concentrate and solvent-water) are separated, the solvent water phase is cooled and water precipitates from the solvent. For the process of salt or metal ion extraction so called ionic liquids can be used [117-119]. Ionic liquids are salts that are in pure form liquid at room temperature. Ionic liquids are composed out of large ions, which are held together by their electrostatic interactions. By changing the structure of the ionic liquid it can be made task specific. Separation and regeneration of the ionic liquid phase is important as ionic liquid may be toxic [119]. Because no or a relatively low amount of energy is involved in heating (no thermal phase shift required), these technologies are promising when further developed. Both technologies are under research and are currently not applied in the field of desalination.

Chapter 2

Seawater predesalination with electrodialysis

Abstract

The suitability of electrodialysis (ED) for seawater desalination was investigated and the energy losses that play a role in ED were quantified. The combination of ED and brackish water reverse osmosis (BWRO) is presented as an alternative desalination strategy for seawater reverse osmosis (SWRO). Experiments have been performed with a recycling batch electrodialyzer. From this we conclude that in most cases the membrane stack is responsible for the main energy loss in the system. Energy losses due to water transport are generally low. At low applied current density, osmotic water transport is relatively large and as such the energy loss, while electro-osmosis was found to be directly proportional to the applied current density. The relative energy loss caused by back diffusion was found to be of minor importance for higher current densities and was only more pronounced at the lowest applied current density of 10 A/m^2. Combining ED with BWRO in a hybrid system does not lead to a reduction in energy consumption compared to ED as standalone technique, when the applied current density becomes lower than 50 A/m^2. At low applied current density (10 A/m^2) ED can perform desalination energetically cheaper at lower operational costs than SWRO.

Nomenclature

A	=	membrane area (m^2)
a	=	activity of an ion (-)
c	=	concentration (mol/m^3)
D_w	=	osmotic water transfer coefficient (m^2/s)
ϕ_0	=	reversible voltage (V)
ϕ_{OCV}	=	open circuit voltage (V)
ϕ_{stack}	=	membrane stack voltage (V)
F	=	Faraday constant (C/mol)
I	=	current (A)
j	=	current density (A/m^2)
m	=	osmotic water transport (mol)
N	=	number of cell pairs (-)
n	=	amount of ions (mol)
Q	=	electric charge (C)
R	=	gas constant (J/mol·K)
R	=	resistance (Ω)
r	=	water recovery factor (-)
T	=	temperature (K)
t	=	time (s)
t_w	=	water transport number (mol H_2O/F)
V	=	volume (m^3)
W	=	volumetric energy (kWh/m^3 diluate)
α	=	membrane permselectivity (-)
α	=	concentration ratio of feed and outlet diluate (-)
β	=	concentration ratio of feed and outlet concentrate (-)
δ	=	membrane thickness (m)
η	=	Coulombic efficiency (-)

2.1 Introduction

2.1.1 Hybrid seawater desalination with ED as first step

Of all water on earth 2.5-3.5 % is fresh water, and only 0.3-0.8% of this fraction is available to us as liquid fresh surface water [1-3]. Due to uneven distribution of the freshwater sources and a growing world population freshwater sources have become scarce; 1.2 billion people live in areas of physical water scarcity and another 500 million people are approaching this situation [4]. Desalination techniques can supply fresh water, wherever salt or brackish water sources are available. By converting only a small fraction of the salty water sources into fresh water, already a significant contribution to solving the problem of water scarcity could be achieved [2].

Seawater desalination is often considered as too energy-consumptive and too expensive [5, 6]. In 2011, Post *et al.* [5] wrote a paper about desalination costs of seawater reverse osmosis (SWRO) and several alternative hybrid desalination strategies. The combination of electrodialysis (ED) and brackish water reverse osmosis (BWRO) is presented as an alternative desalination strategy that could lead to a desalination cost reduction of about 0.15 €/m³ diluate produced, compared to seawater reverse osmosis (SWRO). A benefit of ED is the possibility of adjusting the salt concentration of the water produced. Therefore ED can be used as a predesalination technique, reducing the salt concentration to a desired level. The limitations for ED and BWRO are respectively low conductivity at lower salt concentration for ED and high osmotic pressure at higher salt concentrations for BWRO. When ED-BWRO is used and after a certain degree of salt removal the internal resistance of the ED stack becomes high, brackish water reverse osmosis (BWRO) can continue the desalination process at relatively low pressure [5].

ED has some other benefits over SWRO in seawater treatment. Compared to SWRO, ED requires only little pretreatment efforts [7] and relatively high water recoveries can be reached. Water recovery of an ED (reversal) system is not limited by pressure but depends mainly on the scaling potential of the concentrate [8, 9]. Electrodialysis was successfully used at supersaturated solutions with divalent ions [10] which suggests that high water recoveries should be possible at desalination with seawater. For seawater desalination with ED water recoveries were reported from 50 to 60% [11, 12], and it is expected that with ED reversal higher water recoveries can be obtained [9]. Another benefit is that ED does not need an energy conversion step (e.g. electrical to mechanical energy in the high pressure pumps), but electrical energy can be directly utilized, which makes ED also suitable to combine with renewable energy sources [13], even when the available energy input changes [14].

The proposed use of ED in a seawater desalination scheme is remarkable as it is generally accepted that ED is primarily suitable to desalinate brackish water, whereas SWRO is favourable over ED for seawater desalination [5, 7, 15-17].

2.1.2 Why ED is considered to be a brackish water treatment technique and unsuitable for seawater desalination

In ED, an electrical field is applied to migrate ions through feed water and ion-exchange membranes. Increasing the conductance of the feed water reduces the internal resistance against ion migration and therefore the energy consumption. This would make ED particularly energetically suitable for application on feed water with high salinity, like seawater [11, 12, 18] and RO concentrates [19]. In the literature it is mentioned that ED is less suitable to treat feed water with less than 400 mg/l dissolved solids, because of high energy requirements [14], suggesting high salinity application to be more favourable.

Below we present possible major reasons causing ED to be less suitable for seawater desalination. When applying ED to feed waters with increasing water salinity:

1. **the amount of ions to be transported increases.** In ED the amount of desalination energy is proportional to the ions removed [14, 16, 17], which indicates that ED is less suitable for desalination of high saline feed water. This contrasts with RO, in which the amount of water molecules to be transported for desalination is independent of the salinity of the feed water.
2. **the amount of water molecules that are co transported increases.** With the transport of ions also water will be transported and this influences the efficiency of the separation process. The efficiency losses due to water transport will increase to considerable levels at higher salinity of the feed water.
3. **the coulombic efficiency decreases.** According to [6] the reached separation at high salinity is rather low, which is due to low membrane selectivity at high external salt concentration and limited ion exchange capacity of the membranes which enhances concentration polarization phenomena. As a result, the ratio between electrical current and ionic current (the so-called coulombic efficiency) is low at high salinity.

The relative contribution of these three factors in reducing ED efficiency has not been quantified yet and was therefore the focus of the research reported here.

2.1.3 Objectives

With these three considerations in mind, we investigated the ED process with an experimental set-up as a seawater pre-desalination step. The ED process was analysed in terms of (i) ion transport, (ii) water transport, and (iii) back diffusion (and associated coulombic efficiency loss). This investigation was used to elucidate the contribution of the different processes in ED with respect to energy losses and how these are related to the applied current density. Another goal is to clarify the concentration range of the desalinated water where ED should be succeeded by BWRO when a hybrid ED-BWRO system [5] is used.

2.2 Materials and Methods

2.2.1 Materials

The ED stack comprised ten repeating cells, each consisting of a cation exchange membrane (Neosepta CMS; Tokuyama Co., Japan) and an anion exchange membrane (Neosepta ACS; Tokuyama Co., Japan). These membranes are separated by silicone gaskets that form flow channels for alternating the concentrate and diluate. At the beginning of the stack one extra CEM membrane was placed in order to close the first cell (see Figure 1). The area of each membrane was 104 cm^2. A squared electrode was placed on both sides of the membrane stack. As anode a titanium electrode (mesh 1.7, area 96.04 cm^2) with a mixed metal oxides coating (Magneto Special Anodes BV, The Netherlands) was used, and as cathode a titanium electrode (mesh 1.7, area 96.04 cm^2) with a 50 g/m^2 platinum coating was used (Magneto Special Anodes BV, The Netherlands). The diluate and concentrate compartments between the membranes contained a woven PET fabric spacer (Nitex 06-700/53, Sefar, Switzerland). Typical thickness of the flow channel in this research was 500 μm, further characteristics of the spacer are given in [20].

2.2.2 Methods

In this research electrodialysis experiments were performed in a recycled batch mode. The initial concentration of both the diluate and concentrate was 0.5 M NaCl (29.22 g/l). This is also referred to as the feed water for the ED stack. The flow rates were equal in the concentrate and diluate channels and were set to 15.0 ml/min per channel. A 0.5 M NaCl solution was used as electrode rinse fluid (electrolyte). The electrode rinse fluid was not recirculated and the outflow of both electrodes was collected, degasified and disposed. The concentrate and diluate were recirculated over two 1 l bottles during the experiment. Both the concentrate and diluate had a volume of 0.890 l (stack, tubing, and bottle) at the start of the experiment. The water in the two bottles

was continuously stirred with a magnetic stirrer and weighed with a balance (PL 3001-S ±0.1 g, Mettler Toledo). The actual value of the balances was logged every second on a laptop using LabVIEW (Version 11.0, National Instruments).
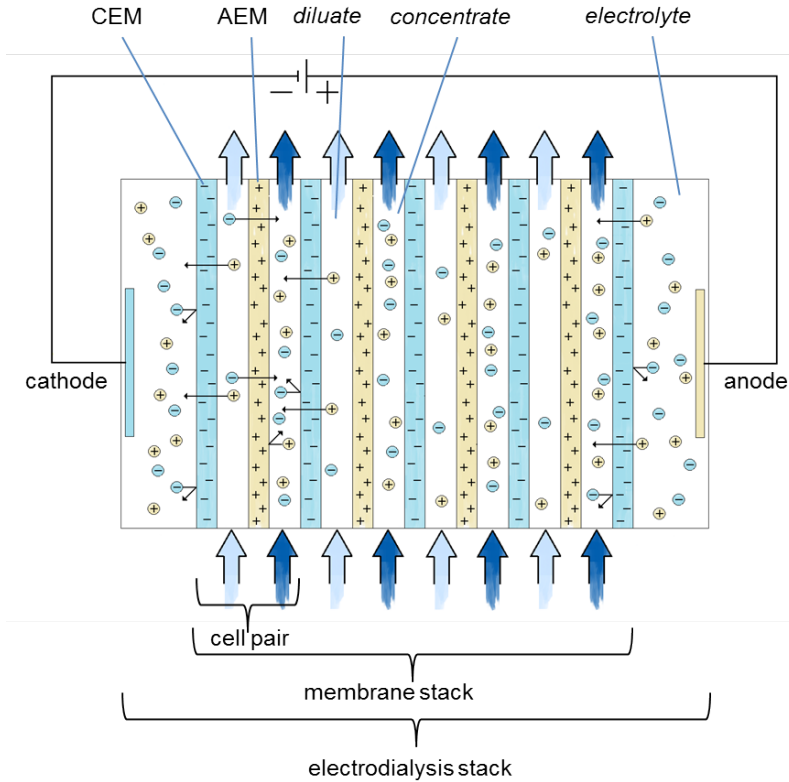
Figure 1. Schematic overview of an electrodialysis stack, where AEM represent the anion exchange membranes and CEM the cation exchange membranes. Cations are depicted with an encircled positive sign and anions by an encircled negative sign.

Conductivity of the diluate and concentrate was measured in line with two conductivity probes (QC205 XC, QIS) directly before the ED stack. These probes were connected through a transmitter box (P862, QIS) with a data logger (Memograph M RSG40, Endress+Hauser). For measurements of the membrane stack voltage, Ag/AgCl reference electrodes (QM711X, QIS) were used. These were located at the inlet of both electrode compartments. As described in [21] the losses associated with electrode reactions are left out of consideration. The potential difference of the two reference electrodes was measured with a high impedance preamplifier (-10/+10 V, Extins technologies). As an additional control the voltage of the anode (anode potential) and cathode (cathode potential) were measured with respect to the reference electrodes with a potentiometer (PPM-3C, Bank Electronic) as was also the ED stack potential, by measuring the

potential over the anode and cathode. The absolute difference in potential of the ED stack with anode and cathode potential resulted also in the membrane stack potential. To apply a constant current to the stack a power supply was used (SM70-AR-24, Delta Elektronika). Actual values of potential, conductivity and current were logged every second.

The electrodialysis desalination experiments were performed under constant current regime. Applied current density, *j* was varied and was set at respectively 10, 50, 100, 200 and 300 A/m². The temperature throughout the experiments was measured as 20±2 °C. All presented experiments were repeatable and performed at least two times. Water transport was measured during the ED process with current density in the range of 50-300 A/m². By constantly measuring the mass of the recirculation bottles, the gain or loss in weight could be determined. Water transport under applied current conditions can be due to; 1) osmotic water transport, 2) electro-osmotic water transport and 3) water losses (see section 2.3.2). Throughout experiments there were no water losses measured. So during the ED experiments the weight change of the batches was caused by osmosis and electro-osmosis. By periodically switching off the current (and as such switching off electro-osmotic flow), the osmotic flow could be determined. At certain points in the desalination process, the current is switched off for about 300 s, of which the first 120 s was used to flush the stack to remove the vertical concentration gradient between the inflow and outflow of the flow channels. The remaining time is used for measuring the osmotic water transport. This periodic switching off of the current was done after every decrease of 5 mS/cm in conductivity of the diluate channel.

2.3 Results and Discussion

2.3.1 Ion transport

Reversible ion transport and energy consumption

To transport ions from the diluate to the concentrate in an electrolytic cell, energy input is required [22]. Without loss, the required energy is equal to the Gibbs free energy of mixing (reversible energy). This reversible energy is independent of the technique but depends on the salt concentration and the extent of desalination [5, 22]. This is also the energy for the electrodialysis process to take place when there is no resistance and no flux of coion transport or water transport. The reversible energy can be calculated via several equations [5, 22, 23]. Based on [23] the reversible volumetric energy, W_r (kWh/m³) is calculated via:

$$W_r = 2RT(c_f - c_d)\left[\frac{\ln\alpha}{1-\alpha} - \frac{\ln\beta}{1-\beta}\right]\cdot\frac{1}{3.6\cdot10^6} \qquad \text{eq. 1}$$

$$\alpha = \frac{c_f}{c_d}$$ eq. 2

$$\beta = \frac{c_f}{c_c}$$ eq. 3

Where R is the gas constant (J/mol·K), T is the absolute temperature (K) and c is the salt concentration (mol/m³). Subscripts f, d, and c refer to feed, diluate and concentrate, respectively. The water efficiency of the desalination technique is expressed by the water recovery factor, r:

$$r = \frac{V_d}{V_d + V_c} = \frac{V_d}{V_f}$$ eq. 4

Where V_d is the volume of the produced diluate (product water) and V_f is the volume of the initial feed water (diluate + concentrate). In Figure 2 the energy requirement per m³ of diluate water is shown as a function of water recovery and final concentration of the diluate.

From a thermodynamic point of view, higher water recovery seems to be only attractive at higher salt concentrations of the diluate, where the volumetric energy consumption is relatively lower. As shown in Figure 2 the required reversible energy to desalinate 500 mM seawater to 0.01 mM freshwater at a water recovery of 50% ($r = 0.5$) is about 0.95 kWh/m³. In comparison, state-of-the-art SWRO installations have a water recovery around 35-45% [3] and have an average energy consumption around 3.4 kWh/m³ [24]. Figure 2 shows that, at 40% recovery, the minimum required amount of desalination energy is 0.88 kWh/m³. This implies that about 75% of the energy use in nowadays SWRO plants is due to irreversible losses. Glancing at Figure 2, one might conclude that it is more beneficial to have low water recovery. However, the concentrated fraction already consumed some energy due to pretreatment and at low water recovery more water intake, pretreatment, storage capacity, pumping and concentrate discharge is required per quantity unit of product water. These factors will cause a shift of the optimal water recovery towards higher values.
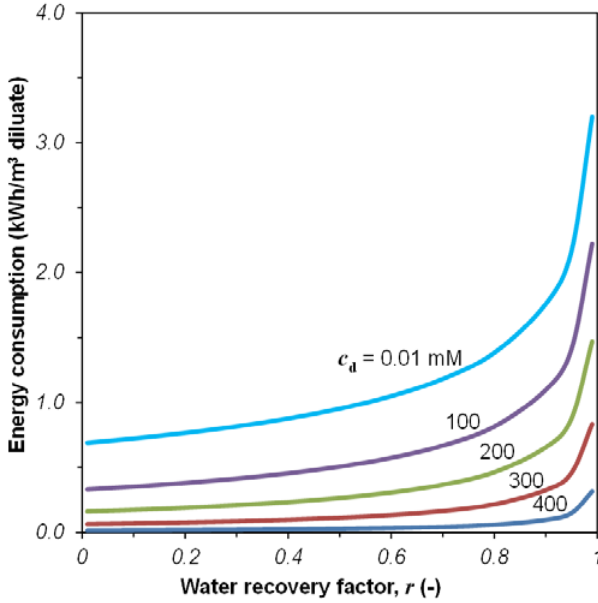
Figure 2. Reversible desalination energy requirement, Wr (kWh/m3) as a function of the water re-covery factor, r (-) and final diluate concentration (mM); Seawater was assumed to consist of a 0.50 M NaCl solution at 293 K.

Membrane stack potential difference as measure for energy consumption

The reversible desalination energy of an ED system can be calculated from the reversible potential difference, ϕ_0 (V). The reversible potential difference (or voltage) could theoretically be measured under open circuit conditions, when 100% permselective membranes are used (i.e., the coulombic efficiency is then 100%). This open circuit voltage, ϕ_{OCV}, can be derived from the adapted Nernst-equation for monovalent ions [25, 26]:

$$\phi_{OCV} = \alpha \cdot \phi_0 = \alpha \cdot 2N \cdot \frac{RT}{F} \ln\left(\frac{a_c}{a_d}\right) \qquad \text{eq. 5}$$

Where α is the membrane permselectivity (-), ϕ_0 is the reversible membrane voltage, N is the number of cell pairs in the stack (-), R is the gas constant (J/mol·K), T is the temperature (K), F is the Faraday constant (C/eq) and a is the ionic activity (-). The ϕ_{OCV} shows the maximum voltage that could possibly be recovered from the diluate and concentrate stream, with e.g. a reverse electrodialysis (RED) process [26]. In Figure 3, we calculated the ϕ_{OCV} with $\alpha = 0.93$. This value was determined in previous work using the same membrane couple (ACS/CMS) [26]. The permselectivity will be discussed in more detail in section 2.3.3.

Lower energy consumption at lower current density?

During the experiments a constant current I (A) was applied. In Figure 3, the measured membrane stack voltages at different current densities, j (A/m^2) are shown as a function of diluate conductivity (mS/cm). From Ohm's law it follows that the membrane stack voltage, ϕ_{stack} (V) increases with current and resistance:

$$\phi_{stack} = \phi_{OCV} + I \cdot R \qquad \text{eq. 6}$$

Where R (Ω) is the resistance of the membrane stack. At a low applied current density of 10 A/m^2, the volumetric desalination energy is relatively close to the minimum obtainable energy consumption with the applied membranes (i.e., close to open-circuit conditions). However, this cannot directly be concluded only from the membrane stack voltage as for calculating the volumetric desalination energy, $W_{desalination}$ (kWh/m^3), also the obtained water recovery should be considered:

$$W_{desalination} = \frac{I \cdot \int \phi_{stack} dt}{3.6 \cdot 10^6 \cdot V_d} \qquad \text{eq. 7}$$

Where t is the time period (s), and V_d is the measured diluate volume (m^3), or obtained water recovery (since $V_d = r\ V_f$). The obtained water recovery depends on the water transport through the membranes, which is discussed in section 2.3.2. Equation 7 will give a good approximation of the energetic costs, but note that e.g. electrode losses and pumping energy are neglected in this formula.
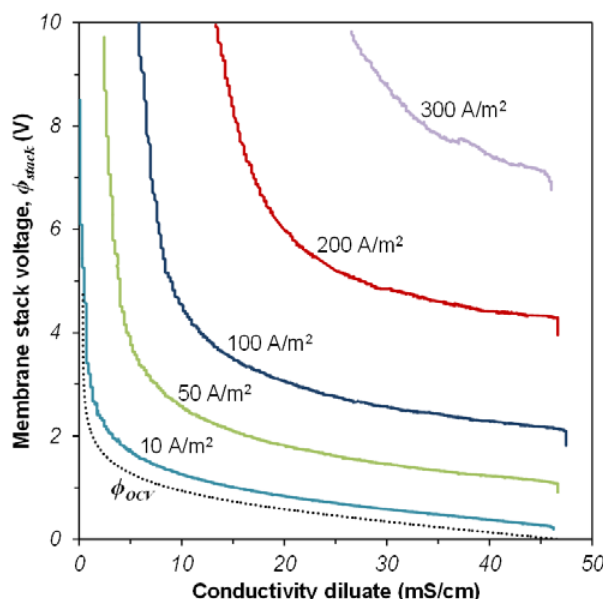
Figure 3. Measured stack voltage over a ten cell-pair ACS/CMS stack at different current densities (10/50/100/200/300 A/m²) and the calculated open circuit voltage as a function of the diluate conductivity. Feed water consisted of a 0.50 M NaCl solution at 293 K.

2.3.2 Water transport

Osmotic and electro-osmotic water transport in ED

ED is known as a technique used to transport ionic bodies through an ion exchange membrane. However, with the transport of ions water will also be transported and consequently influence the efficiency of the separation process [22, 23]. Water transport can occur either as free (osmosis) or as bound water (electro-osmosis). Free water transport will take place especially at larger osmotic pressure differences [22] caused by the difference in concentration of the diluate and concentrate channels (see equation 8) [27]. Transport of water bound to ions, in ED known as electro-osmosis [22, 28], will take place whenever ions are passing through the membrane and has a minimum corresponding to the water in the primary hydration sphere of the ions [23, 29, 30].

Water transport has been studied in the nineteen-fifties by Schmid, Spiegler and Oda and Yawataya [31-35]. The latter two studied electro-osmotic effects in the practical NaCl concentration range (0.05-4 M). In ED desalination processes electro-osmosis can lead to significant water transport through the ion exchange membranes [22, 23]. The unavoidable water transport over the membrane by osmosis and electro-osmosis even limit the usefulness of ED as a method of concentrating electrolyte solutions [23, 29, 33]. This is the case when the migration of ions from diluate to concentrate

does not longer lead to a decrease of concentration, because water is transported proportionally through the membrane. The amount of water that is transported varies for different membranes, but is influenced primarily by the membrane water content and the external salt concentration and secondarily by temperature, degree of crosslinking and the fixed charge density [23, 29, 33-37].

Water transport as indirectly measured from obtained conductivity
During this research the effect of water transport in the ED was observed by measuring the outlet conductivity of the diluate and the concentrate in a recirculating cell. These conductivities are shown in Figure 4. In this figure the measured conductivity of the diluate is placed on the x-axis and the corresponding concentrate conductivity on the y-axis. The dashed 'Ideal' line shows the graph of concentrate conductivity when there is no water transport through the membranes at a water recovery, r of 0.5 (when initial condition: $V_d = V_c$). Due to non-linearity of the relation between concentration and conductivity this is not a perfect straight line. In Figure 4 it is shown that at a low applied current density of 10 A/m², the concentrate conductivity is noticeably lower than at higher applied current density. The same but to less extent is observed for 50 A/m². The reduced concentrate conductivity is caused by enhanced water transport of either osmotic or electro-osmotic origin.
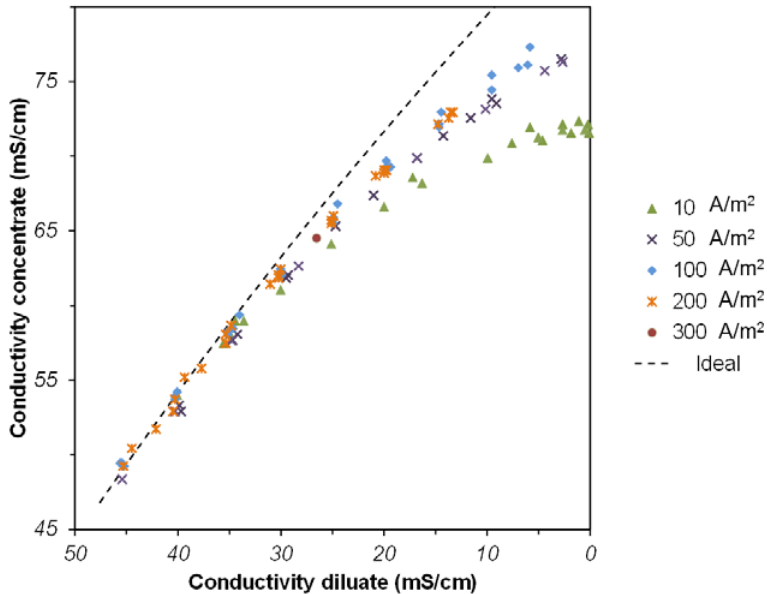
Figure 4. Measured conductivity of the concentrate as a function of the conductivity of the diluate at different current densities. The ideal line is calculated on basis of a stack without water transport and r = 0.5.

Measured osmotic water transport

Osmotic water transport is related to the osmotic pressure difference caused by the ionic concentration difference over the membrane. The amount of water transported by osmosis, Δm (mol) can be calculated by the following equation [27]:

$$\Delta m = D_w \cdot \frac{A(c_c - c_d)}{\delta} t$$

eq. 8

Where D_w is the osmotic water transfer coefficient (m²/s), A is the membrane area (m²), c is the concentration of respectively concentrate and diluate (mol/m³), δ is the membrane thickness (m) and t is the time (s). The measured osmotic water transport is shown in Figure 5.
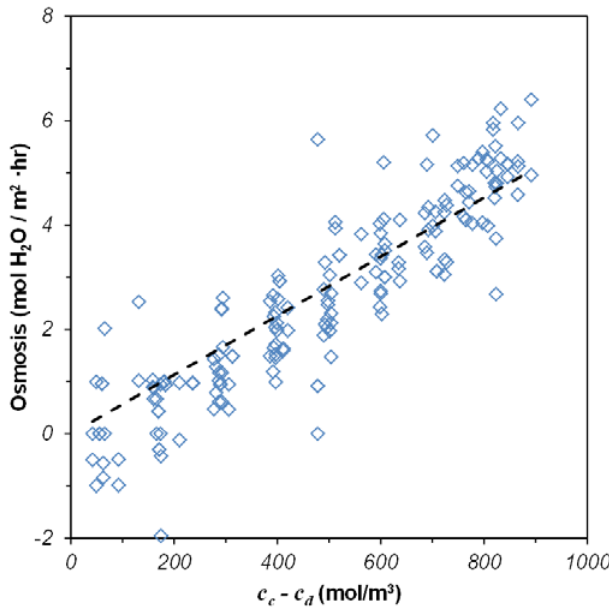
Figure 5. Osmotic water transport in (mol H$_2$O/m²·h) measured at different NaCl concentration (mol/m³) differences of the concentrate (c$_c$) and diluate (c$_d$) channel. Dotted line based on the linear equation 8.

From the measured data the osmotic water transfer coefficient (D_w) for the ACS/CMS membrane pair was estimated by using equation 8 and the plotted regression line in Figure 5. The regression coefficient ($5.66 \cdot 10^{-3}$, standard error 2%) of this line is equal to D_w over δ in equation 8. Membrane thickness δ is taken as the average membrane thickness of the ACS/CMS membranes ($130 \cdot 10^{-6}$ m) which results in $D_w = 2.04 \cdot 10^{-10}$ m²/s. This is about one order of magnitude lower than the diffusion coefficient of water

in pure solution.

Measured electro-osmotic transport

Electro-osmotic water transport is expressed in moles H_2O/F and as such directly related to the number of electrons (coulombs) transported through the stack. The electro-osmotic water transport is calculated as the measured water transport in a time period minus the average osmotic transport of the beginning and end of this time period. The determined electro-osmotic flow is shown in Figure 6. During this research the electro-osmotic water transport was found to be proportional to applied current density and independent of the concentration gradient across the membrane. The average water transport number, t_w of the membrane pair was found to be 6.4 ($\pm$ 1.5) mol H_2O/F. This number is similar to other homogeneous membranes that can be found in literature as various researchers investigated electro-osmotic water transport through ion exchange membranes at external NaCl concentrations within the ED range (0.1-4 M) [29, 36, 38-44]. Water transport numbers, t_w of about 2.0 mol H_2O/F [43] up to 37.2 mol H_2O/F [36] are reported here, however in most cases water transport numbers around 4 – 6 mol H_2O/F are mentioned [29, 36, 38-44].
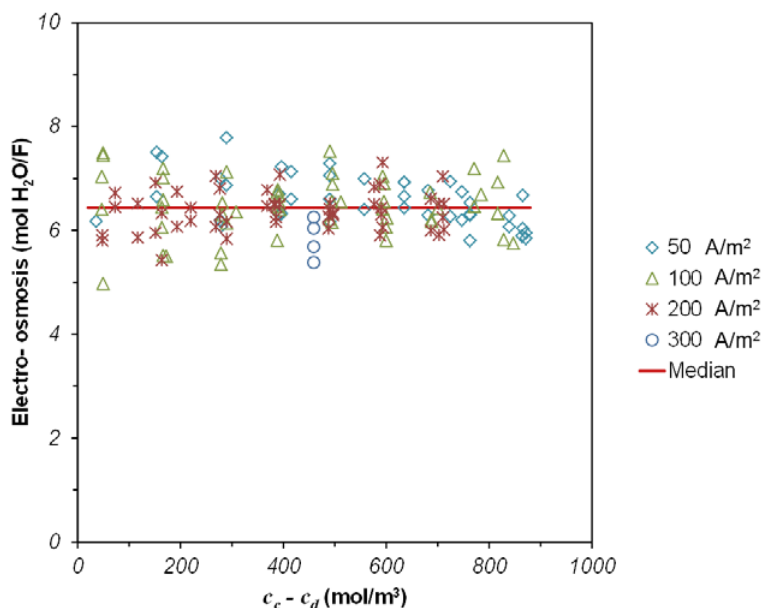
Figure 6. Electro-osmotic water transport number, tw (mol H_2O/F) determined at different NaCl concentration differences of the concentrate (c_c) and diluate (c_d) and at different applied current densities (50/100/200/300 A/m²). The median value is given by the solid line.

Higher water transport at lower current density

As the water transport may limit the possibilities of ED [23], knowing osmotic and electro-osmotic water transport numbers can provide useful input parameters for modelling ED. The limiting character of water transport for concentrating solutions was already shown for different applied current densities in Figure 4. With the measurements of osmosis and electro-osmosis this graph can be further explained. When a low current density is used, desalination of an equal amount of water takes more time than when higher current densities are applied. Osmotic water transport depends on time of operation and, as a result, will increase with reducing current density and increasing concentration gradients. This additional water transport is diluting the concentrate and results in lower conductivity levels. This diluting effect of the water transport on the concentrate conductivity is shown in Figure 4.
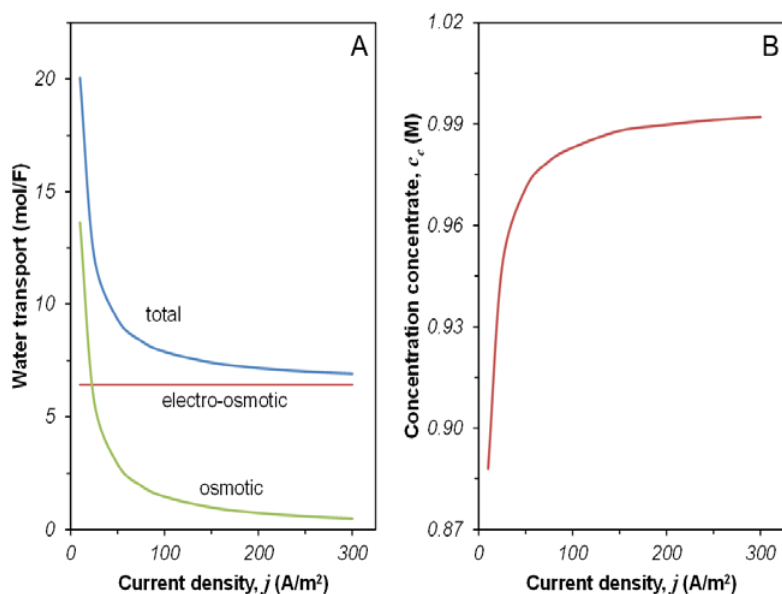
Figure 7 A. Calculated transported water (mol/F) based on in this work determined values of t_w and D_w as a function of the applied current density. B. Calculated concentrate effluent concentration as a result of the water transport shown in A, the diluate effluent concentration is 0.01 M.

The water transport through an ED stack, as used in this study, was modelled with the values that were determined for D_w and t_w. Total water transport and the (electro-) osmotic fractions are shown in Figure 7 A. The calculated concentrate concentration of the stack is given in Figure 7 B. The diluate concentration is in this model reduced from 0.500 to 0.01 M. At current densities lower than 23 A/m², osmotic water transport exceeds the transported amount of water due to electro-osmosis. From this model the

output water recovery is estimated as 49.6% at 300 A/m² and only 43.7% at 10 A/m², where a recovery of 50% would imply no water transport from the diluate to concentrate, since in these experiments the initial condition was $V_d = V_c$.

2.3.3 Back-diffusion

Coulombic efficiency as measure of back-diffusion

In ED systems not all current is used effectively, processes like 'back diffusion' of ions or coion transport can occur due to non-perfect selectivity of the membranes [17]. To measure the effective current utilization the term coulombic efficiency is used. This coulombic efficiency is calculated as the total amount of electric charge transported by ions, divided by the electric charge transported applied to the system. This is shown in equation 9 – 11, where equation 10 is only valid for systems with monovalent ions.

$$\eta = \frac{Q_{transported}}{Q_{applied}} \qquad \text{eq. 9}$$

$$Q_{transported} = \frac{\Delta n_i \cdot F}{N} \qquad \text{eq. 10}$$

$$Q_{applied} = \int I \cdot dt \qquad \text{eq. 11}$$

In these equations, η is the coulombic efficiency (-), Q the electric charge (C) and Δn_i, the moles of ions transported (mol). The experimental results are shown in Figure 8. For applied current densities between 50 and 300 A/m², η was measured between 0.85 and 1.05. However, when 10 A/m² was applied this efficiency was found to be between 0.7 and 0.95. Comparable to this Sadrzadeh and Mohammadi reported a higher coulombic efficiency of seawater desalination with electrodialysis at higher applied voltages [45].

Lower coulombic efficiency at lower current density

Assuming that the coulombic efficiency is influenced by back diffusion of ions, there are two factors playing a role: (i) the concentration gradient over the membrane and (ii) the available diffusion time. At a low current density, the back diffusion will be quite substantial compared to the migration of ions in the opposite direction, due to a long desalination period. Moreover water is transported from diluate to the concentrate, leading to a decrease in product. The coulombic efficiency seems to increase at lower diluate conductivity (especially at 10 A/m² applied). This is explained as an indirect effect of water transport. Due to water transport the diluate volume is decreasing,

shortening the desalination and back diffusion time and consequently increasing the coulombic efficiency.

Shunt (or shortcut) currents are also known to cause a reduction in coulombic efficiencies as current in those situations is running through non-active cell areas [22, 23, 45, 46]. These currents especially take place in the high conductive concentrate channels and manifold. These currents are more likely to be present at higher applied current densities, when internal resistance and membrane stack potential are higher. Therefore this type of losses cannot be used to further explain the lower measured coulombic efficiency at an applied current of 10 A/m².
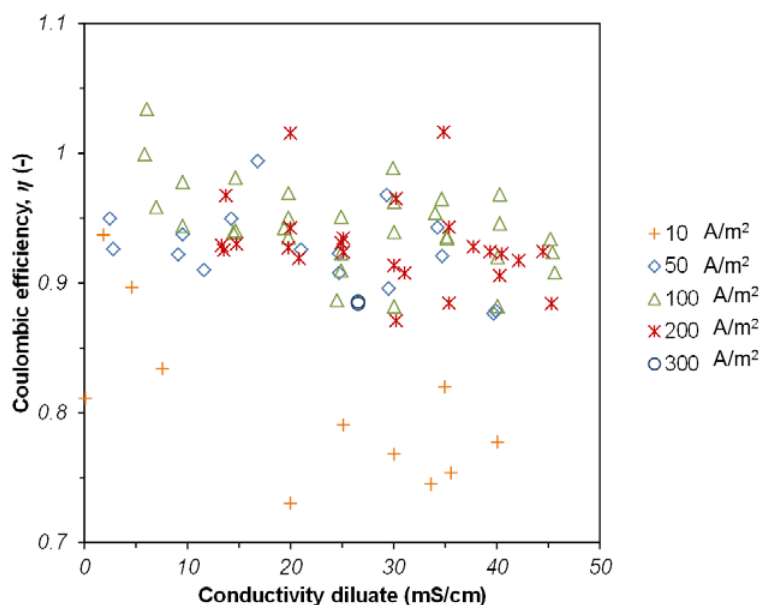
Figure 8. Coulombic efficiency of a ten pair ACS/CMS stack at different applied current densities (10/50/100/200/300 A/m²) as a function of the diluate conductivity.

2.3.4 Associated energy losses

From the membrane stack voltage measurements it is derived that, at low applied current density, the system has low losses (section 2.3.1). From a water transport point of view, however, higher current densities seem to increase the stack efficiency leading to high water recovery (section 2.3.2). From the measurements of energy consumption and water transport, the energy per volume diluate (product) can be determined. The result of this calculation is shown in Figure 9. It should be stressed that this calculation only includes the energy consumption of the membrane stack; energy loss caused by e.g. the electrodes and pumping energy is neglected. Despite the increased water

transport occurring at low applied current density, desalination at reduced energy consumption can be reached. Low diluate conductivity leads in all cases to an enhanced membrane stack resistance and as a result to an increase of the volumetric energy consumption.
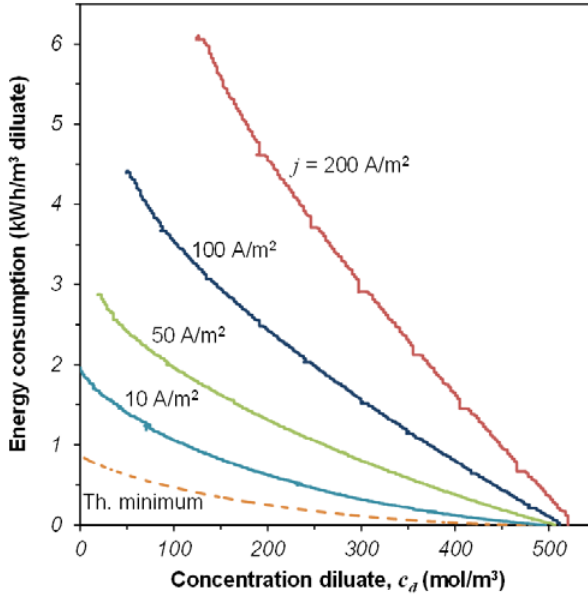
Figure 9. Volumetric energy consumption (kWh/m³) in a ten pair ACS/CMS stack measured at different applied current densities (10/50/100/200 A/m²) and the calculated thermodynamic minimum as a function of the diluate concentration (mol/m³).

The described losses (section 2.3.2-4) cause a difference between the theoretical minimum energy consumption and the energy consumption found at the applied current densities. To show the effect of water transport on this gap between theory and experiments, the energy consumption for a system without water transport is calculated from the experimental data. It has to be mentioned that this is purely theoretical because osmotic and electro-osmotic process will always take place to a certain degree. In Figure 10 A and B the effect of the water transport on the volumetric energy consumption is shown in absolute and relative extent.
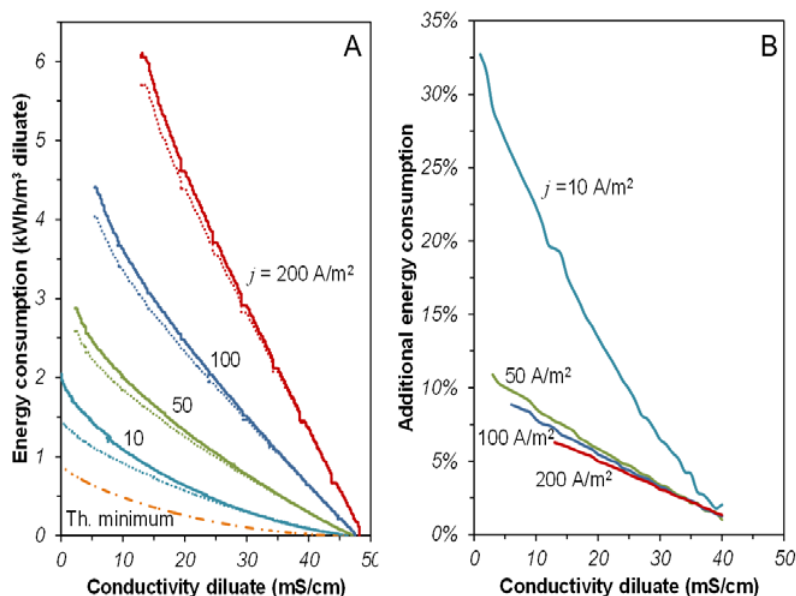
Figure 10 A. Volumetric energy consumption in a ten pair ACS/CMS stack measured at different applied current densities (10/50/100/200 A/m²) (solid lines), the calculated volumetric energy consumption without water transport (dotted lines) and the calculated theoretical minimum (semi dotted line). B. Relative extra energy consumption (%) due to water transport at different current densities as a function of the diluate conductivity.

From Figure 10 it is derived that at low current density (10 A/m²) the influence of water transport is much more pronounced than at higher current densities. The relative extra amount of volumetric desalination energy consumed was found to be as large 32.7%, at 10 A/m². This is in good agreement with section 2.3.2, where water losses are shown to be the largest at 10 A/m².

The loss due to back diffusion is similar in size with the energy loss caused by water transport. When the applied current density is in the range of 50-300 A/m², a loss around 5-10% and maximally 15% is found. For the 10 A/m² the loss was found between 7-25%. It was not determined how large the influence of water transport on the back diffusion (section 2.3.3) is, but when combined they form the total non-ohmic losses. These losses are decreasing at increasing applied current density. When the percentages of the losses are summed up, an absolute maximum value of the non-ohmic losses is found. In that case a maximum of less than 20% of the total loss was found at 50 A/m². However, when 10 A/m² is applied the non-ohmic losses are maximally 51.5% of the total energetic loss. The energy loss due to stack resistances (ohmic) is always the main loss compared to the losses caused by coulombic efficiency and water transport. This implies that the focus of improving the ED process should be on de-

creasing the resistances in the membrane stack (by e.g. adjusting the stack design and flow parameters).

2.3.5 ED-BWRO switching point

If a hybrid desalination scheme of ED and BWRO is used, it is important to know what the outlet concentration of the ED process and thus the inlet of the BWRO module should be. In this paper this specific solution concentration is referred to as the technological switching point. To discover the optimum outlet salinity of the ED unit all process economics should be taken into account. This includes overall energy consumption of the ED and BWRO processes, but also module, operating and facility costs. This is beyond the scope of this paper, as in the present work only experiments with ED are done and energy calculations are based only on the ED membrane stack. Despite this lack of information, still an indication of the technological switching point can be found.

Data on energy consumption of modern low energy BWRO systems are based on [47] and on the international Desalination & Water Reuse quarterly industry website [48]. These data were in good agreement. Plotting the volumetric energy consumption (kWh/m^3), as shown for ED in Figure 9, provides good insight in the energy consumption of the used membrane stack. To compare this ED data with the BWRO data in order to find the technological switching point, it is more useful to determine the actual energy consumption needed to remove a mole of salt. This actual energy consumption (kWh/mol salt removed) is given by the slope of the graphs in Figure 9. The ED and BWRO graphs for the actual energy consumption are shown in Figure 11.

From literature it is known that the applied pressure for BWRO is typically in the range of 10 to 40 bar [3, 49, 50]. The permeate flux can be up to 45 l/m^2·h [3], the water recovery is between 75 and 90% with a salt rejection of 95-99% [3, 47, 49]. In reverse osmosis processes, energy costs depend on the water recovery ratio, the main costs are energy and equipment [51]. The optimal water recovery depends on electricity and membrane prices as well as on feed water salinity, and process efficiency [47]. The membrane life time is estimated as 5-7 years in a pH range of 5.5-7 [3]. Vince *et al.*(2008) performed a BWRO cost optimization leading to an optimal water recovery of 84%, where 75% recovery would lead to the minimal energy use.
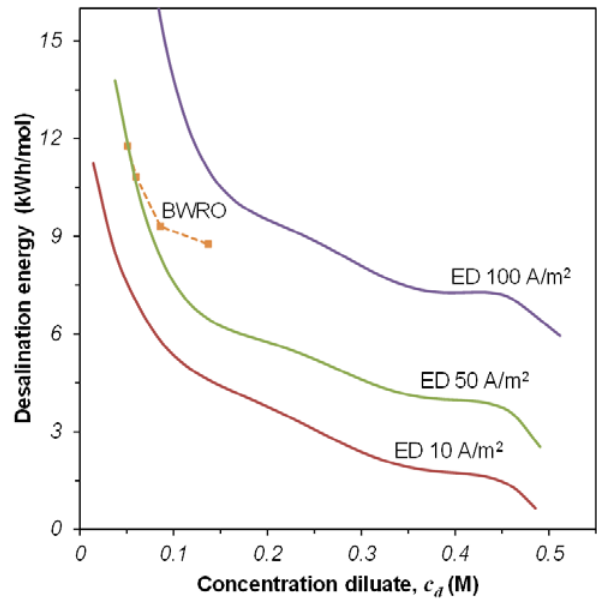
***Figure 11. Calculated actual energy consumption (kWh/mol salt removed) for electrodialysis (j =
10/50/100 A/m²) (solid lines) at different applied current densities and for BWRO (dashed line).***

If ED is performed with a current density of e.g. 50 A/m², the intersection point of the
ED graph with the BWRO graph in Figure 11, will give the technological switching
point. For ED with current density of 50 A/m² this intersection point is found to be at
0.05 M NaCl at an energy consumption of 12 kWh/mol salt removed. When complete
desalination from 0.50 M NaCl is assumed, this will lead to an energy consumption for
ED (from 0.50 to 0.050M) of 2.49 kWh/m³ and an energy consumption for BWRO of
0.55 kWh/m³ (from 0.050 to 0 M). This results in a total energy use for the ED-BWRO
process of 3.04 kWh/m³. If the graph for ED at 50 A/m² is extrapolated to 0 and the
total process energy consumption for ED as a single technique (0.50 to 0M) is calcu-
lated, this would lead to an energy consumption of 3.22 kWh/m³, which is 0.18 kWh/
m³ (6%) more. However, when ED would be performed at 100 A/m², with an assumed
switching point at 0.137 M (assumed maximum BWRO inlet concentration), the ener-
gy consumption decreases with 1.36 kWh/m³ (23%) from 5.98 to 4.62 kWh/m³. Figure
11, shows this decrease in energy consumption as the area between the graphs for
BWRO and for ED at 100 A/m², when these graphs are extrapolated to 0.

2.4 Conclusion

- The transported amount of electro-osmotic water was found to be proportional to the applied current density.

- With homogeneous state of the art ion exchange membranes (Neosepta ACS/CMS; Tokuyama Co., Japan) water transport can have a significant effect on the ionic concentration of the concentrate stream.

- At low applied current density, osmotic water transport can exceed electro-osmotic water transport.

- The volumetric energy consumption (kWh/m^3) in the ED stack can be minimized by using low current densities.

- For ED systems with applied current densities above 50 A/m^2, energy losses due to water transport and back diffusion together were found to be less than 20% of the total losses.

- In all cases, membrane stack resistance causes the main energy loss in the system and therefore this should be the point of focus when improving the stack.

- When the applied current density becomes lower than 50 A/m^2, combining ED with BWRO does not lead to a reduction in energy consumption compared to ED in a standalone configuration.

- Application of ED potentially leads to desalination energy reduction compared to SWRO.

2.5 Literature

[1] P.H. Gleick, Water resources, Oxford University Press, New York USA, 1996.
[2] M.A. Shannon, P.W. Bohn, M. Elimelech, J.G. Georgiadis, B.J. Marĩas, A.M. Mayes, Science and technology for water purification in the coming decades, Nature, 452 (2008) 301-310.
[3] L.F. Greenlee, D.F. Lawler, B.D. Freeman, B. Marrot, P. Moulin, Reverse osmosis desalination: Water sources, technology, and today's challenges, Water Research, 43 (2009) 2317-2348.
[4] U.N. UN, International Decade for Action 'Water for Life', in: Water scarcity, 2005-2015.
[5] J.W. Post, H. Huiting, E.R. Cornelissen, H.V.M. Hamelers, Pre-desalination with electro-membranes for SWRO, Desalination and Water Treatment, 31 (2011) 296-304.
[6] M. Sadrzadeh, T. Mohammadi, Sea water desalination using electrodialysis, Desalination, 221 (2008) 440-447.
[7] B. Pilat, Practice of water desalination by electrodialysis, Desalination, 139 (2001) 385-392.
[8] R.P. Allison, Electrodialysis reversal in water reuse applications, Desalination, 103 (1995) 11-18.
[9] R.P. Allison, High water recovery with electrodialysis reversal, in: AWWA Membrane Technology Conference Proceedings, Baltimore, MD (USA), 1993, pp. 665-673.
[10] M. Turek, P. Dydo, Electrodialysis reversal of calcium sulphate and calcium carbonate supersaturated solution, Desalination, 158 (2003) 91-94.
[11] S.K. Thampy, P.K. Narayanan, W.P. Harkare, K.P. Govindan, Seawater desalination by electrodialysis. Part II: a novel approach to combat scaling in seawater desalination by electrodialysis, Desalination, 69 (1988) 261-273.

[12] T. Seto, L. Ehara, R. Komori, A. Yamaguchi, T. Miwa, Seawater desalination by electrodialysis, Desalination, 25 (1978) 1-7.

[13] A. Al-Karaghouli, D. Renne, L.L. Kazmerski, Technical and economic assessment of photovoltaic-driven desalination systems, Renewable Energy, 35 (2010) 323-328.

[14] S.A. Kalogirou, Seawater desalination using renewable energy sources, Progress in Energy and Combustion Science, 31 (2005) 242-281.

[15] K.S. Spiegler, Y.M. El-Sayed, The energetics of desalination processes, Desalination, 134 (2001) 109-128.

[16] Y. Tanaka, A computer simulation of continuous ion exchange membrane electrodialysis for desalination of saline water, Desalination, 249 (2009) 809-821.

[17] M. Turek, Cost effective electrodialytic seawater desalination, Desalination, 153 (2003) 371-376.

[18] M. Turek, Dual-purpose desalination-salt production electrodialysis, Desalination, 153 (2003) 377-381.

[19] Y. Oren, E. Korngold, N. Daltrophe, R. Messalem, Y. Volkman, L. Aronov, M. Weismann, N. Bouriakov, P. Glueckstern, J. Gilron, Pilot studies on high recovery BWRO-EDR for near zero liquid discharge approach, Desalination, 261 (2010) 321-330.

[20] D.A. Vermaas, M. Saakes, K. Nijmeijer, Doubled Power Density from Salinity Gradients at Reduced Intermembrane Distance, Environmental Science and Technology, 45 (2011) 7089-7095.

[21] J.W. Post, H.V.M. Hamelers, C.J.N. Buisman, Energy recovery from controlled mixing salt and fresh water with a reverse electrodialysis system, Environmental Science and Technology, 42 (2008) 5785-5790.

[22] H. Strathmann, Ion-exchange membrane separation processes, Elsevier, Amsterdam NL, 2004.

[23] J.R. Wilson, Demineralization by electrodialysis, Butterworths Scientific Publications, London, (1960) First edition.

[24] A. Subramani, M. Badruzzaman, J. Oppenheimer, J.G. Jacangelo, Energy minimization strategies and renewable energy utilization for desalination: A review, Water Research, 45 (2011) 1907-1920.

[25] J.N. Weinstein, F.B.J.W. Leitz, Electric power from differences in salinity: the dialytic battery, Science, 191 (1976) 557-559.

[26] J.W. Post, H.V.M. Hamelers, C.J.N. Buisman, Influence of multivalent ions on power production from mixing salt and fresh water with a reverse electrodialysis system, Journal of Membrane Science, 330 (2009) 65-72.

[27] T. Sata, Ion Exchange Membranes; Preparation, Characterization, Modification and Application, The Royal Society of Chemistry, Cambridge UK, 2004.

[28] M. Mulder, Basic Principles of Membrane Technology, Kluwer academic Publishers, second edition, ISBN 0-7923-4247-8 (1996).

[29] V.K. Indusekhar, N. Krishnaswamy, Water transport studies on interpolymer ion-exchange membranes, Desalination, 52 (1985) 309-316.

[30] J. Barret, Inorganic chemistry in aqueous solution, Royal Society of Chemistry, first edition, ISBN 0-85404-471-X (2003).

[31] G. Schmid, Zur elektrochemie feinporiger kapillarsysteme, Zeitschrift Fur Elektrochemie, 55 (1951) 229-237.

[32] K.S. Spiegler, On the electrochemistry of ion-exchange resins - A review of recent work, Journal of the Electrochemical Society, 100 (1953) C303-C316.

[33] Y. Oda, T. Yawataya, On the electro-osmotic water transport through cation-exchange resin membranes, Bulletin of the Chemical Society of Japan, 28 (1955) 263-269.

[34] Y. Oda, T. Yawataya, On the transport number for ion-exchange resin membranes, Bulletin of the Chemical Society of Japan, 29 (1956) 673-679.

[35] Y. Oda, T. Yawataya, On the distribution and behavior of water in cation-exchange resin membranes, Bulletin of the Chemical Society of Japan, 30 (1957) 213-218.

[36] N. Lakshminarayanaiah, Electroosmosis in Ion-Exchange Membranes, Journal of the Electrochemical Society, 116 (1969) 338-343.

[37] A.S. Tombalakian, H.J. Barton, W.F. Graydon, Electroösmotic water transport across ion-exchange membranes, Journal of Physical Chemistry, 66 (1962) 1006-1009.

[38] N.P. Gnusin, O.A. Demina, N.P. Berezina, Water Transport in Ion-Exchange Membranes in an External Electric Field, Soviet electrochemistry, 23 (1987) 1176-1179.

[39] N.P. Berezina, S.A. Shkirskaya, A.A.R. Sycheva, M.V. Krishtopa, The electric transport of pro-

ton-bound water in MF-4SK/PAni nanocomposite membranes, Colloid Journal, 70 (2008) 397-406.

[40] N. Berezina, N. Gnusin, O. Dyomina, S. Timofeyev, Water electrotransport in membrane systems. Experiment and model description, Journal of Membrane Science, 86 (1994) 207-229.

[41] J.H.B. George, R.A. Courant, Conductance and water transfer in a leached cation-exchange membrane, Journal of Physical Chemistry, 71 (1967) 246-249.

[42] N.P. Berezina, E.N. Komkova, A comparative study of the electric transport of ions and water in sulfonated cation-exchange polymeric membranes of the new generation, Kolloidnyj Zhurnal, 65 (2003) 5-15.

[43] N. Berezina, A. Dyomin, O. Dyomina, V. Zabolotsky, Equilibrium and electrotransport properties of the perfluorinated membranes of Nafion and MF-4SC types, Desalination, 200 (2006) 163-165.

[44] N.P. Berezina, N.A. Kononenko, O.A. Dyomina, N.P. Gnusin, Characterization of ion-exchange membrane materials: Properties vs structure, Advances in Colloid and Interface Science, 139 (2008) 3-28.

[45] M. Sadrzadeh, T. Mohammadi, Treatment of sea water using electrodialysis: Current efficiency evaluation, Desalination, 249 (2009) 279-285.

[46] J. Veerman, J.W. Post, M. Saakes, S.J. Metz, G.J. Harmsen, Reducing power losses caused by ionic shortcut currents in reverse electrodialysis stacks by a validated model, Journal of Membrane Science, 310 (2008) 418-430.

[47] F. Vince, F. Marechal, E. Aoustin, P. Bréant, Multi-objective optimization of RO desalination plants, Desalination, 222 (2008) 96-118.

[48] Desalination&WaterReuse, Desalitech closed-circuit technology set for BWRO project, in, 2011.

[49] M.A. Alghoul, P. Poovanaesvaran, K. Sopian, M.Y. Sulaiman, Review of brackish water reverse osmosis (BWRO) system designs, Renewable and Sustainable Energy Reviews, 13 (2009) 2661-2667.

[50] M. Li, Optimal plant operation of brackish water reverse osmosis (BWRO) desalination, Desalination, 293 (2012) 61-68.

[51] R. Semiat, Energy issues in desalination processes, Environmental Science and Technology, 42 (2008) 8193-8201.

Chapter 3

Seawater electrodialysis with preferential removal of divalent ions

Abstract

In this work desalination of a ternary salt mixture and artificial seawater is studied with a lab scale electrodialysis stack, which was used in a recycling batch mode. During the desalination procces samples were taken and the ionic composition of the diluate stream was determined. The effect of applied current density (10-300 A/m^2) on this composition was investigated. A clear effect of applied current density was observed. A lower applied current density leads to a more complete reduction in concentration of divalent ions, in an earlier extent of desalination. This influence of the applied current density could be related to the concentration polarization effects that occur in the stagnant diffusion layer and are explained with a model based on the Nernst-Planck flux equation. It was found that the lower initial ion concentration of Ca^{2+}, Mg^{2+}, but also of K^+, and SO_4^{2-} compared to respectively Na^+ and Cl^-, leads to stronger depletion of these ions in the transport layer adjacent to the membrane. These boundary layer effects are more pronounced at higher applied current densities, resulting in reduced transport of ions with a low initial concentration. High monovalent over divalent ion ratios can be found at low applied current.

Nomenclature

A	=	area (m^2)
c	=	concentration (mol/m^3)
D	=	diffusion coefficient (m^2/s)
F	=	Faraday constant (C/mol)
I	=	current (A)
J	=	ion flux ($mol/m^2 \cdot s$)
j	=	current density (A/m^2)
R	=	gas constant ($J/mol \cdot K$)
r	=	ratio of external over internal (membr.) diffusion coefficient (-)
T	=	temperature (K)
T_i	=	transport number (-)
t	=	time (s)
V	=	volume (m^3)
v	=	velocity (m/s)
X	=	membrane charge (mol/m^3)
x	=	membrane coordinate (m)
z	=	valence (-)
δ	=	thickness (m)
ϕ	=	dimensionless potential (-)
σ	=	conductivity (mS/cm)

3.1 Introduction

There are three widely applied desalination technologies; electrodialysis (ED) [1], reverse osmosis (RO) [2], and distillation [3]. ED and RO are membrane-based processes, whilst distillation deploys heat to vaporize water. RO and distillation techniques generally provide a (close to) complete separation of pure water from the concentrated feed solution. With ED, ions and small charged molecules can be removed from a solution to a chosen extent, which makes ED suitable as a predesalination technique [4, 5].

3.1.1 A background on divalent ions in seawater desalination

When looking into the ionic composition of seawater one will find that it mainly consists of monovalent sodium (Na^+) and chloride (Cl^-) ions, but significant amounts of multivalent ions like calcium (Ca^{2+}), magnesium(Mg^{2+}), and sulphate (SO_4^{2-}) are present as well. A for desalination purposes 'troublesome' property of these divalent ions is that they can form salts with low solubility, which precipitate readily on surfaces in desalination devices.

In RO, water permeates through the membrane under an applied pressure while salts are retained. Water recovery of such a system is limited as the concentration of particles (i.e. colloids) on the retentate side is becoming high, what leads to high osmotic pressures to overcome [6]. RO membranes can typically withstand a hydrostatic pressure of 70 bar, some overpressure (typically 20 bars) is required to generate substantial flux, therefore, the water recovery of a seawater RO process will be limited by the osmotic pressure to a maximum of 35-50% [4]. From an economical point of view, a high water flux is required to minimize the number of RO membrane elements, however, high water fluxes results in larger concentration polarization (i.e. concentration of particles is higher at the membrane-water interphase than in the bulk solution) and higher permeation resistance. Due to concentration polarization, local oversaturation occurs at the membrane-solution interface, leading to precipitation of multivalent ions. Therefore often, not the osmotic pressure, but precipitation of ions on the RO membrane is limiting the SWRO process.

Deposition of salts on (for example) a membrane is known as scaling and causes increased membrane permeation resistance, shortens membrane life time as it can physically damage membranes, but also may cause irreversible clogging of parts of the desalination equipment [7, 8]. Scaling is often caused by precipitation of calcium carbonate ($CaCO_3$), calcium sulphates ($CaSO_4$ / $CaSO_4 \cdot H_2O$ / $CaSO_4 \cdot 2H_2O$), magnesium hydroxide ($Mg(OH)_2$), or silica.

Solubility (and thus scaling potential) depends on ionic strength of the solution, temperature, pressure, velocity, and concentration polarization [7]. When the scaling potential can be lowered, water recovery and overall efficiency of RO systems can be enlarged, and savings can be made on chemical dosing and membrane cleaning. Water recovery is an important factor in RO systems as feed water has undergone typically quite extensive pretreatment. In cases where boron is present in seawater, often the pH is enlarged in the RO to >9.5 as than most boron is present as $H2BO3-$ which can be almost completely removed [9]. However, the scaling potential increases a lot at these alkaline conditions [10], and therefore can be another reason why water softening may be required.
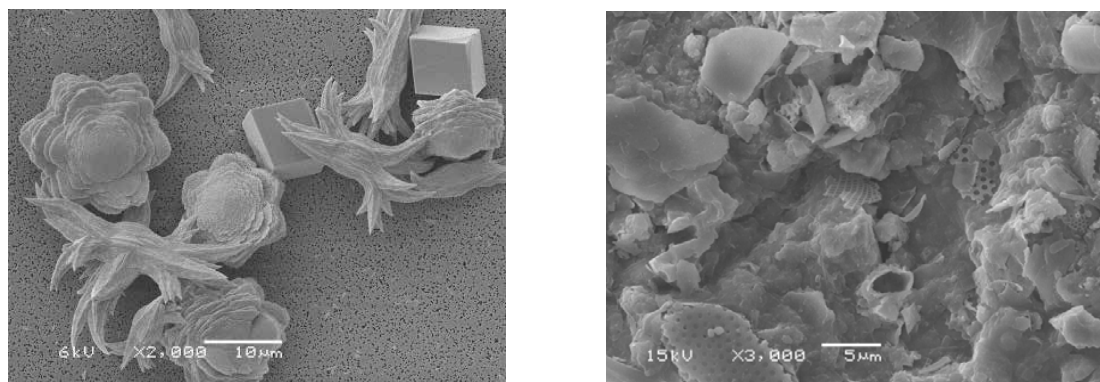
Figure 1. Different CaCO$_3$ crystals (left) and a RO membrane with CaCO$_3$ deposition (right). (Images provided by Martijn Wagterveld, Wetsus).

3.1.2 Specific removal of divalent ions

Scaling problems are not a recent discovered phenomenon, and already for over 50 years people are investigating methods to avoid scaling of desalination equipment. Ion exchange resins were used for seawater desalination and softening [11-13]. However, low selectivity in high concentrated solutions, like seawater, and requirement of a resin regeneration step make the ion exchange process inefficient. Techniques that may provide a selective predesalination of seawater are nanofiltration (NF) and ED [14-16]. In the last decade(s) water softening by an additional pretreatment step with nanofiltration (NF) membranes was applied in large scale plants.

NF membranes are suitable to lower scaling potential as the applied pressure is relative low (up to 9 bar) and the NF membranes show good rejection of divalent ions, while allowing most of the monovalent ions to pass [10, 14, 17-21]. NF is a technology that gained interest as a pretreatment technique for seawater desalination or even as seawater desalination technique [10, 21-23]. Being a pressure driven technique, NF is limited in its water recovery by the osmotic pressure [4, 10, 21, 22]. With the combination

NF-RO the overall water recovery may be somewhat increased but is still at maximum around 50% and typically below 40% [18, 20, 21, 23, 24]. When the water recovery of the NF is high, the removed amount of salts and particles is low and the recovery in the RO is low. Vice versa, when more (also monovalent) ions and silica's are removed, water recovery of the NF element is typically low, and even with high water recovery of the RO unit, overall water recovery will hardly be increased. Although, in a hybrid NF-RO system life time of RO membranes may be increased, also NF membranes need replacement and require periodically cleaning [24]. Therefore, even if higher water recovery is achieved, this does (typically) not make up for the additional costs [25]. Scaling issues are not actually solved with such a hybrid system, but are relocated from the RO to the NF membranes. Therefore, NF is very suitable for water softening of solutions with low salinity and less suitable for pre-desalination of seawater [4] or the production of oil injection water.

In ED, the salts permeate through the membrane under the influence of an applied electrical current. By placing anion exchange membranes (AEM) and cation exchange membranes (CEM) in alternating order between an anode and a cathode an ED stack is formed. When applying a DC current, the cations start to migrate towards the cathode and the anions towards the anode. As a result, desalinated streams (diluate) and concentrated streams (concentrate) are created in alternating channels. Electrodialysis (ED) has the benefits over pressurized membrane filtration techniques that it is less sensitive to fouling and scaling, especially when used in the reversal (EDR) mode, where polarity is switched periodically [26]. ED is shown to be working well at high recovery, very high salt concentrations, and supersaturated solutions of divalent ions [27-31]. To enhance water recovery, a separator can be used to form precipitates in the concentrate, before it is recirculated into the stack [28, 29]. In such systems very high water recovery (>90%) may be achieved, at high concentrations of ions in the feed water.

For the selective transport of monovalent ions from seawater so-called monovalent selective ion exchange membranes can be used. With this type of membranes one can achieve an almost complete separation between monovalent ions and divalent ions [32-36]. However, in this study, the focus was not on the removal of monovalent ions but on the preferential removal of the multivalent ions from seawater using membranes that are anion or cation selective. For this process there is no obvious technique available and there are no membranes that are 'multivalent selective', as transport of monovalent ions through a membrane is easier than transport of divalent ions.

Besides scaling, presence of divalent ions in the feed water may cause other problems. Final drying of seawater originated salt might become more challenging and more expensive (if for instance a drying agent is needed) as these divalent ions form more hygroscopic precipitates. That is why for edible salt production electrodialysis, with monovalent selective membranes, is used to prevent the concentration of multivalents in the seawater brines [34, 37]. Thirdly the presence of divalent ions, sulphate in particular, represents a challenge for the off-shore oil reservoir desalinated water injection. To increase the oil extraction desalinated seawater is injected in to the reservoir. In order to avoid formation of hydrogen sulphide [38], the requirements for the sulphate concentration in the processed injection water are very strict. Sulphate concentrations must be lowered to levels much smaller than the chlorides. From these examples, it is clear that ions have to be selectively transported, either the monovalent ones (e.g. for desalination, for edible salt production), or the multivalent ions (e.g. for pre-desalination, for production of oil recovery injection water).

For ED, it was reported that although small differences in transport rates can be observed for monovalent ions and divalent ions, this does not lead to a selective desalination of practical use [15, 16]. However, some operational measures may improve the selectivity of the process. Van der Bruggen *et al.* [15] proposed that separation efficiency with ED may also be influenced by applied voltage or current.

A selective desalination was found by Kabay *et al.* at decreased applied voltage [39, 40]. Kim *et al.* investigated the properties of the boundary layers and their effect on the membrane selectivity for monovalent and divalent ions [41, 42]. In the second study an indirect effect of applied potential on the membrane selectivity is reported [42]. In these studies, however, the molar concentrations of monovalent and divalent are, unlike seawater, equal [39, 40, 42] or relative close to each other [40]. Moreover, only the selectivity of the cation exchange membrane (CEM) was investigated. In the studies performed by Kabay *et al.* [39, 40] the investigated applied potential range was small. Kim *et al.* were performing their study in a much broader current range (0-200 A/m^2) but also did not apply a constant current.

In the present study, ED is applied on feed water with seawater ion concentrations and the effect of applied current density on the preferential removal of multivalent ions is investigated over a broad current density range (10-300 A/m^2). Furthermore, both the anion and the cation transport are considered.

3.2 Theory

To describe ion transport in electrochemical systems the Nernst-Planck (NP) flux equation is widely used (e.g. [12, 42-48]). In the present study equation 1 is used, both in the SDL in front of the membrane, and in the membrane itself. Here, the NP equation contains a diffusion term and a migration term:

$$J_i = -D_i \left[\frac{dc_i(x)}{dx} + c_i(x)z_i \frac{d\varphi}{dx} \right]$$ eq. 1

Where J is the ion flux (mol/m²·s), D is the diffusion coefficient (m²/s), ϕ is the electrical potential in the SDL or membrane (made dimensionless by scaling the potential to the thermal voltage, $V_T=RT/F$), c_i is the concentration of species i (mol/m³), z is the valence (-), F is the Faraday constant (C/mol), R is the gas constant (J/mol·K), T is the temperature (K) and x the distance from a reference point (m). The convection term $(+ c_i \cdot v)$ was neglected as the convective transport in the direction perpendicular to the membranes is negligible in comparison with the diffusion and migration term [42-44, 48].
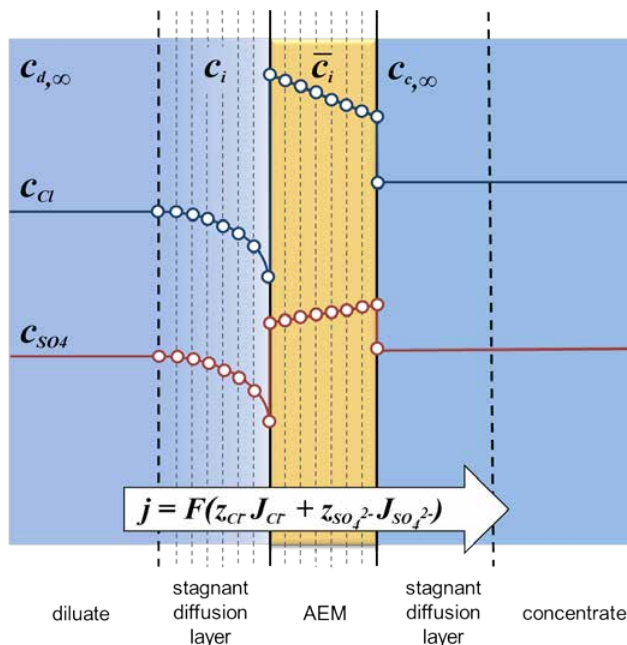
Figure 1. Schematic representation of the diluate, stagnant difusion layer (SDL), anion exchange membrane (AEM), concentrate, and schematically the calculation planes (dotted lines) used in the model.

Based on the NP flux equation, the transport of e.g. chloride and sulphate through an anion exchange membrane (AEM) can be calculated with a fairly simple model. The

CEM can be modeled in the same way. In the model four phases are distinguished: (i) a dilute bulk solution phase (diluate), (ii) a stagnant diffusion layer (SDL) phase at the diluate side of the membrane, (iii) an AEM and (iv) a concentrate bulk solution phase (concentrate). These four phases are schematically shown in Figure 1.

Diluate and concentrate phases are regarded as completely stirred solutions with a concentration changing in time (transient state) from an initial situation where they have the same composition. In the mathematical model, the SDL and AEM are divided in a number of planes (or nodes) where equation 1 is discretized and solved. The transport through the SDL and membrane is assumed to be in steady state, and thus for each ion the flux J of equation 1 is [47, 49] unchanging across SDL and membrane.

An AEM has not only a selectivity towards counterions (anions) or co-ions (cations) but it can also be more selective towards a specific counterion when several counterions are present in the solution [34, 50]. In this model, the affinity of the membrane towards specific counterions is estimated from experimental data by introducing a ratio r_i between the diffusion coefficient of the species in the bulk solution and the SDL (D_i) and the diffusion coefficient in the membrane matrix ($\overline{D_i}$). $\overline{D_i}$ is taken as a function of the value in the (bulk, external) solution, D_i, as described by:

$$\overline{D_i} = \frac{D_i}{r_i}$$

eq. 2

Where the values of r_i are empirically obtained for each ion separately from fitting model to data (see Table 4). As we will discuss, for divalent anions in an AEM, a current-dependent value of this r_i must be used.

For the sake of simplicity the membrane is considered perfectly selective for counterions, (no co-ions are allowed in or through the membrane) and is assumed that no water transport through the membrane takes place. Everywhere in the system electro-neutrality is assumed and accumulation of ions is absent. Because the co-ion is blocked entry in the membrane, in equation 1, the co-ion flux J_{co-ion} is zero, and equation 1 simplifies for the co-ions to Boltzmann's relation [51]:

$$\ln c_{SDL,i}(x) = \ln c_{d,i,\infty} + z_i \cdot \phi_{SDL}(x)$$

eq. 3

Effects of concentration polarization in the SDLs [47, 48] stem from membrane selectivity, leading to high transport numbers, T_i (-), for counterions in the membrane phase and migration of co-ions in opposite direction [34, 50, 52]. In the model of our present study T_i is equal at each position in the SDL and membrane. The transport number is defined as de fraction of the total current, carried by a specific ion [52]:

$$T_i = \frac{z_i J_i}{\sum_i z_i J_i}$$

eq. 4

In contrary, the SDL is also influencing the membrane selectivity [50] as it determines the ionic concentrations just outside the membrane. In the SDL, concentration polarization may be so pronounced that it leads to ion concentrations of (almost) zero at the solution-membrane interface. In that case the limiting current density (LCD) is reached [34, 50, 52, 53]. The SDL on the concentrate side is not modeled, since it is assumed that the effect of this layer is relatively low and while desalination continues further diminishes in importance [54, 55] as during desalination the concentration gradient in this layer is further reduced.

In order to calculate the concentration profiles for all ionic species in the SDL, the NP equation is used together with the assumption of electroneutrality at each point in the SDL:

$$\sum_i z_i \cdot c_i = 0$$

eq. 5

From the ion concentration in the SDL, adjacent to the membrane, $\overline{c}_D$, the counterion concentration of the solution just in the membrane, $\overline{c}_D$ is calculated by the Boltzmann relationship [51, 56]:

$$\ln \overline{c}_{D,i} = \ln c_{D,i} + z_i \cdot \Delta\phi_D$$

eq. 6

Where $\Delta\phi_D$ is the Donnan potential (dimensionless by scaling to the thermal voltage, $V_T = RT/F$), which is the electrical potential difference across the solution-membrane interface. With $\overline{c}_D$ being known, from the calculation over the SDL and the assumption of electroneutrality in the membrane [57]:

$$\sum_i z_i \cdot \overline{c}_i + X = 0$$

eq. 7

Where X is the fixed membrane charge (mol/m³; positive for AEM and negative for CEM). The NP equation is used to calculate the concentration profile over the membrane. Since at the concentrate side of the membrane no SDL is considered the concentration adjacent to the membrane is equal to the concentrate bulk concentration, $c_{c,\infty}$.

Because in this model the duration (time) is not directly considered (only the ongoing

change of concentration in the diluate and concentrate compartments, and the concentration profiles in the SDL and membrane), the exact value of the thickness, δ of the SDL and AEM are not required to be known. In the model, the thickness of the SDL is taken equal to the thickness of the membrane. The effect of thickness of both entities on the ion transport has been lumped with the effect of different diffusivities within the membrane and the SDL. As such, the reported apparent diffusivity in the membrane relative to the diffusion coefficient in the SDL (represented by their ratio r_i) includes the thickness of the SDL and AEM. All model assumptions and input parameters are listed in Table 1.

Table 1. Model assumptions and input parameters.

diluate	*SDL*	*IEM*	*concentrate*
electroneutrality	electroneutrality	electroneutrality	electroneutrality
transient state	steady state	steady state	transient state
no accumulation	no accumulation	no accumulation	no accumulation
completely stirred		selectivity = 100%	completely stirred
		no water transport	

Input parameters: $c_{d,\,initial}$, $c_{c,\,initial}$, X, r_i, $D_{monovalent}$, $D_{divalent}$, V, $A_{membrane}$ **and** I

The volume of the aqueous solution in the experimental setup is V (m^3), and is the sum of the volume of the diluate (V_d) and concentrate (V_c) batches (see section 3.3.2). Volumes are used with the membrane area, $A_{membrane}$ (m^2) in an overall and differential mass balance set up for each of the ionic species, given by:

$$V_d \cdot c_{i,d} + V_c \cdot c_{i,c} = V \cdot c_{i,initial} \qquad \text{eq. 8}$$

$$V_d \cdot \frac{dc_{i,d}(t)}{dt} = -J_i(t) \cdot A_{membrane} \qquad \text{eq. 9}$$

3.3 Materials and Methods

3.3.1 Materials

The ED stack contained nine cell pairs and two electrode compartments. Every repeating cell pair in the membrane stack consisted of a diluate and concentrate compartment, formed with silicone gaskets (~500 μm), that contained a woven PET fabric spacer (Nitex 06-700/53, Sefar, Switzerland). Characteristics of this spacer are given in [58]. The compartments were separated by a cation exchange membrane (Neosepta CMX;

Tokuyama Co., Japan) and an anion exchange membrane (Neosepta AMX; Tokuyama Co., Japan). Characteristics of this membrane pair were determined by [59]. An extra cation exchange membrane was used to separate the last cell pair and the electrode. The active area of each square shaped membrane was 104 cm². On both sides of the membrane stack a squared electrode was placed in the electrode compartments. As anode a titanium electrode (mesh 1.7, area 96.04 cm²) with a mixed metal oxides coating was used (Magneto Special Anodes BV, The Netherlands), and as cathode a titanium electrode (mesh 1.7, area 96.04 cm²) with a 50 g/m² platinum coating was used (Magneto Special Anodes BV, The Netherlands).

3.3.2 Methods

ED experiments were done with two different starting solutions (feed water). The compositions of these solutions are shown in Table 2. The salt solution given by *composition 1* in this table is a ternary mixture with sodium chloride and sodium sulphate concentrations corresponding to those of North Sea water. Whilst magnesium, potassium and calcium were omitted in the first composition, *composition 2* in Table 2 represents a more complete seawater composition.

Table 2. Composition of the salt solutions used in the electrodialysis experiments.

Ion	Composition 1		Composition 2	
	g/l	*mol/l*	*g/l*	*mol/l*
K^+	-	-	0.420	0.011
Na^+	11.150	0.485	11.150	0.485
Ca^{2+}	-	-	0.390	0.010
Mg^{2+}	-	-	1.410	0.058
Cl^-	15.126	0.427	20.310	0.573
SO_4^{2-}	2.800	0.029	2.800	0.029
Total	*29.076*		*36.480*	

The flow rate was set to 15.0 ml/min per channel and was equal for the diluate and the concentrate. Experiments were done in a recirculating batch mode; in this mode the concentrate and diluate are pumped from respectively a concentrate and a diluate batch (with equal initial concentrations of solutes) through the ED stack back into the batches. These batches were kept in glass bottles and were continuously stirred. Both the concentrate and the diluate batches had a volume of 600 ml (including the internal volume of tubes and compartments) at the start of the experiment. A sodium chloride solution (29.22 g/l) was pumped through the electrode compartments with a flow rate

of 100 ml/min per compartment. The electrode rinse solution was not recycled but collected, degasified and disposed.

Before the start of the experiments, the membrane stack was equilibrated with the experimental salt solution by recycling the solution trough the stack for a minimum time of 1 hour. Directly after the experiment the stack was flushed with a solution equal in composition with the start solution as to equilibrate the membranes before the next experiment. This equilibration solution was not recycled, but disposed after leaving the stack. Conductivity probes (QC205 XC, QIS) were placed in line directly before the stack and measured the actual conductivity value of the concentrate and diluate. These probes were connected through a transmitter box (P862, QIS) with a data logger (Memograph M RSG40, Endress+Hauser). The membrane stack voltage was measured with two Ag/AgCl reference electrodes (QM711X, QIS). These were placed at the inlet of the anode and cathode compartments. The potential difference of the two reference electrodes was measured with a high impedance preamplifier (-50/+50 V, Ext-ins technologies). A power supply (SM70-AR-24, Delta Elektronika) was used to apply a constant current. Actual values of potential, conductivity and current were logged every second. Throughout the experiments, the temperature of the water was measured to be 20±2 °C.

Presented experiments were reproducible and repeated at least three times. Electrodialysis was performed under a constant current. The applied current density was varied and set at 10, 30, 100 and 300 A/m^2 respectively, referring to the cross sectional area of the flow compartments. During desalination salt concentrations in the diluate were decreasing, resulting in lower conductance (increasing stack resistance), because a constant current was applied this results in an increasing stack potential (V). This potential increases drastically when the LCD (theory section) was reached. Due to a potential limitation on the power source, at a certain extent of desalination the maximum applicable potential has been reached. From then on the power source applied a lower current at a constant (maximum allowed) voltage. One could interpret this as operating at the LCD. The maximum voltage for the 300 A/m^2 experiment was set to 50 V and for the 100 A/m^2 to 35 V, so to assure that in all cases a higher current was applied for the 300 A/m^2 experiments than for the 100 A/m^2, even after the maximum potential is reached. For experiments with 10 and 30 A/m^2 the maximum stack potential was never reached. At what level of voltage (35 or 50 V) and at what extent of desalination the switching form applied current to applied voltage occurred, can be seen in Table 3.

Table 3. Applied current density (A/m²) and switching point from constant current to constant (maximum) voltage (conductivity of the diluate in mS/cm) to applied voltage (V).

Applied current density (A/m^2)	Composition 1						Composition 2					
	Test 1		Test 2		Test 3		Test 1		Test 2		Test 3	
	mS/cm	V	mS/cm	V	mS/cm	V	mS/cm	V	mS/cm	V	mS/cm	V
300	12	50	13.1	50	13.3	50	12.3	50	12.2	50	12	50
100	3.8	35	3.8	35	3.8	35	3.9	35	3.8	35	3.9	35
30	No switching point, V_{max} =35V						No switching point, V_{max} =35V					
10	N/A											

When the diluate inlet conductivity (concentration) reached a value of 20, 10, 5 and 2 mS/cm samples of the diluate and concentrate were taken for analysis of the ionic compositions. The samples were first diluted with an auto diluter (ML530B, Hamilton) to lower the measurement error propagation. Anions were measured by ion chromatography (IC, 761 Compact IC, Metrohm) and cations by inductive-coupled plasma optical emission spectroscopy (ICP-OES, Optima 5300DV, Perkin Elmer).

3.4 Results

3.4.1 Ternary mixture

Figure 2 shows the linear decrease of the remaining sodium concentration in the diluate, during desalination of a ternary mixture (solution composition 1). This is as expected since the solution conductivity (σ, mS/cm) decreases linearly with salt concentration in this concentration range. Due to electroneutrality in the flow channels, the remaining sodium concentration has to decrease linearly as it is the only type of cation present in the ternary solution (see section 3.3.1). The spread in the results at higher diluate conductivity is larger than at lower diluate conductivity, due to a lower accuracy resulting from the higher required dilution factor for samples with a higher salt concentration (see section 3.3.2).
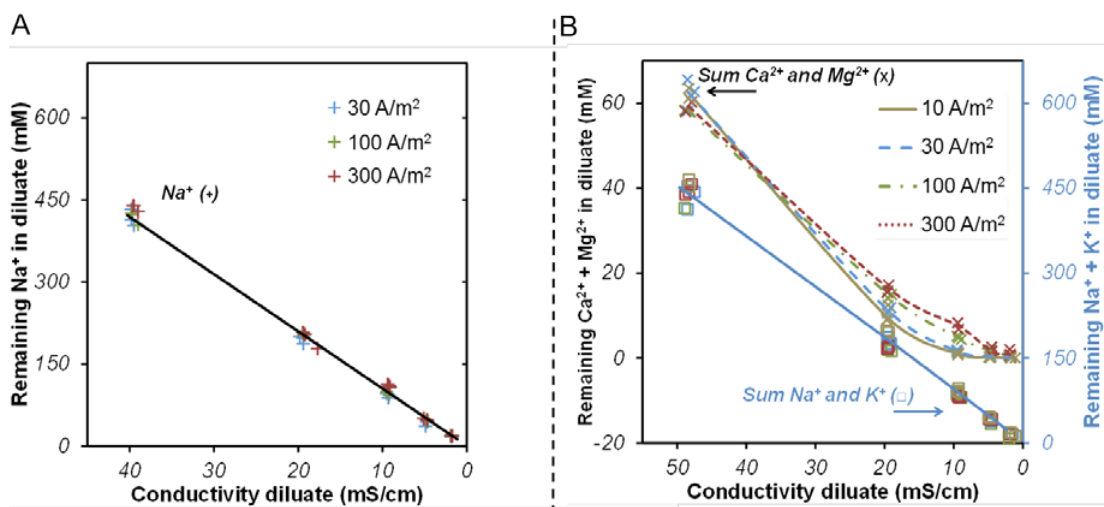
Figure 2 A. Measured remaining sodium concentration (mM) in the diluate during desalination of a ternary mixture (Na$^+$, Cl$^-$ and SO$_4^{2-}$) at an applied current density of 30 A/m^2 (blue), 100 A/m^2 (green) and 300 A/m^2 (red). A linear trend line is drawn through the point clouds. B. Sum of measured remaining monovalent and divalent ion concentrations (mM) in the diluate during desalination of an artificial North Sea water mixture (Na$^+$, K$^+$, Ca^{2+}, Mg^{2+}, Cl$^-$ and SO$_4^{2-}$) at an applied current density of 10 A/m^2 (brown solid), 30 A/m^2 (blue stripe), 100 A/m^2 (green stripe-dot) and 300 A/m^2 (red dot), trend lines along the median values of the measurements.

Results of remaining anion (Cl$^-$ and SO$_4^{2-}$) concentrations obtained by using a ternary mixture are shown in Figure 3. This figure displays that the sulphate concentration shows an increased removal rate, at all applied current densities (j, A/m^2), from a diluate conductivity of about 20 mS/cm. In Figure 3 an effect of applied j is visible at

measurement points at a diluate conductivity of 10, 5 and 2 mS/cm. Although between $j = 100$ and $j = 300$ A/m² there is no observed difference, at $j = 30$ A/m² the remaining sulphate concentrations are found lower, which implies a higher removal rate.
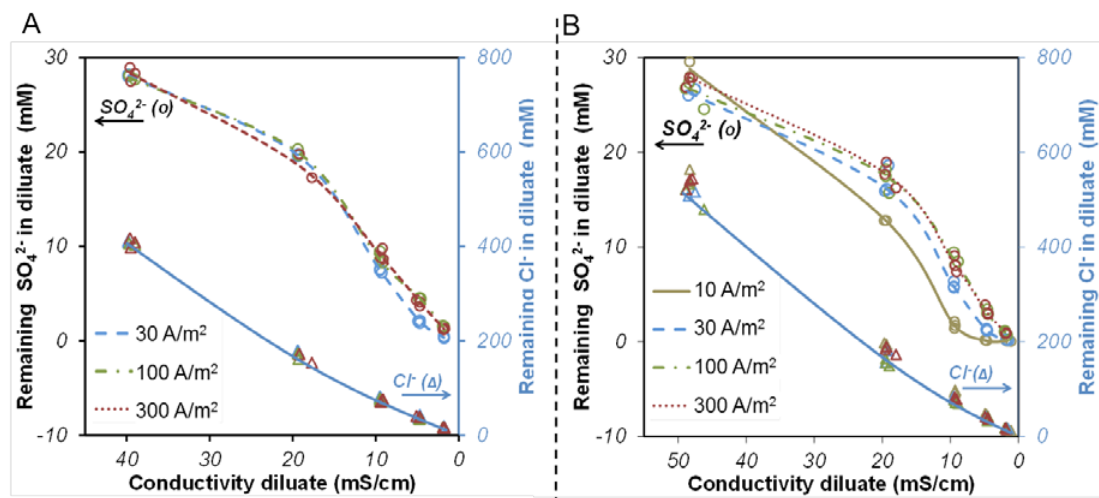
Figure 3 A. Measured remaining SO₄²⁻ (left axis) and Cl⁻ (right axis) concentration (mM) in the diluate during desalination of a ternary mixture (Na⁺, Cl⁻ and SO₄²⁻) at an applied current density of 30 A/m² (blue stripe), 100 A/m² (green stripe-dot) and 300 A/m² (red dot), trend lines along the median values of the measurements. B. Measured remaining SO₄²⁻ (left axis) and Cl⁻ (right axis) concentration (mM) in the diluate during desalination of an artificial North Sea water mixture (Na⁺, K⁺, Ca²⁺, Mg²⁺, Cl⁻ and SO₄²⁻) at an applied current density of 10 A/m² (brown solid), 30 A/m² (blue stripe), 100 A/m² (green stripe-dot) and 300 A/m² (red dot), trend lines along the median values of the measurements.

3.4.2 Artificial North Sea water

When artificial North Sea water (solution composition 2) is used for the experiments, two monovalent (Na⁺, K⁺) and two divalent cations (Ca²⁺, Mg²⁺) are present in the solution. To compare the transport behavior of monovalent and divalent ions, the sum of the monovalent ion concentrations is compared with the sum of the divalent ion concentrations in the diluate (Figure 2 B). In this graph trend lines are drawn to help distinguish the trends at variously applied j. These trend lines are drawn by eye along the median values of the measurements and have no further mathematical meaning.

Both for monovalent ions and divalent ions, Figure 2 B clearly shows that at the beginning of the desalination process the decrease in ion concentration in the diluate is linear with the extent of desalination (here presented as decreasing conductivity). For the divalent ions, however, the last part of the graph is non-linear, while the

curve for the monovalent ions decreases linearly throughout the process and at every applied current density. At lower applied current densities, more charge is transported by divalent ions, which results in a lower residual concentration of these divalent cations in the diluate. The same is valid for the anions as shown in Figure 3. This is in good agreement with data reported in literature [36, 39]. A difference between the two graphs is that in Figure 2 B the decrease of divalent cations is first steeper and then flattens out, whereas in Figure 3 the decrease of divalent anions is first linear and then increased before it reduces in the final stage of desalination. The trend of remaining sulphate in the diluate, obtained with a ternary mixture (Figure 3 A) and with artificial seawater (Figure 3 B) is very similar.

3.5 Discussion

3.5.1 Removal ratio between monovalent and multivalent ions

Analyzing Figure 3 one finds that from the start of the desalination process, monovalent ions are removed at a much higher rate than divalent ions. This difference in removal rate is larger than the initial ionic ratio of monovalent over divalent ions (~19.5 for anions and ~7.5 for cations). As a result this ratio will be lowered in the first part of desalination. This is shown in Figure 4 B. However, at a certain point in the desalination extent (at $\sigma \approx 20$ mS/cm), the chloride removal rate starts to decrease and a relative bigger part of the current is transported by sulphate, resulting in an increase in the remaining Cl^- / SO_4^{2-} ratio of the diluate. At lower applied current density (10 A/m^2) concentration polarization effects are smaller. Therefore the observed membrane selectivity will be affected more by the membrane affinity resulting in a higher transport rate of divalent ions, as will be discussed in paragraph 3.5.2. This will lead to a higher Cl^- / SO_4^{2-} ratio in the diluate, as shown in Figure 4. This monovalent over divalent ratio was found as large as ~410, which is an increase by a factor ~20. For monovalent over divalent cations this ratio was measured as large as ~440, which is an increase by a factor ~60. Hence, preferential removal of divalent ions is taking place at the AEM, and is even more pronounced at the CEM.

The removal rate of divalent ions is reduced again in the very final stage of the experiments, due to almost complete depletion of these divalent ions. This means that there is a maximal ratio that can be obtained, which also can be seen for the data points of the experiment with $j = 10$ A/m^2 (see Figure 4). Another important finding is that during removal of the first ~60% of the salt, the ratio between the monovalent and the divalent ions remains nearly constant.
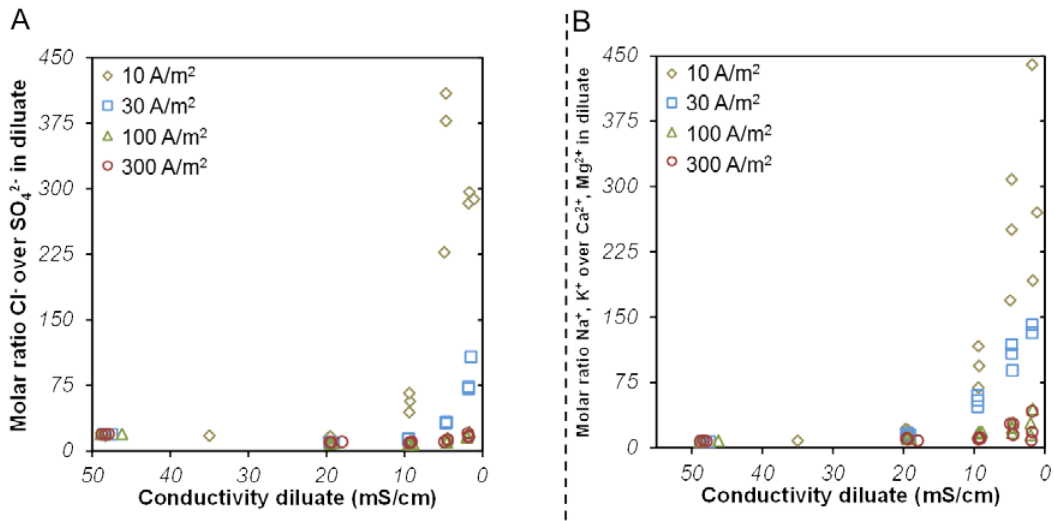
Figure 4. Ratio measured remaining monovalent ion/divalent ion concentration (M) in the diluate during desalination of an artificial North Sea water mixture (Na$^+$, K$^+$, Ca^{2+}, Mg^{2+}, Cl$^-$ and SO$_4^{2-}$) at an applied current of 10 A/m^2 (brown diamond), 30 A/m^2 (blue square), 100 A/m^2 (green triangle) and 300 A/m^2 (red circle).

3.5.2 Preferential removal of multivalent ions at low applied current density

The model as described in section 3.3.2 was used for the further investigation of the preferential removal of multivalent ions that was achieved at low applied current densities. Also the difference in preferential removal between CEMs and AEMs was studied. As shown in Figure 6, the model was fitted to the external monovalent and divalent ion concentrations in the bulk ($c_{d,\,\infty}$, $c_{c,\,\infty}$). The fitting was done by adjusting the ratio r_i between the diffusion coefficient of the specie in the external bulk solution phase and the diffusion coefficient in the membrane matrix, equation 2.2. The model input parameters are shown in Table 4. For the diffusion coefficients of the monovalent cations (Na$^+$, K$^+$) and divalent cations (Ca^{2+}, Mg^{2+}) weighted averages were used (weighted by initial diluate concentrations).

For the CEM, the ratio between external (bulk) and internal (membrane) diffusivity coefficients used for fitting were found to be 10 for both monovalent and divalent cations. According to this, the membrane is not selective between monovalent and divalent cations when an electric field is applied. This is remarkable as in the literature, diffusion coefficients in the membrane of divalent ions are relatively lowered more than those of monovalent ions of [12, 60-62]. Also from sorption experiments (equilibrium)

in literature can be found the divalent ions have a higher affinity to the IEM than the monovalent ions [12, 35, 62, 63], although it was already recognized that this affinity may be subject to operational conditions such as applied current density [35, 64]. The selective transport of divalent ions at higher desalination extent can just be explained by (i) differences in initial concentrations, (ii) differences in diffusivities, and (iii) concentration polarization phenomena and properties of the SDL [42].

Table 4. Model input parameters.

Parameter	Anion exchange membrane		Cation exchange membrane	
X	$4.8 \cdot 10^3$	mol/m^3	$6.0 \cdot 10^3$	mol/m^3
$D_{monovalent}$	20.32	$\cdot 10^{-10}$ m^2/s	13.46[*]	$\cdot 10^{-10}$ m^2/s
$D_{divalent}$	10.65	$\cdot 10^{-10}$ m^2/s	7.77[*]	$\cdot 10^{-10}$ m^2/s
$r_{monovalent}$	10	-	10	-
$r_{divalent}$	$2400 \cdot j^{-0.32}$	-	10	-
$V_{diluate}$, $V_{concentrate} = 0.6 \cdot 10^{-3}$ m^3; A_{AEM}, $A_{CEM} = 0.01$ m^2; $I = 0.1\text{-}3$ A				

[*]*weighted average of* $D_i = \sum_i c_i \cdot D_i / \sum_i c_i$ *, where* D_{Na+}=13.34, D_{K+}=19.57, D_{Ca2+}=7.92 *and* D_{Mg2+}=7.06·10^{-10} m^2/s

Regarding the North Sea water (Table 2, *composition 2*), the initial molar concentration of sulphate is approximately 19.5 times smaller than the chlorine concentration. The molar divalent cation concentration is about 7.5 times smaller than the monovalent cation concentration. Equation 1 shows that the ion concentration has a larger effect than the diffusion coefficient on the ion flux. The smaller D value for divalent ions compared to monovalent ions (about 2-3 times smaller [65, 66]) is, as seen in equation 1, partly compensated by the higher ion valence (z). As such, it can be stated that the difference in ion concentration will mainly determine the difference in ion flux. This is supported by the fact that the monovalent potassium ions were found to have a similar shape of the curve for residual ions in the diluate (Figure 5), as the divalent magnesium and calcium (Figure 2 B).
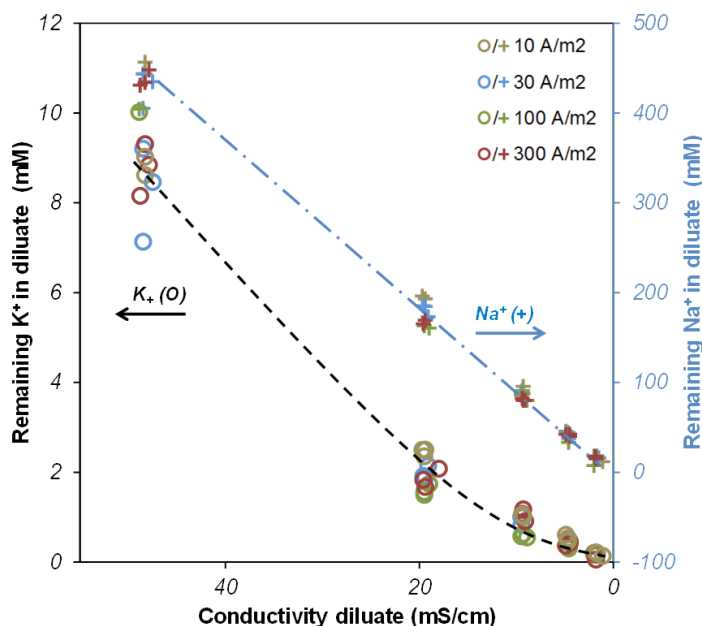
Figure 5. Measured remaining sodium (+) and potassium (O) concentrations (mM) in the diluate during desalination of an artificial North Sea water mixture (Na⁺, Ca²⁺, Mg²⁺, Cl⁻ and SO₄²⁻) Trend lines are drawn through the measurement data clouds of sodium (blue stripe-dot) and potassium (black stripe).

At the applied current densities in this study, concentration polarization effects are considerable. An increase of applied j results in steeper concentration gradients in the SDL. Due to the higher diffusion coefficients of the monovalent ions compared to divalent ions [65, 66] and due to higher concentrations of monovalent ions in the bulk solution, concentration polarization is less pronounced for monovalent ions. This is also found when considering the NP flux equation (equation 1), where the difference in fluxes for monovalent and divalent ions is directly related to the ion concentration and diffusion coefficient of the ionic specie. An increase in the SDL thickness would therefore result in an increased transport of monovalent ions. Thickness of the SDL can be influenced to a certain extent by the hydrodynamic conditions, such as applied cross flow velocity, type of spacer, and stack design [41, 59, 67]. By adjusting this control and design parameters the transport numbers can be influenced. If the SDL thickness has been changed, also another r_i value will be obtained, as the thickness is indirectly included in this ratio (Theory section).
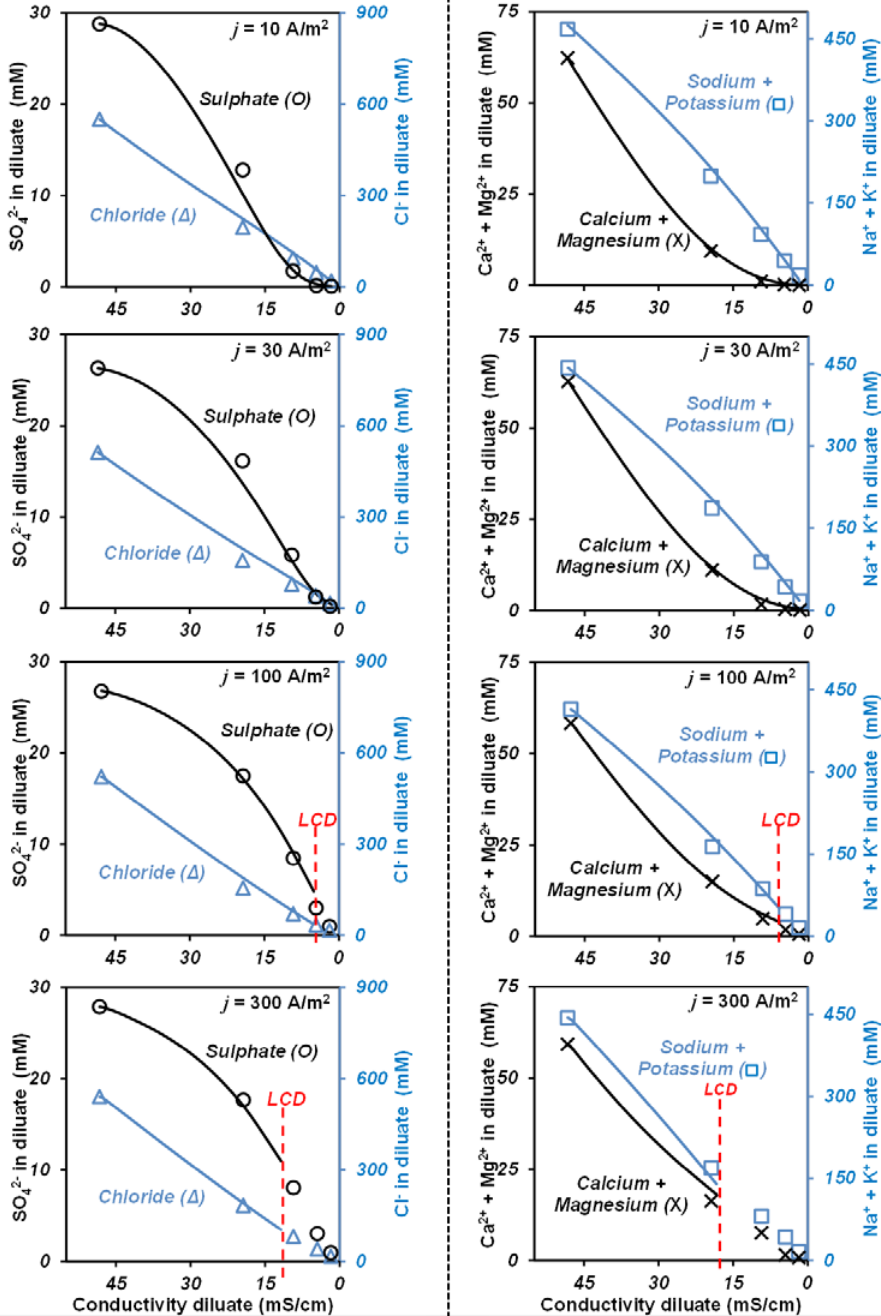
Figure 6. Measured remaining monovalent (blue, right axis) and divalent ion (black, left axis) concentration (mM) in the diluate during desalination of an artificial North Sea water mixture (Na$^+$, K$^+$, Ca^{2+}, Mg^{2+}, Cl$^-$ and SO$_4^{2-}$) at an applied current varying from 10-300 A/m^2 and their modeled ion concentrations (solid line) and limiting current density (LCD).

For the AEM, the ratio between external and internal diffusivity coefficients used for fitting were found to be 10 for monovalent anions and much higher for divalent anions (ranging from 390 at j =300 A/m2 to 1150 at j = 10 A/m²). To obtain a good fit for remaining sulphate in the diluate it was necessary to assume the diffusion coefficient for sulphate in the membrane to be dependent on the applied current density. It was found that the diffusion coefficient of sulphate (membrane) apparently decreases with increasing applied current density. In the present work we observed the empirical relation $r = 2400 \cdot j^{-0.32}$, $\overline{D}_{SO4} = \dfrac{D_{SO4}}{2400 \, j^{-0.32}}$.

This dependency on the applied current density implies that an improved membrane diffusion model is required which should possibly incorporate effects of ion-ion friction in the membrane, or the effect of the solvent flow [68-70]. According to these diffusion coefficients, sulphate ions have a much higher affinity to the AEM than the chloride ions, especially at lower applied current densities. This difference in affinity influences the observed selectivity, what gains importance when concentration polar-ization effects are reduced. Despite of this, sulphate is selectively transported at higher desalination extent and at lower applied current densities due to differences in initial concentrations for chloride and sulphate, differences in diffusivities for chloride and sulphate, and concentration polarization.

When transport of counterions through the CEM and the AEM is compared, the mon-ovalent-divalent ionic ratio of cations maximally increases about 60 times and of anions about 20 times. The difference in affinity of these membranes for divalent ions is partially responsible for this difference in obtained monovalent-divalent ratios. At low applied current density, when the influence of the membrane affinity is expected to be the largest, divalent ions are transported preferentially, which shows that most of the 'membrane selectivity' is actually due to the transport phenomena in the SDL.

The transport numbers of sulphate were calculated from the modeled graphs and are shown in Figure 7. This figure confirms that at low applied current density the observed maximum transport numbers is reached earlier in the desalination process. What is also shown is that indeed the obtained monovalent over divalent ion ratio has a maximum, because the transport number is decreasing till almost zero when the divalent ion concentration in the diluate is nearly depleted.
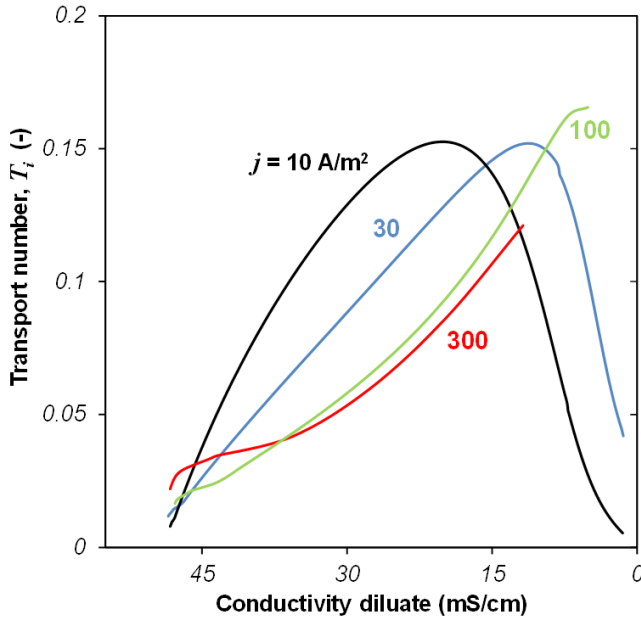
Figure 7. Modeled transport number T_i (-) of SO_4^{2-}, at different applied current densities (10, 30, 100 and 300 A/m²) as a function of the extent of desalination, represented by the conductivity (mS/cm).

Finally, the used model also predicts the extent of desalination when the LCD is reached. The LCD value in the model was reached when the calculated concentrations in the SDL, adjacent the membrane were approaching zero. These modeled values are indicated by a red dotted line in Figure 6 and very well represent the measured values given in Table 3. Only for the diagram of cations with $j = 300$ A/m² this LCD value is not accurately predicted. Possibly this is due to the fact that a ternary mixture of monovalent and divalent ions with chloride was modeled instead of the artificial seawater. Other reasons can be that i) there is a bit of convection taking place (not modeled) that postpones the LCD effects or, ii) due to a local pH shift the membrane is losing some of the effective charge, what leads to lower membrane permselectivity [53].

3.5.3 Use of preferential removal of multivalent ions in desalination with ED

Results shows that the monovalent ion over divalent ion ratio can be increased during desalination with ED operated at low applied current density. A low applied current density, however, makes the process economically less feasible and without further development of low-cost membranes, in practice unattractive for seawater (pre)desali-

nation. As shown by the data, it would be possible to desalinate with a high current density at larger solution conductivity in the first ED stages, and start to fractionate the monovalent and divalent ions (at low applied current density) at later ED stages when conductivity levels are lower. If ED can be used as a predesalination technique for seawater desalination as proposed in [4, 5] scaling potentials of divalent cations and sulphate can be lowered as their relative concentration can be reduced substantially (ratio monovalent ion of divalent ion is increased), especially when lowering the applied current density (as seen at an applied current density of $10 \, A/m^2$). With respect to sulphate removal, this study showed that by applying low current density ($10 \, A/m^2$) the sulphate content of the diluate can be lowered to a larger extent (99.9% removal) than compared to chloride (96.1% removal).

The concentration of divalent ions on the concentrate side is increased during desalination. Precipitation of e.g. $CaSO_4$ can become a scaling problem in membrane systems. During the performed experiments, the water recovery was always below 50% and concentrate concentrations were not high enough to induce precipitation. With the OLI analyzer studio 3.1 software (OLI systems Inc. USA) it was calculated that scaling of gypsum ($CaSO_4 \cdot H_2O$) may occur at a water recovery of over 74% (at 25 °C). As high water recovery is desired, scaling tendencies of especially $CaSO_4$ must be considered. Precipitation in highly concentrated solutions, treated by electrodialysis, was investigated by Korngold et al. [28, 29] and Oren et al. [71]. These studies show that with electrodialysis reversal (EDR), acidification and with a side loop crystallizer it is possible to obtain high solute concentrations without scaling problems on the membrane. Turek et al. [27, 72, 73] presented an alternative approach using hydrodynamic conditions within the stack to avoid precipitation at supersaturated $CaSO_4$ conditions. Both approaches show that EDR can be used at supersaturated conditions without scaling. Consequently, a high water recovery (>90%) should be obtainable.

3.6 Conclusion

A relation between applied current density and desalination with preferential removal of divalent ions was found. This relation was found in a ternary mixture of NaCl and Na_2SO_4 as well as in artificial North Sea water. It was shown that the lower initial ion concentration of Ca^{2+}, Mg^{2+}, SO_4^{2-} and K^+ will lead to larger concentration polarization of these ions in the stagnant diffusion layer, compared to Na^+ and Cl^-. For both cations and anions, the ratio of monovalent ions over divalent ions in the diluate will become larger at lower applied current densities. It was shown to be possible to remove divalent ions at a relative larger extent than monovalent ions.

3.7 Literature

[1] H. Strathmann, Electrodialysis, a mature technology with a multitude of new applications, Desalination, 264 (2010) 268-288.

[2] L.F. Greenlee, D.F. Lawler, B.D. Freeman, B. Marrot, P. Moulin, Reverse osmosis desalination: Water sources, technology, and today's challenges, Water Research, 43 (2009) 2317-2348.

[3] M. Al-Shammiri, M. Safar, Multi-effect distillation plants: State of the art, Desalination, 126 (1999) 45-59.

[4] J.W. Post, H. Huiting, E.R. Cornelissen, H.V.M. Hamelers, Pre-desalination with electro-membranes for SWRO, Desalination and Water Treatment, 31 (2011) 296-304.

[5] A.H. Galama, M. Saakes, H. Bruning, H.H.M. Rijnaarts, J.W. Post, Seawater Predesalination with Electrodialysis, Desalination, 342 (2013) 61-69.

[6] C.Y. Tang, T.H. Chong, A.G. Fane, Colloidal interactions and fouling of NF and RO membranes: A review, Advances in Colloid and Interface Science, 164 (2011) 126-143.

[7] A.S. Al-Amoudi, Factors affecting natural organic matter (NOM) and scaling fouling in NF membranes: A review, Desalination, 259 (2010) 1-10.

[8] A.Y. Al-Borno, M. Abdel-Jaward, Conventional pretreatment of surface seawater for reverse osmosis application, state of the art, Desalination, 74 (1989) 3-36.

[9] M. Rodríguez Pastor, A. Ferrándiz Ruiz, M. Chillon, D. Prats Rico, Influence of pH in the elimination of boron by means of reverse osmosis, Desalination, 140 (2001) 145-152.

[10] N. Hilal, H. Al-Zoubi, N.A. Darwish, A.W. Mohammad, Performance of nanofiltration membranes in the treatment of synthetic and real seawater, Separation Science and Technology, 42 (2007) 493-515.

[11] G. Klein, S. Cherney, E.L. Ruddick, T. Vermeulen, Calcium removal from sea water by fixed-bed ion exchange, Desalination, 4 (1968) 158-166.

[12] F.G. Helfferich, Ion Exchange, McGraw-Hill, New York, (1962).

[13] T. Vermeulen, B.W. Tleimat, G. Klein, Ion-exchange pretreatment for scale prevention in desalting systems, Desalination, 47 (1983) 149-159.

[14] J. Schaep, C. Vandecasteele, Evaluating the charge of nanofiltration membranes, Journal of Membrane Science, 188 (2001) 129-136.

[15] B. Van Der Bruggen, A. Koninckx, C. Vandecasteele, Separation of monovalent and divalent ions from aqueous solution by electrodialysis and nanofiltration, Water Research, 38 (2004) 1347-1353.

[16] Y. Zhang, S. Paepen, L. Pinoy, B. Meesschaert, B. Van Der Bruggen, Selectrodialysis: Fractionation of divalent ions from monovalent ions in a novel electrodialysis stack, Separation and Purification Technology, 88 (2012) 191-201.

[17] L. Llenas, X. Martínez-Lladó, A. Yaroshchuk, M. Rovira, J. de Pablo, Nanofiltration as pretreatment for scale prevention in seawater reverse osmosis desalination, Desalination and Water Treatment, 36 (2011) 310-318.

[18] F. Macedonio, E. Curcio, E. Drioli, Integrated membrane systems for seawater desalination: energetic and exergetic analysis, economic evaluation, experimental study, Desalination, 203 (2007) 260-276.

[19] S. Van Geluwe, L. Braeken, T. Robberecht, M. Jans, C. Creemers, B. Van Der Bruggen, Evaluation of electrodialysis for scaling prevention of nanofiltration membranes at high water recoveries, Resources, Conservation and Recycling, 56 (2011) 34-42.

[20] P. Eriksson, M. Kyburz, W. Pergande, NF membrane characteristics and evaluation for sea water processing applications, Desalination, 184 (2005) 281-294.

[21] B.E. Ryabchikov, A.A. Panteleev, M.G. Gladush, Performance testing of seawater desalination by nanofiltration, Petroleum Chemistry, 52 (2012) 465-474.

[22] M. Pontié, J.S. Derauw, S. Plantier, L. Edouard, L. Bailly, Seawater desalination: Nanofiltration-A substitute for reverse osmosis?, Desalination and Water Treatment, 51 (2013) 485-494.

[23] A. AlTaee, A.O. Sharif, Alternative design to dual stage NF seawater desalination using high rejection brackish water membranes, Desalination, 273 (2011) 391-397.

[24] A.A. Al-Hajouri, A.S. Al-Amoudi, A.M. Farooque, Long term experience in the operation of nanofiltration pretreatment unit for seawater desalination at SWCC SWRO plant, Desalination and Water Treatment, 51 (2013) 1861-1873.

[25] C. Fritzmann, J. Löwenberg, T. Wintgens, T. Melin, State-of-the-art of reverse osmosis desalination, Desalination, 216 (2007) 1-76.

[26] AmericanWaterWorksAssociation, Electrodialysis and Electrodialysis Reversal, manual of water supply practices M38, AWWA, Denver USA, 1999.

[27] M. Turek, P. Dydo, Electrodialysis reversal of calcium sulphate and calcium carbonate supersaturated solution, Desalination, 158 (2003) 91-94.

[28] E. Korngold, L. Aronov, N. Belayev, K. Kock, Electrodialysis with brine solutions oversaturated with calcium sulfate, Desalination, 172 (2005) 63-75.

[29] E. Korngold, L. Aronov, N. Daltrophe, Electrodialysis of brine solutions discharged from an RO plant, Desalination, 242 (2009) 215-227.

[30] Y. Tanaka, R. Ehara, S. Itoi, T. Goto, Ion-exchange membrane electrodialytic salt production using brine discharged from a reverse osmosis seawater desalination plant, Journal of Membrane Science, 222 (2003) 71-86.

[31] M. Reig, S. Casas, C. Aladjem, C. Valderrama, O. Gibert, F. Valero, C.M. Centeno, E. Larrotcha, J.L. Cortina, Concentration of NaCl from seawater reverse osmosis brines for the chlor-alkali industry by electrodialysis, Desalination, 342 (2014) 107-117.

[32] M. Amara, H. Kerdjoudj, A modified anion-exchange membrane applied to purification of effluent containing different anions. Pre-treatment before desalination, Desalination, 206 (2007) 205-209.

[33] L. Firdaous, J.P. Malériat, J.P. Schlumpf, F. Quéméneur, Transfer of monovalent and divalent cations in salt solutions by electrodialysis, Separation Science and Technology, 42 (2007) 931-948.

[34] T. Sata, Ion Exchange Membranes; Preparation, Characterization, Modification and Application, The Royal Society of Chemistry, Cambridge UK, 2004.

[35] A. Chapotot, G. Pourcelly, C. Gavach, Transport competition between monovalent and divalent cations through cation-exchange membranes. Exchange isotherms and kinetic concepts, Journal of Membrane Science, 96 (1994) 167-181.

[36] F. Quéméneur, J.P. Schlumpf, L. Firdaous, M. Stitou, J.P. Malériat, P. Jaouen, Modification of ionic composition of natural salt-waters by electrodialysis, Desalination, 149 (2002) 411-416.

[37] M. Turek, Dual-purpose desalination-salt production electrodialysis, Desalination, 153 (2003) 377-381.

[38] S. Myhr, B.L. Lillebø, E. Sunde, J. Beeder, T. Torsvik, Inhibition of microbial H2S production in an oil reservoir model column by nitrate injection, Applied Microbiology and Biotechnology, 58 (2002) 400-408.

[39] N. Kabay, Ö. Ipek, H. Kahveci, M. Yüksel, Effect of salt combination on separation of monovalent and divalent salts by electrodialysis, Desalination, 198 (2006) 84-91.

[40] N. Kabay, H. Kahveci, Ö. Ipek, M. Yüksel, Separation of monovalent and divalent ions from ternary mixtures by electrodialysis, Desalination, 198 (2006) 74-83.

[41] Y. Kim, W.S. Walker, D.F. Lawler, Electrodialysis with spacers: Effects of variation and correlation of boundary layer thickness, Desalination, 274 (2011) 54-63.

[42] Y. Kim, W.S. Walker, D.F. Lawler, Competitive separation of di- vs. mono-valent cations in electrodialysis: Effects of the boundary layer properties, Water Research, 46 (2012) 2042-2056.

[43] C. Forgacs, N. Ishibashi, J. Leibovitz, J. Sinkovic, K.S. Spiegler, Polarization at ion-exchange membranes in electrodialysis, Desalination, 10 (1972) 181-214.

[44] P. Moon, G. Sandí, D. Stevens, R. Kizilel, Computational modeling of ionic transport in continuous and batch electrodialysis, Separation Science and Technology, 39 (2004) 2531-2555.

[45] V.A. Shaposhnik, O.V. Grigorchuk, Mathematical model of electrodialysis with ion-exchange membranes and inert spacers, Russian Journal of Electrochemistry, 46 (2010) 1182-1188.

[46] A.A. Sonin, R.F. Probstein, A hydrodynamic theory of desalination by electrodialysis, Desalination, 5 (1968) 293-329.

[47] K.S. Spiegler, Polarization at ion exchange membrane-solution interfaces, Desalination, 9 (1971) 367-385.

[48] Y. Tanaka, Concentration polarization in ion-exchange membrane electrodialysis—the events arising in a flowing solution in a desalting cell, Journal of Membrane Science, 216 (2003) 149-164.

[49] J.G. Crespo, K.W. Böddeker, Membrane Processes in Separation & Purification, Kluwer Academic Publishers, Dordrecht NL, 1993.

[50] K. Kontturi, L. Murtomäki, J.A. Manzanares, Ionic Transport Processes : in Electrochemistry and Membrane Science: in Electrochemistry and Membrane Science, OUP Oxford, 2008.

[51] A.H. Galama, J.W. Post, M.A. Cohen Stuart, P.M. Biesheuvel, Validity of the Boltzmann equation to describe Donnan equilibrium at the membrane-solution interface, Journal of Membrane Science, 442

(2013) 131-139.

[52] H. Strathmann, Ion-exchange membrane separation processes, Elsevier, Amsterdam NL, 2004.

[53] M.B. Andersen, M. Van Soestbergen, A. Mani, H. Bruus, P.M. Biesheuvel, M.Z. Bazant, Current-induced membrane discharge, Physical Review Letters, 109 (2012) 108301.

[54] A. Kitamoto, Y. Takashima, Transfer rates in electrodialysis with ion exchange membranes, Desalination, 9 (1971) 51-87.

[55] R. French, Unstirred layer effects on calculations of the potential difference across an ion exchange membrane, Biophysical Journal, 18 (1977) 53-61.

[56] R. Zhao, O. Satpradit, H.H.M. Rijnaarts, P.M. Biesheuvel, A. van der Wal, Optimization of salt adsorption rate in membrane capacitive deionization, Water Research, 47 (2013) 1941-1952.

[57] T. Teorell, Progress in biophysical chemistry, Academic Press Inc., New York USA, 1953.

[58] D.A. Vermaas, M. Saakes, K. Nijmeijer, Doubled Power Density from Salinity Gradients at Reduced Intermembrane Distance, Environmental Science and Technology, 45 (2011) 7089-7095.

[59] P. Długołęcki, P. Ogonowski, S.J. Metz, M. Saakes, K. Nijmeijer, M. Wessling, On the resistances of membrane, diffusion boundary layer and double layer in ion exchange membrane transport, Journal of Membrane Science, 349 (2010) 369-379.

[60] H. Miyoshi, Diffusion coefficients of ions through ion-exchange membranes for Donnan dialysis using ions of the same valence, Chemical Engineering Science, 52 (1997) 1087-1096.

[61] H. Miyoshi, Diffusion coefficients of ions through ion excange membrane in Donnan dialysis using ions of different valence, Journal of Membrane Science, 141 (1998) 101-110.

[62] G. Pourcelly, P. Sistat, A. Chapotot, C. Gavach, V. Nikonenko, Self diffusion and conductivity in NafionR membranes in contact with NaCl+CaCl2 solutions, Journal of Membrane Science, 110 (1996) 69-78.

[63] M. Higa, A. Tanioka, K. Miyasaka, An experimental study of ion permeation in multicomponent ion systems as a function of membrane charge density, Journal of Membrane Science, 64 (1991) 255-262.

[64] P.N. Pintauro, R. Tandon, L. Chao, W. Xu, R. Evilia, Equilibrium partitioning of monovalent/bivalent cation-salt mixtures in nafion cation-exchange membranes, Journal of Physical Chemistry, 99 (1995) 12915-12924.

[65] L. Yuan-Hui, S. Gregory, Diffusion of ions in sea water and in deep-sea sediments, Geochimica et Cosmochimica Acta, 38 (1974) 703-714.

[66] CRC Handbook of Chemistry and Physics, 85th ed., Boca Raton (Florida, U.S.A.), 2004.

[67] D. Vermaas, M. Saakes, K. Nijmeijer, Power generation using profiled membranes in reverse electrodialysis, Journal of Membrane Science, 385-386 (2011) 234-242.

[68] P.M. Biesheuvel, Two-fluid model for the simultaneous flow of colloids and fluids in porous media, Journal of Colloid and Interface Science, 355 (2011) 389-395.

[69] J.A. Wesselingh, P. Vonk, G. Kraaijeveld, Exploring the Maxwell-Stefan description of ion exchange, The Chemical Engineering Journal and the Biochemical Engineering Journal, 57 (1995) 75-89.

[70] K.S. Spiegler, Transport processes in ionic membranes, Transactions of the Faraday Society, 54 (1958) 1408-1428.

[71] Y. Oren, E. Korngold, N. Daltrophe, R. Messalem, Y. Volkman, L. Aronov, M. Weismann, N. Bouriakov, P. Glueckstern, J. Gilron, Pilot studies on high recovery BWRO-EDR for near zero liquid discharge approach, Desalination, 261 (2010) 321-330.

[72] M. Turek, K. Mitko, M. Chorzewska, P. Dydo, Use of the desalination brines in the saturation of membrane electrolysis feed, Desalination and Water Treatment, 51 (2013) 2749-2754.

[73] M. Turek, P. Dydo, J. Waś, Electrodialysis reversal in high CaSO4 supersaturation mode, Desalination, 198 (2006) 288-294.

Chapter 4

Fractioning electrodialysis: a current induced ion exchange process

Abstract

In desalination often multi ionic compositions are encountered. A preferential removal of multivalent ions over monovalent ions can be of interest to prevent scaling in the desalination process. Recently, a novel fractionating electrodialysis stack is described by Zhang *et al.* 2012 (in *Sep. purify. Technol. 88*). In the present work a small modification to such a stack was made, to create a current induced ion exchange process, in which no longer desalination occurs. This was done by building a membrane stack in which monovalent-selective ion-exchange membranes and standard grade ion-exchange membranes, with similar charge sign (so either anion or cation exchange groups), were placed alternatingly between an anode and a cathode to form a membrane stack. A proof of principle of the fractioning electrodialysis technology is given. Ternary mixtures, with a divalent-monovalent ion ratio similar to seawater, were used as feed water. For a cation and an anion fractioning stack, maximum fractionations of divalent ions were obtained of approximately 90 and 60%. At higher applied current density, ions can be fractionated to a larger extent than at lower applied current density. For both stacks the water recovery was ~50%. Coulombic efficiency of both processes decrease rapidly after the start of the experiment. This leads to relatively large volumetric energy consumptions.

Nomenclature

c	=	concentration (mol/m^3)
F	=	Faraday constant (C/mol)
I	=	current (A)
N	=	number of membrane pairs (-)
n	=	number of moles (mol)
Q	=	charge (C)
r	=	water recovery factor (-)
t	=	time (s)
V	=	volume (m^3)
X	=	fixed membrane charge (mol/m^3)
z	=	ion valence (-)
β	=	unit conversion factor (kWh/J)
η	=	coulombic efficiency (-)
$\widetilde{\mu}$	=	electrochemical potential (J/mol)
ξ	=	membrane porosity (-)
τ	=	endpoint time interval (s)
ϕ	=	potential (V)

4.1 Introduction

In desalination often multi ionic compositions are encountered. A preferential removal of multivalent ions over monovalent ions can be of interest to in order to meet quality standards, or to prevent scaling in subsequent processes [1]. It can be required to lower the total dissolved solids (TDS), but often just a selective decrease of specific ions is needed. Especially the separation (or fractionation) of monovalent and multivalent ions in saline streams can be challenging [2]. As an example, sulfate should be removed from seawater before it is injected in oil reservoirs to avoid sulfate scaling in the wells or souring of the reservoirs. At the same time the injection water needs compatible TDS of the reservoir formation water [3]. State-of-the-art ion exchangers or nanofiltration membranes could provide, to a certain extent, a selective removal of divalent ions from a saline feed water [4]. However, the nanofiltration process may need relatively high feed pressure when applied on a feed water with a high level of TDS [5]. Ion exchange resins also could provide a selective ion removal, even without lowering the TDS. Despite the fact that divalent ions have a higher affinity to the ion exchange resin than monovalent ions, the ion exchange process becomes less effective when the resin is equilibrated with a feed water with high concentrations of monovalent ions (i.e., a high TDS).

Recently, a novel fractionating electrodialysis stack is described in the work of Zhang *et al.* (2012) [6]. This electrochemical process (called 'selectrodialysis') is capable to separate ions of the same charge sign but different valence. It consists of a repetitive arrangement of three compartments which are formed by stacking a non-selective cation-exchange membrane (CEM), a non-selective anion-exchange membrane (AEM), and a monovalent-selective anion-exchange membrane (mvs-AEM). When an electric field (i.e. current) is applied over this stack, three major effects occur. The feed water between the CEM and AEM is getting lower in TDS. The multivalent ion concentration in the product between the AEM and the mvs-AEM increases (without a considerable change in TDS). The TDS in the brine between the mvs-AEM and CEM increases. Hence, in this process desalination is taking place (salt is transferred from feed to brine) combined with fractionation (multivalent ions are collected in a separate product). With a first concept of this stack a desalination of feed water containing 8 mM NaCl and 8 mM Na_2SO_4 was demonstrated, combined with fractionation resulting in a Na_2SO_4 solution with a purity of over 85% [6].

Only a small modification of this process is needed to make this process a pure fractioning process, i.e. without desalination work. This can be achieved by leaving the CEM out of the configuration. In this fractioning electrodialysis, the applied current

is merely used to exchange multivalent ions for monovalent ions of same charge sign. Such an electrodialysis stack contains ion exchange membranes (IEMs) with fixed charged groups of the same charge sign; either AEMs or CEMs. Monovalent-selective ion-exchange membranes (mvs-IEMs) and non-selective ion-exchange membranes were placed alternatingly between an anode and a cathode to form a membrane stack. The principle of this fractionating electrodialysis stack for anions is given in Figure 1 (for a cation fractionating electrodialysis stack, the AEMs are replaced for CEMs and the mvs-AEMs for mvs-CEMs).
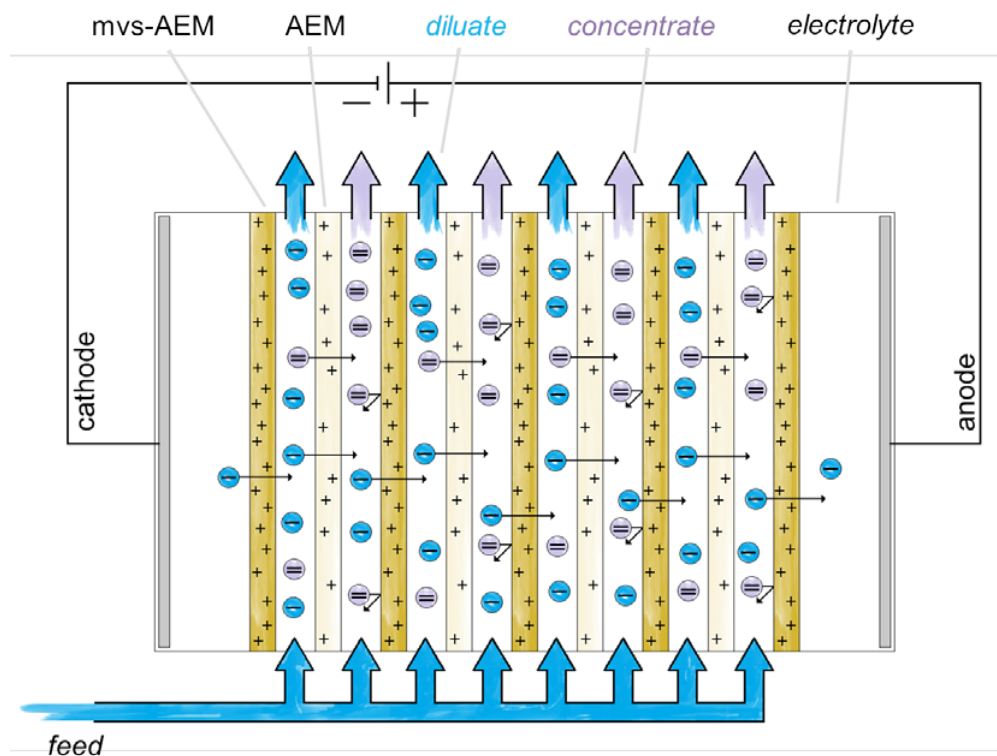
Figure 1. Schematic representation of an anion fractioning electrodialysis stack. Where, AEM indicates an anion exchange membrane and mvs-AEM a monovalent selective anion exchange membrane.

When an electric field is applied, anions migrate in direction of the anode. Monovalent anions transfer through both the non-selective AEMs and the mvs-AEMs, whereas divalent anions transfer through the non-selective AEM and are retained by the mvs-AEMs. As a result, in the compartment between an mvs-AEM and a non-selective AEM, the concentration of the multivalent ions is decreasing and the concentration of monovalent ions is increasing; and in the compartment between a non-selective AEM

and an mvs-AEM, vice versa. Overall, the multivalent ions in the one compartment are exchanged for monovalent ions in the other by applying a current. In this paper, the batch with lowering concentration of divalent ions is referred to as 'divalent diluate' and the batch with increasing concentration of divalent ions is referred to as 'divalent concentrate'.

In this work a proof of principle of the fractioning electrodialysis is given for seawater applications. Experiments are carried out both for fractionation of cations (sodium, magnesium) and of anions (chloride, sulfate) from ternary mixtures with relatively high sodium chloride concentrations. The coulombic efficiency and the energy consumption of these fractioning processes were investigated as well.

4.2 Theory

It can be hypothesized that the success of the fractioning electrodialysis may be determined by following factors: (i) the selectivity of monovalent-selective ion-exchange membranes, (ii) the differences in migration of monovalent and divalent ions through the non-selective ion-exchange membranes and the respective stagnant diffusion layers (SDLs), and (iii) the back diffusion resulting from concentration gradients over the membrane.

The monovalent selectivity of monovalent-selective membranes is reasonable but limited [2, 7-9] and therefore a perfect separation in the fractioning electrodialysis should not be expected. The standard-grade membranes are not selective between monovalent and divalent ions, at least not in an application on seawater at the early stages of desalination [1], and therefore the efficiency of the process will largely depend on the concentration ratio between monovalent and divalent ions. The fractioning electrodialysis efficiency will decrease with increasing monovalent ion concentration.

Membranes are not perfectly perm selective and therefore substantial back diffusion from the high concentration side towards the low concentration side will occur [10]. Because this transport of ions is in opposite direction of the migration, the back diffusion has a negative influence on the coulombic efficiency of the system. Despite the fact that the concentration gradient in terms of TDS is almost absent in the fractioning electrodialysis stack, the concentration gradient of the divalent (and monovalent) ions causes diffusion of these ions. In a stack as shown in Figure 1, concentration gradients of monovalent ions and divalent ions are in opposite direction, as a result enforced by the diffusion potential also inter-diffusion of ions can take place [11-14]. So diffusion of ions in direction opposite of the migration (back diffusion) will take place.

If a concentration gradient is present over a membrane a membrane potential arises. This membrane potential that is present when no electrical current is applied is referred to as the open cell voltage (OCV) and this potential increases with an increasing gradient in chemical potential. The OCV indicates the change in entropy of the system and represents the potential that can be regained in the reversed process. This OCV is partly formed due to unequal mobility of the diffusing co-ions and counterions, which causes a charge separation and as such an electric potential (diffusion potential) that is aiding the slower ion [11, 15, 16]. Another part of the membrane potential arises due to the ion concentration difference of the solution in the membrane and the surrounding solution. This potential, formed at both membrane-water interface is known as the Donnan potential drop [12, 17]. The membrane potential, ϕ_m (V) can be estimated by [11, 18-20]:

$$\phi_m = \Delta\phi_D^{'} - \Delta\phi_D^{''} + \phi_{diff}$$

<div align="right">eq. 1</div>

Where $\Delta\phi_D^{'}$ and $\Delta\phi_D^{''}$ are the Donnan potential drops on both membrane-water interfaces and ϕ_{diff} is the diffusion potential. When two permeating counterions are present, as in case of fractioning electrodialysis, the membrane potential is known as the bi-ionic potential [11, 13, 21]. When ion valences of the permeating ionic species are dissimilar, an estimation of the bi-ionic potential is rather complex [11, 22-24], as the concentration gradients, the activity coefficients and the diffusion potentials of the individual ions in the membrane are required as input [11]. In general divalent ions were found to have a lowering effect on the membrane potential [25, 26].

4.3 Materials and Methods

4.3.1 Materials

The fractioning electrodialysis stack comprised fourteen cell pairs and two electrode compartments. Every repeating cell pair in the membrane stack consists of a divalent diluate and a divalent concentrate compartment, formed with silicone gaskets (~500 μm). These compartments contained a woven PET fabric spacer (Nitex 06-700/53, Sefar, Switzerland). The divalent diluate and the divalent concentrate flow channels are alternatingly separated by a standard grade ion exchange membrane (Neosepta CMX / AMX; Tokuyama Co., Japan) and a monovalent selective ion exchange membrane (Neosepta CMS / ACS; Tokuyama Co., Japan). These membranes possess high chemical stability. An extra monovalent selective exchange membrane was used to close the stack and separate the last cell pair and the electrode compartment. The total

area of each square shaped membrane was 104 cm². On both sides of the membrane stack a squared electrode was placed in the electrode compartments. As anode a titanium electrode (mesh 1.7, area 96.04 cm²) with a mixed metal oxide coating was used (Magneto Special Anodes BV, The Netherlands), as cathode a titanium electrode (mesh 1.7, area 96.04 cm²) with a 50 g/m² platinum coating was used (Magneto Special Anodes BV, The Netherlands).

4.3.2 Methods

Experiments were done with an anion fractioning electrodialysis stack and a cation fractioning electrodialysis stack. For both type of stacks a ternary mixture was used as feed water. For anion fractioning this ternary mixture contained sodium, chloride and sulfate ions. For cation fractioning this ternary mixture contained chloride, sodium and magnesium ions. Compositions of these ternary mixtures are given in Table 1. These compositions were based on the North Sea water concentrations of the counterions (ions with a charge opposite to the membrane).

Table 1. Composition of the ternary solutions used in the fractioning electrodialysis experiments.

Ion	Anion ternary mixture		Cation ternary mixture	
	g/L	*mol/L*	*g/L*	*mol/L*
Na^+	11.150	0.485	11.15	0.485
Mg^{2+}	-	-	1.41	0.058
Cl^-	15.126	0.427	21.31	0.601
SO_4^{2-}	2.800	0.029	-	-
Total	**29.076**		**33.87**	

The flow rate was set to 15.0 ml/min per channel (0.5 cm/s). Experiments were done in a recirculating batch mode, in which the batch was kept in a glass bottle that was continuously stirred. These batches had a volume of 340 ml (including the internal volume of tubes and compartments) at the start of the experiment. Throughout the experiments the weight changes of the batches were measured and registered as explained in [27].

The actual composition of the batches was measured by periodically taking samples of these batches from the bottles (in total up to 7 samples of 5 ml). These samples were prepared for analysis by dilution with an auto diluter apparatus (ML530B, Hamilton). Anions were measured by ion chromatography (IC, 761 Compact IC, Metrohm) and cations by inductive-coupled plasma optical emission spectroscopy (ICP-OES, Optima 5300DV, Perkin Elmer). Samples for anion measurement were diluted 250 times and samples for cation measurement were diluted 1200 times. Before the start of the experiments, the membrane stack was equilibrated with the experimental salt solution

by recycling the solution trough the stack for a minimum time of 1 hour. Directly after the experiment the stack was flushed with a solution equal in composition with the start solution as to equilibrate the membranes before the next experiment.

A sodium chloride solution (29.22 g/l) was pumped through the anode compartment with a flow rate of 120 ml/min per compartment. At the anode, oxygen and chlorine is formed and the pH of the electrolyte is lowered. This anolyte is used as influent for the cathode compartment. After flowing through the cathode, where hydrogen is formed, the electrolyte was degasified and disposed.

The membrane stack voltage was measured with two Ag/AgCl reference electrodes (QM711X, QIS). These were placed at the inlet of the anode and cathode compartments. The potential difference of the two reference electrodes was measured with a high impedance preamplifier (-50/+50 V, Ext-ins technologies). A power supply (SM70-AR-24, Delta Elektronika) was used to apply a constant current. Actual values of potential and current were logged every second with a data logger (Memograph M RSG40, Endress+Hauser). Throughout the experiments, the temperature of the water was measured to be 20±2 °C. Temperature sensors were located in the solution stream directly in front of the ED stack and directly after the ED stack (i.e. 2 in the divalent diluate and 2 in the divalent concentrate). Presented experiments were reproducible and repeated at least two times. Electrodialysis was performed with a constant applied direct current. The applied current density was varied and set at 20, 100 or 200 A/m², where the area is referring to the active area of a single membrane.

4.3.3 Definitions

The purpose of the fractioning electrodialysis stack is to concentrate divalent ions. Therefore the coulombic efficiency, η_2 (-) is defined as the amount of divalent ions in the divalent diluate that is exchanged with monovalent ions from the divalent concentrate, Q_{exch} (C) per membrane pair N (-), divided by the applied electrical charge, $Q_{applied}$ (C):

$$Q_{exch} = \frac{(c_i^0 - c_i^\tau) \cdot z_i \cdot F \cdot V}{N} \qquad \text{eq. 2}$$

$$Q_{applied} = \int_0^\tau I dt \qquad \text{eq. 3}$$

$$\eta_2 = \frac{Q_{exch}}{Q_{applied}} \qquad \text{eq. 4}$$

Where, c is the ion concentration (mol/m³), z_i is the ion valence (-), F the Faraday constant (C/mol), V the volume of the solution (m³), I the applied current (A), t the time (s), and τ the end of the time interval (s). The ions that are initially present in the solution can be expressed as a charge. This charge ($Q_{initial}$) is given by:

$$Q_{initial} = \sum_i c_i \cdot z_i \cdot F \cdot V \qquad \text{eq. 5}$$

In this paper the ratio of the applied charge over the initial charge is taken as a measure for relative charge input in the system.

$$Q_{rel} = \frac{Q_{applied}}{Q_{initial}} \qquad \text{eq. 6}$$

Where Q_{rel} (-) is the relative charge applied to the system, which can be used to compare electrodialysis experiments with unequal applied current density and unequal starting volume. Water recovery, r (-) of the system is defined as the product (divalent diluate) fraction of the total water input.

$$r = \frac{V_d}{V_d + V_c} = \frac{V_d}{V_f} \qquad \text{eq. 7}$$

Where the subscripts f, d, and c refer to feed, divalent diluate and divalent concentrate.

4.4 Results

4.4.1 Cation fractioning stack

In the cation fractioning stack the purpose was to decrease the amount of divalent magnesium ions (Mg^{2+}) in one batch (divalent diluate) and concentrate it in the other batch (divalent concentrate). Sodium ions (Na^+) are effectively transported from the divalent concentrate to the divalent diluate, whilst the chloride ion (Cl^-) concentration is not expected to change as only cation exchange membranes are used. The relative change in cation concentration (%) is shown in Figure 2.
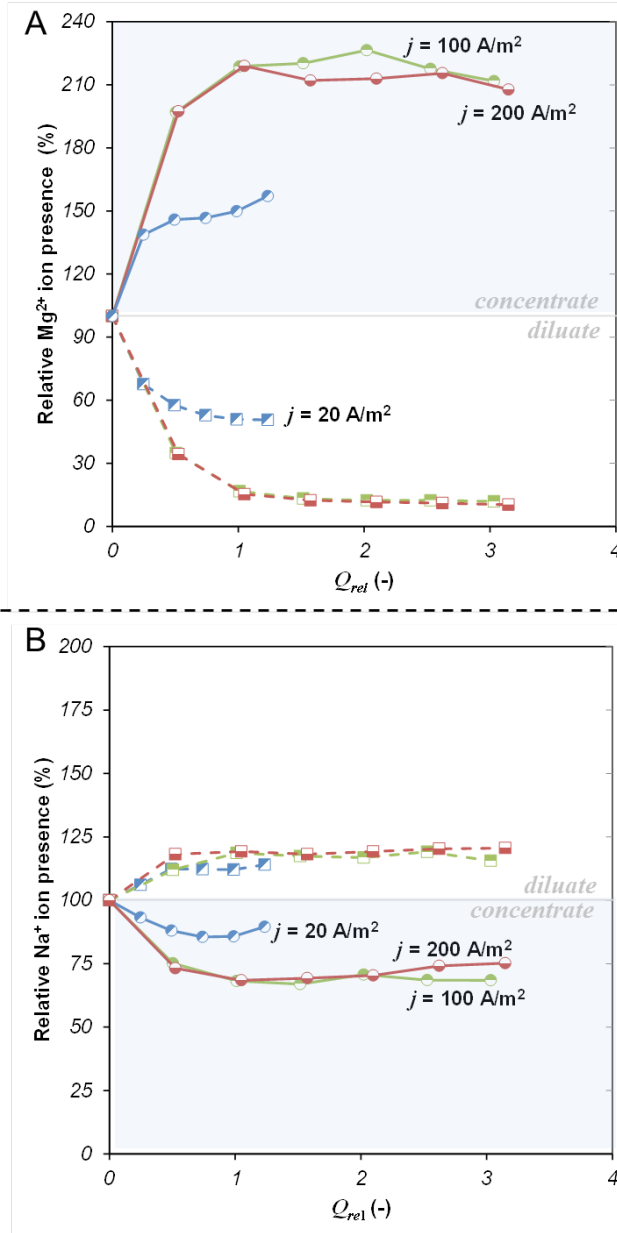
Figure 2. Measured Mg²⁺ (A) and Na⁺ (B) ion concentrations (%) in the divalent diluate (□) and in the divalent concentrate (○) at an applied current density of 20 (blue, diagonal filled), 100 (green, upper half filled) and 200 (red, lower half filled) A/m² as a function of the relative charge applied to the system. Q_{rel} is the applied charge ($Q_{applied}$) over the charge of the ions initially present in the divalent diluate ($Q_{initial}$).

Figure 2 shows the proof of principle for the current-induced ion exchange in an electrodialysis stack containing only CEMs. In the divalent diluate, the Mg^{2+} concentration was decreased and the Na^+ concentration was increased. Most of the ion exchange occurred in the beginning of the experiment, when a relative small amount of charge was applied. Results obtained at an applied current density of 100 and 200 A/m² do not differ significantly, however when the applied current density was 20 A/m², the obtained fractionation was much smaller.

Furthermore, it is shown that the Mg^{2+} ion concentration in the divalent concentrate is increased more than it is decreased in the divalent diluate. For the Na^+ ions this is the other way around, the decrease is larger than the increase. Water transport could have been an explanation for such differences (by effectively diluting the divalent concentrate and concentrating the divalent diluate), but no net water transport was observed during the experiments. However, the disappearing of monovalent ions and the appearing of divalent ions can be explained by the fact that under operating conditions the distribution of the monovalent and divalent counterions in the ion-exchange membranes is changing. Sorption experiments, under equilibrium conditions, show that divalent ions have a higher affinity to the IEM than the monovalent ions [11, 28-30]. Monovalent counterions that were originally present in the membrane are (partly) replaced by divalent ions, when the membrane stack is equilibrated in a solution containing divalent ions. When a current is applied, the affinity towards divalent ions may change [28, 31, 32], and divalent counterions are replaced by monovalent counterions. The results are further interpreted as follows. The amount of counterions (assuming no co-ions in the membrane) is approximately given by:

$$\sum_i z_i \overline{n_i} \approx (2N+1) \cdot V_{mem} \cdot \xi \cdot X \qquad \text{eq. 8}$$

Where $\overline{n_i}$ is the number of moles present in the membrane phases of the stack (mol), V_{mem} is the volume of the membrane (m³), ξ is the membrane porosity (-), X the fixed membrane charge density (mol/m³). With membrane porosity, $\xi = 0.327$, $X = 5700$ mol/m³ [33], and with the stack characteristics given in section 4.3, it can be calculated that at maximum ~25 mmol of divalent ions or ~50 mmol of monovalent ions can be present in the membranes. The number of moles that are initially present in the feed water, n_i (mol) is given by:

$$n_i = c_i \cdot V_{sol} \qquad \text{eq. 9}$$

Where c_i is the ion concentration (mol/m³) and V_{sol} is the volume of the solution (m³).

Initially ~165 mmol Na^+ and ~20 mmol Mg^{2+} was present. So if the membrane is equilibrated with the $NaCl/MgCl_2$ solution a substantial amount of Mg^{2+} ions might be present in the membrane prior to the experiment. This implies that that if ~30% of the fixed charge sites changes from divalent to monovalent counterion association, the change in concentration (observed in Figure 2) could be explained. A change in composition of the counterions in the membrane, may therefor explain the imbalance in Mg^{2+} concentrations between divalent diluate and divalent concentrate as shown in Figure 2.

4.4.2 Anion fractioning stack

In the anion fractioning stack the purpose was to decrease the amount of divalent sulfate ions (SO_4^{2-}) in one batch (divalent diluate) and concentrate it in the other batch (divalent concentrate). Consequently chloride ions (Cl^-) are transported from the divalent concentrate to the divalent diluate, whilst the sodium ion (Na^+) concentration is not expected to change as only anion exchange membranes are used. Change of the anion concentration (%) is shown in Figure 3.

Figure 3 shows that also in this stack configuration the principle of current induced ion exchange was also working. Concentration of SO_4^{2-} was lowered and concentration of Cl^- was increased in the divalent diluate. Also in this case fractionation of ions took place mostly in the beginning of the experiment, although it is less pronounced than with the cation fractioning stack.

A maximum ion separation is reached at a higher value of Q_{rel} and the obtained ion exchange is smaller than with the cation fractioning stack. Figure 3A shows that the divalent concentrate concentration of SO_4^{2-} of the experiment done with an applied current density of 200 A/m² is lower than when 100 A/m² was applied. Moreover, with an applied current density of 200 A/m², the concentration of SO_4^{2-} decreased after Q_{rel} = 1 both in the divalent diluate and in the divalent concentrate. This means that SO_4^{2-} disappears from the solutions either to the membranes (as previously explained, the counterion distribution may be subject to changes) or to the anode compartment. The divalent concentrate stream was separated from the anode compartment by a monovalent-selective anion-exchange membrane. Since this type of membrane is not perfectly selective a small loss could be expected. This loss will diminish when the number of membrane pairs is further increased. At higher applied current density more SO_4^{2-} ions were found to be transported to the anolyte.
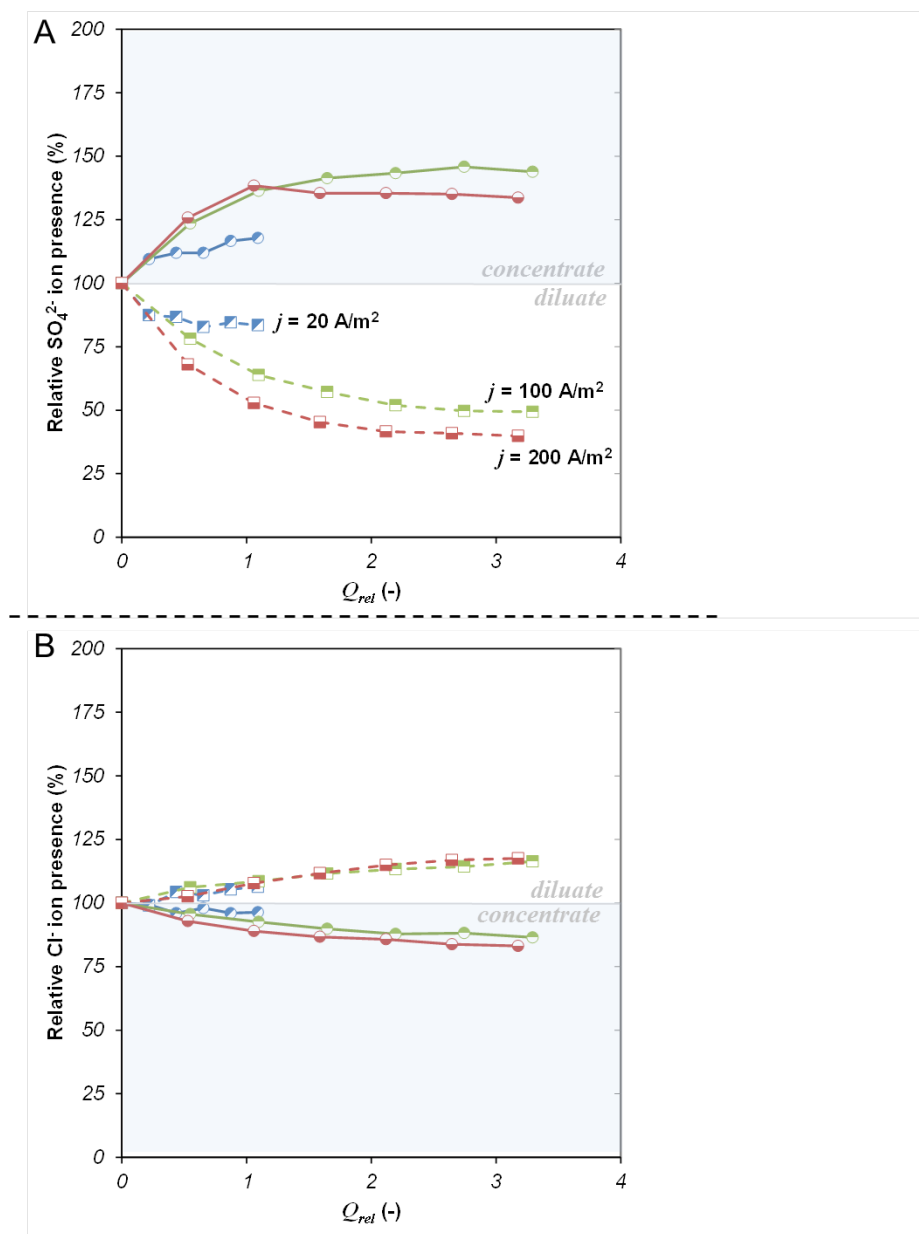
Figure 3. *Measured SO$_4^{2-}$ (A) and Cl$^-$ (B) ion concentrations (%) in the divalent diluate (□) and in the divalent concentrate (○) at an applied current density of 20 (blue, diagonal filled), 100 (green, upper half filled) and 200 (red, lower half filled) A/m^2 as a function of the relative charge applied to the system. Q_{rel} is the applied charge ($Q_{applied}$) over the charge of the ions initially present in the divalent diluate ($Q_{initial}$).*
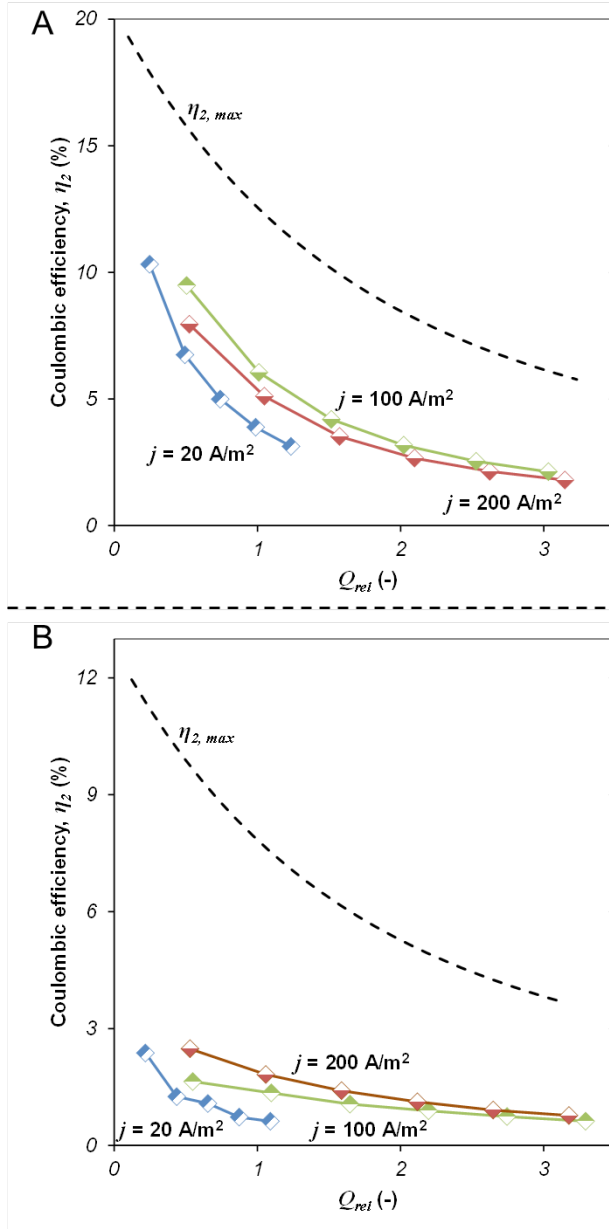
Figure 4. Coulombic efficiency regarding the transport of divalent ions, η₂ (-) of a cation fractioning ED stack (A) and an anion fractioning ED stack (B), at an applied current density of 20 (blue, diagonal filled), 100 (green, upper half filled) and 200 (red, lower half filled) A/m², as a function of the relative charge applied to the system. Q_rel is the applied charge (Q_applied) over the charge of the ions initially present in the divalent diluate (Q_initial). The theoretically maximum coulombic efficiency, η₂, max is shown as a dashed line.

4.4.3 Coulombic efficiency

The coulombic efficiency of the system, η_2 (-), as defined in the materials and methods section (paragraph 4.3), was calculated for the fractionation stacks. The result is shown in Figure 4. When a current density of 20 A/m^2 was applied, the coulombic efficiency of the cation exchanging electrodialysis stack was found as low as 3.9 % at Q_{rel} = 1. For the anion fractioning stack this was even lower (0.65%). These are much lower than the calculated theoretically maximum coulombic efficiencies, $\eta_{2, max}$ at Q_{rel} = 1. This $\eta_{2, max}$ for the different fractioning stacks was calculated with the assumptions that; i) there is a complete non-selective transfer through the non-selective CEMs, ii) a complete selectivity by the monovalent-selective membranes, and iii) there is no (back) diffusion or water transport.

What Figure 4A & B have in common is that η_2 was found to decrease with the relative applied charge, where the decrease was the fastest at lower applied current density. Just as for the maximum coulombic efficiency, the decrease in coulombic efficiency is in the beginning larger and is than flattening of (asymptotic) towards the end of the process. This decrease corresponds to the observation that most of the ion exchange takes place in the beginning of the experiment. When the curve flattens of almost no exchange is taking place and the actual coulombic efficiency of the process will become close to 0%. The effect of the coulombic efficiency will be discussed in the next paragraphs.

4.4.4 Energy consumption

The volumetric energy consumption of the system required for the fractionation, $W_{fractionation}$ (kWh/m^3) was calculated with:

$$W_{fractionation} = \frac{I \cdot \int_0^\tau \phi_{stack} dt}{\beta \cdot V_d} \qquad \text{eq. 10}$$

Where ϕ_{stack} the measured stack voltage (V), V_d is the measured divalent diluate volume (m^3), and $\beta = 3.6 \cdot 10^6$ kWh/J. The results of the calculations are shown in Figure 5 (note: these numbers do not include pumping energy and energy for electrode reactions).
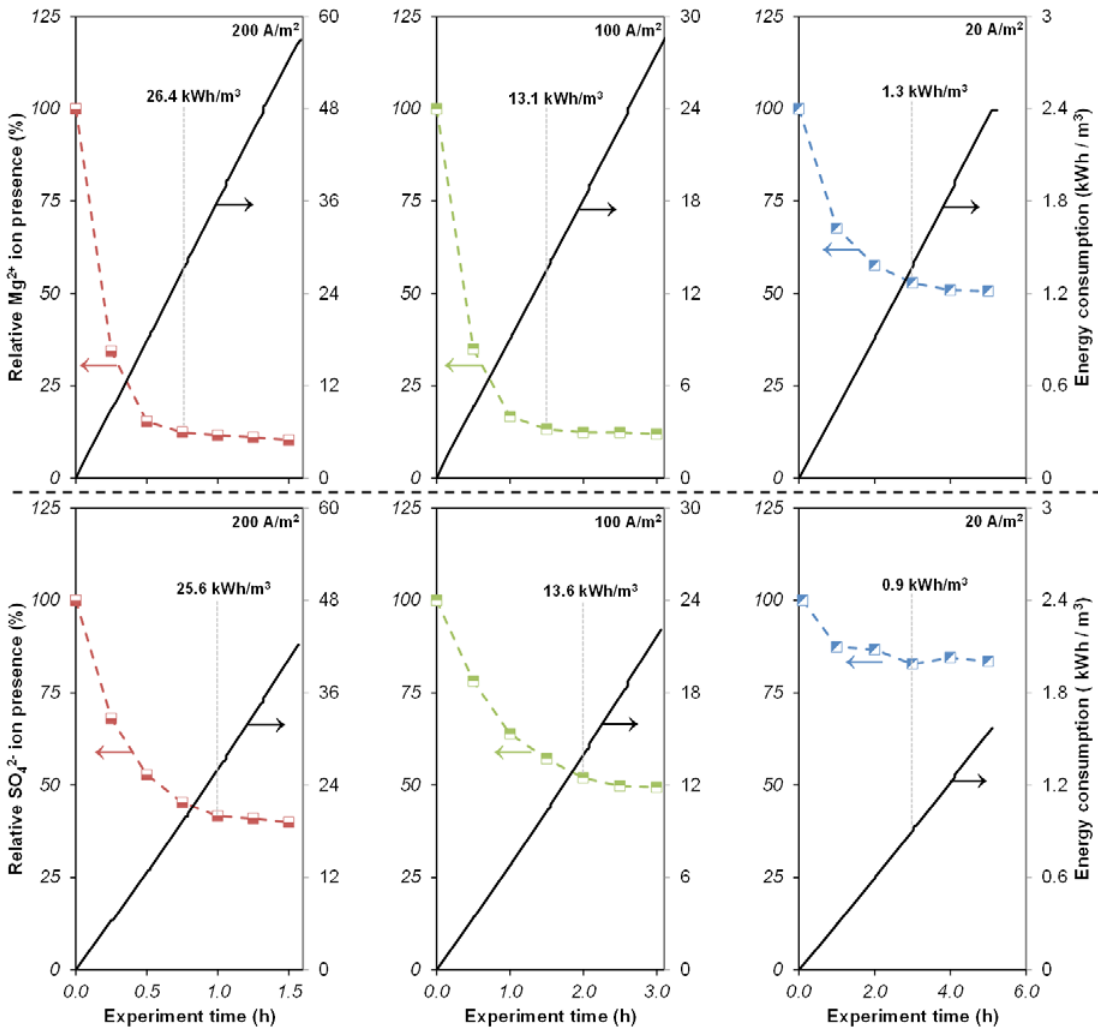
Figure 5. Relative divalent ion presence in the divalent diluate (%) on the left axis and the accompanying energy consumption (kWh/m³) on the right axis as function of time (h). Where, the applied current density was 20 (right hand), 100 (middle) and 200 (left hand) A/m² in a cation fractioning electrodialysis stack (upper plane) and an anion fractioning electrodialysis stack (lower plane).

Figure 5 shows the relative divalent ion presence and the corresponding volumetric energy consumption. The grey dotted lines indicate the point from which, no or little further ion exchange takes place. What comes forward from these indication points is that the energy consumptions for both fractioning electrodialysis stacks, to reach some minimum divalent ion concentration, are very similar. However, here should be noted that the reached cation exchange is much larger than the reached anion exchange, both on a relative (%) as absolute scale (the initial magnesium concentration is about two times higher, see Table 1). A better performance of the cation exchanging elec-

trodialysis stack was also expected, based on the coulombic efficiencies found for both systems and for the calculated maximum coulombic efficiency. Figure 5 displays that continuing the electrodialysis processes after the indicative points, would lead to higher energy consumption, with hardly any added result as the actual coulombic efficiency is (approaching) zero.

4.5 Discussion

The fractioning electrodialysis stack has many similarities with the selectrodialysis process (further referred to as SED) that was described by Zhang *et al.* [6, 34]. In SED three different aqueous stream are produced and in the experimental studies with this system low water recoveries were obtained ($r \approx 0.1$-0.2) [6, 34]. SED differs from fractioning electrodialysis as SED is not only separating ions, it is also desalinating the feed stream. This unavoidably leads to an increasing stack resistance. With fractioning electrodialysis these two issues may be avoided. Although, the water recoveries of SED can be increased, the overall water recovery of the product, is likely to be higher in a technology where only two streams are needed (divalent concentrate, divalent diluate). In the performed fractioning experiments the observed water recovery of the divalent diluate was ~ 0.5. No desalination takes place and therefore the entropy decrease is lower.

A higher water recovery however causes a larger concentration gradient of the ionic species over the membrane, which leads to a higher diffusion potential of the ionic species (back diffusion flux increases). This is shown by the decreasing coulombic efficiency, η_2 when the concentration gradient is increased. At certain moment the back transport of divalent ions from the divalent concentrate to the divalent diluate is balanced with the divalent ion migration. This results in an actual coulombic efficiency of 0%. Back transport of ions can take place through both, back diffusion and effectively by transport of divalent ions through the monovalent selective membranes, being not perfectly selective [26]. The first part is becoming larger, whereas the latter can be expected to be constant. By creating multiple stages, where the divalent diluate of stack *n* forms the influent of stack *n+1*, the concentration gradient of divalent ions over the ion can be reduced and as there will be less back diffusion, a better separation can be obtained. However, the water recovery factor would also drop tremendously. This illustrates that back-diffusion and product water recovery, are unavoidably connected.

The volumetric energy consumption of the fractionation process (Figure 5) was found to be surprisingly high and being even higher than the energy required for e.g. seawater desalination [27, 35]. This may come as a surprise, because the net change in entropy

is only small since no desalination is taking place. Moreover the high conductivity of the divalent diluate and the divalent concentrate throughout the process does not lead to an increase of the stack resistance as would be the case whenever desalination is taking place. The measured membrane stack voltage, which is directly related through ohm's law with the membrane stack resistance is shown in Figure 6. The open circuit voltage (OCV), which is represented by the dotted lines in Figure 6, shows the reversible membrane potential. This OCV does not seem to change after the first OCV measurement and is small compared to the OCV that can be found at desalination with electrodialysis in a comparable cell [1], what shows that the entropy change in the fractioning system is indeed relatively small. A small change in entropy indicates that from a thermodynamic point of view only a small amount of work is required to obtain the actual fractionation extent.

The membrane stack voltage of the cation fractioning electrodialysis stack was found higher compared to the membrane stack voltage of the anion fractioning electrodialysis stack. This higher voltage can be caused by the higher membrane resistance of the cation exchange membranes compared to the anion exchange membranes [36]. This higher resistance is also the cause of the steeper graphs for energy consumption for the cation exchange stack compared to the anion exchange stack, which were shown in Figure 5. The peak shown in the graphs in Figure 6 A, may be explained by the Mg^{2+} that was released from the CEM (replacement by Na^+) to the divalent concentrate. Apparently the membrane resistance decreased when the divalent ions in the internal fluid were replaced by the more mobile monovalent ions.

When the coulombic efficiency of the fractioning stack (η_2) is compared with the coulombic efficiency of (seawater) desalination with electrodialysis, it is seen that during the desalination process the coulombic efficiency is much higher and can be well above 90% [27, 37, 38]. This large difference has several reasons. The main reason is that the divalent ions have a much lower concentration than the monovalent ions. That is also why the maximum reachable coulombic efficiencies (Figure 4) are not starting at a 100%, but much lower at only ~20% (cations), or at ~12% (anions). The major part of current will be transported by monovalent ions that readily migrate through the membranes without any effective work done. If the concentration of divalent ions and monovalent ions would have been equal at the start, $\eta_{2,\,max}$ would be ~67% at the beginning of the process (taking into account the earlier mentioned assumptions on $\eta_{2,\,max}$).
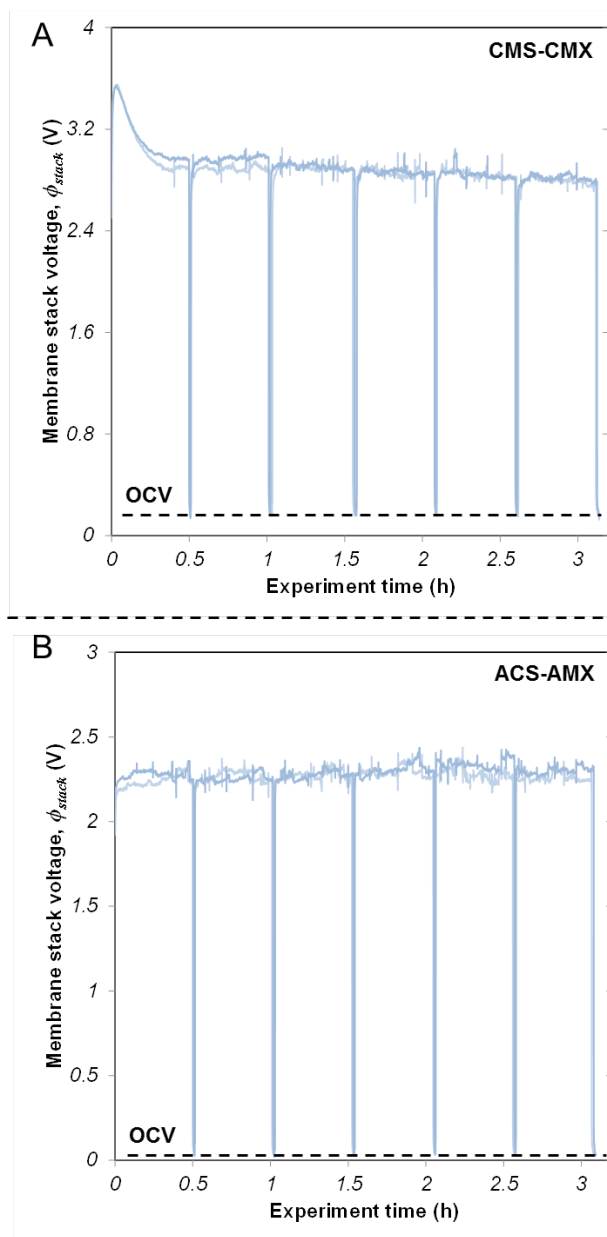
Figure 6. Membrane stack voltage (V) of a cation fractioning electrodialysis stack (A) and an anion fractioning electrodialysis stack (B) as a function of time (h), at an applied current density of 100 A/m². Open circuit voltage (OCV) is indicated by a black striped line and average membrane stack voltage by a black solid line.

Deviation of the obtained η_2, from the maximum is due to the selectivity of the IEMs. As shown by Güler *et al.*[8] anion exchange membranes do not possess high selectivity

towards monovalent ions and considerable amount of divalent ions can be transported through the monovalent selective ACS membranes that are used in the present work. Balster *et al.* [7] reported that cation exchange membranes are selective towards monovalent ions, and the monovalent selective CMS membrane, utilized in the present work, was shown to have a high selectivity towards monovalent cations [7].

However, the observed selectivity is not a pure membrane property, but is also due to concentration polarization effects occurring in the SDLs [39-42], that influence the migration rates of monovalent and divalent ions, as shown in previous work [1]. Concentration polarization is influenced by the applied current density and as the divalent ion concentrations are rather low, the limiting current density of these individual species are easily reached [43, 44]. Hydrodynamic properties of the stack will influence the SDL thickness and as such also the migration rates of monovalent and divalent ions [45]. With increasing SDL thickness, concentration polarization effects increase and more monovalent ions will be transported [1].

On top of these effects the earlier mentioned back diffusion of divalent ions will increase in size during the process. High energy requirements for the fractioning process are a direct result of the low specific coulombic efficiency of the system.

If the principle of fractioning electrodialysis, as an ion exchange process, is compared to ion exchange with resins, the system has several advantages. An important feature is that with the fractioning electrodialysis stack ion exchange can take place in an environment of highly concentrated solutions. Also exchange of divalent ions from a polluted feed solution to a clean draw solution is possible and there is no need for the use of chemicals (used for the regeneration of ion exchange resins).
The fractioning electrodialysis process has similar application possibilities as the SED process described by Zhang *et al.* [6, 34]. But also application similar to Donnan dialysis; e.g. concentrating of metal contaminations in aqueous environments [46, 47].In principle the technique can be used for any purpose where fractionation of monovalent and multivalent ions is desired.

4.6 Conclusion

In this work it is shown that the principle of current induced ion exchange, or fractioning electrodialysis works. Ternary mixtures, with a divalent-monovalent ion ratio similar to seawater were used. A maximum fractionation of divalent cations of ~90% and a maximum fractionation of divalent anions of ~60% was obtained. In all cases the lowest applied current density (20 A/m^2) also resulted in the lowest fractionation. In the performed experiments the water recovery was ~50%. Coulombic efficiency of both processes decrease rapidly after start of the experiment, leading to relative large volumetric energy consumption. When almost no further fractionation of divalent ions is taking place, the energy consumption can be around 25 kWh/m^3 for the highest applied current density (200 A/m^2). The main reason for the low coulombic efficiency is the relative small amount of divalent ions, compared to monovalent ions in the ternary mixtures used in the experimental work.

4.7 Literature

[1] A.H. Galama, G. Daubaras, O.S. Burheim, H.H.M. Rijnaarts, J.W. Post, Journal of Membrane Science, 452 (2014) 219-228.
[2] B. Van Der Bruggen, A. Koninckx, C. Vandecasteele, Water Research, 38 (2004) 1347-1353.
[3] M.S.H. Bader, Journal of Petroleum Science and Engineering, 55 (2007) 93-110.
[4] J. Schaep, C. Vandecasteele, Journal of Membrane Science, 188 (2001) 129-136.
[5] J.W. Post, C.H. Goeting, J. Valk, S. Goinga, J. Veerman, H.V.M. Hamelers, P.J.F.M. Hack, Desalination and Water Treatment, 16 (2010) 182-193.
[6] Y. Zhang, S. Paepen, L. Pinoy, B. Meesschaert, B. Van Der Bruggen, Separation and Purification Technology, 88 (2012) 191-201.
[7] J. Balster, O. Krupenko, I. Pünt, D.F. Stamatialis, M. Wessling, Journal of Membrane Science, 263 (2005) 137-145.
[8] E. Güler, W. van Baak, M. Saakes, K. Nijmeijer, Journal of Membrane Science, (2013).
[9] T. Sata, T. Sata, W. Yang, Journal of Membrane Science, 206 (2002) 31-60.
[10] H. Strathmann, Ion-exchange membrane separation processes, Elsevier, Amsterdam NL, 2004.
[11] F.G. Helfferich, McGraw-Hill, New York, (1962).
[12] F.G. Donnan, Chemical Reviews, 1 (1924) 73-90.
[13] L. Dammak, C. Larchet, B. Auclair, Journal of Membrane Science, 155 (1999) 193-207.
[14] E. Korngold, L. Aronov, N. Belayev, K. Kock, Desalination, 172 (2005) 63-75.
[15] K.N. Mikhelson, A. Lewenstam, S.E. Didina, Electroanalysis, 11 (1999) 793-798.
[16] G.B. Westermann-Clark, C.C. Christoforou, Journal of Electroanalytical Chemistry, 198 (1986) 213-231.
[17] K. Kontturi, L. Murtomäki, J.A. Manzanares, Ionic Transport Processes : in Electrochemistry and Membrane Science: in Electrochemistry and Membrane Science, OUP Oxford, 2008.
[18] T. Teorell, Proc. Soc. Exp. Biol. Med., 33 (1935) 282-285.
[19] K.H. Meyer, J.F. Sievers, Helvetica Chimica Acta, 19 (1936) 649-664.
[20] N. Lakshminarayanaiah, Transport phenomena in membranes, 1st ed., Academic Press, Philadelphia, 1969.
[21] L. Dammak, C. Larchet, B. Auclair, V. Nikonenko, V. Zabolotsky, European polymer journal, 32 (1996) 1199-1205.
[22] M.R.J. Wyllie, Journal of Physical Chemistry, 58 (1954) 67-73.
[23] M. Higa, A. Kira, Journal of Physical Chemistry, 96 (1992) 9518-9523.
[24] Y. Lanteri, A. Szymczyk, P. Fievet, Journal of Physical Chemistry B, 113 (2009) 9197-9204.

[25] D. Liu, Y. Zhang, Membrane potentials across the cation exchange membrane in aqueous mixed electrolyte solutions, in, 2012, pp. 1825-1828.

[26] J.W. Post, H.V.M. Hamelers, C.J.N. Buisman, Journal of Membrane Science, 330 (2009) 65-72.

[27] A.H. Galama, M. Saakes, H. Bruning, H.H.M. Rijnaarts, J.W. Post, Desalination, 342 (2013) 61-69.

[28] A. Chapotot, G. Pourcelly, C. Gavach, Journal of Membrane Science, 96 (1994) 167-181.

[29] G. Pourcelly, P. Sistat, A. Chapotot, C. Gavach, V. Nikonenko, Journal of Membrane Science, 110 (1996) 69-78.

[30] M. Higa, A. Tanioka, K. Miyasaka, Journal of Membrane Science, 64 (1991) 255-262.

[31] A. Galama, G. Daubaras, O. Burheim, H. Rijnaarts, J. Post, Journal of Membrane Science, 452 (2014) 219-228.

[32] P.N. Pintauro, R. Tandon, L. Chao, W. Xu, R. Evilia, Journal of Physical Chemistry, 99 (1995) 12915-12924.

[33] A.H. Galama, J.W. Post, M.A. Cohen Stuart, P.M. Biesheuvel, Journal of Membrane Science, 442 (2013) 131-139.

[34] Y. Zhang, E. Desmidt, A. Van Looveren, L. Pinoy, B. Meesschaert, B. Van Der Bruggen, Environmental Science and Technology, 47 (2013) 5888-5895.

[35] A. Al-Karaghouli, L.L. Kazmerski, Renewable and Sustainable Energy Reviews, 24 (2013) 343-356.

[36] P. Długołęcki, P. Ogonowski, S.J. Metz, M. Saakes, K. Nijmeijer, M. Wessling, Journal of Membrane Science, 349 (2010) 369-379.

[37] S.K. Thampy, P.K. Narayanan, W.P. Harkare, K.P. Govindan, Desalination, 69 (1988) 261-273.

[38] T. Seto, L. Ehara, R. Komori, A. Yamaguchi, T. Miwa, Desalination, 25 (1978) 1-7.

[39] K.S. Spiegler, Desalination, 9 (1971) 367-385.

[40] Y. Tanaka, Journal of Membrane Science, 216 (2003) 149-164.

[41] C. Larchet, S. Nouri, B. Auclair, L. Dammak, V. Nikonenko, Advances in Colloid and Interface Science, 139 (2008) 45-61.

[42] B. Levich, Discussions of the Faraday Society, 1 (1947) 37-49.

[43] V.I. Zabolotsky, J.A. Manzanares, V.V. Nikonenko, K.A. Lebedev, E.G. Lovtsov, Desalination, 147 (2002) 387-392.

[44] M.A.-K. Urtenov, E.V. Kirillova, N.M. Seidova, V.V. Nikonenko, The Journal of Physical Chemistry B, 111 (2007) 14208-14222.

[45] Y. Kim, W.S. Walker, D.F. Lawler, Desalination, 274 (2011) 54-63.

[46] A.L. Nolan, M.J. McLaughlin, S.D. Mason, Environmental Science and Technology, 37 (2003) 90-98.

[47] Y. Çengeloğlu, E. Kir, M. Ersöz, Journal of Colloid and Interface Science, 244 (2001) 342-346.

Chapter 5

Validity of the Boltzmann equation to describe Donnan equilibrium at the membrane-solution interface

Abstract

To describe Donnan equilibrium at the solution-membrane interface, the simplest approach uses the classical Boltzmann equation, based on a mean-field description of ions as ideal point charges, in combination with the assumption of fully overlapped electrical double layers in the membrane pores. We test the Boltzmann equation by measurement of the equilibrium counterion and co-ion concentration in densely charged membranes equilibrated with various NaCl solutions (0.01-3 M). To obtain a good fit of data it was found necessary to express the membrane charge and ion concentrations per volume of aqueous solution phase in the membrane, and to include a small energetic term in the Boltzmann relation. A discrepancy between theory and experiment data is found at low external NaCl concentrations. Similar deviations from the Donnan model have been reported for over half a century, but do not yet have a convincing explanation. Agreement between experiment data and theory at low external NaCl concentrations is obtained when we model the desorption experiment taking into account the role of H^+ and OH^- ions in closing the charge balance, and postulating the presence in the membrane of a tiny amount of fixed groups with a charge opposite to overall fixed membrane charge.

Nomenclature

c	=	concentration (mol/m^3)
F	=	Faraday constant (C/mol)
h	=	pore width (nm)
R	=	gas constant (J/mol·K)
T	=	temperature (K)
k	=	Boltzmann constant (m^2·kg/s^2·K)
V	=	volume (m^3)
V_T	=	thermal voltage (= RT/F)
w_u	=	membrane water content (g solution / g dry membrane)
X	=	fixed membrane charge (mol/m^3)
z	=	ion valence (-)
α	=	ionization degree (-)
$\Delta\phi_D$	=	Donnan potential (-)
λ_D	=	Donnan layer thickness (nm)
μ	=	chemical potential (= kT)
ω	=	charge sign of X
ξ	=	membrane porosity (-)

5.1 Introduction

Densely charged nanoporous membranes are found throughout science and technology, especially in the field of water treatment for the harvesting of valuable metals from water, concentrating protein molecules, and the desalination of seawater [1] and brackish water [2]. Ion transport through such membranes takes place as a result of gradients in concentration (dialysis, concentration diffusion) and electrical potential (electrodialysis [3]), while water transport due to an applied pressure (reverse osmosis [4]) also advects ions [5].

To describe the transport fluxes of ions across the membrane, one of the key elements is a model for the ion partitioning, or ion distribution, at the membrane/solution interface [6-12], see Figure 1. This is the Donnan equilibrium, or Donnan layer. Even under conditions of transport, we can assume that local equilibrium is established in this interfacial layer which has an extension of no more than a few nanometers. Here the ion concentration changes from its value in the external salt solution (where $c_{cation} = c_{anion} = c_\infty$ for a 1:1 salt), to a different value just within the membrane matrix. Within the membrane, fixed charged groups are present with a charge density, X [13]. The counterions are the ions of a charge sign opposite to that of the membrane fixed groups, while the co-ions are those of the same charge sign as the membrane. In the membrane, counterions have an increased concentration relative to the external solution outside the membrane, while the co-ion concentration is lower. Assuming electroneutrality in the membrane, the concentration of the counterions must necessarily be larger than X by the concentration of the co-ions because $c_{counterion} = X + c_{co-ion}$ [14]. During transport, across the membrane both c_{co-ion} and $c_{counterion}$ gradually change, but because of electroneutrality their difference remains equal to X, as schematically depicted in Figure 1. The co-ion concentration, as well as the difference $c_{counterion} - X$, are commonly referred to as the concentration of "free ions" or "free salt". This free salt is expected to be totally released from the membrane when the external salt concentration is reduced to very low values, e.g. of a few mM.

At the solution-membrane interface there is local charge separation [15, 16] with a slight excess of charge just outside the membrane, compensated by an equally large, but opposite, excess charge located just within the membrane. Thus, an electrical double layer (EDL) is formed [17-19]. Across this EDL, or transition zone, the concentration changes abruptly, as well as the electrical potential, ϕ (Figure 1). This Donnan equilibrium (or Donnan layer, Donnan effect) can be described by appropriate ion distribution models assuming local equilibrium [9]. A consequence of Donnan equilibrium is the exclusion of almost all co-ions from entering the membrane, while counterions

are absorbed and transported, which is called Donnan exclusion [16, 20-24]. Note that for currents beyond the overlimiting current when the equilibrium EDL expands, the concept of an equilibrium Donnan layer is no longer valid, but this situation will not be considered in the present work [25-27]. The most classical and basic model for the Donnan layer is the Boltzmann equation which describes the ions as point-charges only interacting with the electrical field. The Boltzmann equation assumes that the salt molecules are fully dissociated into single ions, both in solution and in the membrane, and it includes no other contribution to the ion chemical potential but charge and concentration. Furthermore, in the Donnan approach the membrane pores are assumed to be small enough for the electrical potential to be constant across the pore. Boltzmann's equation has been successfully used to describe Donnan equilibrium in many prior ion transport studies [20, 28-37] and will be tested in the present work.

Modifications of the Boltzmann equation to describe Donnan equilibrium have been developed over time. E.g., Geise *et al.* [14] extend the Donnan theory with two empirical parameters (K_∞ and f_D) and consider both phase-separated and non-phase-separated membranes. Fundamental modifications to the Donnan equilibrium theory have been proposed over the past decades mainly in the context of nanofiltration membranes [34, 35, 38, 39]. An important discussion point is whether ion concentrations must be defined per unit total (wet) membrane volume [14, 27, 40-42], or per unit solution phase in the membrane [7, 43-45]. In the present contribution the latter approach is used, based on the point of view that ions can only be present in the water-filled pores [46-49] the polymeric phase is excluding the ions. The approach is in line with the view that on the nm and sub-nm scale a porous material has a structure, and one can distinguish that at a certain position there is either pore water containing ions, or there is polymer phase. The same approach is followed in many other fields from polyelectrolyte solution theory [50] to porous carbon electrodes [51].

To experimentally test models for the ion distribution between solution and ion exchange membranes (IEMs), two general approaches are found in literature. In one approach, ion transport studies are used to indirectly derive insight in the solution/membrane equilibrium and the state of the ions in the membrane [20, 28-35]. Based on such studies, it has been suggested that part of the ions in the membrane must be in the form of associated salt pairs [7, 31, 44, 52], an effect not captured by the Boltzmann equation. In the other approach, ion concentrations in the membrane are directly measured in equilibrium studies [42, 53, 54]. For nanofiltration membranes with a low charge per volume of solution in the membrane of 0.05 M, Higa *et al.* [53] follow this approach and determine the equilibrium concentration of co-ions and counterions, and find excellent agreement between data and a Poisson-Boltzmann model for a cylindrical

membrane pore. For highly charged Nafion 117 cation exchange membranes, the co-ion concentration was measured by Jones *et al.* [55] as function of external NaCl salt concentration, c_∞. Recently, Geise *et al.* (2012) [14] measure for highly charged cation exchange membranes both the co-ion and counterion concentration as function of c_∞ in the range of 10 mM to 1 M NaCl, see their data in Figure 3. The advantage of such sorption studies is that the ion solution/membrane distribution is directly probed, without having the risk that the transport process distorts the analysis.
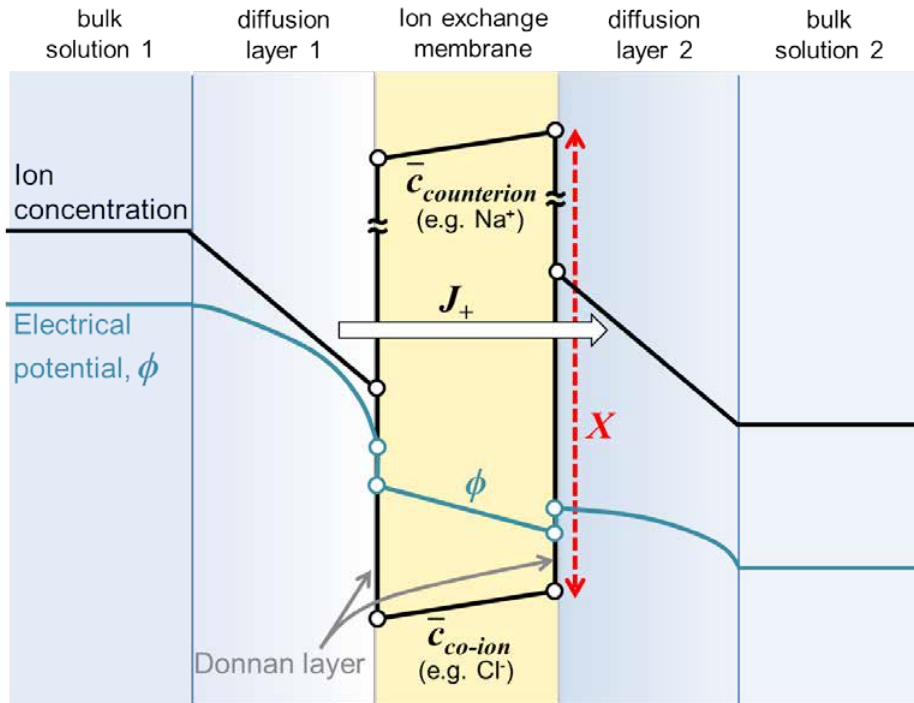
Figure 1. Schematic view of profiles of ion concentration, c, and electrical potential, φ, in an ion exchange membrane (IEM) process model. Arrows indicate the location of the interfacial EDL region, or Donnan layer, at the edge of solution and IEM. The difference between counterion and co-ion concentration is the membrane charge density, X.

In the present study, co-ion and counterion sorption in commercial anion and cation exchange membranes (AEMs, CEMs) with a very high internal fixed charge density, are measured by two routes. After "soaking" the membranes in water of predefined NaCl-concentrations, c_∞, the monovalent counterions are exchanged by contacting the membrane with a $MgSO_4$ solution. To measure the co-ion concentration, in separate experiments the ions are desorbed in the membrane into initially deionized water. In

this desorption method, both ions that are released from the membrane are measured, what led to the surprising finding that at low values of c_∞, the concentrations of Na$^+$ and Cl$^-$ in the desorption solution are markedly different. This difference in concentration implies a role for H$^+$ and OH$^-$ ions in closing the charge balance, both in the desorption solution, and in the membrane. Recalculating the measured concentrations to an apparent free ion membrane concentration a plateau at low c_∞ was found for both Na$^+$ and Cl$^-$. A simple chemical model will be used to interpret these results of the desorption experiment.

5.2 Materials and Methods

In the experiments, the equilibrium co-ion and counterion concentration in ion exchange membranes as function of the external NaCl concentration in a soak solution, c_∞, were measured. Both anion (AMX) and cation (CMX) exchange membranes (Neosepta, Tokuyama Soda Inc., Japan) were tested. AMX membranes contain quaternary ammonium groups as fixed charges, while CMX membranes contain sulfonic acid groups [1, 21, 56, 57].

Pre-treatment

As pretreatment, membranes pieces (~17 cm^2, typical thickness 130 μm (AMX) and 190 μm (CMX), typical dry density of membrane sheet 1.1 g/ml) are stored in 0.5 M NaCl solution for several days to make sure Na$^+$ and Cl$^-$ replace any other ions that may be present in the material as obtained from the manufacturer. Next, the pieces are washed in deionized water for several days, with regular intermediate replacement of the water.

Soak

Next, the membrane pieces are equilibrated (soaked) for at least 24 h in 200 ml of a NaCl-solution of a precise salt concentration c_∞ (0.01 − 3 M), see Figure 2A. During this period, the beaker was sealed with parafilm to prevent water evaporation and contamination.

Exchange

A first experiment is to establish the *counterion* concentration. To extract the counterions from the membrane we transfer the membrane pieces from the NaCl soak solution to a beaker with MgSO$_4$ exchange solution. But first the membrane piece (held with tweezers) is completely submerged and dragged quickly (1-2 s) through a beaker with 1000 ml deionized water, allowing salt solution on the membrane external

surface to be washed off, see Figure 2B. It is assumed that this period is short enough to prevent diffusion of salt out of the membrane. After placing the membrane piece into the exchange solution (200 ml, 50 mM MgSO$_4$), the beaker is again covered with parafilm and left for at least 24 h, see Figure 2C.

After this exchange period, samples were taken from the exchange solution and after the required dilution with deionized water were analyzed by ICPOES/IC to determine the ion content of the water. As exchange ions, the divalent ions Mg^{2+} and SO$_4$$^{2-}$ were used in the form of magnesium sulfate heptahydrate (MgSO$_4$·7H$_2$O, Boom b.v., Meppel, the Netherlands). A solution prepared only of this compound does not contain a measurable level of Na$^+$ or Cl$^-$ when analyzed using ICP-OES/IC.

Figure 2. Schematic view of ion exchange experiment to determine membrane counterion composition. A) Equilibration of membrane in NaCl solution; B) Short rinse in deionized water; C) Ion exchange in MgSO$_4$ solution.

For salt mixtures it has been reported that under equilibrium conditions (no electrical current), the affinity of divalent counterions with the IEM is larger than for monovalent counterions [44, 58]. And, additionally, because the MgSO$_4$ concentration is about 100x larger than the final NaCl concentration in the exchange solution, a complete exchange of the monovalent counterions in the membrane for the divalent ions of the same charge sign (e.g., Na$^+$ replaced by Mg^{2+}) can be assumed. Separate tests confirmed this: some membrane pieces equilibrated once with MgSO$_4$ (as just described) were subsequently put into fresh MgSO$_4$ solution, but after 24 h still no Na$^+$ or Cl$^-$ could be detected in this second exchange solution. The amount of Cl$^-$ and Na$^+$ ions in the

(diluted) exchange solution is measured by ion chromatography (IC, 761 Compact IC, Metrohm, Schiedam, Netherlands) for Cl⁻, and by inductive-coupled plasma optical emission spectroscopy (ICP-OES, Optima 5300DV, Perkin Elmer, Groningen, Netherlands) for Na⁺.

Desorption experiments

To measure the co-ion concentration in the membrane, we use the classical method of desorbing the ions from the membrane by placing the soaked membrane pieces (again after a short rinse, see Figure 2B) in a volume of deionized water of known volume, V_d. Equal amounts of Na⁺ and Cl⁻ are expected to desorb from the membrane, representing the "free ion" concentration in the membrane, which can be equated to the co-ion concentration in the membrane. After 24 h of desorption, we measure by IC and ICP both the concentration of Na⁺ and Cl⁻ in this solution. In a standard experiment, the desorption volume is V_d=200 ml, while the water content of a membrane piece is $V_{aq,mem}$ = 0.065 ml (AMX) or ~0.090 ml (CMX). The measured ion concentration in the desorption solution, $c_{i,d}$ is multiplied by $V_d / V_{aq,mem}$ to obtain the apparent free ion membrane concentration, $c_{i,mem,app}$, see Figure 4 bottom row.

Water content

To determine the water content of the membrane pieces, in separate experiments the water uptake as function of NaCl concentration was measured by first soaking samples in NaCl solution for 48 h, then by careful and quick wiping off of adhering electrolyte with filter paper [27, 40, 42, 54, 59] and by weighing on a mass balance. Next, these samples were placed in a crucible and dried for 24 h in a 105 °C stove. From the stove the membranes are directly transferred to an exsiccator to cool down under low pressure for 1 h, after which they are weighted again. The mass fraction of water relative to the dry membrane weight, is for the AEM membrane described by: w_u = 0.3 g/g independent of NaCl concentration (up to 3 M), and described by $w_u = a - b \cdot c_\infty$ for CEM with a = 0.3113, b = 0.0167, and c_∞ the external NaCl-concentration in M. These data are used to calculate the ion uptake in the membrane per volume of aqueous pore solution, as presented in Figure 4.

Additional experiments

Additional experiments were performed with N_2 bubbling in the soak and desorption solutions (to remove possible carbonate ions). Also, experiments were performed where the ions in the membrane are exchanged with $MgSO_4$ (as described above) but now the co-ion concentration in the exchange solution is measured. Results of these experiments are discussed in paragraph 5.3.

5.3 Results and Discussion

This section presents the counterion and co-ion concentration in highly-charged IEMs (up to $X\sim6.8$ M charge density, expressed in moles of fixed charge per unit pore volume) equilibrated with a monovalent (NaCl) salt solution, up to an external salinity of $c_\infty = 3$ M. To our knowledge, in the field of IEMs at least, materials of such high charge density have not been used in co- and counterion sorption experiments, and neither up to the external salt concentrations used. To measure the membrane counterion concentration, the counterions in the membrane are exchanged for ions of a bivalent salt solution ($MgSO_4$), a strongly absorbing salt, which is a procedure resulting in a complete extraction of the monovalent counterions from the membrane (Figure 2). To measure co-ion concentration, just as in the work of Jones *et al.* [55] and Geise *et al.* [14] (Figure 3), the membrane pieces are soaked in monovalent salt solution of concentration c_∞ and then desorbed in initially deionized water, of which the salinity increases to a non-zero level, c_d, which relates to the co-ion concentration in the membrane. As we will show, for low c_∞, the concentration of Na^+ and Cl^- in the desorption solution is not the same, and the amount of ions extracted is a strong function of the desorption volume, even though c_d is low (order of 1-100 μM).

To theoretically model ion sorption, it is possible to make use of the Poisson-Boltzmann (PB) model as used by Higa *et al.* [53]. One disadvantage, besides the mathematical complexity, is that one must make an assumption on the pore size and geometry. This assumption does not need to be made when the material has small pores, smaller than the Debye length. The Debye length relates to the ionic strength of the external salt solution, i.e., outside the membrane, and is $\lambda_D = 3$ nm at $c_\infty = 10$ mM of a monovalent salt solution. In that case gradients in the pore potential can be neglected in a first approximation, and a single membrane potential suffices to describe the pore potential, irrespective of pore geometry. This is the Donnan approach [60]. The commercial IEMs that were tested have pores that are around 1 nm in dimension [56], and thus this assumption seems appropriate. In Figure 3 (right graph) to be discussed below, also a PB-calculation was included (for slit-shaped pores of 1 and 2 nm in width [30, 61-63]), which shows that the co-ion concentration is shifted upward compared to the Donnan approach, and that in a log-log representation this shift is by a constant amount. For 1 nm-pores the difference between a Donnan- and PB-calculaton is very minor (<10%), while for pores 2 nm in width, the difference is a factor of 2. Thus, the Donnan model is a good approximation of the full PB model for strongly charged microporous membranes when pores are of the order of 1 nm. A more detailed double layer models for the ion distribution in micropores including e.g. ion correlation and volume exclusion effects, effects which are important for a more detailed under-

standing [63-67] was not considered here.

Experimental data from literature [14] for the ion concentration in a cation exchange membrane (BPSH-32) are presented in Figure 3, expressed per unit solution volume in the membrane. Data are compared with the Donnan model based on the Boltzmann equation, to be discussed below, using a membrane charge density of 0.88 meq/gr dry material ($X = 2.2$ M at $c_\infty = 1$ M when expressed per unit solution volume). Data analysis and the calculations include the measured decrease of the water fraction (g solution/g dry), w_u, with external salinity c_∞ (in M) according to $w_u = a \cdot c_\infty^b$ where $a = 0.395$ and $b = -0.0136$. The most important observation is that solely by fitting X, we can quite accurately describe the sorption data both for counterions and co-ions. The only exception is when the co-ion concentration in the membrane is below 10 mM, a region where $\log_{10}(c_{co-ion})$ depends on $\log_{10}(c_\infty)$ with a slope of approximately unity ("1:1" in Figure 3b), a classical observation also made in refs. [20] and [43]. This dependence of c_{co-ion} on c_∞ contradicts the Donnan theory which predicts a slope of 2:1, based on c_{co-ion} being proportional to c_∞^2. Deviations from this proportionality have been noted more often [7, 44, 68].

Figure 3. Data for NaCl absorption in the cation exchange membrane BPSH-32, tested by Geise *et al.*, 2012 [14]. Ion absorption and membrane charge, X, expressed per volume of solution phase in membrane. The same data on linear-linear scale to the left, on log-log scale to the right. Solid lines based on Donnan theory, dashed line based on Poisson Boltzmann theory for a slit-shaped pore of *h* = 1 nm or 2 nm width.

Results of our own experiments are presented in Figure 4 for anion exchange membranes (left), and cation exchange membranes (right). Presented are counterion concentrations, $c_{counterion}$, and co-ion concentrations, c_{co-ion}, both per volume of aqueous

phase in the membrane as function of the external salt concentration, $c_{NaCl,external}$, further denoted as: c_∞. Data are plotted on a linear-linear scale (top row) and on $\log_{10}$-$\log_{10}$ scale (bottom row). Insert pictures show in detail c_{co-ion} for $c_\infty < 1.2$ M. Lines are based on the modified Donnan model using Boltzmann's equation, see Eqs. 1-7 below.

Very similar behaviour for both AEMs and CEMs was found, with the ion concentrations gradually increasing when increasing c_∞, starting for the counterions at a value of ~4.8 M for the AMX membrane and ~5.7 M for the CMX membrane, and for the co-ions starting at values below 0.02 M. For the co-ions was found that co-ion sorption is not proportional to c_∞, but increases more than linearly (see insert pictures in top row of Figure 4), in agreement with Eq. 6 to be discussed below, and different from the proportional relationship reported in ref. [55].

When comparing CMX with AMX, for CMX more absorption of counterions and at the same time less of co-ions is measured. This observation that increasing $c_{counterion}$ corresponds to a lower c_{co-ion} is in line with the Donnan theory, see Eq. 1 below. In the data, it is furthermore observed that for the AMX membrane, the difference between c_{Cl} and c_{Na} is independent of c_∞, which suggests that the membrane charge, X, is constant, as is also expected because the water fraction in the AMX membrane is independent of c_∞. For the CMX membrane, because of a decrease of water fraction with increasing c_∞, the membrane charge (per unit aqueous volume) increases, and thus the difference c_{Na} - c_{Cl} increases with c_∞.

The classical Donnan model based on the Boltzmann equation is based on the following two equations:

$$c_{counterion} \cdot c_{co-ion} = c_\infty^2 \qquad \text{eq. 1}$$

And [24, 69]:

$$c_{counterion} + c_{co-ion} = \sqrt{X^2 + (2 \cdot c_\infty)^2} \qquad \text{eq. 2}$$

Which can be derived from the underlying Boltzmann relationship:

$$c_i = c_\infty \cdot \exp(-z_i \cdot \Delta\phi_D) \qquad \text{eq. 3}$$

Together with membrane electroneutrality [28]:

$$X + c_{co-ion} = c_{counterion} \qquad \text{eq. 4}$$

Where z_i is the ion valence (e.g. $z_i = -1$ for a monovalent anion), and where $\Delta\phi_D$ is the Donnan potential (dimensionless by scaling to the thermal voltage, $V_T = RT/F$), which is the electrical potential difference across the solution-membrane interface. Combining Eqs. 2 and 4 results in an explicit expression for the co-ion concentration [24]:

$$c_{co-ion} = \frac{1}{2}\left(\sqrt{X^2 + (2 \cdot c_\infty)^2} - X\right) \qquad \text{eq. 5}$$

When $c_{co-ion} \ll c_{counterion}$, then $X \sim c_{counterion}$, and thus [20, 24]:

$$c_{co-ion} \approx \frac{c_\infty^2}{X} \qquad \text{eq. 6}$$

This implies that under the given conditions and when plotted on a log-log scale, the Donnan model predicts a slope of ~2:1 for c_{co-ion} vs c_∞, see Figure 3 and Figure 4.

The question is, should concentrations be based on the total (wet) membrane volume, or should they be based on the volume of the water-filled pore solution? In our view, because solely the aqueous solution phase is available to the ions, concentrations (c_i, X) must be defined per unit (pore) solution phase in the membrane. More formal is to define all concentrations per unit total (wet) membrane volume, but then a volume-exclusion term must be added to the ion chemical potential, which for ions as point charges is given by $\mu_{exc} = -\ln(\xi)$, where μ_{exc} is in units of kT, and where ξ is the porosity, which is the volume fraction of the membrane taken up by aqueous solution [70, 71]. Including this term leads to the exact same result as when concentrations per unit solution phase are directly taken and the μ_{exc}-term is left out.

Figure 5 shows results for the Donnan model as just described (lines denoted "per volume solution") while the steep lines denoted by "per volume wet membrane" are based on a Donnan model which assumes that all concentrations c and X are defined per total membrane volume (assuming a polymer density of 1.34 g/ml). Note that in Figure 5, these calculated ion concentrations per unit total volume are subsequently multiplied by $1/\xi$, with $\xi = 0.23$ based on $\xi = w_u / (1 + w_u)$ with $w_u = 0.30$. This is just a redefinition of concentrations by a constant factor to aid the comparison. Figure 5 quite clearly shows how defining ion concentrations per unit aqueous solution in the membrane has a very positive effect on the predictive power of the Donnan theory, resulting in a rather good fit to the data, whereas when taking the total volume as the reference volume, there is no fit at all.

Figure 4. Measurement data (symbols) and modified Donnan theory (solid lines, $\mu^*=0.2$ kT) for co-ion and counterion concentration as function of external NaCl solution concentration, $c_{NaCl,external}=c_\infty$, in commercial anion exchange membranes (left, Neosepta AMX) and cation exchange membranes (right, Neosepta CMX) on linear-linear scale (top row) and log-log scale (bottom row). Concentrations defined per volume of aqueous solution phase in the membrane. Insert graphs show detailed view of c_{co-ion} vs. c. The difference between $c_{counterion}$ and c_{co-ion} is the membrane charge density, X, which for CMX is a function of c_∞. Dashed lines in lower panels describe theoretical prediction for apparent free ion concentration in desorption experiment (pK=6, $X_{minority}=5$ mM, $V_d/V_{aq,mem}=2000$). The "2:1" slope in the theoretical curves for co-ion concentration is the Donnan model prediction in the limit $c_{co-ion} << c_{counterion}$.

Next a modified Donnan theory is proposed that includes an extra contribution to the chemical potential of the ion, μ^*, when present in the membrane. This term can be interpreted as being due to volumetric exclusion effects, either because of an interaction of the ion with the membrane pore walls, or due to a volumetric interaction between the ions themselves [70, 71]. In the membrane pores the total ion concentration is beyond 5 M, and with ions (hydrated or not) having a size of at least a few Ångstrom, this implies that the ion volume fraction is not insignificant. The ion size also excludes them from approaching the membrane pore walls infinitely close which also effectively

leads to a non-zero value of μ^*. Thus, in general, a balance of ion chemical potential between outside and inside the membrane pore can be written as:

$$\ln c_\infty = \ln c_i + z_i \cdot \Delta\phi_D + \mu^* \qquad \text{eq. 7}$$

Eq. 7 can be combined with Eq. 4 to obtain modified expressions in the Donnan model for $c_{co\text{-}ion}$ and $c_{counterion}$. For instance, Eq. 2 becomes:

$$c_{counterion} + c_{co\text{-}ion} = \sqrt{X^2 + (2 \cdot c_\infty \cdot \exp(-\mu^*))^2} \qquad \text{eq. 8}$$

As Figure 5 shows, including the term μ^* further improves the fit of the (now, modified) Donnan model to the data. To obtain this fit, for μ^* a small value of $\mu^* = 0.2$ kT is sufficient. It is possible to make μ^* an explicit function of ion volume fraction, ion size, and pore size and thus to include the volume of the ions (either with or without their hydration shell). To this end, expressions available for the osmotic pressure of hard-sphere fluids can be applied, which can be modified to describe volume constriction effects caused by the membrane matrix [70, 72, 73].

Calculation results using the modified Donnan model for ion concentration in the membrane as function of c_∞ are shown in Figure 4 as solid lines. For AMX the membrane charge X is constant, while for CMX it increases because of membrane deswelling with increasing c_∞ according to $X = X_0 \cdot w_{u,0} / w_u$ where $w_{u,0} = 0.31$ and $X_0 = 5.7$ M and, leading to values at $c_\infty = 3$ M of $w_u = 0.26$ and $X = 6.8$ M. For both membranes, the ion exchange capacity per unit dry weight is assumed constant, being IEC = 1.35 meq/g for AMX, and IEC = 1.93 meq/g for CMX. After fitting the modified Donnan model to the data by using $\mu^* = 0.2$ kT, we find for the counterions a very good agreement, where, for both types of membranes, the theory accurately reproduces the gradual increase of $c_{counterion}$ with c_∞.

Also for the co-ions we find a very good fit of the modified Donnan model to the data. The model well reproduces that up to $c_\infty = 1$ M, $c_{co\text{-}ion}$ increases more than linearly with c_∞ (see insert graphs). Also, at higher values of c_∞, co-ion concentrations are very well predicted. It may be noted that the data have quite some dispersion which could be due to sample-to-sample variation, which makes the test of the model less rigorous. Still, the good fit of the modified Donnan model to the data justifies its use in a full problem of ion sorption and transport in ion exchange membranes. Since Donnan equilibrium is so widely applied, also for many problems outside the field of ion exchange membranes [74-78], it is argued that the degree of agreement as evidenced in Figure 4 is an important finding.

When our data is plotted on a log-log scale (bottom row in Figure 4), it is observed that for c_∞=0.5 M and beyond, the measured values of the apparent free membrane concentration, $c_{i,mem,app}$, are the same for Na$^+$ and Cl$^-$, and thus it can be assumed that indeed the co-ion concentration in the membrane was measured by the desorption method (as plotted in the top row in Figure 4). But more strikingly is the observation that below c_∞ = 0.5 M, the predicted 2:1 slope is not followed at all. Instead, both for the AMX and the CMX membrane was found that $c_{i,mem,app}$ is not steadily decreasing with lowering c_∞, to disappear below the detection limit, but $c_{i,mem,app}$ levels off at measurable values in the range of ~3 mM to ~30 mM. Note that the corresponding ion concentrations in the desorption solution are more than three orders of magnitude lower, down to values as low as 1 μM (because the volume ratio $V_d / V_{aq,mem} > 10^3$). Interestingly, in previous literature often a 1:1 slope is found in c_{co-ion} vs c_∞, see Figure 3 above, and taken as evidence for a deviation from Donnan's law, but the presence of two plateaus was not reported before. That these plateaus are now found may be related to the very high membrane charge X of the tested materials.

These data rises various questions: Why do the data deviate so strongly from Donnan theory? Why do the counter- and co-ions have different concentration in the desorption solution? and, Why is there a plateau? Do these discrepancies lead us to question the validity of the Donnan theory, either in total or in part [16, 20, 68, 79], is there an experimental artifact, or are ions interacting with the membrane by other mechanisms than considered? The first question is whether there is a real effect. The anomalously high concentration of free counter-ions seems possible, for instance by having some of the ionic countercharge released. For the co-ions, the question is, is it possible that our findings are wrong, and that although we think we measure their release from the membrane, actually these ions were not there. However, we are quite certain it is a real effect that we measure all of these co-ions coming out of the membrane, though it is in such striking contradiction to Donnan theory in this regime (which predicts there are hardly any co-ions in a membrane soaked in e.g. c_∞=10 mM NaCl solution). To support this view we can bring forward the following information. Firstly, membranes are washed in deionized water for prolonged times to wash out the initial conditioning in 0.5 M NaCl, before being transferred to beakers at the specified values of c_∞. Secondly, ICP analysis measures Na$^+$ and Cl$^-$ to be below the detection limit when no membrane is placed in the desorption solution. Thirdly, also exchange experiments with MgSO$_4$ were done where the co-ion concentration was measured. This different experimental program gives us exactly the same data for the free co-ion concentration as the desorption experiment. Therefore it is believed that our measurement of the "higher-than-Donnan" value of free co-ions in the membrane is a real effect.

Theoretically, various model modifications come to mind to explain the anomalous free (co-)ion concentration, such as the role of pairing of the co-ion in the membrane with the counterions there (or directly with the membrane charge) [31, 43, 56]. A mathematical model set up to describe this effect based on a mass-action law association-dissociation reaction certainly predicts an increase in co-ion concentration. However, this increase results in an upward shift of the entire curve of c_{co-ion} vs c_∞ in a log-log representation, and does not lead to the prediction of a plateau-region in c_{co-ion} for low values of c_∞. Likewise, the effect of including direct counterion association with the membrane (a chemical interaction of the counterion with the oppositely charged membrane [80, 81]) neither led to a useful model improvement. All of these modifications predict (just as the Donnan model) that in the low-c_∞ limit, when c_∞ goes down by an arbitrary factor α, c_{co-ion} must go down by a factor α^2.

In the literature it is often argued that such effects are due to membrane inhomogeneities, either because the electrical potential varies across the pore, or because the membrane charge density is not homogeneously distributed [24, 45, 82, 83]. However, calculations demonstrated that, though both explanations will increase the predicted co-ion concentration in the membrane, still, the co-ion concentration consistently scales with the square of c_∞, without a deviation from the predicted 2:1 ratio (in a log-log plot) at low c_∞. Results of a Poisson-Boltzmann (PB) calculation, which considers the potential profile across a slit-shaped pore, are presented in Figure 3 (right) and show that c_{co-ion} vs c_∞ follows the 2:1 limiting law. Charge inhomogeneity was included in a separate Donnan calculation where the membrane charge was not constant at 5 M, but was distributed equally over a range from 0.1 to 9.9 M (leading to an average value of 5 M). Though this modification leads to an increase of the predicted co-ion concentration in the membrane, the increase is by a constant factor of about 2.5, independent of c_∞. Thus, also this explanation does not lead to an explanation of the measured deviation from the 2:1 law for $c_{co-ion,mem}$ vs c_∞.

Here a different route to explain the deviation from Donnan theory is proposed that is suggested by the desorption experiment. A simple chemical model is set up based on ion balances, which as will be shown quite accurately describes the plateau in the two apparent free membrane ion concentrations. The fact that the chemical model fits the data (see dashed lines in lower row in Figure 4) suggests that results of the desorption experiment cannot be used without model interpretation, and that these results do not indicate a fundamental problem with the Donnan theory. In the chemical modelwhere first of all H^+ and OH^- ions are included in the charge balance, both in the membrane and in the very large desorption volume. Note that here the difference in concentration between cation and anion can be as high as 25 µM which implies a pH 4.6 for an AMX

membrane and pH 9.4 for a CMX membrane. With ion concentration in the desorption volume of the order of 1-100 μM, it is clear that the H^+/OH^- concentrations are not insignificant. This modification is sufficient to explain the development of the plateau in the free counterion concentration (highest of the two dashed lines in Figure 4 lower row). However, the deviation from Donnan's limiting law of the measured free co-ion concentration remains then unexplained. To obtain a model which predicts the plateau in co-ion concentration, the suggestion made in previous work [20, 43, 44] that the membrane may contain a small fraction of fixed charge groups of opposite sign (to be called: the minority groups), was considered. These groups have an affinity to their counterion (which is the co-ion of the membrane as a whole, called ion* from this point onward) described by the intrinsic pK-value [84]. When placed in the soak solution, the concentration of ion* in the membrane (though low) is still high enough for the minority groups to be fully associated with their counterion, ion*. In the desorption solution, the concentration of ion* in the membrane drops dramatically (its concentration in the desorption solution is very low, and the Donnan potential is huge, beyond $\Delta\phi_D = 10$, with a sign such that ion* is repelled from the membrane) and thus ion* is desorbed from the minority groups in the desorption step.

Thus, the chemical model includes an overall charge balance, $c_{Na} - c_{Cl} + c_H \ c_{OH} + \omega X$ $(1 - \alpha) \cdot \omega X_{minority} = 0$, to be solved both in the soak and desorption solutions, and in the membrane. The final two terms in this balance are only evaluated in the membrane, and include: ω: the charge sign of the matrix (majority) fixed membrane group; α: the fraction of the minority groups that have an association with ion*; $X_{minority}$: the charge density of minority groups. The ionization degree α is described by: $\alpha / (1 - \alpha) = c_{ion*} \cdot$ 10^{pK}, where c_{ion*} is equal to $c_{Na,mem}$ for an AEM, and $c_{Cl,mem}$ for a CEM. To relate concentrations in the membrane with those in the soak and desorption solution, for all ions the modified Boltzmann's relation, Eq. 7, is used. For the desorption step, two additional ion balances are used, one stating that all Na^+ leaving the membrane ends up in the much larger desorption solution, and likewise an ion balance for Cl^-.

Figure 4 (lower row) shows using dashed lines the predicted apparent free ion membrane concentrations, $c_{i,mem,app}$, based on this model. Remarkably, quite like the data, it predicts values for $c_{i,mem,app}$ that deviate strongly from the standard Donnan model, including the development of two plateaus at low c_∞, and at different levels. Though the qualitative fit is quite good, it is not perfect (values are too low for $c_{counterion}$), and thus the role of CO_2 was investigated. In a theory without the minority groups, including the role of carbonate ions in the charge balance (assuming an initial pH of 5.5 due to carbonate from air) made the plateau in $c_{counterion}$ shift up by about this factor. However, experiments where all samples were saturated with N_2 gas to

remove possible dissolved CO_2, led to the same values for $c_{i,mem,app}$. Thus, based on this experiment it is concluded there is no role for carbonate ions in the results of the desorption experiments.

Thus, our results show a role for H^+ and OH^- ions in describing the desorption experiment. In addition, it is suggested that there may exist minority groups in the membrane of an opposite charge sign. Note that there is no direct spectroscopic or chemical evidence for the presence of these groups. Our results suggest that measured results of the desorption experiment cannot be used directly to estimate the free ion concentration in membranes soaked at values of c_∞ below 0.5 M. This point is strengthened by results of desorption experiments at various desorption volumes (not reported). Here a significant effect of desorption volume on the apparent membrane ion concentration is found, demonstrating that not a unique value of the membrane ion concentration is measured. Note that these effects only happen for c_∞ of 0.2 M and lower, when $c_{i,mem,app}$ is different between the co-ion and counterion. At higher values of c_∞, the two ion concentrations are the same, and theoretically there is also no effect of desorption volume. Thus, in the latter case the desorption experiment can be used to determine the membrane free salt concentration, which is the co-ion concentration. However, for lower values of c_∞, a model such as the one presented is required to analyze the experiment. Additional experiments at different pH levels in the soaking and desorption volumes, and different volume of the desorption volume, can provide valuable extra information on the details of ion adsorption and desorption, and on the presence and properties of the minority groups of opposite charge.

The presented chemical model for the desorption experiment assumes the presence of minority fixed membrane groups of a charge opposite to that of the membrane (or at least, there must be groups that have a strong affinity with the co-ion). Interestingly, such oppositely charged groups are deliberately present in monovalent selective membranes in the form of a thin film [1, 40, 56, 85] but are also found in RO membranes [86]. Our analysis suggests that a concentration of a few mM of these groups (~0.1 % of the membrane charge density) suffices to explain the anomalous behavior in the desorption experiment. However, additional experiments (such as verification of oppositely charged functional groups on the polymer chains) would need to be performed before the model can truly be considered to describe the physical situation at hand.

What would be the effect of these groups that attract their counterions (co-ions to the membrane as a whole) on membrane performance? When these ions are quite immobile, they will probably not play a significant role during the membrane transport

process. But assuming instead that these ions are just as mobile as the ions in the rest of the membrane, then they provide an extra source of mobile co-ions. This would limit the membrane permselectivity to lower values than expected based on the Donnan model. It is often argued that higher membrane charge is required for better permselectivity (lower co-ion leakage) [56, 87, 88]. If however, these ions associated with minority membrane groups have sufficient mobility, lower-than-expected membrane permselectivities in actual (electrodialysis) applications may also be due to the presence of a slight amount of fixed charged groups with a charge sign opposite to that of the membrane matrix.
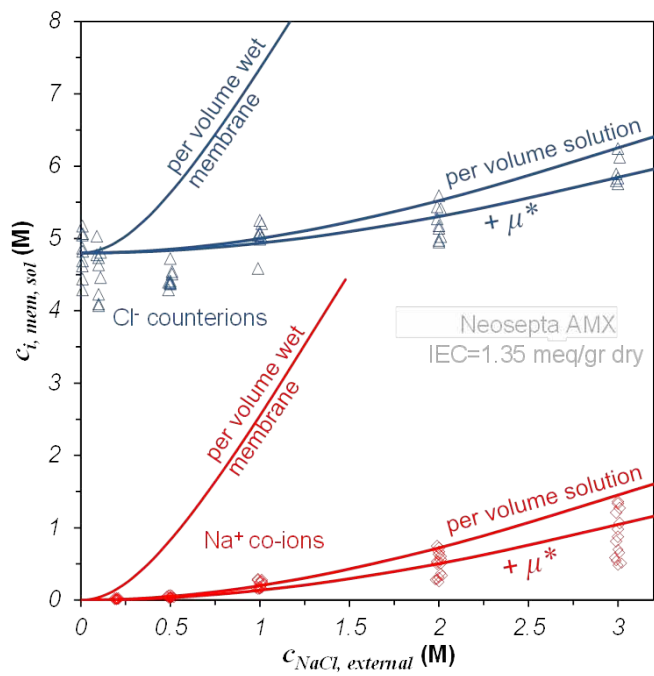
Figure 5. Data for ion absorption in anion exchange membrane (Neosepta AMX) per unit aqueous phase (solution pore volume) in the membrane, just as Figure 4A. Model calculations based on the Boltzmann equation with concentrations and membrane charge X defined either per volume of total (wet) membrane (steepest lines), or per volume of aqueous phase (more horizontal lines). The most horizontal lines include an additional contribution to the ion chemical potential in the membrane of $\mu^* = 0.2\ kT$ per ion.

5.4 Conclusion

Equilibrium counterion and co-ion concentrations inside highly charged ion exchange membranes as function of external NaCl solution concentration, c_∞, were measured. Donnan theory correctly predicts the gradual increase of both $c_{co\text{-}ion}$ and $c_{counterion}$ in the membrane with increasing c_∞, with $c_{co\text{-}ion}$ increasing non-linearly for c_∞ up to 1 M. Using the ion exchange capacity IEC to fit the data, together with an extra contribution to the ion chemical potential in the membrane, μ^*, both $c_{counterion}$ and $c_{co\text{-}ion}$ are very well described by a modified Donnan theory, except for desorption experiments when c_∞ is lower than 0.5 M. These experiments have both Na$^+$ and Cl$^-$ diffusing from the membrane into initially salt-free water and lead to apparent "free" membrane ion concentrations with different plateaus for the two ions, i.e., this free membrane concentration does not drop off steadily when c_∞ is decreased, as would be predicted by Donnan theory. These anomalies are due to the very low ionic strength of the desorption solution, leading to a very high Donnan potential. Because of this situation, proton and hydroxyl ions play a role in the charge balance, both in the desorption solution and in the membrane. Furthermore there may be minority groups in the membrane of a charge sign opposite to that of the membrane. The counterions of these groups are released into the desorption solution and lead to the observation of a plateau in the apparent free membrane concentration of that ion.

In conclusion, the presented methods of measurement and analysis directly probes the solution-membrane interface, and points out that the Boltzmann equation, underlying the classical Donnan theory, remains an excellent starting point. For an optimum fit of the Donnan model, ion concentrations and membrane charge must be defined per unit solution volume in the membrane and not be based on the total wet membrane volume.

5.5 Literature

[1] H. Strathmann, Ion-Exchange Membrane Separation Processes, Elsevier, Amsterdam NL, 2004.
[2] R. Zhao, P.M. Biesheuvel, A. Van Der Wal, Energy consumption and constant current operation in membrane capacitive deionization, Energy and Environmental Science, 5 (2012) 9520-9527.
[3] H. Strathmann, Electrodialysis, a mature technology with a multitude of new applications, Desalination, 264 (2010) 268-288.
[4] L.F. Greenlee, D.F. Lawler, B.D. Freeman, B. Marrot, P. Moulin, Reverse osmosis desalination: Water sources, technology, and today's challenges, Water Research, 43 (2009) 2317-2348.
[5] J.A. Wesselingh, R. Krishna, Mass Transfer in Multicomponent Mixtures, VSSD, Delft NL, 2006.
[6] F.G. Donnan, The theory of membrane equilibria, Chemical Reviews, 1 (1924) 73-90.
[7] E.H. Cwirko, R.G. Carbonell, Ionic equilibria in ion-exchange membranes: a comparison of pore model predictions with experimental results, Journal of Membrane Science, 67 (1992) 211-226.
[8] J.R. Bontha, P.N. Pintauro, Water orientation and ion solvation effects during multicomponent salt partitioning in a Nafion cation exchange membrane, Chemical Engineering Science, 49 (1994) 3835-3851.

[9] F.G. Donnan, Theory of membrane equilibria and membrane potentials in the presence of non-dialysing electrolytes. A contribution to physical-chemical physiology, Journal of Membrane Science, 100 (1995) 45-55.

[10] T. Xu, W. Yang, B. He, Partition equilibrium between charged membrane and single electrolyte aqueous solution, Chinese Journal of Chemical Engineering, 9 (2001) 326-330.

[11] D. Gillespie, R.S. Eisenberg, Modified Donnan potentials for ion transport through biological ion channels, Physical Review E - Statistical, Nonlinear, and Soft Matter Physics, 63 (2001) 061902.

[12] S. Déon, A. Escoda, P. Fievet, A transport model considering charge adsorption inside pores to describe salts rejection by nanofiltration membranes, Chemical Engineering Science, 66 (2011) 2823-2832.

[13] J. Schaep, C. Vandecasteele, Evaluating the charge of nanofiltration membranes, Journal of Membrane Science, 188 (2001) 129-136.

[14] G.M. Geise, L.P. Falcon, B.D. Freeman, D.R. Paul, Sodium chloride sorption in sulfonated polymers for membrane applications, Journal of Membrane Science, 423-424 (2012) 195-208.

[15] Y. Oren, A. Litan, The state of the solution-membrane interface during ion transport across an ion-exchange membrane, Journal of Physical Chemistry, 78 (1974) 1805-1811.

[16] A.E. Yaroshchuk, Non-steric mechanism of nanofiltration: Superposition of donnan and dielectric exclusion, Separation and Purification Technology, 22-23 (2001) 143-158.

[17] P. Długołecki, P. Ogonowski, S.J. Metz, M. Saakes, K. Nijmeijer, M. Wessling, On the resistances of membrane, diffusion boundary layer and double layer in ion exchange membrane transport, Journal of Membrane Science, 349 (2010) 369-379.

[18] H. Ohshima, S. Ohki, Donnan potential and surface potential of a charged membrane, Biophysical Journal, 47 (1985) 673-678.

[19] G.M. Geise, H.S. Lee, D.J. Miller, B.D. Freeman, J.E. McGrath, D.R. Paul, Water purification by membranes: The role of polymer science, Journal of Polymer Science, Part B: Polymer Physics, 48 (2010) 1685-1718.

[20] E. Glueckauf, R.E. Watts, The Donnan law and its application to ion exchanger polymers, Proceedings of the Royal Society A, 269 (1962) 339-349.

[21] P. Długołecki, K. Nymeijer, S. Metz, M. Wessling, Current status of ion exchange membranes for power generation from salinity gradients, Journal of Membrane Science, 319 (2008) 214-222.

[22] M. Jardat, J.F. Dufrêche, V. Marry, B. Rotenberg, P. Turq, Salt exclusion in charged porous media: A coarse-graining strategy in the case of montmorillonite clays, Physical Chemistry Chemical Physics, 11 (2009) 2023-2033.

[23] M. Rendueles, A. Fernández, M. Díaz, Sorption of counter and co-ions at high concentration in ion exchangers, Solvent Extraction and Ion Exchange, 15 (1997) 665-688.

[24] K. Kontturi, L. Murtomäki, J.A. Manzanares, Ionic Transport Processes : in Electrochemistry and Membrane Science: in Electrochemistry and Membrane Science, OUP Oxford, 2008.

[25] V.V. Nikonenko, N.D. Pismenskaya, E.I. Belova, P. Sistat, P. Huguet, G. Pourcelly, C. Larchet, Intensive current transfer in membrane systems: Modelling, mechanisms and application in electrodialysis, Advances in Colloid and Interface Science, 160 (2010) 101-123.

[26] M.B. Andersen, M. Van Soestbergen, A. Mani, H. Bruus, P.M. Biesheuvel, M.Z. Bazant, Current-induced membrane discharge, Physical Review Letters, 109 (2012) 108301.

[27] J.-H. Choi, S.-H. Moon, Structural change of ion-exchange membrane surfaces under high electric fields and its effects on membrane properties, Journal of Colloid and Interface Science, 265 (2003) 93-100.

[28] T. Teorell, Progress in biophysical chemistry, Academic Press Inc., New York USA, 1953.

[29] I.A. Stenina, P. Sistat, A.I. Rebrov, G. Pourcelly, A.B. Yaroslavtsev, Ion mobility in Nafion-117 membranes, Desalination, 170 (2004) 49-57.

[30] A. Szymczyk, Y. Lanteri, P. Fievet, Modelling the transport of asymmetric electrolytes through nanofiltration membranes, Desalination, 245 (2009) 396-407.

[31] S. Bason, V. Freger, Phenomenological analysis of transport of mono- and divalent ions in nanofiltration, Journal of Membrane Science, 360 (2010) 389-396.

[32] V.M. Barragán, J.P.G. Villaluenga, M.P. Godino, M.A. Izquierdo-Gil, C. Ruiz-Bauzá, B. Seoane, Experimental estimation of equilibrium and transport properties of sulfonated cation-exchange membranes with different morphologies, Journal of Colloid and Interface Science, 333 (2009) 497-502.

[33] P.N. Pintauro, D.N. Bennion, Mass transport of electrolytes in membranes. 1. Development of

mathematical transport model, Industrial and Engineering Chemistry Fundamentals, 23 (1984) 230-234.

[34] Y. Lanteri, P. Fievet, A. Szymczyk, Evaluation of the steric, electric, and dielectric exclusion model on the basis of salt rejection rate and membrane potential measurements, Journal of Colloid and Interface Science, 331 (2009) 148-155.

[35] A. Szymczyk, P. Fievet, Investigating transport properties of nanofiltration membranes by means of a steric, electric and dielectric exclusion model, Journal of Membrane Science, 252 (2005) 77-88.

[36] P.M. Biesheuvel, Two-fluid model for the simultaneous flow of colloids and fluids in porous media, Journal of Colloid and Interface Science, 355 (2011) 389-395.

[37] P.M. Biesheuvel, R. Zhao, S. Porada, A. van der Wal, Theory of membrane capacitive deionization including the effect of the electrode pore space, Journal of Colloid and Interface Science, 360 (2011) 239-248.

[38] L. Bruni, S. Bandini, The role of the electrolyte on the mechanism of charge formation in polyamide nanofiltration membranes, Journal of Membrane Science, 308 (2008) 136-151.

[39] Y. Lanteri, A. Szymczyk, P. Fievet, Influence of steric, electric, and dielectric effects on membrane potential, Langmuir, 24 (2008) 7955-7962.

[40] G. Saracco, Transport properties of monovalent-ion-permselective membranes, Chemical Engineering Science, 52 (1997) 3019-3031.

[41] V.M. Barragán, M.J. Pérez-Haro, Correlations between water uptake and effective fixed charge concentration at high univalent electrolyte concentrations in sulfonated polymer cation-exchange membranes with different morphology, Electrochimica Acta, 56 (2011) 8630-8637.

[42] P.N. Pintauro, D.N. Bennion, Mass transport of electrolytes in membranes. 2. Determination of NaCl equilibrium and transport parameters for nafion, Industrial and Engineering Chemistry Fundamentals, 23 (1984) 234-243.

[43] D.H. Freeman, Electrolyte uptake by ion-exchange resins, Journal of Physical Chemistry, 64 (1960) 1048-1051.

[44] F.G. Helfferich, Ion Exchange, McGraw-Hill, New York, (1962).

[45] J.H. Petropoulos, Membrane transport properties in relation to microscopic and macroscopic structural inhomogeneity, Journal of Membrane Science, 52 (1990) 305-323.

[46] C. Larchet, S. Nouri, B. Auclair, L. Dammak, V. Nikonenko, Application of chronopotentiometry to determine the thickness of diffusion layer adjacent to an ion-exchange membrane under natural convection, Advances in Colloid and Interface Science, 139 (2008) 45-61.

[47] V.I. Zabolotsky, V.V. Nikonenko, Effect of structural membrane inhomogeneity on transport properties, Journal of Membrane Science, 79 (1993) 181-198.

[48] K.D. Kreuer, S.J. Paddison, E. Spohr, M. Schuster, Transport in proton conductors for fuel-cell applications: Simulations, elementary reactions, and phenomenology, Chemical Reviews, 104 (2004) 4637-4678.

[49] N.P. Berezina, N.A. Kononenko, O.A. Dyomina, N.P. Gnusin, Characterization of ion-exchange membrane materials: Properties vs structure, Advances in Colloid and Interface Science, 139 (2008) 3-28.

[50] A.V. Dobrynin, M. Rubinstein, Theory of polyelectrolytes in solutions and at surfaces, Progress in Polymer Science (Oxford), 30 (2005) 1049-1118.

[51] S. Porada, R. Zhao, A. Van Der Wal, V. Presser, P.M. Biesheuvel, Review on the Science and Technology of Water Desalination by Capacitive Deionization, Progress in Materials Science 58 (2013).

[52] G.M. Geise, B.D. Freeman, D.R. Paul, Sodium chloride diffusion in sulfonated polymers for membrane applications, Journal of Membrane Science, 427 (2013) 186-196.

[53] M. Higa, A. Kira, A. Tanioka, K. Miyasaka, Ionic partition equilibrium in a charged membrane immersed in a mixed ionic solution, Journal of the Chemical Society, Faraday Transactions, 89 (1993) 3433-3435.

[54] K.L. Huang, T.M. Holsen, J.R. Selman, Anion partitioning in and diffusion through a Nafion membrane, Industrial and Engineering Chemistry Research, 42 (2003) 3620-3625.

[55] L. Jones, P.N. Pintauro, H. Tang, Co-ion exclusion properties of polyphosphazene ion-exchange membranes, Journal of Membrane Science, 162 (1999) 135-143.

[56] T. Sata, Ion Exchange Membranes; Preparation, Characterization, Modification and Application, The Royal Society of Chemistry, Cambridge UK, 2004.

[57] AmericanWaterWorksAssociation, Electrodialysis and Electrodialysis Reversal, manual of water supply practices M38, AWWA, Denver USA, 1999.

[58] A. Chapotot, G. Pourcelly, C. Gavach, Transport competition between monovalent and divalent cations through cation-exchange membranes. Exchange isotherms and kinetic concepts, Journal of Membrane Science, 96 (1994) 167-181.

[59] P.N. Pintauro, R. Tandon, L. Chao, W. Xu, R. Evilia, Equilibrium partitioning of monovalent/bivalent cation-salt mixtures in nafion cation-exchange membranes, Journal of Physical Chemistry, 99 (1995) 12915-12924.

[60] K. Dähnert, D. Huster, Comparison of the Poisson–Boltzmann Model and the Donnan Equilibrium of a Polyelectrolyte in Salt Solution, Journal of Colloid and Interface Science, 215 (1999) 131-139.

[61] X. Xing, Poisson-Boltzmann theory for two parallel uniformly charged plates, Physical Review E - Statistical, Nonlinear, and Soft Matter Physics, 83 (2011) 041410.

[62] S.H. Behrens, M. Borkovec, Exact Poisson-Boltzmann solution for the interaction of dissimilar charge-regulating surfaces, Physical Review E - Statistical Physics, Plasmas, Fluids, and Related Interdisciplinary Topics, 60 (1999) 7040-7048.

[63] J. Daicic, A. Fogden, I. Carlsson, H. Wennerström, B. Jönsson, Bending of ionic surfactant monolayers, Physical Review E - Statistical Physics, Plasmas, Fluids, and Related Interdisciplinary Topics, 54 (1996) 3984-3998.

[64] S. Basu, M.M. Sharma, An improved Space-Charge model for flow through charged microporous membranes, Journal of Membrane Science, 124 (1997) 77-91.

[65] I. Borukhov, D. Andelman, H. Orland, Steric effects in electrolytes: A modified Poisson-Boltzmann equation, Physical Review Letters, 79 (1997) 435-438.

[66] J. Cervera, V. García-Morales, J. Pellicer, Ion size effects on the electrokinetic flow in nanoporous membranes caused by concentration gradients, Journal of Physical Chemistry B, 107 (2003) 8300-8309.

[67] J. Cervera, P. Ramírez, J.A. Manzanares, S. Mafé, Incorporating ionic size in the transport equations for charged nanopores, Microfluidics and Nanofluidics, 9 (2010) 41-53.

[68] S. Mafé, P. Ramírez, J. Pellicer, Activity coefficients and Donnan co-ion exclusion in charged membranes with weak-acid fixed charge groups, Journal of Membrane Science, 138 (1998) 269-277.

[69] R. Zhao, O. Satpradit, H.H.M. Rijnaarts, P.M. Biesheuvel, A. van der Wal, Optimization of salt adsorption rate in membrane capacitive deionization, Water Research, 47 (2013) 1941-1952.

[70] P.M. Biesheuvel, W.M. De Vos, V.M. Amoskov, Semianalytical continuum model for nondilute neutral and charged brushes including finite stretching, Macromolecules, 41 (2008) 6254-6259.

[71] W.M. De Vos, M. Biesheuvel, A. De Keizer, M. Kleijn, M.A. Cohen Stuart, Adsorption of anionic surfactants in a nonionic polymer brush experiments, comparison with mean-Field theory, and implications for brush-Particle interaction, Langmuir, 25 (2009) 9252-9261.

[72] F.G. Smith III, W.M. Deen, Electrostatic effects on the partitioning of spherical colloids between dilute bulk solution and cylindrical pores, Journal of Colloid and Interface Science, 91 (1983) 571-590.

[73] F.G. Smith III, W.M. Deen, Electrostatic double-layer interactions for spherical colloids in cylindrical pores, Journal of Colloid and Interface Science, 78 (1980) 444-465.

[74] M.N. Tamashiro, Y. Levin, M.C. Barbosa, Donnan equilibrium and the osmotic pressure of charged colloidal lattices, European Physical Journal B, 1 (1998) 337-343.

[75] A. Philipse, A. Vrij, The Donnan equilibrium: I. on the thermodynamic foundation of the Donnan equation of state, Journal of Physics Condensed Matter, 23 (2011) 194106.

[76] K. Tsujii, Donnan equilibria in microbial cell walls: A pH-homeostatic mechanism in alkaliphiles, Colloids and Surfaces B: Biointerfaces, 24 (2002) 247-251.

[77] E.H. Cwirko, R.G. Carbonell, A theoretical analysis of Donnan dialysis across charged porous membranes, Journal of Membrane Science, 48 (1990) 155-179.

[78] S. Porada, B.B. Sales, H.V.M. Hamelers, P.M. Biesheuvel, Water desalination with wires, Journal of Physical Chemistry Letters, 3 (2012) 1613-1618.

[79] B. Jamnik, V. Vlachy, Ion partitioning between charged micropores and bulk electrolyte solution. Mixtures of mono- and divalent counterions and monovalent co-ions, Journal of the American Chemical Society, 117 (1995) 8010-8016.

[80] S. Mafé, P. Ramírez, A. Tanioka, J. Pellicer, Model for counterion-membrane-fixed ion pairing and donnan equilibrium in charged membranes, Journal of Physical Chemistry B, 101 (1997) 1851-1856.

[81] S. Bandini, Modelling the mechanism of charge formation in NF membranes: Theory and application, Journal of Membrane Science, 264 (2005) 75-86.

[82] J.M. Crabtree, E. Glueckauf, Structural analysis of ion semi-permeable membranes by co-ion uptake and diffusion studies, Transactions of the Faraday Society, 59 (1963) 2639-2654.

[83] E. Glueckauf, A New Approach to Ion Exchange Polymers Proceedings of the Royal Society A, 268 (1962) 350-370.

[84] K. Köhler, P.M. Biesheuvel, R. Weinkamer, H. Möhwald, G.B. Sukhorukov, Salt-induced swelling-to-shrinking transition in polyelectrolyte multilayer capsules, Physical Review Letters, 97 (2006) 188301.

[85] L. Firdaous, J.P. Malériat, J.P. Schlumpf, F. Quéméneur, Transfer of monovalent and divalent cations in salt solutions by electrodialysis, Separation Science and Technology, 42 (2007) 931-948.

[86] O. Coronell, B.J. Mariñas, X. Zhang, D.G. Cahill, Quantification of functional groups and modeling of their ionization behavior in the active layer of FT30 reverse osmosis membrane, Environmental Science and Technology, 42 (2008) 5260-5266.

[87] A. Yaroshchuk, Y. Boiko, A. Makovetskiy, Electrochemical perm-selectivity of active layers and diffusion permeability of supports of an asymmetric and a composite NF membrane studied by concentration-step method, Desalination, 245 (2009) 374-387.

[88] A.V. Sokirko, J.A. Manzanares, J. Pellicer, The Permselectivity of Membrane Systems with an Inhomogeneous Distribution of Fixed Charge Groups, Journal of Colloid and Interface Science, 168 (1994) 32-39.

Chapter 6

Membrane resistance: The effect of salinity gradients over a cation exchange membrane

Abstract

Ion exchange membranes (IEMs) are used for selective transport of ions between two solutions. These solutions are often different in concentration or composition. The membrane resistance (R_M) is an important parameter affecting power consumption or power production in electrodialytic processes. In contrast to real applications, often R_M is determined while using a standard 0.5 M NaCl external solution. It is known that R_M increases with decreasing concentration. However, the detailed effect of a salinity gradient present over an IEM on R_M was not known, and is studied here using alternating and direct current. NaCl solution concentrations varied from 0.01-1.1 M. The results show that R_M is mainly determined by the lowest external concentration. R_M can be considered as two resistors in series i.e. a gel phase (concentration independent) and an ionic solution phase (concentration dependent). The membrane conductivity is limited by the conductivity of the ionic solution when the external concentration, c_{ext} < 0.3 M. The membrane conductivity is limited by the conductivity of the gel phase when $c_{ext} \geq 0.3$ M, then differences of R_M are small. A good approximation of experimentally determined R_M can be obtained. The internal ion concentration profile is a key factor in modeling R_M.

Nomenclature

A	=	area (m^2)
a	=	constant ($\Omega\ m^2$)
b	=	constant ($\Omega\ m^2$)
c	=	concentration (mol/m^3)
$\bar{c}$	=	concentration in the membrane (mol/m^3)
D_w	=	osmotic water transfer coefficient (m^2/s)
F	=	Faraday constant (C/mol)
f	=	volume fraction (-)
G	=	conductance (S)
j	=	current density (A/m^2)
k	=	dimensionless concentration (-)
N	=	number of membrane pairs in the membrane stack (-)
n	=	curvature parameter (-)
R	=	resistance (Ω , $\Omega\ cm^2$)
T_i	=	transport number (-)
t	=	time (s)
t_w	=	water transport number (-)
v_f	=	flow velocity (m/s)
w_u	=	membrane water content (g solution / g dry membrane)
X	=	membrane charge (mol/m^3)
x	=	membrane coordinate (m)
z	=	valence (-)
Δm	=	transported water (mol)
δ	=	thickness (m)
η	=	coulombic efficiency (-)
Λ	=	molar conductivity (S m^2 / mol)
μ	=	chemical potential ($= kT$)
ρ	=	resistivity ($\Omega\ m$)
σ	=	conductivity (S/m)
ϕ	=	phase shift (˚)
Ψ	=	permselectivity (-)

6.1 Introduction

Ion exchange membranes are widely used for concentrating and/or selective transport of dissolved charged particles, for example in electrodialysis (ED) for desalination purposes [1-3]. Although ED is in practice most used for brackish water desalination, it recently gained interest as a seawater (pre) desalination technology [4, 5]. In addition, an electrodialysis stack can be used for the production of salinity gradient energy in the opposite process i.e. reversed electrodialysis (RED), by mixing river water and seawater [6-9]. The salt concentrations of the solutions in a RED stack are comparable to those in a seawater ED stack. In the ED process low energy consumption is desired and in RED high power production is targeted. In both situations low stack resistances are a prerequisite.

Generally, membrane resistances are determined at an external salt concentration of 0.5 M NaCl and a temperature of 25 °C. Literature shows that membrane resistance depends on the concentration of the external solution [10-16]. In practical applications of ED or RED, the concentration at either side of the ion exchange membrane differs. It is, however, unknown how this determines the membrane resistance. Recent research indicated that the membrane resistance is significantly higher compared to high salinities at both sides of the membrane when a solution low in salinity is present at one side of the membrane and liquid with a high salinity at the other side [16]. This previous research indicated that the actual membrane resistance in practical applications may be an order of magnitude higher than specified in standard resistance characterization measurements with 0.5 M solutions at both sides of the membranes.

Although the membrane resistance between external solutions of unequal concentration is particularly interesting for many practical applications, no systematic quantitative experimental research has been performed on this topic. Veerman *et al.* attempted to model the membrane resistance in cases with different salinity at both sides quantitatively [8]. To validate this model, and gain fundamental knowledge on membrane resistance in practical applications, this paper presents experimental results on the resistance of ion exchange membranes, having different salinities at both sides (0.01-1.1 M NaCl). This experimental data provides a solid fundament for a model, presented in this research, to estimate the (cat-) ion exchange membrane resistance, even when using different salt concentrations at either side of the membrane. This knowledge improves the modeling of processes in ED and RED [17, 18] and furthermore provides insight in how to influence the membrane resistance for practical applications.

6.2 Theory

Determination of the 'membrane resistance' is not straightforward as the measurement is influenced by changes in the membrane environment. Długołęcki *et al.* [11, 12] investigated single membranes at several NaCl concentrations (range 0.017-0.5 M) and distinguished the ohmic (true) membrane resistance (R_M), the resistance of the electric double layer (R_{DL}), and the resistance of the diffusional boundary layer (R_{DBL}). Długołęcki *et al.* [11, 12] showed that, at low external NaCl concentrations (<0.1 M), the diffusion boundary layer resistance (R_{DBL}) is the main resistance, while at 0.5 M the true membrane resistance (R_M) accounts for the largest part of the observed membrane resistance [11, 12].

In the present article, the electric double layer resistance as defined in [12, 19] is not included as a separate resistance, as there is no convincing evidence for it to be significant; the effect is considered here to be part of the diffusion boundary layer, which is further referred to as stagnant diffusion layer (SDL) [20, 21]. Consequently the observed membrane resistance is given by the summation of the true membrane resistance and the resistance of the SDL:

$$R_{M+SDL} = R_M + R_{SDL} \qquad \text{eq. 1}$$

Ion exchange membranes (IEMs) contain a fixed charge, which stems from the ion exchange groups covalently bound to the membrane polymer. For cation exchange membranes e.g. sulfonic acid groups are used, while for anion exchange membranes e.g. quaternary ammonium groups are used [1, 2]. Ions with a charge opposite to the fixed membrane charge density, X (mol/m^3 of internal solution [22]) are called counterions, while ions with a charge similar to X are called co-ions. So for a cation exchange membrane Na$^+$ ions are the counterions and Cl$^-$ ions are the co-ions. The degree to which counterions can pass the membrane and the passage of co-ions is prevented, is reflected by the permselectivity (ψ^m), which was defined by Winger *et al.* [23] as:

$$\psi^m = \frac{T_{cou}^m - T_{cou}^s}{T_{co}^s} \qquad \text{eq. 2}$$

Where T_{cou}^m, T_{cou}^s, and T_{co}^s are the transport numbers (-) of respectively the counterions in the membrane, the counterions in solution and the co-ions in solution. Assuming electro neutrality within the membrane, the fixed membrane charge density, X, the counterion concentration in the membrane ($\bar{c}_{counterion}$), and the co-ion concentration in

the membrane ($\bar{c}_{co-ion}$) are related according to eq. 3:

$$X + \bar{c}_{co-ion} = \bar{c}_{counterion} \qquad \text{eq. 3}$$

The counterion concentration in excess to the membrane charge is referred to as 'free ion concentration' and is equal to the co-ion concentration, therefore $\bar{c}_{co-ion} \equiv \bar{c}_{free}$. These free ions could be of particular interest to model membrane conductance, as these ions are not associated with a fixed charge and depend on the external concentration [24]. Previously, the relation between the external NaCl concentration and the internal concentration was investigated [22]. This research concluded that the Boltzmann equation underlying the classical Donnan theory is valid to use for densely charged ion exchange membranes. In the original Boltzmann theory ions are regarded as point charges, in very narrow pores (~1 nm), ion size is no longer completely negligible. Therefore it is necessary to include a small (energetic) size exclusion term ($\mu^* = 0.2\,kT$), leading to the relationship given by eq. 4 [22]:

$$\bar{c}_{counterion} + \bar{c}_{co-ion} = \sqrt{X^2 + (2 \cdot c_{ext} \cdot \exp(-\mu^*))^2} \qquad \text{eq. 4}$$

Where c_{ext} is the external salt concentration (mol/m³). The fixed membrane charge density, X is not a constant because it is expressed per unit volume and therefore changes with the swelling degree of the membrane according to eq. 5 [22]:

$$X = X_0 \cdot \frac{w_0}{w} \qquad \text{eq. 5}$$

Where X_0 is the fixed membrane charge density estimated at an external NaCl solution concentration of zero (=5.7 M, in case of a Neosepta CMX membrane [22]), w_0 is the accompanying CMX membrane water content (0.3113 g/g [22]), and w is the actual water content (= w_0 - 0.0167 $\cdot$ c_{ext}, g/g [22]) of a CMX membrane at the given external solution concentration, c_{ext} (M). By combining eq. 3 and 4, the equation to determine the co-ion (or free ion) concentration becomes:

$$\bar{c}_{co-ion} = \frac{1}{2}(\sqrt{X^2 + (2 \cdot c_{ext} \cdot \exp(-\mu^*))^2} - X) \qquad \text{eq. 6}$$

Eq. 6 shows that, due to the Donnan equilibrium, a decrease in ion concentration of the external solution (c_{ext}) leads to a decrease of the (free) ion concentration of the internal membrane solution [22, 24-27]. If the ion concentration of a solution decreases, the conductivity of the solution decreases proportionally (and almost linear below 1.0 M).

Resistance of a salt solution (*R, Ω*) is related to the conductivity (*σ*, S/m) as shown in eq. 7:

$$R = \frac{1}{G} = \frac{\delta}{\sigma \cdot A} = \frac{\delta}{\Lambda \cdot c \cdot A}$$
eq. 7

Where *G* is the conductance (S), *A* is the area (m²), *δ* is the thickness (m), *σ* is the conductivity (S/m), *Λ* is the molar conductivity (S m²/mol), and *c* is the concentration (mol/m³). The conductivity of a material is defined by the concentrations and mobilities of the charge carriers it contains [25]. In ion exchange membranes, the charge is carried by ions. The mobility of these ions is expressed by their diffusion coefficient (related through the Einstein-Smoluchowski equation [28, 29]). As described by Helfferich [25], a high membrane conductivity is favored by: i) a high membrane charge density, ii) low degree of cross-linking, iii) small ion size, iv) low ion valence, v) high external solution concentration and vi) elevated temperature.

The membrane resistance is only one part of the total ED/RED stack resistance. Additional resistance is created by electrodes and liquid phase. By adjusting the electrolyte system or the electrode coating, the overpotential (due to concentration polarization) and the electrode resistance can be minimized [8, 30, 31]. Channel thickness, and consequently liquid resistance, can also be optimized for the system. Membrane resistance especially becomes important for processes where electrode and flow channel resistances are minimized, or when the membrane resistance is relatively large compared to the other resistances, e.g. when very thin flow channels or profiled membranes are used [7, 32].

NaCl concentrations of the external solutions, which are unequal at both sides of an ion exchange membrane result in a chemical potential gradient over the membrane. This induces ionic diffusion and osmotic water transport. In electrochemical systems such as ED and RED, water transport can take place due to osmosis (free water) or due to electro-osmosis (water transport together with the ion, as its hydration sphere) [1, 2, 33-35]. In electrodialysis, the osmotic and electro-osmotic water flux are in the same direction (towards the concentrate) and can have a large influence on the separation process [2, 5, 33, 34, 36]. For RED, water transport is of less influence as electro-osmosis and osmosis are in opposite direction and effectively cancel out partially at current densities typical for RED [37].

The utilized membrane will influence the water flux through the membrane. The size of the flux is primarily influenced by the membrane water content and external solution concentrations. Secondly it is influenced by the degree of cross-linking, the fixed

membrane charge density and the temperature [33, 34, 36, 38-41]. Electro-osmosis is proportional to the applied current density, osmosis is indirectly affected by the current density [5]. The osmotic water transport, Δm_{osm} (mol) is calculated by eq. 8 [1]:

$$\Delta m_{osm} = D_w \cdot \frac{A \cdot (c_{high} - c_{low})}{\delta} \cdot \Delta t \qquad \text{eq. 8}$$

Where t is the time (s) and D_w is the osmotic water transfer coefficient (m²/s), which depends on the specific membrane type and temperature. For a system with one counterion type and one co-ion type (such as NaCl), the net electro-osmotic water transport Δm_{e-osm} (mol) is given by eq. 9:

$$\Delta m_{e-osm} = t_w \cdot \frac{j \cdot A \cdot \eta \cdot N}{z_i \cdot F} \cdot \Delta t \qquad \text{eq. 9}$$

Where t_w is the water transport number (mol H$_2$O/mol ion), j the applied current density (A/m²), η is the coulombic efficiency (-), N is the number of membrane pairs in the membrane stack (-), z_i is the ion valence (-), and F is the Faraday constant (C/mol). Similar as for D_w also t_w is membrane specific. Furthermore t_w also depends on the ion type and ionic composition. Unlike the osmotic water flux, the direction of the electro-osmotic water flux does depend on the direction of the electric field.

6.3 Materials and Methods

6.3.1 Materials

Membrane resistance was investigated in a six compartment stack as shown in Figure 1. A detailed description of this stack is given by Długołęcki *et al.* [11, 42]. The effective area of the membrane under investigation in this stack was 2.835 cm². This effective area was obtained by placing two shields (Perspex 2 mm) on either side of the membrane, which, without shields, has an effective area of 23.8 cm². In contrast to previous research [11, 42], all membranes in the setup for this research are cation exchange membranes (CMX, Neosepta®, Tokuyama Corporation, Japan). Consequently, no concentration changes occur when a direct current (DC) is applied on the electrodes. The active area of the auxiliary membranes was 23.8 cm² each. The volume of each of the compartments was 95.0 cm³.

A galvanostat (Ivium Technologies, The Netherlands) was used to apply a (fixed) current density (DC or alternating current, AC) and at the same time measure the voltage drop over the membrane under investigation. In order to measure this voltage drop, two Haber-Luggin capillaries were placed on either side of the membrane. The

distance from the tip of the capillaries to the membrane was ~4.5 mm. These capillaries were filled with the same solution (and same concentration) as present in the specific compartment and each was connected to a small reservoir. In these reservoirs Ag/AgCl gel electrodes (QM711X, QIS, The Netherlands) were placed and connected to the galvanostat.
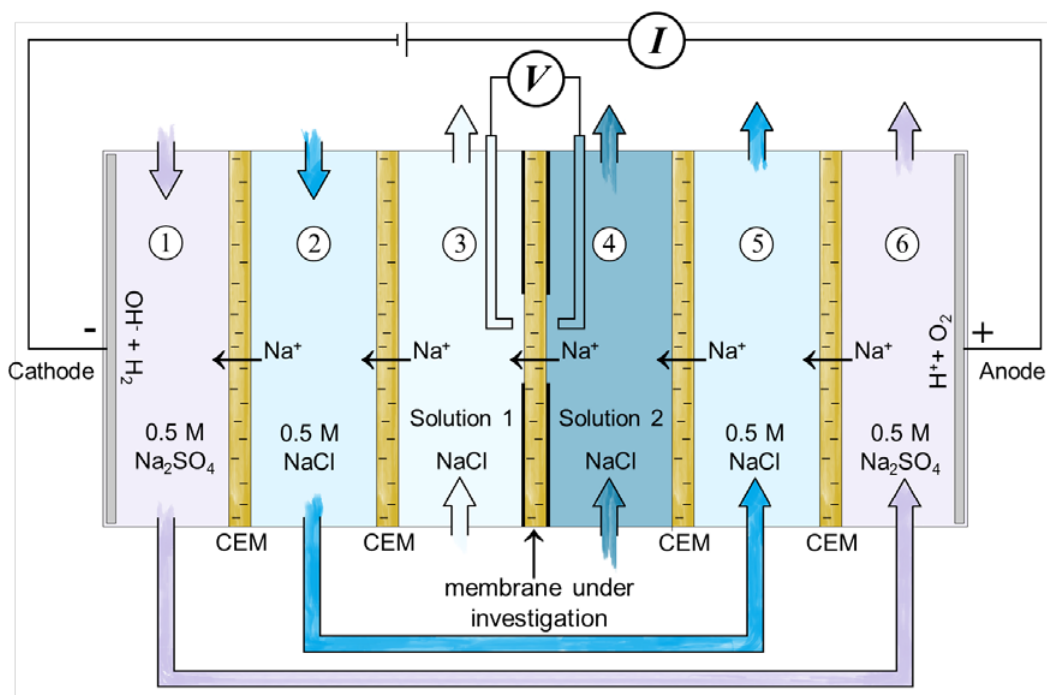
Figure 1. Schematic representation of the six compartment cell used to determine the membrane resistance. The NaCl solution concentration (c_{low} and c_{high}) of the compartments adjacent to the membrane under investigation (CMX, Neosepta), was varied between 0.01-1.1 M. CEM is a cation exchange membrane, I is the electrical current (A) and V is the potential difference over the Haber-Luggin capillaries (V). Drawing based on [11, 42].

6.3.2 Methods

Determining membrane resistance

Throughout the experiments, the temperature of the solutions was controlled at 25°C with a thermostatic bath. In this bath, the solutions were kept in 1 l bottles and circulated through the compartments at a flow rate of 170 ml/min (average flow velocity at the solution-membrane interface ≈ 0.07 cm/s). The temperature of the solutions was checked with a glass thermometer before the start of each experiment. Salt solutions were prepared with distilled water and NaCl (analytical grade, Boom B.V., The Netherlands). The concentrations varied from 0.01 - 1.1 M.

Preliminary to installing the investigated membrane in the stack, it was equilibrated with a 0.5 M NaCl solution for 3 days, while refreshing the solution daily. Preliminary to the experiment, the membrane was equilibrated for 1 hour with the specific measurement solutions in the stack. After the equilibration, the solutions in the stack were refreshed with solutions of the same initial concentration as the measurement solution (solutions were also kept at 25 °C). This was done to exclude possible effects of diffusion when a large concentration gradient was present over the membrane, e.g., 0.01 M in compartment 3 and 1.1 M in compartment 4 (see Figure 1). Even at the largest possible concentration gradient, only negligible difference in conductivity (< 1%) was observed directly before and after the experiments. This indicates that the concentrations of the solutions could be considered constant during the experiments.

To determine the membrane resistance, chronopotentiometry using DC in the under limiting current regime was applied [11, 42], as well as impedance spectroscopy (which creates an AC). DC was applied to determine the resistance of the membrane and the SDL (see eq. 1). The measurement was performed in 3 series. Each series started with 5 minutes open circuit conditions (0 A), followed by a defined array of applied current densities. At a concentration of 0.01 M at one of the membrane sides (compartment 3 or 4), the applied current density steps were 5, 10, 15, 20, 25, 30 A/m^2 (2 minutes per step). When the lowest concentration adjacent to the membrane under investigation was 0.1 M or higher, the current density steps (1 minute per step) were 5, 10, 15, 20, 25, 30, 40, 60, 80, 100 A/m^2.

During the chronopotentiometric experiments the potential is constantly measured. The resistance (ohm cm^2) was taken as the slope of the graph with the applied current density (mA/cm^2) on the x-axis and the potential (mV) on the y-axis. The polarity of the stack was fixed throughout the experiments, i.e. the electrical current was always applied in the same direction.

To distinguish the effect of the SDL from the true membrane resistance, the impedance was measured applying a high frequency AC while measuring the voltage with the galvanostat. The AC density was varied in ten steps between 1.8-35.3 A/m^2, always at a frequency of 1000 Hz. At this frequency, the phase shift, ϕ (°) is minimized and the measured resistance only includes the true membrane resistance, while SDL effects are excluded, as is shown in previous investigations [12, 43]. Also no relation between applied AC density and measured resistance within this current density range was found in the present work, wat confirms that the SDL formation can be neglected under these conditions. The AC resistance was determined from 17 measurements per

experimental setting.

When determining AC and DC resistances it is important to correct for the aqueous phase between the capillary and the membrane. Also a possible asymmetry of the right side and the left side of the membrane should be taken into account. Therefore, for every resistance data point, 4 individual measurements were performed. Considering the resistance of the membrane between two different solutions with a concentration c_1 and c_2, we determined the resistance of these 4 systems: R_1) $c_1|membrane|c_2$, R_2) $c_2|membrane|c_1$, R_3) c_1 only, and R_4) c_2 only. R_{M+SDL} (in case of DC) and R_M (in case of AC) can then be calculated as:

$$R_{M+SDL} / R_M = \frac{(R_1 + R_2 - R_3 - R_4)}{2}$$

eq. 10

Concentration profiles within the membranes

To study the ion transport through the membranes, the relative concentration of co-ions (Cl$^-$) and counterions (Na$^+$) in the cation exchange membrane cross-section was identified with energy dispersive X-ray spectra (SEM-EDX or EDS). As the Neosepta CMX membrane used in the chronopotentiometry experiments was not suitable for this, among others because its reinforcement contains the element Cl [44], a Ralex CMH membrane (MEGA A.S., Czech Republic) was selected for this experiment. This membrane was used in a stack with typical RED conditions, fed with 0.51 M NaCl as concentrate and 0.017 M NaCl as diluate, both at a flow velocity, v_f of 1.3 cm/s. Feed water passed the stack only once, i.e. a constant concentration was supplied on either side of the membrane continuously. A current density of 10 A/m^2 was generated in RED-operation for four hours to equilibrate the ionic composition in the membrane interior.

After this operation, the membranes were removed from the stack and the external liquid was quickly removed by rinsing with demineralized water. The membranes were directly frozen in liquid nitrogen to conserve the position of the ions in the membranes. The process to stop the stack operation, dismantle the stack, and freeze the membranes took approximately 1 min. Subsequently, the frozen membranes were broken and freeze dried (Edwards, United Kingdom).

EDX analysis (JEOL, JSM 6010LA, United States) was performed over two cross-sectional lines, each comprising 13 scan points, equally distributed over the membrane cross-section. The dry thickness of these membranes was approximately 400 μm. The average atomic percentages of the detected elements of Na and Cl were calculated.

Because the EDX analysis only yields a relative contribution of several elements, no absolute concentrations can be derived. Therefore, the ratio between the amount of counterions (Cl⁻) and the total amount of ions (Na⁺ + Cl⁻) in a cross-section of the membrane was determined.

6.4 Results & Discussion

6.4.1 Experimentally determined membrane resistance

Figure 2 shows the membrane resistance as a function of the two external NaCl solutions (c_1 and c_2), for a range of concentrations, varying from 0.01-1.1 M.
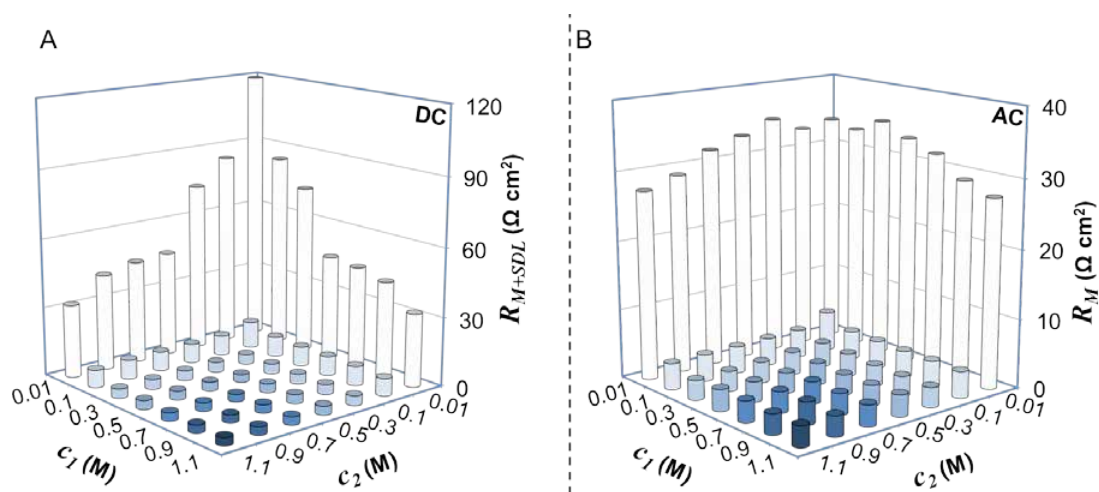
Figure 2. A) Observed membrane resistance (R_{M+SDL}, Ω cm²) determined with DC measurements and B) membrane resistance (R_M, Ω cm²) determined with AC measurements, at defined external NaCl solution concentrations (c_1 and c_2, M). Both Figures are mirrored in their diagonal axes where $c_1 = c_2$. Exact values of the measurements are given in Table A 1 (DC) and Table A 2 (AC) in Appendix A.

The left graph (A) shows the observed membrane resistance (R_{M+SDL}) determined while applying DC. The data includes the true membrane resistance (R_M) and the stagnant diffusion layer resistance (R_{SDL}) adjacent to the membrane at both sides. The primary and secondary x-axis represent the concentrations on each side of the membrane. Highest R_{M+SDL} was obtained at a concentration of 0.01 M on either side of the membrane. Lowest R_{M+SDL} was obtained at a concentration of 1.1 M on either side of the membrane.

The right graph (B) shows the determined membrane resistance (R_M) obtained while applying AC. Again the primary and secondary x-axis represent the concentrations on

each side of the membrane. Highest R_M was observed at a concentration of 0.01 M on one side and 0.3 M on the other side. Lowest R_M was obtained at a concentration of 1.1 M on either side of the membrane. Exact values of the data shown in Figure 2 A and B are provided in Table A 1 (A) and Table A 2 (B) in Appendix A.

Considering the value of R_M at the diagonal (where $c_1 = c_2$) in Figure 2A and 2B, it is remarkable that increasing the external salt concentration results in a significant decrease of the membrane resistance (and the SDL resistance). Similar trends are reported by others [10-12, 16, 45, 46]. Comparing Figure 2 A and B (mind the different scale on the y-axes) reveals that the mutual difference in the measured values with 0.01 M NaCl solution present at one side is much larger in Figure 2 A, than in Figure 2 B. This small mutual difference of R_M, shown in Figure 2 B, is remarkable as it suggests that the effect of the concentrated side on R_M is only very limited. In case the concentrated side would have a large influence, the R_M obtained for a membrane with $c_1 = 0.01$ and $c_2 = 1.1$ M would be much closer to the R_M obtained at $c_1 = c_2 = 1.1$ M. Furthermore when c_1 and $c_2 \geq 0.3$ M, the difference in R_M (2.9-3.5 Ω cm^2) is relatively small.

Minor deviations, e.g., the higher R_M at 0.01 and 0.3 M in the AC measurements compared to the R_M at 0.01M at both sides of the membrane, are most likely due to measurement errors. As each data point given in the graph is based on four measurements (see eq. 10), each having its own uncertainty, the four uncertainties propagate. It was estimated that the uncertainty in one measurement with 0.01M at one side of the membrane can be as large as 5%. This implies that the uncertainty of the displayed data can be as large as 10%. This error mainly stems from the error in solution concentration as the error between the measurements (without changing the solutions) was found to be < 0.5%.

6.4.2 Dependency of R_M on lowest external solution concentration

Figure 2 B suggests that R_M is mainly determined by the lowest external solution salt concentration present. Figure 3 A shows the dependency of the measured membrane resistance on the lowest external solution concentration (c_{low}), disregarding the external concentration at the other side of the membrane. In the low concentration range (< 0.3 M), the observed membrane resistance ($R_M + R_{SDL}$) obtained with DC measurements and the true membrane resistance (R_M) obtained with AC measurements, both rapidly decrease with increasing c_{low}. If however, $c_{low} \geq 0.3$, the decrease of the membrane resistance flattens off and seems to reach a plateau. Figure 3 B shows the dependency of the measured membrane resistance on the average of the external solution concentrations ($c_{average}$). This Figure shows that no clear relation exists between $c_{average}$ and the

membrane resistance obtained with DC or AC measurements.
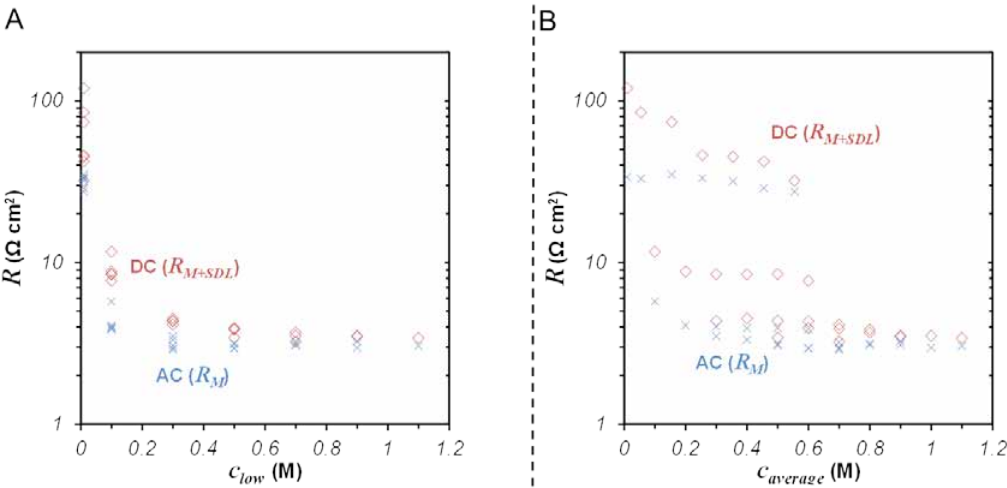
Figure 3. Membrane resistance (R, Ω cm²) determined with DC (◇) and AC (✕) measurements as a function of A) lowest external NaCl solution concentration (c_{low}, M) and B) average of the two external NaCl solution concentrations (c_{average}, M).

In addition to the relations shown in Figure 3 also the dependency of the membrane resistance on the highest external solution concentration (c_{high}) and the harmonic average ($\sqrt{c_{low} \cdot c_{high}}$) of the external solution concentrations was investigated (graphs not shown). These two variables showed even lower correlation with the measured membrane resistance, as is shown by the corresponding R^2 values (Table 1). These R^2 values are obtained from the differences in experimental values and a LOESS fit on these measurements. A LOESS fit gives a locally weighted polynomial regression [47], in this case applied with a span that covers 50% of the domain. This method is especially suitable since an assumption of the parametric form of the regression surface is not required [47]. Figure 3 and Table 1 clearly indicate that the membrane resistance depends mainly on c_{low}. This observation is important in e.g. ED and RED processes but was not studied before or reported in literature.

Table 1. R² values defined for four variables and obtained using a LOESS fit [47] .

Variable	R^2_{DC}	R^2_{AC}
c_{low}	0.951	0.993
c_{high}	0.570	0.401
$c_{average}$	0.608	0.417
$c_{harmonic}$	0.601	0.401

As this work focuses mainly on the membrane resistance (R_M), and not on the SDL

effect, the results in Figure 2 B will be further discussed and explained in this article, including some additional remarks on the DC measurements.

6.4.3 Limiting factor in membrane conductance

In Figure 4, the experimentally determined R_M values shown in Figure 2 B, are displayed as conductivity (σ_M, mS/cm), as a function of the external solution concentration (with $c_{ext} = c_{low}$). Figure 4 shows also the conductivity of the external solution (c_{ext}), and the conductivity of free ion concentration of the solution in the membrane ($\bar{c}_{free}$), both at 25 ºC. This free ion concentration is the concentration of counterions in excess to the fixed membrane charge density and is equal to the concentration of co-ions calculated with eq. 6 (where $\bar{c}_{co-ion} \equiv \bar{c}_{free}$).
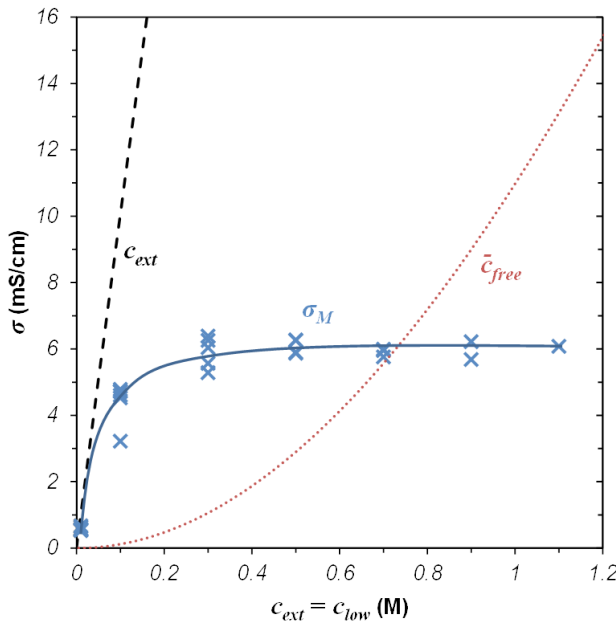
Figure 4. Conductivity (σ, mS/cm) of the membrane determined with AC measurements (σ_M, ×, solid line) as a function of the external NaCl concentration (c_{ext}, M), which is considered equal to the lowest external concentration, compared to the corresponding conductivity of the external solution (c_{ext}, dashed line), and the conductivity of the internal solution based on the free ion concentration ($\bar{c}_{free}$, dotted line).

Figure 4 shows that the conductivity of the external NaCl solution (c_{ext}) is rapidly increasing and is always higher than the measured membrane conductivity (σ_M). The external concentration at which the membrane conductivity is equal to the external solution conductivity is known as the equiconductance point [25] (or isoconductivity

point [14, 48]). For this membrane such point may be found when $c_{ext} < 0.01$ M, but this was outside our measurement range. The conductivity of the internal solution, taking into account only the free ions according to the Donnan equilibrium (eq. 6), is equal to the membrane conductivity at around 0.7 M. However, the concentration of these free ions does not seem to influence the membrane conductivity. It is remarkable to see that at low external solution concentration ($c_{ext} < 0.3$) the membrane conductivity is strongly influenced by the conductivity of the external solution, while at higher external concentrations ($c_{ext} \geq 0.3$ M) the measured membrane conductivity remains almost constant, whereas the conductivity of both the external and of the free ions in the internal solution further increases.

It can be reasonably assumed that most of the membrane's ion conductivity stems from the counterions associated with the fixed membrane charge (X). In previous investigations [22, 49] was shown that the concentration of counterions associated with X was affected by c_{ext} only to a very limited extent in the concentration range of 0.01-0.3 M. When assuming a homogenous internal membrane phase, the sudden flattening out of the membrane conductivity when $c_{ext} \geq 0.3$ M cannot be explained. Moreover, if the internal water existed only from one phase, an effect of the free ions in the internal solution would be expected. To explain the membrane conductivity curve as shown in Figure 4, a different approach is required. An approach which involves at least two internal conductive phases: One phase that is strongly influenced by the external concentration and limits the measured membrane conductivity when $c_{ext} < 0.3$ M, and another phase which is (almost) not influenced by the external concentration and is limiting the measured membrane conductivity when $c_{ext} \geq 0.3$ M.

6.4.4 The two conductive water phases of ion exchange membranes

Literature describes that at the micro level, also membranes known as 'homogenous' ion exchange membranes (as CMX) are spatially non-uniform, which influences the membrane properties [50-54]. This is known as the microheterogeneity of the membrane. According to previous research [14, 15, 50, 51, 55] the membrane can be divided into two phases. Phase I comprises a gel like phase that contains the charged polymer matrix with fixed ionic groups, and a charged solution of mobile counterions (and, in the minority, co-ions), which compensates the charge of the matrix. Phase I also contains the membrane reinforcements or inert fillers in the polymer. Phase II is defined as the electrically neutral solution (identical to the external solution) that is for instance present in structural cavities and at the center of the larger pores of the swollen membrane. The volume fraction of phase I and II (f_I and f_{II}) are defined as the volume fractions of the swollen membrane.

Membrane conductivity stems from ions in the mobile phase. From that point of view it might be advantageous to regard not just the two described phases but to make a further distinction of phase I in conductive and nonconductive regions. Yaroslavtsev [52] and Mafé *et al.* [56] have a similar approach and, with respect to the ion conductivity, only consider the water phases I and II.

The internal membrane water phase (pore) can be divided into a gel phase, similar to phase I, but now without e.g. reinforcements and polymer fillers, and an ionic solution (which is exactly the described phase II), with concentration $\bar{c}_i$ (with $\bar{c}_i = c_{ext}$). Mafé *et al.* [56] showed that the conductance of this ionic solution phase is influenced by the pore radius of the membrane (due to increased cross sectional area of phase II at increased pore radius) and the external solution concentration. A low external concentration results in a higher swelling degree and a larger fraction of phase II. At the same time, it reduces the conductivity of this phase as the concentration is equal to the external solution. The conductance of the gel phase is rather independent of pore radius and external concentration [56, 57]. Assuming the co-existence of these two phases, implies that the presence of microcavities and microchannels [52] influences the membrane conductance. As Zabolotsky *et al.* [51] pointed out, the micro structural inhomogeneity of the membrane is the main factor determining the concentration dependence of the 'electrical' conductivity. In literature, a distinction between water phases in the membrane is also made based on freezing water and non-freezing water, which would correspond respectively to the ionic solution and the gel phase [58-61]. Besides these two water phases also the membrane structure is considered, following [52], four phases can be distinguished within a CMX membrane:

- I) fixed membrane charge associated counterion solution with a vast minority of co-ions (gel phase).
- II) ionic solution existing of co-ions and counterions with concentration equal to the external solution.
- III) non-conductive polymer matrix.
- IV) non-conductive reinforcement.

Phase II is directly influenced by c_{ext}, and phase I is for now considered to be independent of c_{ext}. In fact, this latter assumption is not completely true, as the fixed membrane charge density of a CMX membrane is slightly influenced by the external concentration due to membrane swelling [22]. The two non-conductive phases (III and IV), do not provide any membrane conductance.

Literature reports that the fraction of phase II is typically small (up to $f_{II} \approx 0.1$) in homogenous membranes [50] , although also considerable fractions (up to $f_{II} \approx 0.45$) are reported [48]. These fractions were however taken as the fraction of the total membrane volume and not as the fraction of the pore. If taken as fraction of the water volume, which is ~0.3 for the CMX membranes [22], this fractions are much larger. Therefore it is important to express fractions based on pore volume.

6.4.5 A structure model based on serial conductors

In [52, 56] the ionic solution phase is considered to be in the center of the membrane pores, while the gel phase effectively acts as an electric double layer (EDL) at the internal membrane surface. This approach suggests presence of two parallel conductors in the membrane. In the microheterogeneity theory, utilized in e.g. [14, 15, 48, 50, 51, 55] both serial and parallel configurations can be evaluated by changing a parameter (α) for characterizing the arrangement of phases in the material [14]. The conductance of the membrane (G_M) for two parallel resistors (phase I and phase II) is given by $1/R_I + 1/R_{II}$. This implies that an increase in conductivity of phase II, would result in a linear increase of the total membrane conductivity. Our experimental results (Figure 4) however, show that the membrane conductivity flattens off, while the conductivity of phase II increases (represented by the conductivity of c_{ext}). The conductance of two serial resistors (Figure 5) is given by $1/(R_I + R_{II})$. In this case an increase in conductivity of phase II will result in an increase of the total membrane conductivity as well. However, this increase is not linear but levels of since the value of $1/(R_I + R_{II})$ reaches its limit ($1/R_I$) at higher external concentrations. Consequently our findings suggest that phase I and phase II act as serial conductors instead of parallel conductors.
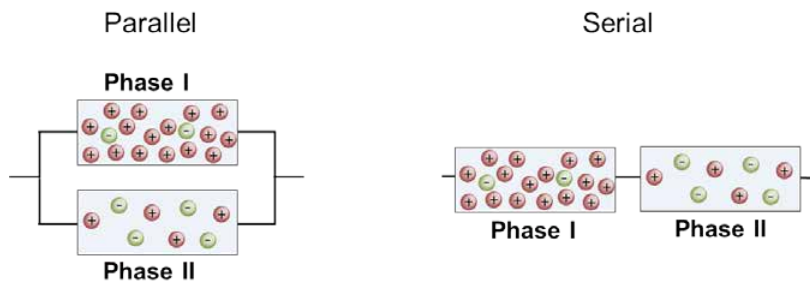

Figure 5. Parallel and serial resistors of phase I and phase II in a cation exchange membrane. Phase I represents the gel phase mainly existing of counterions associated with the fixed membrane charge density and phase II represents the electro neutral ionic solution which has a concentration equal to the external solution concentration.

Considering this serial approach, Figure 4 shows that the membrane conductivity is limited by the conductivity of the ionic solution when $c_{ext} < 0.3$ M, and the membrane conductivity is limited by the conductivity of the gel phase when $c_{ext} \geq 0.3$ M. In agreement with literature, the effect of c_{ext} on this gel phase conductivity is very small. So, although the counterion concentration in the gel phase can be around ~6 M, the conductivity of this phase is limiting when $c_{ext} \geq 0.3$ M. This can be explained by the intensive interactions between ions, water and fixed charges that occur at such high concentrations [62]. These interactions lower the ion mobility and effectively the conductivity of the phase. This is in agreement with the work of Berezina *et al.* [14, 15], who show that membrane conductivity as a function of the external solution concentration can show a maximum, as with increasing concentration the membrane water content decreases. This membrane dehydration results in higher viscosity, more ion-ion interaction (friction), and as such lower conductivity than expected regarding ion concentration. Swelling of ion exchange membranes is a well-known phenomenon and depends on many conditions, under which membrane cross-linking and membrane reinforcement [1].
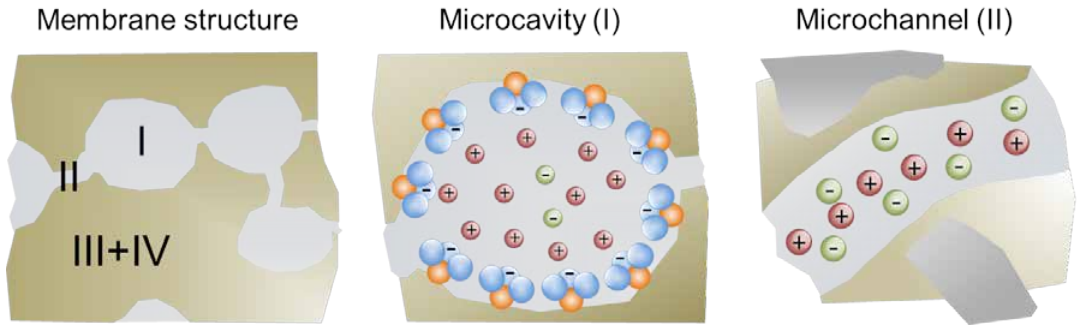
Figure 6. Schematic representation of a part of a cation exchange membrane structure as used in the model, with separately shown phase I and phase II. Phase I represents the assumed microcavities with fixed membrane charges (negative for cation exchange membranes) and an ion concentration based on the electro neutrality assumption and the Donnan equilibrium (eq. 3 and eq. 6). Phase II represents the assumed microchannels with a solution concentration equal to the external concentration.

In reinforced or cross-linked areas (phase III and IV) polymer swelling is minimized and the fixed membrane charge density in these phases can be assumed zero. It is assumed that due to the presence of these reinforced or cross-linked areas, small microchannels of ionic solution (phase II) can exist. The non-cross-linked polymer area contains the fixed membrane charge and can swell and as such form microcavities. In these microcavities, the gel phase is present (phase I). To obey the Donnan equilibrium [24], in the gel phase also free ions at a concentration equal to eq. 6 should be present.

These co-ions cause Donnan failure, and lead to a non-perfect permselectivity of the membrane (eq. 2). The four membrane phases that were defined earlier are illustrated in Figure 6.

6.4.6 Membrane resistance when $c_1 = c_2$

Taking into account the previously described membrane structure, R_M can be expressed in two terms, one depending on the external solution salt concentration and one (for simplicity assumed) independent of the external salt concentration. This leads to eq. 11, or in terms of conductance, eq. 12 (S/cm²).

$$R_M = a + \frac{b}{k_{ext}} = \frac{1}{G_I} + \frac{\frac{1}{G_{II}}}{k_{ext}} = \frac{1}{G_I} + \frac{1}{G_{II} \cdot k_{ext}} \qquad \text{eq. 11}$$

$$G_M = \frac{k_{ext}}{a \cdot k_{ext} + b} = \frac{G_I \cdot G_{II} \cdot k_{ext}}{G_I + G_{II} \cdot k_{ext}} \qquad \text{eq. 12}$$

Where a and b are constants, which can be written as G_I and G_{II} that represent the conductance (S/cm²) resulting from the ions in the microcavities (phase I) and from the ions in the microchannels (phase II), and k_{ext} is the dimensionless external concentration (by dividing c_{ext} with the reference concentration, $c^0 = 1$ M). For the CMX membrane considered in this research, the values of the two constants are $a = 2.674$ and $b = 0.311$. These values where obtained by fitting to the measurement data obtained with $c_1 = c_2$ only.

Figure 7 shows the experimental membrane resistance together with the modeled resistance according to eq. 11. The measured data seems to fit the model. Moreover, using this approach of different serial conductive phases in the membrane (eq. 11-12), membrane resistance data of different membranes presented in literature [10, 11, 45] can be well fitted and explained, as shown in Appendix B. However, the fact remains that the suggested structure is hypothetical and simplified, as in reality the three dimensional internal structure of a membrane is likely to be much more complex. As shown, the model can be used for reinforced homogenous membranes, but for, e.g., heterogeneous membranes, non-reinforced membranes or membranes with larger pore size adjustments may be required.
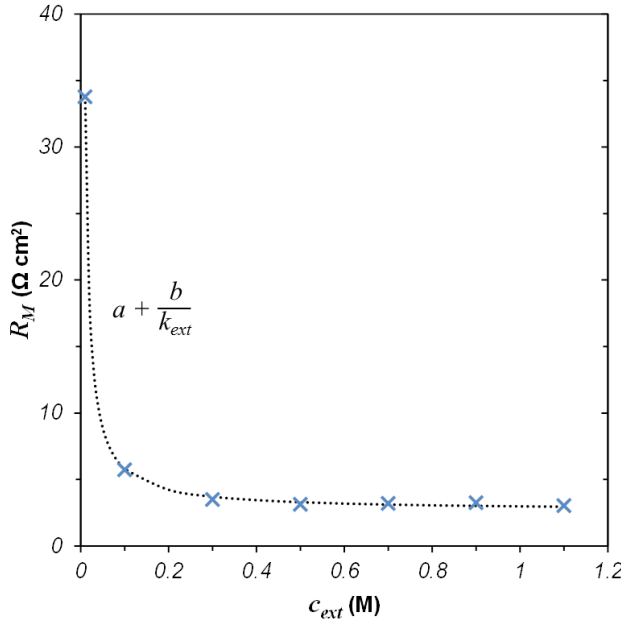
Figure 7. Membrane resistance (R_M, Ω cm²) of a CMX membrane determined with AC measurements (✕) as a function of the external NaCl concentration (c_{ext}, M). The external solution concentrations at both sides of the membrane were equal. The dotted line represents the calibrated result of eq. 11.

6.4.7 Membrane resistance when $c_1 \neq c_2$

The same model is also used to model R_M when external concentrations are unequal. As it was shown in Figure 3, R_M mainly depends on the lowest concentration of the external solutions. This implies that the solution in the microchannels (phase II) is almost similar to the lowest external concentration ($c_i \approx c_{low}$), although some influence of c_{high} is present. This finding suggests that the membrane obeys an internal concentration profile that largely follows c_{low} and shows towards the interface with c_{high} a sudden steep increase in concentration. Such a concentration profile can be explained by water transport from the low to the high salinity side (osmosis) and NaCl transport (by diffusion) in the opposite direction. Eq.8 shows that osmosis depends on the difference in salt concentration between the external solutions. During open circuit conditions, osmosis is in a direction opposite to ion diffusion, i.e. from c_{low} to c_{high}. The internal diffusion coefficient of water is estimated to be about one order of magnitude larger than that for salt [37]. A diffusive water flux through the membrane may therefore cause such a steep concentration profile. Also water-ion interaction (or friction [62]) might be enhanced. However, this is hypothetical and the internal concentration profile should be subject to further investigations. In literature, both linear concentration gradients [1, 2, 25, 33, 63, 64], and non-linear concentration profiles are considered

[25-27, 65-68]. This non linearity can become large due to water flow through the membrane by (anomalous) osmosis, electro osmosis, convection or differences in mobilities of co-ions and counterions in the membrane [27, 65-68]. Schlögl [27] shows how water flows can arise from local pressure differences in the membrane, however, to use this equation assumptions on water velocity and ion mobility in the membrane are required. More recent model concepts for the transport processes and resulting gradients in microheterogeneous models have been developed [14, 55]. In the present work, investigation of the exact form of the concentration profile is outside the scope of this work, therefore the assumed concentration profile is described by an arbitrary and rather simple function, as shown in eq. 13.

$$\bar{c}_i(x) = c_{low} + \left(c_{high} - c_{low}\right) \cdot \left(\frac{x}{\delta}\right)^n \qquad\qquad \text{eq. 13}$$

Where x is the membrane coordinate i.e. the position in the membrane (m), δ is the membrane thickness (m), and n is a fit parameter that indicates the curvature (steepness) of the graph that describes the concentration profile between two points as dictated by the two external solution concentrations ($n = 1$ gives a linear profile). In this equation, all parameters except n are boundary conditions. This function requires only one parameter without a physical meaning. It is of course a harsh simplification of reality, but for now fits the purpose to model the internal concentration profile in a first approximation. Figure 8 shows the effect of n on the internal concentration profile of a membrane with $\delta = 180 \cdot 10^{-4}$ cm. When the effect of water transport from the low concentration side to the high concentration side increases, the internal concentration profile is better described by an increasing n. Similar effect of water flow on the internal concentration profile is shown in [27].
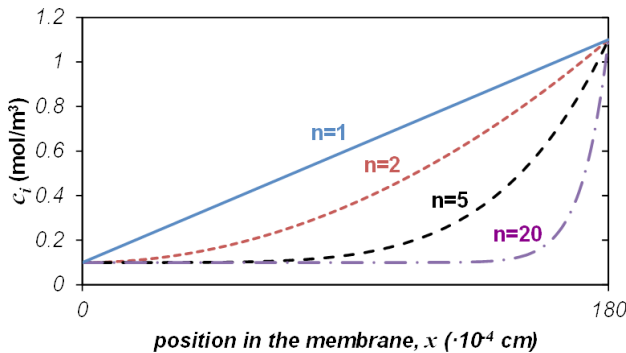
Figure 8. Ion concentration (c_i, mol/m³) as a function of the position in the membrane (x, 10^{-4} cm) when different input values of n are used in eq. 13.

The internal concentration profile (of phase II) is calculated with eq. 13. The result of this calculation is used as input for eq. 11 to calculate the membrane resistance, which is subsequently divided by the wet membrane thickness (δ) to obtain the membrane resistivity profile, ρ (Ω cm). Figure 9 shows the internal concentration profile and local resistivity in a CMX membrane present between a 0.01 M and 1.1 M NaCl solution ($n = 42.3$).
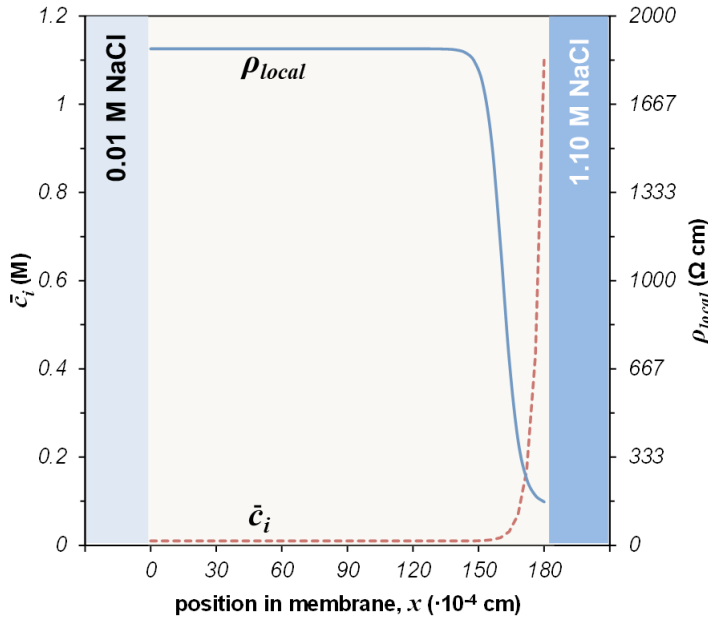
Figure 9. Modeled internal concentration profile ($\bar{c}_i$, M, dashed line), and local membrane resistivity profile (ρ_{local}, Ω cm, solid line) in a CMX membrane between a 0.01 M and 1.10 M NaCl external solution.

By integrating the local resistivity over the membrane thickness, the modeled membrane resistance is obtained. With eq. 13 an approximation of the internal concentration profile is obtained; however, the choice for the value for n is critical. In the present article the actual profile in a CMX membrane was not studied experimentally and therefore three different values for n were used. In all cases where $c_{low} = 0.01$ an n value of 42.3 was used and in all cases where $c_{low} = 0.1$ an n value of 1.4 was used. When $c_{low} \geq 0.3$, a straight line is assumed for the internal concentration profile ($n = 1$) because the conductivity of the gel phase is limiting in these cases, as stated earlier. The n values for the 0.1 M and 0.01 M series were chosen by minimizing the difference between the modeled membrane resistance and the experimental membrane resistance (Figure 2 B) of the whole series. More experimental data would provide

a better estimation of R_M and the n value might be determined as a function of both external solution concentrations.

6.4.8 Modeled membrane resistances

Figure 10A shows the modeled membrane resistance ($R_{M, model}$) as a function of c_1 and c_2. Figure 10B shows the model offset if $R_{M, model}$ is compared with the experimentally determined R_M, shown in Figure 2 B, also as a function of c_1 and c_2. The values of all modeled resistances are given in Appendix A (Table A 3).
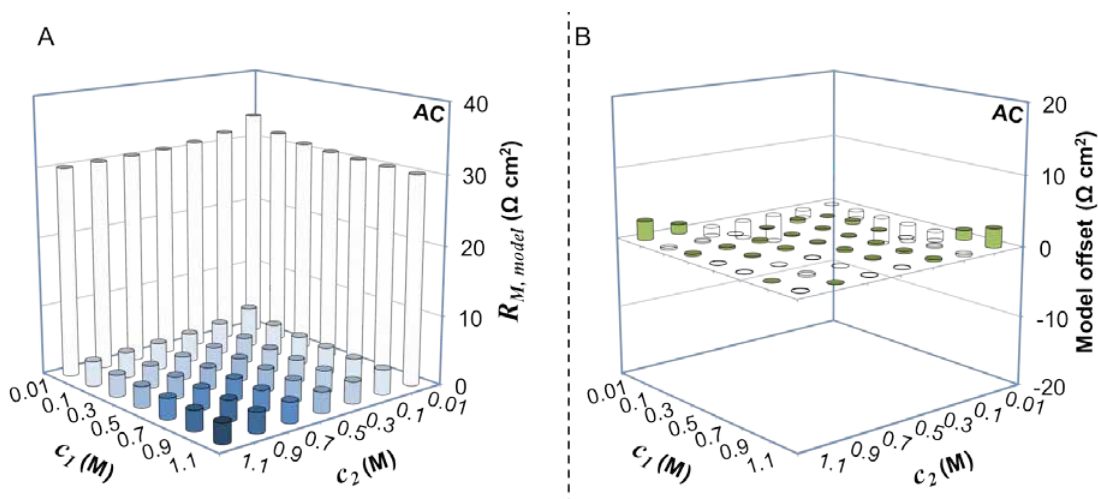
Figure 10. A) modeled membrane resistance ($R_{M, model}$, Ω cm²), calibrated with experimental data and B) the difference between the modeled and measured membrane resistance (R_M, Ω cm²) at defined external NaCl solution concentrations (c_1 and c_2, M). Negative values (model underestimation) are shown as unfilled bars and positive values (model overestimation) as solid filled bars. Both Figures are mirrored in their diagonal axes, where $c_1 = c_2$. Exact values of $R_{M, model}$ are given in Table A 3 in Appendix A.

Figure 10 A shows in general that $R_{M, model}$ increases with a decrease in c_1 and c_2. Figure 10 A shows large similarity with Figure 2 B, although some differences occur. For example, the earlier described outlier at external solution concentrations of 0.01 and 0.3 M, which was due to relative large uncertainty in the measurement value, has vanished in the modeled data. These differences are visualized in Figure 10 B (y-axes same magnitude as in Figure 10 A). This figure shows that, despite several simplifications, the model gives a good approximation of the experimentally determined R_M values. A second observation from this figure is that all values on the diagonal, where $c_1 = c_2$, show some offset, in line with the modeled values and the measured data shown in Figure 7. The largest deviation in this diagonal was found at $c_1 = c_2 = 0.9$ M (7.1%). This deviation is hardly noticed in Figure 7, as the absolute difference is

small (0.23 Ω cm²). Thirdly, Figure 10 B shows that the model does not notoriously overestimates or underestimates the experimentally determined membrane resistance when $c_{low} \geq 0.3$. This confirms that a straight internal concentration profile can be used in those cases. Further investigations should be done to lower the uncertainty of the measured resistances.

6.4.9 Experimental concentration profile

The concentration profile of the internal membrane solution ($\bar{c_i}$) was shown of great importance for the explanation of the measured R_M values when $c_1 \neq c_2$. To investigate the actual internal concentration profile in the membrane an elemental analysis was done. For CMX membranes, this method was not suitable as the membrane reinforcement contains Cl atoms that disturb the analysis of sorbed co-ions and counterions. However, for a Ralex CMH cation exchange membrane this method can be used. Figure 11 shows the relative concentration of the co-ions (Cl⁻) with respect to the total concentration of sorbed ions (Cl⁻ + Na⁺), as derived from the elemental analysis. This membrane was operated in typical RED conditions.
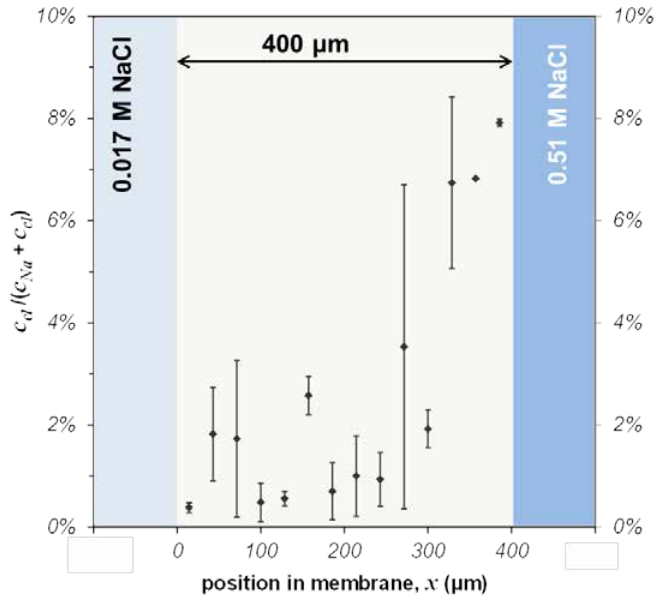
Figure 11. Relative concentration of the co-ions (Cl⁻) with respect to the total ion concentration (Cl⁻ & Na⁺), as derived from the elemental analysis with EDX on a Ralex CMH membrane that was operated in RED mode between 0.017 M and 0.51 M NaCl. Average values from 2 measurements are shown with error bars that indicate the standard error. For the most right data point the standard error is too small to show, the data point at x = ~350 μm is a single measurement.

Figure 11 indicates that the fraction of counterions is approximately 8 % at the side of the concentrated NaCl solution, while these ions contribute for only ~0.5 % at the side with diluted NaCl solution. This is in agreement with previous research, which indicated that both the concentration of co-ions and counterions in the membrane increases when the external concentration increases [22]. Because the absolute concentration of co-ions is much smaller than that of counterions inside the membrane, an increasing external solution concentration results in an increase in the relative co-ion concentration. Although, the uncertainty in some measurement points is large, Figure 11 suggests that the relative internal solution concentration of co-ions is not linear but decreases rapidly from the side with concentrated solution towards the side with diluted solution. This justifies the theory that osmosis reduces the internal ion concentration ($\bar{c}_i$) in a large part of the membrane.

6.4.10 Outlook

Membrane conductivity depends on various parameters [25], amongst others, the concentration of the external solution(s), as is clearly shown by the results in this paper. As two external solutions of different concentration are present adjacent to the membrane, a certain ion concentration profile arises within the internal solution of the membrane. The concentration profile in the membrane is influenced by water transport. This water transport can be substantial in ED processes [5], but is typically hardly observed during RED [37]. This is due to the opposite direction of the osmotic and electro-osmotic flow in RED. Also (applied) current density and direction of the current can influence the ion concentration profile in the membrane. Therefore, we infer that the electrochemical process occurring (e.g. ED or RED) will influence the membrane conductance. This idea of process depending membrane conductance is supported by the data shown in Appendix C, which shows that the applied current density affects the cell pair resistance.

To improve modeling of membrane conductance, further investigations are required. Focus of these studies should be on the effects of (applied) current density and current direction on the measured membrane resistance (R_M). Also the development of the suggested concentration gradient in the membrane and the influence of water transport require further investigations, as it is found to be of great importance with respect to the membrane conductivity. There might also be an effect of the membrane thickness on the internal concentration profile, this is interesting to investigate as often the membrane thickness is reduced to lower membrane resistance.

6.5 Conclusion

The conductance of ion exchange membranes is influenced by the ion concentrations of the external solutions at both sides of the membrane. Classical membrane resistance measurements, at fixed external ion concentrations, are therefore not always representative for processes where the ion concentrations of the external solutions change during the process. In the present work, the effect of the ion concentration of the external solution(s) on the membrane conductance was investigated, and the following conclusions could be drawn:

- Membrane conductance is largely determined by the external solution with the lowest ion concentration.
- By describing the membrane as a structure of microcavities and microchannels in serial order, experimentally determined membrane resistances can be explained.
- The ion concentration profile in the membrane is a key factor determining membrane conductance, and as such:
    - An increase of the osmotic water flux through the membrane results in a decrease in the membrane conductance.
    - The electrochemical process, more specifically the current density and direction, influences the osmotic water flux through the membrane and thus the membrane conductance.

It was known before that an external solution with low ion concentration can largely increase membrane resistance, compared to the measured resistance under standard test conditions (0.5 M). Until now there was no established way on estimating the membrane resistance when two solutions of unequal concentration are present adjacent to the ion exchange membrane, and for which the results presented here offer the fundaments. This is of great importance as many processes are known where ion exchange membranes are used with two external solutions of unequal concentration.

6.6 Literature

[1] T. Sata, Ion Exchange Membranes; Preparation, Characterization, Modification and Application, The Royal Society of Chemistry, Cambridge UK, 2004.

[2] H. Strathmann, Ion-exchange membrane separation processes, Elsevier, Amsterdam NL, 2004.

[3] H. Strathmann, Electrodialysis, a mature technology with a multitude of new applications, Desalination, 264 (2010) 268-288.

[4] J.W. Post, H. Huiting, E.R. Cornelissen, H.V.M. Hamelers, Pre-desalination with electro-membranes for SWRO, Desalination and Water Treatment, 31 (2011) 296-304.

[5] A.H. Galama, M. Saakes, H. Bruning, H.H.M. Rijnaarts, J.W. Post, Seawater Predesalination with Electrodialysis, Desalination, 342 (2013) 61-69.

[6] J.W. Post, H.V.M. Hamelers, C.J.N. Buisman, Energy recovery from controlled mixing salt and fresh water with a reverse electrodialysis system, Environmental Science and Technology, 42 (2008) 5785-5790.

[7] D.A. Vermaas, M. Saakes, K. Nijmeijer, Doubled Power Density from Salinity Gradients at Reduced Intermembrane Distance, Environmental Science and Technology, 45 (2011) 7089-7095.

[8] J. Veerman, M. Saakes, S.J. Metz, G.J. Harmsen, Reverse electrodialysis: Performance of a stack with 50 cells on the mixing of sea and river water, Journal of Membrane Science, 327 (2009) 136-144.

[9] R.E. Pattle, Production of electric power by mixing fresh and salt water in the hydroelectric pile, Nature, 174 (1954) 660.

[10] K. Urano, Y. Masaki, M. Kawabata, Electric resistances of ion-exchange membranes in dilute solutions, Desalination, 58 (1986) 171-176.

[11] P. Długołęcki, B. Anet, S.J. Metz, K. Nijmeijer, M. Wessling, Transport limitations in ion exchange membranes at low salt concentrations, Journal of Membrane Science, 346 (2010) 163-171.

[12] P. Długołęcki, P. Ogonowski, S.J. Metz, M. Saakes, K. Nijmeijer, M. Wessling, On the resistances of membrane, diffusion boundary layer and double layer in ion exchange membrane transport, Journal of Membrane Science, 349 (2010) 369-379.

[13] S.M. Hosseini, S.S. Madaeni, A.R. Khodabakhshi, The Electrochemical Characterization of Ion Exchange Membranes in Different Electrolytic Environments: Investigation of Concentration and pH Effects, Separation Science and Technology, 47 (2011) 455-462.

[14] N.P. Berezina, N.A. Kononenko, O.A. Dyomina, N.P. Gnusin, Characterization of ion-exchange membrane materials: Properties vs structure, Advances in Colloid and Interface Science, 139 (2008) 3-28.

[15] N. Berezina, N. Gnusin, O. Dyomina, S. Timofeyev, Water electrotransport in membrane systems. Experiment and model description, Journal of Membrane Science, 86 (1994) 207-229.

[16] G.M. Geise, A.J. Curtis, M.C. Hatzell, M.A. Hickner, B.E. Logan, Salt Concentration Differences Alter Membrane Resistance in Reverse Electrodialysis Stacks, Environmental Science and Technology Letters, 1 (2014) 36-39.

[17] J. Veerman, M. Saakes, S.J. Metz, G.J. Harmsen, Reverse electrodialysis: A validated process model for design and optimization, Chemical Engineering Journal, 166 (2011) 256-268.

[18] V.A. Shaposhnik, O.V. Grigorchuk, Mathematical model of electrodialysis with ion-exchange membranes and inert spacers, Russian Journal of Electrochemistry, 46 (2010) 1182-1188.

[19] S. Sang, H. Huang, Q. Wu, An investigation on ion transfer resistance of cation exchange membrane/solution interface, Colloids and Surfaces A: Physicochemical and Engineering Aspects, 315 (2008) 98-102.

[20] M.B. Andersen, M. Van Soestbergen, A. Mani, H. Bruus, P.M. Biesheuvel, M.Z. Bazant, Current-induced membrane discharge, Physical Review Letters, 109 (2012) 108301.

[21] A.H. Galama, G. Daubaras, O.S. Burheim, H.H.M. Rijnaarts, J.W. Post, Seawater electrodialysis with preferential removal of divalent ions, Journal of Membrane Science, 452 (2014) 219-228.

[22] A.H. Galama, J.W. Post, M.A. Cohen Stuart, P.M. Biesheuvel, Validity of the Boltzmann equation to describe Donnan equilibrium at the membrane-solution interface, Journal of Membrane Science, 442 (2013) 131-139.

[23] A.G. Winger, G.W. Bodamer, R. Kunin, Some electrochemical properties of new synthetic ion exchange membranes, Journal of the Electrochemical Society, 100 (1953) 178-184.

[24] F.G. Donnan, The theory of membrane equilibria, Chemical Reviews, 1 (1924) 73-90.

[25] F.G. Helfferich, Ion Exchange, McGraw-Hill, New York, (1962).

[26] R. Schlögl, Elektrodiffusion in freier Losung und geladenen Membranen, Z. Physik. Chem., 1 (1954) 305.

[27] R. Schlögl, Stofftransport durch Membranen, Dr. Dietrich Steinkopff Verlag, Darmstadt, 1964.

[28] A. Einstein, Über die von der molekularkinetnschen Theorie der Wärme geforderte Bewegung von in ruhenden Flüssigkeiten suspendierten Teilchen, Annalen der Physik, 322 (1905) 549-560.

[29] M. von Smoluchowski, Zur kinetischen Theorie der Brownschen Molekularbewegung und der Suspensionen, Annalen der Physik, 326 (1906) 756-780.

[30] O.S. Burheim, F. Seland, J.G. Pharoah, S. Kjelstrup, Improved electrode systems for reverse electro-dialysis and electro-dialysis, Desalination, 285 (2012) 147-152.

[31] D.A. Vermaas, S. Bajracharya, B.B. Sales, M. Saakes, B. Hamelers, K. Nijmeijer, Clean energy generation using capacitive electrodes in reverse electrodialysis, Energy & Environmental Science, (2013).

[32] D. Vermaas, M. Saakes, K. Nijmeijer, Power generation using profiled membranes in reverse electrodialysis, Journal of Membrane Science, 385-386 (2011) 234-242.

[33] J.R. Wilson, Demineralization by electrodialysis, in, Butterworths Scientific Publications, London (UK), 1960.

[34] V.K. Indusekhar, N. Krishnaswamy, Water transport studies on interpolymer ion-exchange membranes, Desalination, 52 (1985) 309-316.

[35] J. Barret, Inorganic chemistry in aqueous solution, in: E.W. Abel (Ed.), Royal Society of Chemistry, Cambridge (UK), 2003.

[36] Y. Oda, T. Yawataya, On the electro-osmotic water transport through cation-exchange resin membranes, Bulletin of the Chemical Society of Japan, 28 (1955) 263-269.

[37] J. Veerman, R.M. de Jong, M. Saakes, S.J. Metz, G.J. Harmsen, Reverse electrodialysis: Comparison of six commercial membrane pairs on the thermodynamic efficiency and power density, Journal of Membrane Science, 343 (2009) 7-15.

[38] N. Lakshminarayanaiah, Electroosmosis in Ion-Exchange Membranes, Journal of the Electrochemical Society, 116 (1969) 338-343.

[39] Y. Oda, T. Yawataya, On the distribution and behavior of water in cation-exchange resin membranes, Bulletin of the Chemical Society of Japan, 30 (1957) 213-218.

[40] Y. Oda, T. Yawataya, On the transport number for ion-exchange resin membranes, Bulletin of the Chemical Society of Japan, 29 (1956) 673-679.

[41] A.S. Tombalakian, H.J. Barton, W.F. Graydon, Electroösmotic water transport across ion-exchange membranes, Journal of Physical Chemistry, 66 (1962) 1006-1009.

[42] P. Długołęcki, K. Nymeijer, S. Metz, M. Wessling, Current status of ion exchange membranes for power generation from salinity gradients, Journal of Membrane Science, 319 (2008) 214-222.

[43] J.-S. Park, J.-H. Choi, J.-J. Woo, S.-H. Moon, An electrical impedance spectroscopic (EIS) study on transport characteristics of ion-exchange membrane systems, Journal of Colloid and Interface Science, 300 (2006) 655-662.

[44] J.-H. Choi, S.-H. Moon, Pore size characterization of cation-exchange membranes by chronopotentiometry using homologous amine ions, Journal of Membrane Science, 191 (2001) 225-236.

[45] J.-H. Choi, S.-H. Kim, S.-H. Moon, Heterogeneity of ion-exchange membranes: the effects of membrane heterogeneity on transport properties, Journal of Colloid and Interface Science, 241 (2001) 120-126.

[46] K. Sollner, Recent advances in the electrochemistry of membranes of high ionic selectivity, Journal of the Electrochemical Society, 97 (1950) 139C-151C.

[47] W.S. Cleveland, S.J. Devlin, Locally Weighted Regression: An Approach to Regression Analysis by Local Fitting, Journal of the American Statistical Association, 83 (1988) 596-610.

[48] A. Elattar, A. Elmidaoui, N. Pismenskaia, C. Gavach, G. Pourcelly, Comparison of transport properties of monovalent anions through anion-exchange membranes, Journal of Membrane Science, 143 (1998) 249-261.

[49] J. Mackie, P. Meares, The diffusion of electrolytes in a cation-exchange resin membrane. I. Theoretical, Proceedings of the Royal Society of London. Series A. Mathematical and Physical Sciences, 232 (1955) 498-509.

[50] E. Volodina, N. Pismenskaya, V. Nikonenko, C. Larchet, G. Pourcelly, Ion transfer across ion-exchange membranes with homogeneous and heterogeneous surfaces, Journal of Colloid and Interface Science, 285 (2005) 247-258.

[51] V.I. Zabolotsky, V.V. Nikonenko, Effect of structural membrane inhomogeneity on transport properties, Journal of Membrane Science, 79 (1993) 181-198.

[52] A.B. Yaroslavtsev, Perfluorinated ion-exchange membranes, Polym. Sci. Ser. A, 55 (2013) 674-698.

[53] M.-S. Kang, Y.-J. Choi, I.-J. Choi, T.-H. Yoon, S.-H. Moon, Electrochemical characterization of sulfonated poly(arylene ether sulfone) (S-PES) cation-exchange membranes, Journal of Membrane Science, 216 (2003) 39-53.

[54] T.D. Gierke, G.E. Munn, F.C. Wilson, The morphology in nafion perfluorinated membrane products, as determined by wide- and small-angle x-ray studies, Journal of Polymer Science: Polymer Physics Edition, 19 (1981) 1687-1704.

[55] V.V. Nikonenko, A.B. Yaroslavtsev, G. Pourcelly, A. Ciferri, A. Perico, Ion transfer in and through charged membranes, Structure, properties, theory. Chapter 9 in Ionic Interactions in Natural and Synthetic Macromolecules, in, John Wiley & Sons, Inc, 2012, pp. 267-336.

[56] S. Mafé, J.A. Manzanares, P. Ramirez, Modeling of surface vs. bulk ionic conductivity in fixed charge membranes, Physical Chemistry Chemical Physics, 5 (2003) 376-383.

[57] G. Pourcelly, P. Sistat, A. Chapotot, C. Gavach, V. Nikonenko, Self diffusion and conductivity in NafionR membranes in contact with NaCl+CaCl2 solutions, Journal of Membrane Science, 110 (1996) 69-78.

[58] M. Tasaka, S. Suzuki, Y. Ogawa, M. Kamaya, Freezing and nonfreezing water in charged membranes, Journal of Membrane Science, 38 (1988) 175-183.

[59] R. Wycisk, W.M. Trochimczuk, Water states in PE-poly(MA-co-DVB) interpolymer type carboxylic ion-exchange membranes, Journal of Membrane Science, 66 (1992) 89-96.

[60] K. Yonetake, T. Seo, T. Iijima, Ion transport and states of water in charged poly(allylamine) membranes, Journal of Polymer Science Part B: Polymer Physics, 28 (1990) 303-314.

[61] H. Yoshida, Y. Miura, Behavior of water in perfluorinated ionomer membranes containing various monovalent cations, Journal of Membrane Science, 68 (1992) 1-10.

[62] K.S. Spiegler, Transport processes in ionic membranes, Transactions of the Faraday Society, 54 (1958) 1408-1428.

[63] K. Kontturi, L. Murtomäki, J.A. Manzanares, Ionic Transport Processes : in Electrochemistry and Membrane Science: in Electrochemistry and Membrane Science, OUP Oxford, 2008.

[64] M. Higa, A. Tanioka, K. Miyasaka, Simulation of the transport of ions against their concentration gradient across charged membranes, Journal of Membrane Science, 37 (1988) 251-266.

[65] R. Schlögl, The significance of convection in transport processes across porous membranes, Discussions of the Faraday Society, 21 (1956) 46-52.

[66] M. Tasaka, Y. Kondo, M. Nagasawa, Anomalous osmosis through charged membranes, Journal of Physical Chemistry, 73 (1969) 3181-3188.

[67] T. Kressman, F. Tye, The effect of concentration on the transport of ions through ion-selective membranes, Transactions of the Faraday Society, 55 (1959) 1441-1450.

[68] V. Sasidhar, E. Ruckenstein, Anomalous effects during electrolyte osmosis across charged porous membranes, Journal of Colloid and Interface Science, 85 (1982) 332-362.

Appendix A

Table A 1. Observed membrane resistance (R_{M+SDL}, Ω cm^2) determined with DC measurements at external NaCl solutions with concentration c_1 and c_2 (M).

$c_1 \backslash c_2$	0.01	0.1	0.3	0.5	0.7	0.9	1.1
0.01	119.47	84.71	73.90	46.04	45.06	42.18	32.05
0.1	84.71	11.65	8.80	8.48	8.44	8.49	7.71
0.3	73.90	8.80	4.35	4.52	4.37	4.34	4.13
0.5	46.04	8.48	4.52	3.43	3.93	3.91	3.84
0.7	45.06	8.44	4.37	3.93	3.24	3.69	3.53
0.9	42.18	8.49	4.34	3.91	3.69	3.47	3.52
1.1	32.05	7.71	4.13	3.84	3.53	3.52	3.41

Table A 2. Membrane resistance (R_M, Ω cm^2) determined with AC measurements at external NaCl solutions with concentration c_1 and c_2 (M).

$c_1 \backslash c_2$	0.01	0.1	0.3	0.5	0.7	0.9	1.1
0.01	33.78	33.03	35.01	33.27	31.85	28.93	27.47
0.1	33.03	5.74	4.08	4.02	3.92	3.92	3.87
0.3	35.01	4.08	3.50	3.32	3.06	2.95	2.89
0.5	33.27	4.02	3.32	3.13	2.95	2.95	3.15
0.7	31.85	3.92	3.06	2.95	3.21	3.09	3.11
0.9	28.93	3.92	2.95	2.95	3.09	3.25	2.97
1.1	27.47	3.87	2.89	3.15	3.11	2.97	3.04

Table A 3. Modeled membrane resistance ($R_{M-model}$, Ω cm^2) at external NaCl solutions with concentration c_1 and c_2 (M).

$c_1 \backslash c_2$	0.01	0.1	0.3	0.5	0.7	0.9	1.1
0.01	33.77	31.83	31.06	30.71	30.48	30.31	30.18
0.1	31.83	5.78	4.54	4.11	3.87	3.72	3.60
0.3	31.06	4.54	3.71	3.46	3.33	3.24	3.17
0.5	30.71	4.11	3.46	3.30	3.19	3.13	3.08
0.7	30.48	3.87	3.33	3.19	3.12	3.06	3.02
0.9	30.31	3.72	3.24	3.13	3.06	3.02	2.98
1.1	30.18	3.60	3.17	3.08	3.02	2.98	2.96

Appendix B

Equation B.1, with *a* and *b* being constants and k_{ext} the dimensionless external concentration (by dividing the external concentration with the reference concentration, $c^0 = 1$ M), was used to explain and fit data on the membrane resistance, R_M determined by Urano *et al.*[10], Długołęcki *et al.* [11], and Choi *et al.* [45]. These researchers presented data on Neosepta AMX/CMX membranes and Selemion AMV/CMV membranes for a range of external concentrations. In all cases, the external concentration was equal at both sides of the membrane. This data is used to validate the model presented in eq. B 1. Figure B 1 shows the experimentally obtained resistances and the modeled resistances for these four membrane types.

$$R_M = a + \frac{b}{k_{ext}}$$ eq. B.1
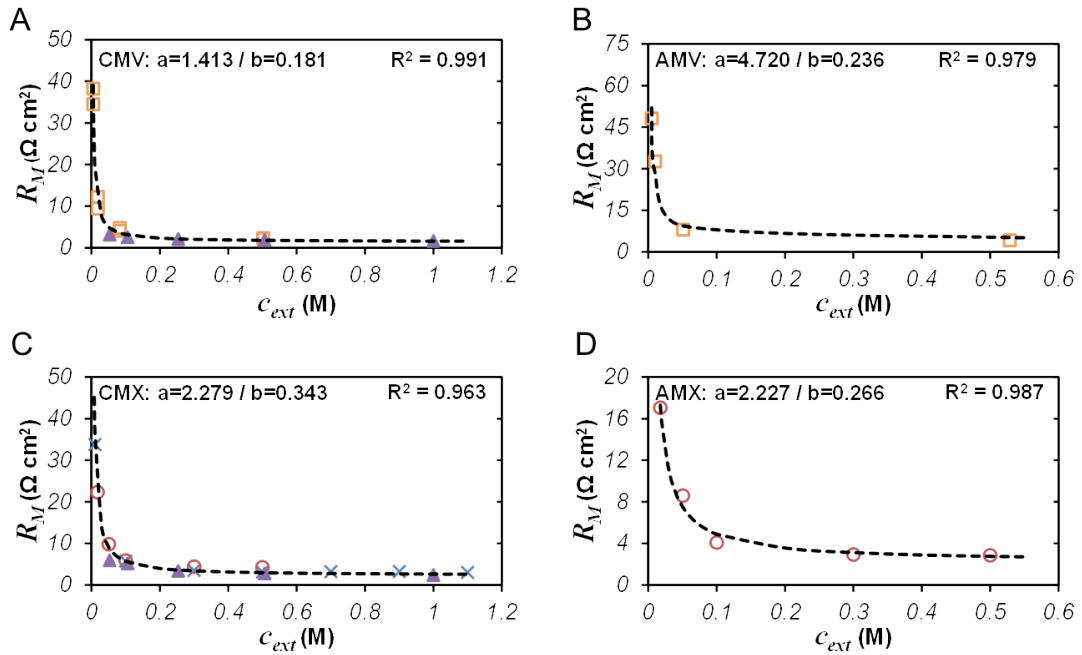
Figure B 1. Experimentally determined membrane resistance (R_M, Ω cm^2) and the modeled resistance (dotted line) as a function of the external NaCl concentration (c_{ext}, M). A) R_M of Selemion-CMV membranes as in [10] (□) and [45] (▲). B) R_M of Selemion-AMV membranes as in [10] (□). C) R_M of Neosepta-CMX membranes as in [11] (○), in [45] (▲), and in the present article (✕). D) R_M of Neosepta-CMX membranes as in [11] (○). Values of the constants a and b from eq. B.1, and the R^2 values are depicted for each of the graphs.

Figure B 1 shows high correlations ($R^2 = 0.962$-0.991) between the model line and the experimentally determined R_M values. The parameters *a* and *b* for the CMX membrane based on data of the present research ($a = 2.674$ / $b = 0.311$), are very close to the values for *a* and *b* as determined based on the experiments done by others [11, 45] ($a = 2.279$ / $b = 0.343$). If all CMX data is combined (literature and present research) the obtained constants are, $a = 2.569$ and $b = 0.319$ ($R^2 = 0.987$).

Considering differences in the membrane batches, also variance in the obtained membrane resistances is expected. Having many experimentally determined R_M values is important for a more exact estimation of the constants *a* and *b*, which then can be used for a more general description of R_M of a specific membrane type.

Appendix C

Desalination experiments were done by varying the applied current density in an electrodialysis stack. The effect on the stack voltage, resulting from the stack resistance, was investigated. An ED stack with 10 membrane pairs was used and the applied current density which was set at 10, 20, 40, 60, 80, and 100 A/m². After removing three membrane pairs the experiments were done again. All experiments were performed at least three repeatable times. The membrane stack potential measurement and the ED stack are described in previous research [5], with exception of the utilized membranes. For these experiments, CMX/AMX membranes (Neosepta, Tokuyama Co., Japan) were used instead of the CMS/ACS membranes that were used in [5]. When the membrane stack potentials were measured for both stacks the resistance of a single membrane pair, $R_{cell\,pair}$ (Ω), was obtained with:

$$R_{cell\,pair} = \frac{\phi_{mem.stack}^{N_1} - \phi_{mem.stack}^{N_2}}{N_1 - N_2} \frac{1}{I} \qquad\text{eq. C.1}$$

Where N (-) is the number of membrane pairs (N_1=10 & N_2=7), $\phi_{mem.stack}$ (V) the membrane stack potential (including electrode reactions) at respectively N_1 and N_2, and I (A) is the applied current. Figure C 1 shows that the applied current density (j) has an influence on the resistance of a cell pair.
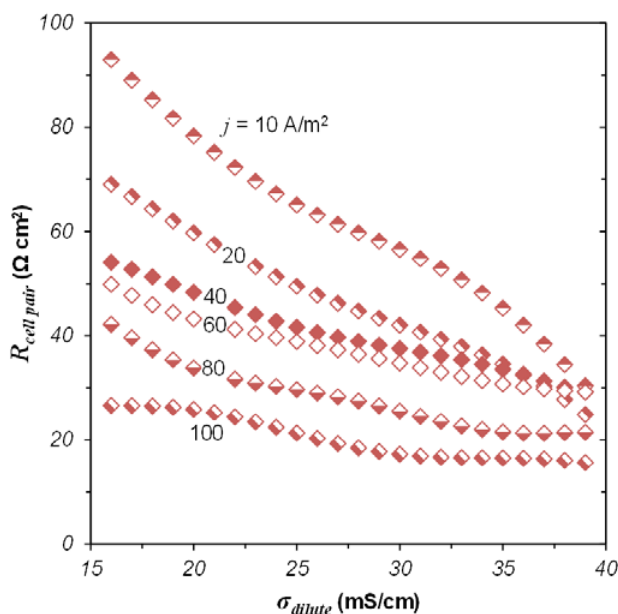
Figure C 1. Measured area resistance of a cell pair (R$_{cell\ pair}$, Ω cm²) in an electrodialysis stack with an under limiting applied fixed current density, j of 10-100 A/m² as function of the conductivity (NaCl concentration) of the dilute compartment (σ$_{dil}$, mS/cm).

A cell pair includes the dilute stream and concentrate stream. Resistance of these liquid streams is similar for all applied current densities at equal conductivity. So, the difference in resistance is due to the membrane and stagnant diffusion layer (SDL). Concentration polarization increases with j, resulting in larger resistance of this SDL (at under limiting current conditions). Figure C 1 shows exactly opposite behavior. This is believed to be an effect of water transport through the membrane, which increases the membrane resistance. The smaller j, the larger the influence of osmotic water transport [5]. At lower j, the net water flux through the membrane becomes larger with the same ion flux. Effectively this may lead to dilution of the membrane channels (or pores), which reduces membrane conductivity.

Chapter 7

On the origin of the membrane potential arising across densely charged ion exchange membranes

Abstract

A difference in salt concentration between two solutions separated by a membrane leads to an electrical potential difference across the membrane, also without applied current. A literature study is presented on proposed theories for the origin of this membrane potential (ϕ_m). The most well-known theoretical description is Teorell-Meyer-Sievers (TMS) theory, which is analyzed and extended. Experimental data for ϕ_m were obtained using a cation exchange membrane (CMX, Neosepta) and NaCl solutions (salt concentration from 1 mM to 5 M). Deviations between theory and experiments are observed, especially at larger salt concentration differences across the membrane. At a certain salt concentration ratio, a maximum in ϕ_m is found, not predicted by the TMS theory. Before the maximum, TMS theory can be used as a good estimate of ϕ_m though it overestimates the actual value. To improve the theory, various corrections to TMS theory were considered: A) Using ion activities instead of ionic concentration in the external solutions leads to an improved prediction; B) Inhomogeneous distribution of the membrane fixed charge has no effect on ϕ_m; C) Consideration of stagnant diffusion layers on each side of the membrane can have a large effect on ϕ_m; D) Reducing the average value of the fixed membrane charge density can also largely affect ϕ_m; E) Allowing for water transport in the theory has a small effect; F) Considering differences in ionic mobility between co-ions and counterions in the membrane affects ϕ_m significantly. Modifications C) and F) may help to explain the observed maximum in ϕ_m.

Nomenclature

a_i	=	ion activity (mol/m^3)
c	=	concentration (mol/m^3)
D	=	diffusion coefficient (m^2/s)
F	=	Faraday constant (C/mol)
$f_m\delta$	=	friction coefficient ($mol\ s/m^4$)
J_i	=	ion molar flux ($mol/m^2\ s$)
K_{ij}	=	coupling coefficient (-)
P	=	pressure (Pa)
P_i	=	ion specific permeability (m/s)
u_i	=	electric mobility ($m^2/V\ s$)
R	=	gas constant (J/mol K)
r_p	=	pore radius (m)
T	=	temperature (K)
T_i	=	ion transport number (-)
v_f	=	fluid velocity (m/s)
X	=	fixed membrane charge density per unit aqueous phase in mem brane (mol/m^3)
x	=	distance perpendicular to the membrane (m)
z	=	valence (-)
β_i	=	ion partition coefficient (-)
γ_i	=	activity coefficient (-)
$\Delta\phi_D$	=	Donnan potential (V)
δ	=	thickness (m)
λ_D	=	Debye length (m)
μ	=	chemical potential (J/mol)
$\widetilde{\mu}$	=	electrochemical potential (J/mol)
Π	=	osmotic pressure (Pa)
ϕ	=	electrical potential (V)
ω	=	indicator for charge sign (-)

The overbar refers to membrane phase (e.g. $\bar{c}$)

7.1 Introduction

7.1.1 Membrane potential

Whenever there is a concentration difference over the membranes of, for instance, an electrodialysis (ED) stack, an electrical potential (or voltage) can be measured. In the absence of a current, this membrane potential is also referred to as the open circuit voltage (OCV), the reversible potential, the concentration potential, or by the more general term, electro motive force (emf). This 'reversible' potential determines the minimum energy that is required to transport charge, as for example in the ED process [1]. Vice versa, it is also a measure of the maximum amount of energy that can be recovered in for instance reversed electrodialysis [2, 3], or during the energy recovery step in membrane capacitive deionization [4, 5]. Recently the membrane potential of living cells was identified as a key indicator of normal cell growth, and changes in the membrane potential to be related to carcinogenesis [6-8].

7.1.2 An early history

The phenomenon of the membrane potential at zero current conditions is intriguing and has fascinated many scientists for over a century. Already in 1890, Wilhelm Ostwald [9] sketched the situation of two electrolyte solutions separated by a semi permeable membrane and drew attention to the (electrical) effects in these kinds of systems. The equilibration of such a system and the potential differences provided proof for the ionization theory [10] which was published by Svante Arrhenius [11]. Between 1887 and 1890 Walther Nernst worked along with Arrhenius in Ostwald's laboratory at the University of Leipzig, where he formulated his theory on diffusion potentials [12], which formed a foundation for the membrane potential theory and ionometry [13]. Twenty one years later (1911), Frederick Donnan wrote his seminal paper on the equilibrium of ions between two phases, separated by a semi permeable membrane, of which one phase contains a fixed charge (non permeating species) [14]. The work of these men became very important in the development of theories to explain the membrane potential that arises over biological membranes or artificial IEMs.

With the development of the theory also practical applications of separation systems were developed, and it was already in 1890 that the ED apparatus was patented [15]. A decade later (1903) the first scientific publication on ED followed [16]. In 1939 the first desalinating stack, with anion and cation selective membranes and three compartments was presented [17], and only one year later a multi compartment stack was described [18]. These two publications form a milestone in desalination history as the ED process, as used today, was defined. However, membranes were at that time still 'primitive' and had only low selectivities [19-21]. In the 1930-40s ion exchange mem-

branes (IEMs) were developed with higher selectivities but, a drawback was the high electrical resistance of these membranes [20, 21]. The preparation of IEMs with high selectivity and 'low' resistance was first published in 1950 [22, 23]. During the 1950s there was a great interest in demineralization of saline waters [20] and consequently also a great interest in the development of IEMs with high selectivities as illustrated by the review of Juda *et al.* [24]. Since then, IEMs are further developed and applied in a broad field [25, 26].

7.1.3 Approach

Many attempts have been done to precisely investigate, explain, and quantify the membrane potential. It may be difficult to get a clear picture of what has been written, especially when original theories are further expanded, and assumptions done in the original theory become less clear, or when for instance, different names or definitions for the same phenomena are in fashion. With this work is attempted to provide a clarification of the basics of the membrane potential theory, the underlying considerations in this theory, and the phenomena occurring when a semi permeable membrane separates two electrolyte solutions that differ in concentration.

Generally there are two approaches which can be followed; a thermodynamical approach or a physical approach. The theory of the thermodynamics of irreversible processes provides a mathematical description of the membrane processes by defining a number of thermodynamic coefficients based on three driving forces which are: an electrical gradient, a pressure gradient, and a chemical gradient [27]. For the use of the theory no detailed information about the membrane pores and structure is required, and the membrane may be regarded as a black box [28, 29]. The theory, concerning IEMs was further developed by Spiegler [30] and Kedem and Katchalsky [31, 32]. In contact with a single electrolyte, in this approach there are six independent 'practical' transport parameters defined that allow complete characterization of the IEM transport properties [32-35]. These parameters enter three flux equations, which are related to the driving forces, as six phenomenological coefficients. This pure phenomenological description of the membrane process, does not provide information on the transport mechanism on a molecular level [36]. To do so, it is necessary to give a physical interpretation to the phenomenological thermodynamic coefficients [31, 32, 36], which is done in friction and distribution coefficients [30-32]. In these models, where the membrane is used as a frame of reference, can be accounted for fluid, particle and membrane interactions. Determining the six individual practical transport parameters can be done with long and delicate experiments [27, 33]. Zabolotsky and Nikonenko [37] showed the importance of relating the membrane structure and the transport coefficients, as the membrane structure is the main factor determining the concentration

dependence of membrane transport properties.

Despite being an exact approach, the thermodynamical approach is very case specific and provides no deep insight in factors that influence the membrane potential. In the present work is attempted to provide a more general description, therefore, a physical approach is considered to be more suitable. The basic and most often used theoretical approach is the Teorell-Meyer-Sievers (TMS) theory [38, 39]. With this theory the membrane potential, arising under zero current conditions, can be well predicted within certain concentration ranges. However, as will be shown, due to certain assumptions made for simplification, deviations between predictions of the TMS theory and experimental data can occur. In the present work the TMS theory and its assumptions, as well as the space charge model (SCM), which is an extension of the TMS theory, are thoroughly analyzed. Experimental data for the membrane potential, obtained in the absence of current (zero current conditions), are compared with the basic TMS theory, and with different extensions of the TMS theory. It is demonstrated how each extension influences the theoretical results. Differences between measured data and theory are discussed, as well as the origin of these differences.

7.2 Theory

In this theoretical section, the basic thermodynamic equations used to describe mass transport in membrane processes are given. It is shown how under zero current conditions a chemical potential gradient induces the rise of an electric potential. Mass transport due to water flow will first be neglected. The origin of the TMS theory in the basic thermodynamic equations will be clearly described. Also the extension of the TMS theory to the SCM will be discussed with respect to densely charged IEMs.

7.2.1 Potentials and transport

Transport of ions through a membrane can take place through migration, diffusion and convection. Migration is the movement of ions caused by an electric potential gradient ($\nabla \phi$), diffusion is the movement of ions caused by a chemical potential gradient ($\nabla \mu$), and convection is the movement of ions due to a pressure gradient (∇P). These three different gradients act as driving forces for mass transfer and result respectively in; i) electrical current, ii) ionic flow, and iii) liquid flow [27, 30, 40]. These three 'currents' are interrelated, and to predict the transport direction and velocity of a certain ionic species, all three forces acting on the ions should be taken into account simultaneously. In the simplest 1:1 salt solution (e.g. NaCl) two ions are present and as such two electrochemical potential gradients should be considered. In solutions with many ionic species, e.g. seawater, the electrochemical potential can be calculated for all individual

ionic species, as shown by Leyendekkers [41] and Whitfield [42]. Due to the combination of different gradients acting on the ions in solutions, the direction and velocity of the ionic flows is not obvious. Even without an applied electrical current and applied pressure, it is possible that ions are transported through the membrane against their own chemical potential gradient, a phenomenon known as uphill ion transport [40, 43, 44].

In the ED process [20, 45], the largest driving force for transmembrane ionic transport is in most cases the electrically applied potential difference. In ED, a dilute and concentrate stream are formed. The concentration difference between these two streams can be large, and as such a large chemical potential gradient can arise during the process. This increasing chemical potential gradient results in an increasing chemical driving force in opposite direction of the electric driving force that leads to a decrease of the ion flux. This decrease of the ion flux is sometimes considered to be diffusion of ionic species in opposite direction of the migrative flux and therefore sometimes referred to as back diffusion of ions. Convective ion transport through the IEM is usually assumed to be negligible and is often left out of the ion transport equations [25, 28, 46]. The chemical potential, μ_i (J/mol) and the electric potential, ϕ (V) are combined in the electrochemical potential, $\widetilde{\mu}_i$ (J/mol), which is calculated as:

$$\widetilde{\mu}_i = \mu_i + z_i F \phi = \mu_i^0 + RT \ln c_i + z_i F \phi \qquad \text{eq. 1}$$

Where, z_i is the ion valence (-), F is the Faraday constant (C/mol), R is the gas constant (J/mol·K), T is the temperature (K), and c is the ion concentration (mol/m³). For now, thermodynamic non-idealities are not discussed [47-49]. According to the Donnan equilibrium, two phases in contact with each other eventually possess the same electrochemical potential [10, 14]. The electric potential arising over an interface (with side L and side R) for a single solute solution can then be obtained according to the following balance:

$$\mu_i^0 + RT \ln c_i^L + z_i F \phi^L = \mu_i^0 + RT \ln c_i^R + z_i F \phi^R \qquad \text{eq. 2}$$

$$RT \ln c_i^L = RT \ln c_i^R + z_i F(\phi^R - \phi^L) \qquad \text{eq. 3}$$

$$\Delta \phi = \phi^R - \phi^L = \frac{RT}{z_i F} \ln\left(\frac{c_i^L}{c_i^R}\right) \qquad \text{eq. 4}$$

Eq. 4 is the well-known Nernst equation (for general cases and for an electrode-solu-

tion interface) or Donnan relation (for a solution-membrane interface). This equation is often used to estimate the electric potential over the membrane in absence of a current, as it gives the theoretically maximum membrane potential (ϕ_{max}) [21, 50]. In biological cells, an unbalanced situation between the internal and the external solution is often maintained by ion pumps, the resulting membrane potential is then known as the resting membrane potential, also described by eq. 4.

Eqs. 1-4 show that the measured electrical potential results from the electrochemical potential gradient ($\nabla\tilde{\mu}$), which is present in a defined system. When differentiating eq. 1 in the transport direction, x (i.e. perpendicular to the membrane), this electrochemical potential gradient can be expressed as:

$$\frac{d\tilde{\mu}_i}{dx} = RT\frac{d\ln c_i}{dx} + z_i F\frac{d\phi}{dx}$$ eq. 5

This gradient is the negative of the driving force on an ion and causes mass transport in the solutions and membrane, as described by the ion molar flux, J_i (mol/m² s). By definition a molar flux is the product of molar concentration and velocity. This velocity is the product of the mobility and the (applied/present) driving force. Combined in one formula, the ionic flux is given by:

$$J_i = -\frac{u_i}{F}c_i\frac{d\tilde{\mu}_i}{dx}$$ eq. 6

Where u_i is the electric mobility (m²/V·s), which is related to the ion diffusion coefficient, D_i (m²/s) through the Einstein (-Smoluchowski) relation [51, 52]:

$$D_i = \frac{u_i RT}{F}$$ eq. 7

Inserting eq. 5 and eq. 7 in eq. 6 gives:

$$J_i = -\frac{D_i}{RT}c_i\left(RT\frac{d\ln c_i}{dx} + z_i F\frac{d\phi}{dx}\right)$$ eq. 8

This is the well-known Nernst-Planck flux equation that can be rewritten to the more commonly used form:

$$J_i = -D_i\left[\frac{dc_i(x)}{dx} + c_i(x)\frac{z_i F}{RT}\frac{d\phi}{dx}\right]$$ eq. 9

In electrochemical system, the convective transport in the direction perpendicular to the membranes is often assumed to be negligible in comparison with the diffusion and migration terms [53-59]. Therefore the convective term ($+\ c_i\ v_f$), where, v_f is the fluid

velocity (m/s), was for now neglected in eq. 9. The water velocity results from the ion concentrations and a specified friction coefficient ($f_m \delta$, mol·s/m⁴), which was further defined in ref. [60]. The fluid velocity can be calculated according to eqs. 29 and 30 in ref. [60].

In eq. 4, membranes are regarded like a black box and membrane characteristics do not influence the calculated membrane potential. However, membrane properties (e.g. water content, fixed membrane charge density, pore size) do have an effect on concentration gradients and potentials in the membrane phase and the two solution-membrane interfaces. These properties affect the ion transport through the membrane, and thus the potential over the membrane. Also in the case when a potential is applied (as in electrodialysis), membrane selectivity becomes important. The fraction of the current transported by a certain ionic species is expressed in the transport number, T_i (-) [25]:

$$T_i = \frac{z_i J_i}{\sum_i z_i J_i} \qquad \text{eq.10}$$

In electrochemistry the term 'transport number' is strictly used for the ion fluxes due to migration, when no concentration and no pressure gradient are present. If there is no restriction on these gradients, T_i is called integral [28, 61] or effective [62-64] transport number. In steady state, this effective T_i is the same in the membrane and solution, as directly follows from the assumption of no accumulation.

When there are multiple permeating monovalent species the membrane potential (ϕ_m) is sometimes (especially in biological systems [65]) calculated with the Goldman-Hodgkin-Katz (GHK) voltage equation [54, 66]. This equation takes the permeability of each permeating species into account. The GHK equation is given as:

$$\phi_m = \frac{RT}{F} \ln \frac{\sum_{i=1}^{N} P_i c_i^L + \sum_{j=1}^{M} P_j c_j^R}{\sum_{i=1}^{N} P_i c_i^R + \sum_{j=1}^{M} P_j c_j^L} \qquad \text{eq. 11}$$

With:

$$P_i = \frac{RT}{F \delta_m} u_i \beta_i \qquad \text{eq. 12}$$

Where P is the ion specific permeability (m/s), c are concentrations (mol/m³) of the cation or anion of respectively the left hand (^{L}) and the right hand (^{R}) side of the membrane, δ_m is the membrane thickness (m), u is the electrical mobility, β is the

partition coefficient (-) between the membrane and solution (defined by the Donnan equilibrium on the solution-membrane interface), and N and M refer to the number of ionic species. The GHK equation (eq. 11) can be derived from the Nernst-Planck (NP) flux equation (eq. 9) as described in [54, 55, 66]. When there is only one permeating monovalent ion present, the GHK reduces to the Nernst equation, which was shown as eq. 4.

7.2.2 The membrane potential in IEMs

IEMs contain a high concentration of fixed charges. These charges are due to ion exchange groups that are covalently bound to the membrane polymer structure. For anion exchange membranes (AEMs) quaternary ammonium groups can be used, while cation exchange membranes (CEMs) can be based on sulphonic acid groups [25, 67]. For commercial IEMs the fixed membrane charge concentration, here denoted by X, can be around 5-6 M when defined per volume of aqueous phase in the membrane [26, 68]. This fixed membrane charge can be regarded as a non-diffusible ionic species [69] and as such participates in the Donnan equilibrium. Ions in the external solution with a charge sign opposite to that of the fixed charge groups, are called counterions, these ions readily enter the membrane. Ions with the same charge sign as the fixed membrane charge are called co-ions, these ions enter the membrane in small amounts. The large difference between the internal concentration of co- and counterions in the membrane is often referred to as Donnan exclusion, and it determines the selectivity of the membrane [69-73].

Donnan potential and diffusion potential

When there is a concentration difference over a membrane or over a stagnant layer (a layer through which ions can migrate, but without tangential fluid flow or fluid mixing), a diffusion potential (ϕ_{diff}) can arise due to differences in ionic mobility of the diffusing ions [71, 72, 74]. If one ionic species diffuses faster than the other ($D_+ \neq D_-$), this will results in a charge separation that causes an electrical potential [72]. This potential aids the slower ions across the membrane, while at the same time it retards the more mobile ions [72]. The diffusion potential (also known as the constrained liquid junction potential) is directly influenced by the concentration gradient in the membrane and by the number of different ionic species [33]. In order to calculate the diffusion potential, first off all the local electroneutrality in the membrane. For a 1:1 solution, electroneutrality relates at every position the concentration of counterions and co-ions according to:

$$\bar{c}_{counterion} - \bar{c}_{co-ion} + \omega X = 0 \qquad \text{eq. 13}$$

Where the parameter ω indicates the charge sign of the fixed membrane charge (ω = -1 for CEMs, and ω = +1 for AEMs). The diffusion potential can be obtained by integration of the mass flux balance of the counterions and co-ions (eq. 14) over the membrane, as shown in Appendix A.

$$J_{counterion} - J_{co-ion} =$$

$$-\overline{D}_{cou}\left[\frac{d\overline{c}_{cou}(x)}{dx} + \overline{c}_{cou}(x)\frac{z_{cou}F}{RT}\frac{d\phi}{dx}\right] + \overline{D}_{co}\left[\frac{d\overline{c}_{co}(x)}{dx} + \overline{c}_{co}(x)\frac{z_{co}F}{RT}\frac{d\phi}{dx}\right] = 0$$

eq. 14

The overbar refers to the membrane phase. In the theoretical case of a 100% permselective membrane, no mobile co-ions are present in the membrane phase, only counterions and fixed membrane charges. In that specific case, due to the electroneutrality condition [38], no diffusion can take place and the diffusion potential is zero.

According to Donnan equilibrium, the electrochemical potential must be equal in the external and internal phase. When using eq. 4, and replacing left and right side by external and internal phase, one finds that there can be a substantial difference between the electric potential in the external phase (ϕ_{ext}) and in the internal phase (ϕ_{in}). The difference is the Donnan potential, $\Delta\phi_D$, and relates to the electrical double layer (EDL) that is formed in the interfacial region [10, 71]. Because there are two solution-membrane interfaces, there are also two Donnan potentials, which are given by:

$$\Delta\phi_D^L = \frac{RT}{z_iF}\ln\left(\frac{\overline{c}_i^{\,L}}{c_i^L}\right) \quad \text{and} \quad \Delta\phi_D^R = \frac{RT}{z_iF}\ln\left(\frac{\overline{c}_i^{\,R}}{c_i^R}\right)$$

eq.15

Addition of these two potentials to the diffusion potential, inside the membrane phase, these two Donnan potentials form the membrane potential, ϕ_m [28, 53, 68, 72, 75-82].

$$\phi_m = \Delta\phi_D^L + \Delta\phi_D^R + \phi_{diff}$$

eq. 16

Where ϕ_m is the membrane potential (V), $\Delta\phi_D$ the Donnan potential (V) on the left hand (^{L}) and the right hand (^{R}) side of the membrane, and ϕ_{diff} is the diffusion potential (V). Figure 1 shows these potentials schematically. The Donnan potential is also referred to as the exclusion potential as it can include both electrostatic (repulsion) and steric (size exclusion) effects [72]. For ionic solutions steric effects are much smaller than electrostatic effects and are not further discussed in this work.
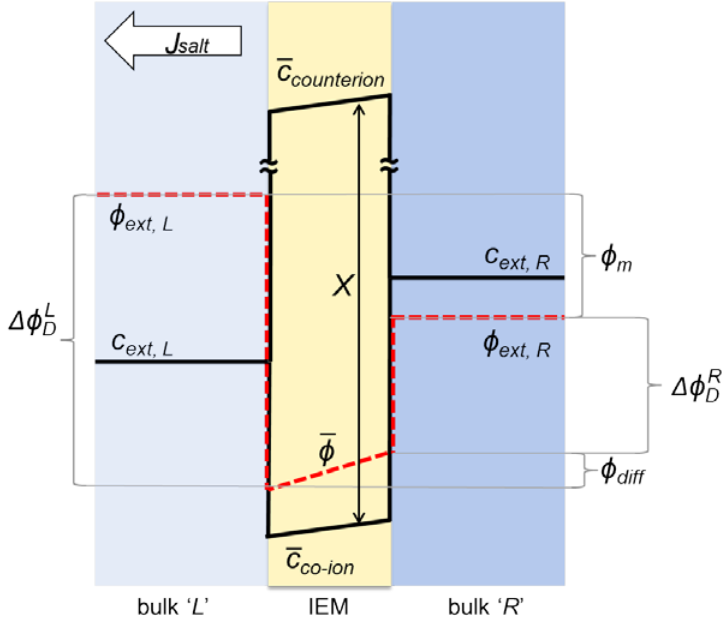
Figure 1. Schematic representation of concentration, c, and potential, ϕ, profile in an ion exchange membrane (IEM) between two electrolyte phases of different concentration, bulk L and bulk R, when no current is applied. Here X is the fixed membrane charge, ϕ_diff the diffusion potential, Δϕ_D the Donnan potential of side L or R, and ϕ_m is the resulting membrane potential.

Effect of the stagnant diffusion layer

With transport through the membrane, on either side of the membrane a stagnant diffusion layer (SDL) develops [28, 40, 46, 47, 83]. This layer, or film, is also known as the Nernst diffusion layer [28, 84-86], diffusion layer [25, 28] or (diffusion) boundary layer [46, 67, 71]. In the absence of current, diffusion initiates mass transport, and in case ions have different diffusion coefficients, migration develops as a driving force upon the ionic species in an SDL, which results in a diffusion potential across the SDL. Therefore, eq. 16 can be extended with the potentials arising over the SDLs adjacent to the membrane, and the total membrane potential is then composed as [47, 87-90]:

$$\phi_m = \phi_{diff}^{SDL,L} + \Delta\phi_D^L + \phi_{diff}^m + \Delta\phi_D^R + \phi_{diff}^{SDL,R} \qquad \text{eq. 17}$$

Figure 2 shows these potentials schematically. Generally, the diffusion potentials due to transport across the SDLs are neglected when considering the membrane potential, which is justified at low concentration differences over the membrane, very thin SDLs, and densely charged IEMs.
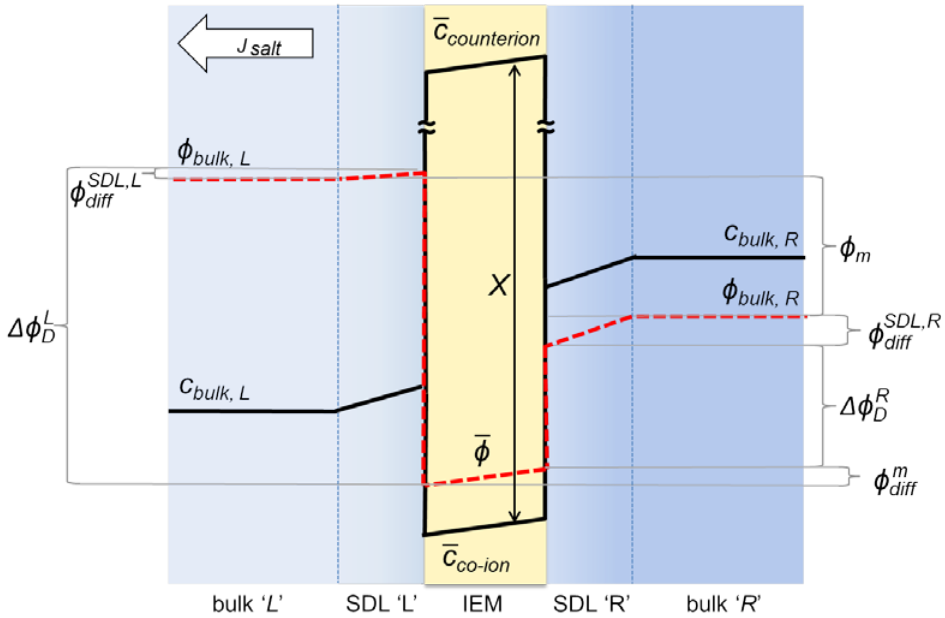
Figure 2. Schematic representation of concentration, c, and potential, φ, profile in the bulk solutions, the stagnant diffusion layers (SDLs), and in an ion exchange membrane (IEM) when no current is applied. Here X is the fixed membrane charge, ϕ_{diff} the diffusion potential, $\Delta\phi_D$ the Donnan potential of side L or R, and ϕ_m is the resulting membrane potential.

Effects of the SDLs are often considered in processes where an electric potential is applied over one or multiple IEMs, such as in electrodialysis. In that case, when an electric current is applied over an IEM (and the accompanying SDLs), concentration polarization takes place in these SDLs [58, 85, 87, 91]. Concentration polarization is then caused by the membrane selectivity between counterions and co-ions [25, 67, 71]. The diffusional and migrational forces acting on ions when a current is applied are schematically shown in Figure 3. So, besides formation of a diffusion potential in the SDL, concentration polarization in the SDL affects the ion concentrations at the membrane-solution interfaces, which also affects the membrane potential.

The relative influence of the SDL depends on i) the ratio of SDL thickness, δ_{SDL}, over the membrane thickness, δ_m (m), ii) the ratio of the ion diffusion coefficient in the SDL, D, over the ion diffusion coefficient in the membrane, $\overline{D}$ (m²/s), and iii) the ratio of the external ion concentration, c, over the internal ion concentration, $\overline{c}$ (mol/m³) [28, 47].
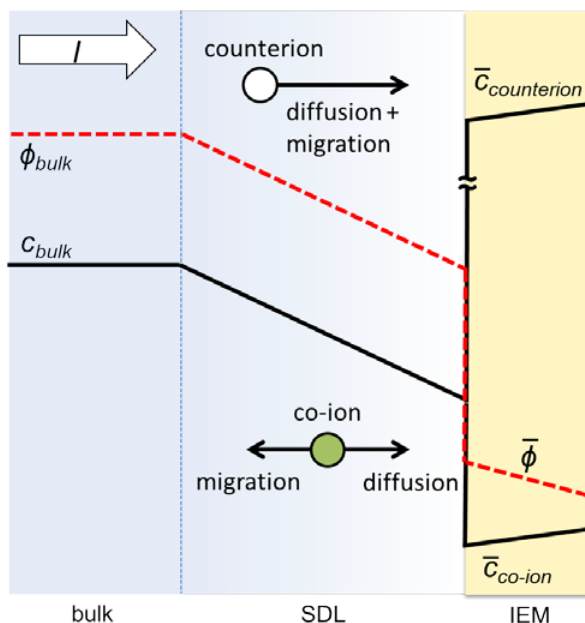
Figure 3. Schematic representation of concentration, c, and potential, φ, profile in the bulk solution, the stagnant diffusion layer (SDL), and in an ion exchange membrane (IEM) when a current is applied. Additionally, the driving forces acting on the ions in solution are shown as vectors.

7.2.3 Modeling the IEM potential

The membrane potential across an IEM is widely studied, especially for situations were only monovalent ions are present, e.g. [75, 77, 80, 92-94]. A more limited number of studies discussed the membrane potential when the membrane is separating ionic mixtures with divalent ions, e.g. [75, 76, 78, 79, 95-98], while for multi-ionic mixtures, the membrane potential is not often studied [75, 98]. Prediction of membrane potentials with multi-ionic electrolytes of different concentrations or different ion valencies is complicated and mathematically complex [75, 98].

The earlier mentioned GHK equation (eq. 11), that is often used in relation with biological membranes, is in most cases not suitable for calculation of the membrane potentials across IEMs. Attempts were made to expand the GHK equation to incorporate effects of surface charge and divalent ions [43, 65, 99, 100], but an adequate prediction of the membrane potential of IEMs with the GHK equation is difficult [46, 65]. For IEMs, many models were developed in an attempt to model the membrane potential. Basically three approaches to investigate the membrane potential are widely used; i) the Teorell-Meyer-Sievers theory, ii) the (electrokinetic) space charge model (SCM), and iii) the theory of irreversible thermodynamics. Of these three, the first two use the

most physical and chemical information. In the present the work focus is on the TMS theory, but also the SCM will be discussed. The theory of irreversible thermodynamics [27, 30-35] is not further discussed in this work.

Teorell-Meyer-Sievers theory

Eq. 16 is the starting point of the Teorell-Meyer-Sievers (TMS) theory [38, 39, 46, 101-104], which is used to predict the membrane potential across an IEM. An expression for the standard TMS theory, given by eq. 18, was derived in Appendix A of this work.

$$\phi_m = \frac{RT}{F}\left(\omega \ln\frac{c_R}{c_L}\left[\frac{X + \sqrt{X^2 + 4c_L}}{X + \sqrt{X^2 + 4c_R}} \right] + \overline{U}\ln\left[\frac{-\overline{U}\omega X + \sqrt{X^2 + 4c_L}}{-\overline{U}\omega X + \sqrt{X^2 + 4c_R}} \right] \right)$$ eq. 18

With:

$$\overline{U} = \frac{\overline{u}_+ - \overline{u}_-}{\overline{u}_+ + \overline{u}_-}$$ eq. 19

In eq. 18, the first term on the right hand side is the Donnan potential, while the second term is the diffusion potential. Similar results can be obtained with the equation defined in [104]. Eq. 18 differs from the equation given by Lakshminarayanaiah [46] and Barragan et al. [105], as there a ω term (or minus sign) in front of the Donnan part is missing (the diffusion part in those equations equals eq. 18 for $\omega = -1$, but for the Donnan part $\omega = +1$ is implicitly assumed). The TMS theory is often used, as it is a one dimensional (1D) model that is mathematically not very complicated. The original TMS theory assumes only gradients perpendicular to the membrane, membrane pores substantially larger than the ion radius, an ideal solution of point ions (activity coefficients of the ions to be equal to unity, so $a_i = c_i$), no pressure-volume term (no convection), and an equal and evenly distributed membrane charge at all external concentrations [38, 39, 46, 101, 102, 104]. And although the TMS theory can predict the reversible membrane potential (OCV) for certain external concentration ranges [46], also (large) deviations are reported [72, 79, 80, 102, 104-107].

In the TMS theory one of the three driving forces, the pressure gradient, is neglected. The TMS theory was extended with the convective water flow in the 'uniform potential model' [40, 47, 108-110].

The space charge model

The SCM, or capillary pore model, developed by Osterle and co-workers [29, 111, 112] is a two dimensional (2D) model that takes into account gradients both in the axial and radial direction. Also, solvent transport is included in this model. In contrast

to the TMS theory, the SCM includes assumptions about the membrane structure. This is necessary because radial gradients within the membrane pores are taken in account. In the original SCM, presence of parallel cylindrical pores with the fixed membrane charge uniformly distributed over the pore walls, while ions are regarded as point charges.

In the SCM, the NP equation, extended with a convection term, is used to describe the ion and water fluxes through the membrane. The Navier-Stokes equation is used for the fluid velocity in the pore. The Poisson-Boltzmann (PB) equation is used to describe the ion and electrical distribution (in the EDL) within the pore.

The SCM is based on the three earlier mentioned driving forces that determine the membrane potential: the electric potential gradient, the chemical (osmotic) potential gradient, and the pressure gradient [29, 111-113]. These three driving forces are not independent but are linked by three equations with each three terms and three coupling coefficients (K_{ij}). The resulting 9 coupling coefficients reduce to 6 by Onsager's reciprocal theorem ($K_{ij} = K_{ji}$) [114]. It was already mentioned that whenever a concentration gradient ($\nabla\mu$) is present in a (charged) membrane, this will lead to the development of an electric potential ($\nabla\phi$). However, due to differences in concentration (or composition) of the external solutions there is as well a difference in osmotic pressure (Π) in these external solutions, which leads to an effective pressure gradient (∇P). So even if no (hydrostatic or hydraulic) pressure is applied (P_{hyd}), effectively a pressure gradient is present in the membrane, resulting in of fluid flow (osmosis) through the membrane pores. The effective pressure gradient in the membrane is defined as [60, 104, 115, 116]:

$$\nabla P = \nabla P_{hyd} - \nabla\Pi \qquad \text{eq. 20}$$

By this definition, movement of fluid against a hydrostatic pressure, toward location of higher osmotic pressure (e.g. in seawater reverse osmosis) can be understood.

Water transport

Across the membrane-solution interface (*I*) of a highly charged IEM exist a sudden change in the osmotic pressure ($\Delta\Pi^I$) of the solution, as the ion concentration changes from the concentration in the external solution to the value in the internal solution (within the membrane) over a distance of the order of a few times the Debye length [108]. As shown by refs. [60, 108, 117], the change in the osmotic pressure results in an equal change in the hydrostatic pressure across the solution-membrane interface ($\Delta\Pi^I$

$= \Delta P_{hyd}{}^I$). The pressure increase from the bulk to the internal solution will be larger on the membrane side facing the lower external solution ion concentration, resulting in a pressure gradient in the membrane pore, which leads to fluid flow towards the high salt concentration (positive or normal osmosis) [40, 60, 108, 117, 118]. Besides the pressure gradient, also the electric potential gradient (electric field) in the pore is a driving force for osmosis [60, 108, 119, 120]. This fluid transport which is induced by ion migration is known as electro-osmosis [25, 121]. Finally, water can be 'bound' to ions in the primary hydration sphere [122-124] or dragged along in a secondary hydration sphere or as 'free' water [123-125], which can lead to large water transport numbers [121, 125]. Membrane properties influence the amount of water that is transported by the ions and in general a small pore size and hydrophobicity, or a low water content of the membrane, limit water transport [124-127]. Electro-osmotic transport depends on ion fluxes and ion diffusion coefficients and is independent of osmotic pressure. Direction and velocity of the fluid flow may vary with different ionic mixtures as described in refs. [40, 108, 117, 120], so just as the solute (ions) also the fluid (water) can be transported against its chemical potential gradient (anomalous osmosis). Neglecting convection in the SCM, or including convection in the TMS theory, was found to have for most cases only a small effect on the calculated membrane potential [72, 102, 128].

Radial concentration gradients

In the SCM besides axial ion gradients, also radial ion gradients in the membrane pore are considered. It was found that the assumption of a uniform distribution of ions across the pore diameter leads to an overestimation of the co-ion exclusion effect, which results in incorrect estimation of the ion fluxes and the membrane potential in the TMS approach [72, 104]. In the limit when EDLs in the membrane pores are fully overlapped, gradients in the radial direction disappear, and differences between the SCM and TMS theory (with convection included) must vanish. The thickness of the EDL is roughly represented by the Debye length and is a function of the external concentration, c_{ext} (mol/m³) at the membrane-solution interface [72, 113]. At room temperature and for a monovalent 1:1 salt, the Debye length, λ_D (nm), can be approximated by $\lambda_D \approx 10/\sqrt{c_{ext}}$ (λ_D in nm, c_{ext} in mol/m³) [129]. It should be noted that the Debye length is not based on the ion concentration within the EDL but on the concentration of the external solution [129]. For densely charged IEMs a typical pore radius (r_p) of ~1-2 nm may be assumed [67, 104]. If c_{ext} is 10 mol/m³, and $\lambda_D \approx 3$ nm, then assuming fully overlapped EDLs is valid. However, at higher external concentrations, where, $\lambda_D < r_p$, the assumption of fully overlapping EDLs would not be correct [130, 131].

Radii of hydrated ions are several Ångström [132, 133], so in densely charged IEMs, with nanoscopic pores, the volume fraction of ions in the pore is not insignificant [68,

134]. Therefore, ions cannot be infinitely close to the wall, or to each other, and both the TMS theory, and the SCM (both of which assume ions as point charges) will over-estimate the concentration of ions in the membrane pore [68, 104]. Also the thickness of the EDL will be influenced when the ion size is included, and will be larger than calculated with the PB equation. Fully overlapping EDLs may therefore be present at higher c_{ext} than estimated on the basis of the earlier given Debye length approximation. Detailed consideration of concentration profiles [135-137] will therefore be of less importance in very narrow and highly charged pores (r_p ~1-2 nm) where radial gradients diminish.
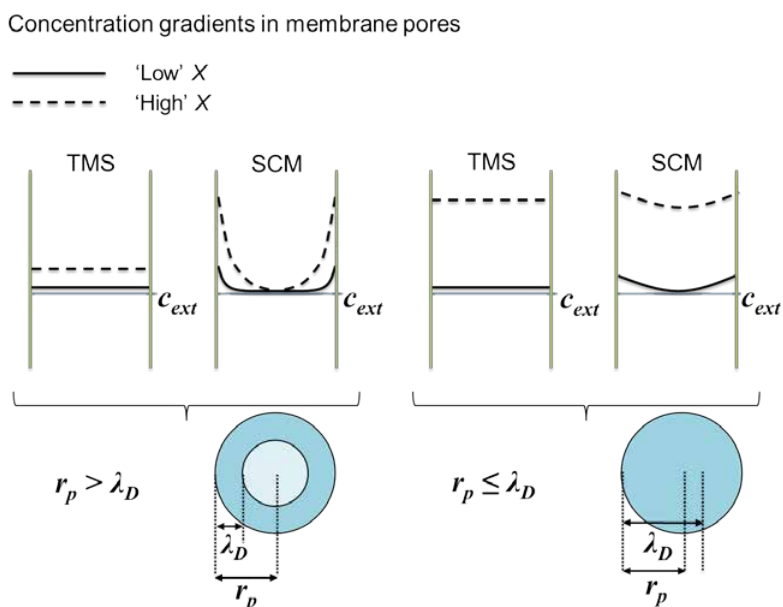
Figure 4. Schematic representation of a membrane pore and the concentration gradients in the radial direction according to the theory of Teorell-Meyer-Sievers (TMS) and the space charge model (SCM). The solid line refer to membranes with a relative low fixed charge density, X, and the dashed lines to a membrane with a high fixed charge density. The external salt concentration, c_{ext}, is indicated by the thin line, pore radius is shown as r_p and the Debye length as λ_D.

For membranes with larger r_p (e.g. used in nanofiltration, NF) and a considerable fixed charge density, these gradients are more important, as 'there is space' to develop a concentration gradient. For membranes with large r_p and low fixed charge density, the gradient is also of less importance and predictions of the membrane potential between the TMS theory and the SCM will become closer again. Interesting are the cases with a low external concentration on one side and a high concentration on the other side

of the membrane. In this situation, the EDLs can change from (fully) overlapping to (partly) non-overlapping along the axial direction. Proper estimation of the internal ion concentration is in that case required. Figure 4 gives a schematic representation of the concentration gradients in membrane pores according to the TMS theory and the SCM.

To overcome some of the shortcomings of the SCM, Basu and Sharma [138] and Cervera *et al.* [104, 134] extended the SCM theory and included effects of ion size, dielectric saturation, hydration, and surface charge regulation. By incorporating finite ion size the ionic selectivity increases, while on the other hand conductance will decrease as a result of lower internal concentrations and decreased diffusion coefficients [134, 138]. Charge regulation, dielectric saturation and ion hydration significantly influence the model results and a good agreement with experimental results was obtained [138]. The effects of finite ion size and hydrodynamic retardation only become important for small pore diameters and high salt concentrations [138], e.g., for dense and highly charged IEMs.

7.3 Materials and Methods

7.3.1 Materials

The membrane potential over a CEM was experimentally investigated in a six compartment stack, of which the details are described in refs. [139, 140], and which is schematically shown in Figure 5. Two shields (Perspex 2 mm), with a circular hole were placed on either side of the membrane under investigation. These shield lowered the effective area of the membrane under investigation to 2.84 cm^2, instead of its standard effective area of 23.8 cm^2. These shields stabilize the membrane and lower the diffusion area between the measuring solutions. All membranes in the setup are CEMs (CMX, Neosepta®, Tokuyama Corporation, Japan). Therefore, no concentration changes occurred when a direct current (DC) was applied to the electrodes (i.e. no formation of diluate/concentrate). The effective area of the four auxiliary membranes (indicated by CEM in Figure 5) was 23.8 cm^2 each, and all six compartments had a volume of 95.0 cm^3.

A galvanostat (Ivium Technologies, The Netherlands) was used to measure the electrical potential over the membrane under investigation. To measure this potential, two Haber-Luggin capillaries were placed on either side of the membrane. These capillaries were connected with a reservoir by silicon tubes (inner diameter 4 mm, length ~100 mm). Both reservoir and capillary were filled with the same solution (and same concentration) as present in the specific compartment. In these reservoirs Ag/AgCl gel

electrodes (QM711X, QIS, The Netherlands) were placed, which were connected to the galvanostat. The distance between the capillary tip and the membrane was 4.5 ± 0.1 mm and was equal for all measurements.
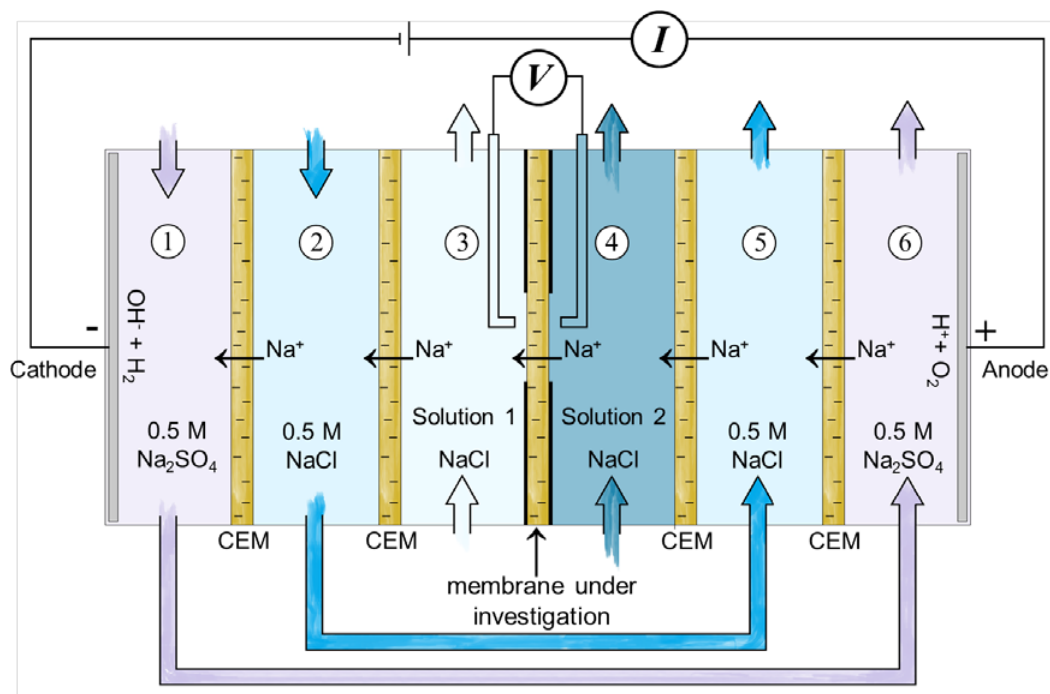
Figure 5. Schematic representation of the six compartment stack used to determine the membrane potential. The NaCl concentration of the solutions (1 and 2) in the compartments adjacent to the membrane under investigation (CMX, Neosepta), was varied between 0.001-5.0 M. CEM is a cation exchange membrane, I is the electrical current (A) and V is the potential difference between the Haber-Luggin capillaries (V). Drawing based on refs. [139, 140].

Salt solutions were prepared with demineralized water and NaCl (analytical grade, Boom B.V., The Netherlands). The concentrations of the measurement solutions were varied between 0.01-1.1 M in the first series of experiments, also described in ref. [140] and shown in Figure 6. For the second series experiments, of which the results are shown in Figure 9, the solution concentration was in the range of $0.001 - 5.0$ M.

7.3.2 Methods

With a thermostatic bath the temperature of the solutions in the six compartment stack was controlled at 25 ± 0.5 °C. The solutions were kept in 1 l bottles, which were sub-merged for 75% in the thermostatic bath. Solutions were circulated through the stack

with a flow rate of 170 ml/min. Before the start of each experiment the temperature was checked with a glass thermometer.

The membranes under investigation were stored in a 0.5 M NaCl solution. After installing the membrane in the stack, the membrane was equilibrated for at least 1 hour with the measurement solutions on each side of the membrane before the experiment was started. After this time, solutions in the system were refreshed and continuously flushed through the stack in order to undo possible concentration changes in the solution due to diffusion effects. The largest concentration gradient over the membrane was present when the measurement solutions of 0.001 and 5.0 M were used. The difference in conductivity of these two solutions was measured directly before and after the experiment. The change in conductivity was observed to be <1%. Therefore, concentrations of the solutions could be considered constant during the experiments.

The membrane potential was measured under open circuit conditions (1 measurement/second) by chronopotentiometry [140]. Three series of measurements were made. Each series started with 5 minutes open circuit conditions, followed by a defined range of applied current densities [140]. From this period of 5 minutes, the first minute was not used for measuring the membrane potential. Based on the remaining (3 times) 4 minutes, the average membrane potential was determined. The same measurements were also made with the salt concentration gradient reversed, i.e., the solutions on either side of the membrane were switched around. A second, independent measurement value of the membrane potential was then obtained. When there is no concentration gradient over the membrane, the membrane potential is by definition zero. However, due to offset between the two reference electrodes still a potential can be measured. This offset was determined as 1.4 ± 0.1 mV. The experimentally determined values were corrected for this electrode offset.

7.4 Results & Discussion

7.4.1 Experimental results

Figure 6 shows the experimentally determined, and theoretically calculated, membrane potential for different NaCl concentrations of the two external solutions (c_{low} and c_{high}).
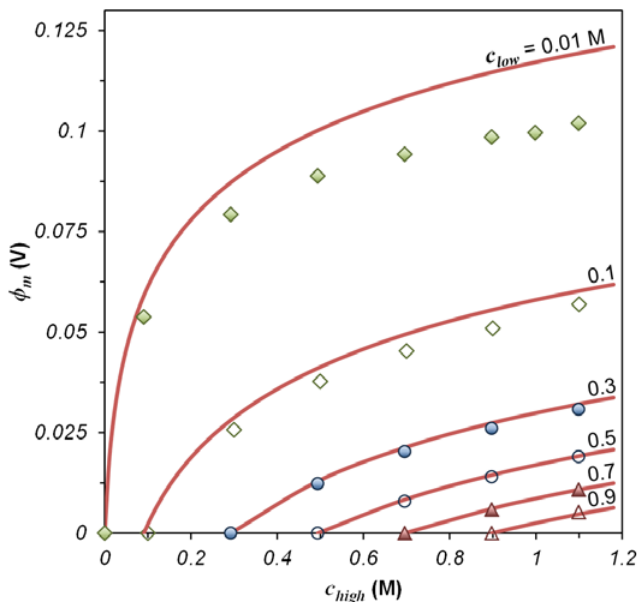

Figure 6. Measurement of the membrane potential, ϕ_m (V), with a lowest external NaCl solution concentration, c_{low} (M), as displayed in the figure as a function of the highest external NaCl solution concentration, c_{high} (M), which is plotted on the x-axis. Solid lines represent the theoretical potential according to the standard TMS theory.

When the two external solutions are equal ($c_{low} = c_{high}$), there is no gradient in any property and consequently there is no membrane potential (as $\nabla\phi = \nabla P = \nabla\mu = 0$). For $c_{low} \geq 0.3$ M, Figure 6 shows that the experimental and theoretical potentials are very close. However, when $c_{low} = 0.1$ M, a small, but distinct, difference develops between the experimental and theoretical value of ϕ_m, and the deviation of the TMS theory increases when $c_{low} = 0.01$ M. The TMS theory (eq. 18) overestimates the experimentally obtained membrane potential. This overestimation of the membrane potential was also reported in refs. [46, 72, 79, 105, 106, 141]. These deviations imply that certain assumptions in the TMS theory are no longer valid for the dense and highly charged CMX membranes which are used here, under the experimental conditions. The assumptions that are made in the TMS theory are that:

i.)   there is no concentration gradient in the radial direction in the membrane pores,

ii.)   membrane pores are substantially larger than the ion radius,

iii.)   the ions behave as thermodynamically ideal point charges (so $a_i = c_i$),

iv.)   membrane pores are homogeneous throughout the membrane, and the fixed membrane charge is evenly distributed,

v.)   the membrane surfaces are in a state of permanent, instantaneously established Donnan equilibrium,

vi.)   the membrane structure does not change, the pore volume is constant, and the membrane charge density is equal at all external concentrations,

vii.)   the convective water transport is negligible,

viii.) the ion mobility ratio in the external solution is equal to the ion mobility ratio in the internal solution.

Assumptions i) and ii) from this list are considered valid for the dense and highly charged IEM used in the experiments. These assumptions were already discussed in the theoretical section (7.2.3). The effect of the other assumptions (iii-viii) on the calculated membrane potential according to the TMS theory is investigated in the next section. These six assumptions are then investigated in six different situations (A-F) based on several modifications or extensions of the TMS theory.

7.4.2 Theoretical results

Figure 7 shows in panels A – F how different parameters, which correlate to assumptions iii – viii, influence the predicted membrane potential according to the TMS theory. The different panels show the effect of: ion activity (A), inhomogeneous distribution of the fixed membrane charge (B), including SDLs in the TMS theory (C), assuming a decreased (effective) membrane charge density (D), including osmotic water transport (E), and changing the ion mobility ratio (F). The lowest concentration of the external solution was fixed at 0.01 M, while the highest concentration is indicated on the x-axis. In all cases the solid line represents the standard TMS theory, and the experimental results (diamonds) are for $c_{low} = 0.01$ M.
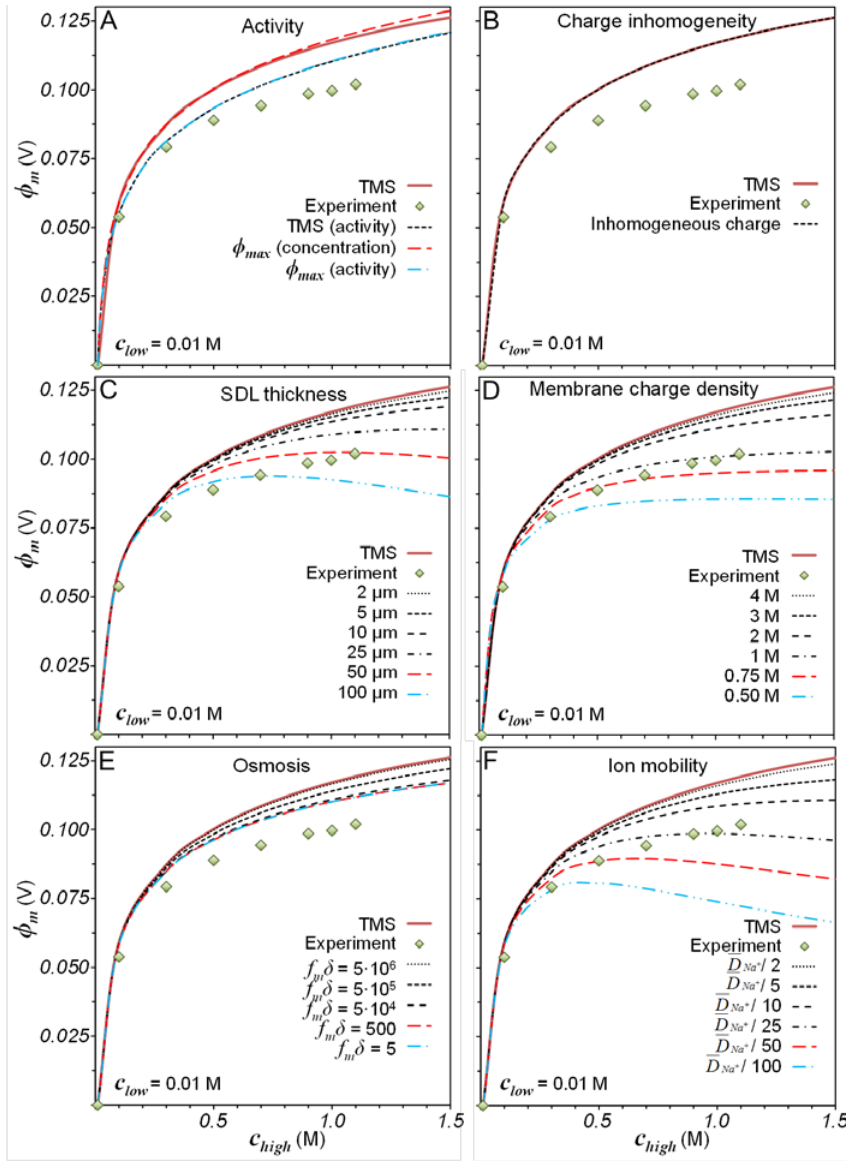
Figure 7. Testing of six modifications of the TMS theory. Diamonds indicate experimental values of the membrane potential, ϕ_m (V), with a low external NaCl solution concentration of 0.01 M and a high external NaCl solution concentration, c_{high} (M), plotted on the x-axis. The solid line is the standard TMS theory. The effect of A) Ion activity (activity coefficients according to [142]); B) Inhomogeneous charge distribution; C) Stagnant diffusion layers adjacent to the membrane of specified thickness, δ_{SDL}; D) Lowering the fixed membrane charge density; E) Osmosis at different water-membrane friction coefficients, $f_m\delta$, through the membrane; F) Lowering the diffusion coefficient of the counterion ($\overline{D}_{Na+}$) in the membrane.

Figure 7 A shows the differences between the theoretical maximum potential (eq. 4) and the TMS theory when the ion concentrations of the external solutions are replaced by the ion activities that are calculated according to:

$$a_i = \gamma_i c_i \hspace{8cm} \text{eq. 21}$$

Where, a_i is the ion activity (mol/m^3) and γ_i the ion activity coefficient (-). For the used concentrations, the assumption that all solutions are sufficiently diluted, so that $\gamma_i = 1$, is not valid [46, 102]. The activity coefficients were obtained from ref. [142]. Figure 7 A shows the difference between the TMS theory and the pure thermodynamical approach. The membrane potential calculated with the TMS theory is very close to the maximum membrane potential (ϕ_{max}) according to the Donnan relation (eq. 4). This observation implies that the effect of the diffusion potential is very small, which is expected as $X \gg c_{ext}$. In this case, activity coefficients in the membrane can be neglected. For that reason only the ion concentrations of the external solutions is replaced by the ion activities, as this difference is the actual driving force for solute transport [104], and no integration is performed of the flux equations using activities.

Use of ion activities greatly improves the prediction of the membrane potential when $c_{high} = 0.1 - 0.3$ M, where the value of γ changes rapidly. In absolute terms, the effect is the largest when the activity coefficient reaches a minimum (at ~1 M). The effect of using ion activity instead of ion concentration diminishes when the concentration gradient is small and $\gamma_i^{\,L} \approx \gamma_i^{\,R}$. In literature, activity coefficients of ions in the membrane and their effects on the membrane potential are discussed for instance in refs. [46, 48, 82, 103, 104, 141, 143-146], and also ion size effects, as observed in a previous work [68], can be included in this membrane activity coefficient [104]. However, activity coefficients in the membrane are unknown [145] and therefore, its usefulness for highly charged membranes is still a question [48].

Figure 7 B shows that the membrane potential is not affected by inhomogeneous distribution of the fixed membrane charge concentration, X. A heterogeneous distribution of charge across the membrane thickness, thus along the membrane pores from one side to the other side of the membrane, can be due to structural or chemical heterogeneities of the membrane [37, 146-148], but can also be due to unequal swelling of the two membrane sides when the membrane is separating a dilute and a concentrate solution. Ramirez *et al.* [149] showed different options of the spatial charge distributions, of which in this work the influence of the most straightforward distributions (beside the average distribution) will be investigated, namely i) an asymmetrical linear distribution, and ii) a symmetrical linear distribution. These two distributions are sketched in

Figure 8. X was previously determined as ~5.7 M for the used membranes [68], and therefore this value is used as the average fixed membrane charge density (indicated as $\langle X \rangle$).
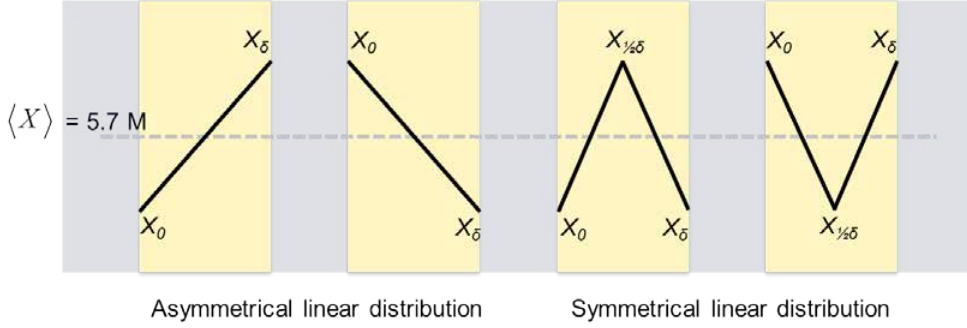
Figure 8, Asymmetrical and symmetrical linear distribution of the fixed membrane charge X (M), where $\langle X \rangle$ is the average membrane charge density.

With the asymmetrical fixed charge distribution, there is a gradient in X across the membrane from position 0 to δ (left and right sides of the membrane). At one side the charge is lowered, on the other side the charge is increased relative to $\langle X \rangle$. With the symmetrical linear charge distribution, X is equal at both membrane-solution interfaces ($X_0 = X_\delta$), but these values are respectively above or below $\langle X \rangle$. In the model of an asymmetrical linear distribution in a CEM, X depends on the position in the membrane according to:

$$X(x) = X_0 + \frac{x}{\delta}\left(X_\delta - X_0\right)$$

eq. 22

With:

$$X_\delta = 2\langle X \rangle - X_0$$

eq. 23

Where x (m) refers to a certain position in a membrane of thickness δ (m). For the symmetrical linear distribution ($X_0 = X_\delta$) the local fixed membrane charge density can be calculated, when $2x < \delta$ by:

$$X(x) = X_0 + \frac{2x}{\delta}\left(X_{\frac{1}{2}\delta} - X_0\right)$$

eq. 24

And when $2x > \delta$ by:

$$X(x) = X_{\frac{1}{2}\delta} + \frac{2x}{\delta}\left(X_{\delta} - X_{\frac{1}{2}\delta}\right)$$

eq. 25

With:

$$X_{\frac{1}{2}\delta} = 2\langle X \rangle - X_0$$

eq.26

In the theoretical calculations performed for the present study, using a modified TMS theory including the charge distribution, based on numerically solving eq.18, no effect of the charge distribution was observed. Small deviations (<1 mV) were found (which cannot be distinguished in the graphs of Figure 7 B) which may be due to the numerical procedure, especially when there is a large gradient of fixed charges. Effect of inhomogeneous fixed membrane charge distribution on the membrane potential was also studied in refs. [148-153]. It was suggested by data in [150, 153] that when membranes with an asymmetrical fixed charge distribution separate two solutions of equal composition, and no current is applied, the membrane potential is unequal to zero ($\phi_m \neq 0$). Here is stressed that according to theory this outcome is not possible, as was already discussed in the early 1970s in refs. [151, 152]. These works conclude that such a potential can only be observed when no ions can penetrate the membrane, otherwise an internal diffusion potential will arise equal in size, but of reversed direction as the difference in Donnan potentials [152]. In ref. [148] it is mathematically proven that under zero-current conditions, regardless of the fixed membrane charge distribution of an IEM, the membrane potential and salt transport must be zero when the membrane is separating two identical external solutions. In approximate models, non-zero equilibrium potentials can for instance arise due to invalidity of the Henderson equation [148]. This Henderson assumption is only valid when the external ion concentration is at least one order of magnitude smaller than the internal ion concentration ($c_{ext} \ll X$) [49, 143, 148].

When a current is applied over a membrane with a distribution of membrane charge, effects of the fixed charge distribution can be observed as described in refs. [149, 154].

Whereas the permselectivity is mainly determined by $\langle X \rangle$, other transport properties, such as the selectivity through an asymmetrical membrane, can be observed when diluate and concentrate are switched [149, 154].

Figure 7 C shows the effect of including two SDLs (as shown by eq. 17 and Figure 2) in the TMS theory (based on eq. 16 and Figure 1). By including SDLs, assumption v) is affected, as the ion concentrations on the solution-membrane interface will change.

Including SDLs in the model lowers the theoretical membrane potential. The effect increases with SDL thickness (δ_{SDL}), as was also experimentally confirmed in ref. [90]. When an SDL thickness δ_{SDL} is used of 50 or 100 µm, the membrane potential shows a maximum in the given concentration range. However, the shape of the curves differs significantly from the measurement. Therefore, the simple addition of SDLs to the theory will not explain the observed differences between experimental and theoretical membrane potentials.

Figure 7 D shows the effect of the fixed membrane charge density on the membrane potential. As mentioned, X was determined as ~5.7 M per unit aqueous volume in the membrane [68]. Ref [68] showed that X slightly increases with increased external solution concentration. An increase of X, however, leads to a higher membrane potential, as directly follows from eq. 18. In literature, it is sometimes assumed that the effective fixed membrane charge density (X_{eff}), is lower than the actual value of X [105, 106, 141]. The effect on the calculated membrane potential can be large when X is lowered substantially. However, this leads to the situation that X is no longer much larger than the external salt concentration. Barragán *et al.* [105, 106] found similar differences between practical and theoretical membrane potentials as in the present work. They explained these differences by assuming that X_{eff} is lower than the actual membrane charge due to tight binding of counterions to the fixed membrane charge sites, as described in ref. [141].

In the present work, it is argued that the effective membrane charge is equal to the actual membrane charge, at least as long as only NaCl is used as the salt. The ions Na^+ and Cl^- do not bind to the fixed charges sites [28]. In Figure 7 D shows that a lower X results in a reduced membrane potential. Lower values of X do not lead to a better prediction of the experimentally determined shape of the membrane potential curve, as the theoretical potential is leveling off when c_{high} is further increased, while the experimental values continue to increase in the concentration range considered. It was shown in literature that with a further increase of c_{high} eventually membrane potentials are lowered [106, 155]. These maximum membrane potentials were investigated and are discussed later on.

Figure 7 E shows that adding water transport to the TMS equation [40, 47, 108-110] (i.e. adding the $+c_i v_f$ term to eq. 9 and solving the model numerically) lowers the theoretical membrane potential. The water velocity (v_f) is a result from the ion concentrations and a specified friction coefficient between membrane and water, $f_m \delta$ [60], as mentioned in the theory section. The water velocity is maximized at the highest concentration differences (largest osmotic pressure difference) and for a minimum friction

with the membrane, and is in opposite direction to the ion flux. In the standard TMS theory there is no water flow. When water flow with a high friction coefficient ($f_m\delta = 5\cdot10^6$) is included, the water velocity in the membrane is low and comparable to the counterion velocity (both in the order of 10 nm/s at a concentration difference of 0.01-1 M). In the membrane the water velocity is constant because, the ion are assumed to have no volume in the Nernst-Planck equation. The ion velocity depends on the local ion concentration (as the ion flux across the membrane is constant). The counterion concentration is almost constant throughout the membrane and thus the counterion velocity may be considered everywhere the same in the membrane.

For co-ions, however, the concentration is strongly related to the ion concentration in the external solution [68] and, therefore, the ion velocity can be much higher at the membrane side that is facing the lowest external concentration (i.e. ~10.000 times higher at a concentration difference (0.01-1 M). When the water-membrane friction coefficient is lowered ten times ($f_m\delta = 5\cdot10^5$), this results in an increase of the water velocity (~6 times higher) and a slight decrease of the ion flux. Now the water velocity (~100 nm/s) becomes substantially higher than the counterion velocity, but is still much lower than the velocity of the co-ions. When the friction coefficient is lowered another ten times ($f_m\delta = 5\cdot10^4$), this only leads to a doubling of the water velocity to ~200 nm/s (at the concentration difference of 0.01-1 M). A further decrease of the friction coefficient does not lead to substantial higher water velocities, and the additive effect on the water flux diminishes. Thus the effect of water transport by itself seems too small to explain the deviation that is observed between experimentally determined and theoretical membrane potentials, even when there is assumed (almost) no friction between water and membrane. Earlier investigations on the effect of water transport on the membrane potential, led to similar conclusions [72, 82, 102, 128]. Sollner argues that measurement of correct stable potentials can be done long before any significant movement of water occurs [21], which underpins the conclusion that water flow cannot be the origin of the discrepancy in the membrane potential.

Figure 7 F shows the effect of a difference in the ratio of mobility (or diffusion coefficient) of the counterion versus co-ion in the membrane compared to solution. In this case the ion mobility of the counterion is lowered to a greater extent when moving into the membrane, than for the co-ion. Usually it is assumed that the ionic mobility (of monovalent ions) in the membrane is around one order of magnitude smaller than the ionic mobility in the external solution, and that the ionic mobility ratio of counterions over co-ions is equal in the membrane and external solution (both ions are retarded in the membrane to the same extent). It is, however, unknown to what extent individual counterion and co-ion mobility changes from the external to the internal solutions.

Thus, it is rather difficult to say what will be the sign of the diffusion potential across the membrane. However, changing the ion mobility ratio has a direct effect on the membrane potential as shown by eq. 18 and eq. 19. Lower ionic mobility occurs due to enhanced ion-ion / ion-membrane / and ion-fluid interactions [72]. As shown in Figure 7 F, the membrane potential decreases when (effectively) the mobility of the counterion is lowered. The effect is very similar to the effect shown in Figure 7 C, which can be explained by the fact that in both cases the transport of the counterion is more restricted than the co-ion.

To conclude, the effects of the parameters shown in Figure 7 A-F do not (each by itself) explain the difference between experimental and theoretical membrane potentials that are shown in Figure 6. So, until now the TMS theory and the discussed modifications cannot explain the experimental results shown in Figure 7. It is most likely that a combination of the presented variables must be considered to explain the discrepancy between the experimentally observed and theoretical potential. With six variables to play with it will certainly be possible to fit the model to the experimental data in several ways [156], although the physical soundness of the different 'fitting' parameters should then be carefully examined. The effect of each parameter is difficult to isolate [144], moreover, the fitting parameters in the model affect each other (e.g. using activities leads to a lowered theoretical driving force for osmotic water transport). A better fit at larger concentration differences, does not necessarily improve also the fit for cases with smaller concentration differences (i.e. when c_{low} is increased), especially when assumptions are made that are physically not correct. Isolation of effects of different parameters may only be possible with very precise experiments.

7.4.3 Maximum membrane potential

The experimental data in Figure 6 show that the membrane potential increases with an increasing concentration difference (Δc) of the two external solutions; c_{low} and c_{high}. This increasing membrane potential, however, seems to level off to a certain maximum value. Such a maximum value was also observed in the membrane potential data of previous investigations related to the membrane potential, see refs. [106, 155, 157-160]. When Δc is further increased, this eventually leads to a decrease of the membrane potential. An 'ideal' membrane, which possesses perfect selectivity, will have exactly the potential given by eq. 4. In that ideal membrane case there would be no maximum potential, but the potential keeps increasing with increasing Δc. To further investigate this interesting phenomenon of decreasing membrane potential, additional experiments were performed according to the same methodology as the experiments of section 4.1. The salt concentration on the low/concentration side, c_{low} was either 0.001 M or 0.01 M NaCl, and c_{high} was between 0.001 and 5, or between 0.01 and 5 M NaCl.

Resulting membrane potentials from these experiments and the theoretical maximum potential (eq. 4) are shown in Figure 9. To be consistent with ref. [155], the x axis shows the activity ratio instead of the concentration ratio of the two external solutions.
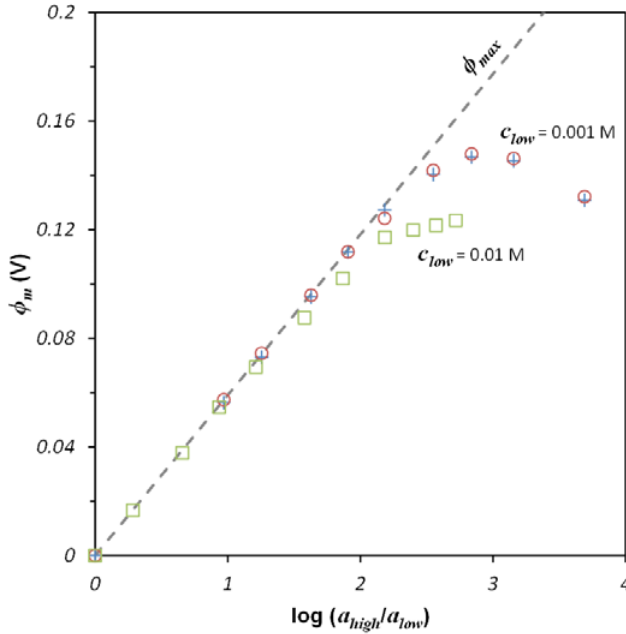

Figure 9. Experimental membrane potential (ϕ_m) as a function of the logarithm of the ratio of the activity of the external solution with the high NaCl concentration (a_{high}) over the activity of the external solution with the low NaCl concentration (a_{low}). The dashed line indicates the activity based maximum potential, ϕ_{max}, according to eqs. 4 and 21. The lowest external solution concentration (c_{low}) was either 0.001 M (circles, crosses) or 0.01 M (squares). When c_{low} = 0.001 M, the highest concentration (c_{high}) was respectively 0.001, 0.01, 0.02, 0.05, 0.1, 0.2, 0.5, 1, 2, or 5 M (from left to right in the graph). When c_{low} = 0.01 M, c_{high} was respectively 0.01; 0.02; 0.05; 0.1; 0.2; 0.5; 1, 2, 3, 4, or 5 M (from left to right in the graph).

Figure 9 shows for the CEM a perfect cation selective behavior, up to a ratio of external activities of ~100 (log 2). Beyond that, a deviation between the experimentally obtained membrane potential and the ideal membrane potential develops, which can be explained by the decrease of membrane selectivity [46, 155, 159, 160]. When the 'fixed' external concentration c_{low} was 0.01 M, no decrease in membrane potential is observed, not even when the variable concentration c_{high} was 5 M. However, when c_{low} is decreased to 0.001 M and the experiments are repeated, a maximum potential is shown, when c_{high} ≈1-2 M NaCl. For even higher salinities the membrane potential decreases again, as was also observed in refs. [155, 159]. So, what is the mechanism

behind this decreasing membrane potential when Δc becomes very large?

In literature was shown that a decrease in pore diameter and an increase in the fixed charge density, postponed the deviation of the ideal potential (and formation of a maximum potential) to a larger external concentration ratio [155, 159]. It was suggested in literature [159, 160] that if the concentration of the external solution is similar to, or larger than, the fixed membrane charge density, the membrane loses its permselectivity, which then leads to a decrease in membrane potential. However, in a previous investigation it was found that the fixed membrane charge density of the membrane is ~5.7 M [68], a concentration that was not reached in the experiments of Figure 9, but still a decrease was observed. Figure 9 furthermore shows that when c_{low} is increased from 0.001 to 0.01 M, no decrease in membrane potential can be observed anymore. Moreover, when in that case c_{high} is 1 M (log $(a_{high}/a_{low}) \approx 1.9$) the membrane potential is still very close to the Nernst potential, while if $c_{low} = 0.001$ M and $c_{high} = 1$ M (log $(a_{high}/a_{low}) \approx 2.8$) a much large deviation of the Nernst potential is observed. From these observations it can already be concluded that not only the absolute value of the highest external concentration is important, but also the concentration ratio. This suggests that the diffusive ion flux (of counterions and co-ions) through the pores is of influence to the membrane potential, as is also recognized by Makra *et al.* [159]. At the solution-membrane interfaces 'large' ion fluxes can cause concentration polarization. Figure 7 shows that including concentration polarization layers in the theory can help to explain the maximum in the membrane potential. Also further restriction of the counterion mobility compared to the co-ion mobility in the membrane can lead to the observation of a maximum membrane potential.

Note that in this work only three driving forces were considered, but it should be kept in mind that in fact also the thermal difference (ΔT) acts as a driving force for mass transport [161, 162]. This driving force for instance becomes important when membranes are used in fuel cells and in membrane distillation [162, 163]. Direction of the water flux due to temperature differences depends on the hydrophobicity of the membrane. Through hydrophilic membrane pores water is transported from the cold side to the hot side, while in a membrane with hydrophobic pores water is transported from the hot side to the cold side [162, 163]. Because in most membrane systems there is no, or a very small, temperature difference between the external solutions, this driving force is neglected in most theories, although in electrochemical systems significant temperature gradients can locally be found.

7.5 Conclusion

With respect to the title question: 'How well does the Teorell-Meyer-Sievers theory work?', for the case of densely charged IEMs, it can be concluded that: when the concentration difference across the membrane is small, the TMS theory predicts the measured membrane potential fairly well. When the concentration difference increases, TMS theory starts to deviate. In the parameter analysis, it was found that using the ion activity instead of the ion concentration of the two solutions adjacent to the membrane in all cases leads to a better prediction of the membrane potential. Charge inhomogeneity (charge distribution) has no effect on the membrane potential under zero current conditions. The effect of the two stagnant diffusion layers on either side of the membrane can be relatively large, but just like all other tested parameters it cannot by itself explain the deviation of the theoretical membrane potential from the measured potential. Lowering the effective charge density can improve the theoretical prediction to some extent, but the physical justification thereof is questionable. The effect of osmosis is small, even when in the theory the membrane-water friction is set to a very low value. Considering differences in the ionic mobility of the ions in the membrane phase can have large effect on the membrane potential and can, just as including the SDLs, be beneficial to explain the maximum membrane potential.

7.6 Literature

[1] H. Strathmann, Electrodialysis, a mature technology with a multitude of new applications, Desalination, 264 (2010) 268-288.
[2] R.E. Pattle, Production of electric power by mixing fresh and salt water in the hydroelectric pile, Nature, 174 (1954) 660.
[3] J.W. Post, H.V.M. Hamelers, C.J.N. Buisman, Energy recovery from controlled mixing salt and fresh water with a reverse electrodialysis system, Environmental Science and Technology, 42 (2008) 5785-5790.
[4] S. Porada, R. Zhao, A. Van Der Wal, V. Presser, P.M. Biesheuvel, Review on the Science and Technology of Water Desalination by Capacitive Deionization, Progress in Materials Science 58 (2013) 1388-1442.
[5] B. Sales, M. Saakes, J. Post, C. Buisman, P. Biesheuvel, H. Hamelers, Direct power production from a water salinity difference in a membrane-modified supercapacitor flow cell, Environmental science & technology, 44 (2010) 5661-5665.
[6] M. Levin, Molecular bioelectricity in developmental biology: new tools and recent discoveries, Bioessays, 34 (2012) 205-217.
[7] M. Yang, W.J. Brackenbury, Membrane potential and cancer progression, Frontiers in physiology, 4 (2013).
[8] L. Pardo, C. Contreras-Jurado, M. Zientkowska, F. Alves, W. Stühmer, Role of voltage-gated potassium channels in cancer, The Journal of membrane biology, 205 (2005) 115-124.
[9] W. Ostwald, Elektrische Eigenschaften halbdurchlässiger Scheidewände, Zeitschrift für Physikalische Chemie, 6 (1890) 71-82.
[10] F.G. Donnan, The theory of membrane equilibria, Chemical Reviews, 1 (1924) 73-90.
[11] S. Arrhenius, Über die gleichgewichtsverhältnisse zwischen Elektrolten, Zeitschrift für Physikalische Chemie, 1 (1890) 1-22.
[12] M.D. Archer, Genesis of the Nernst equation, in, 1989, pp. 115-126.
[13] V.A. Shaposhnik, Evolution of the membrane electrochemistry, Russian Journal of Electrochemis-

try, 38 (2002) 800-805.

[14] F.G. Donnan, Theorie der Membrangleichgewichte und Membranpotentiale bei vorhandensein von nicht dialysierenden elektrolyten. Ein beitrag zur Physikalisch-chemischen Physiologie., Zeitschrift Für Elektrochemie, 17 (1911) 572-581.

[15] E. Maigrot, J. Sabates, Apparat zur Lauterung von Zuckersaften mittels Elektrizitat. Germ. Pat. Nr. 50443, (1890).

[16] H.N. Morse, J.A. Pierce, Diffusion und Übersättigung in Gelatine Mit., Zeitschrift für physikalische Chemie, 45 (1903) 589-607.

[17] E. Manegold, C. Kalauch, Über kapillarsystem, XXII die wirksamkeit verschiedener reinigungs-methoden (filtration, dialyse, electrolyse und ihre kombinationen), Kolloid Zeitschrift, 86 (1939) 93-101.

[18] K.H. Meyer, W. Straus, La perméabilité des membranes VI. Sur le passage du courant electrique a travers des membranes sélectives, Helvetica Chimica Acta, 23 (1940) 795-800.

[19] V.A. Shaposhnik, K. Kesore, An early history of electrodialysis with permselective membranes, Journal of Membrane Science, 136 (1997) 35-39.

[20] J.R. Wilson, Demineralization by electrodialysis, in, Butterworths Scientific Publications, London (UK), 1960.

[21] K. Sollner, Recent advances in the electrochemistry of membranes of high ionic selectivity, Journal of the Electrochemical Society, 97 (1950) 139C-151C.

[22] W. Juda, W.A. McRae, Coherent ion-exchange gels and membranes, Journal of the American Chemical Society, 72 (1950) 1044-1044.

[23] T. Kressman, Ion exchange resin membranes and resin-impregnated filter paper, Nature, 165 (1950) 568.

[24] W. Juda, J.A. Marinsky, N.W. Rosenberg, Ion exchange, Annual Review of Physical Chemistry, 4 (1953) 373-398.

[25] H. Strathmann, Ion-exchange membrane separation processes, Elsevier, Amsterdam NL, 2004.

[26] T. Xu, Ion exchange membranes: State of their development and perspective, Journal of Membrane Science, 263 (2005) 1-29.

[27] A. Staverman, Non-equilibrium thermodynamics of membrane processes, Transactions of the Faraday Society, 48 (1952) 176-185.

[28] F.G. Helfferich, Ion Exchange, McGraw-Hill, New York, (1962).

[29] R.J. Gross, J.F. Osterle, Membrane transport characteristics of ultrafine capillaries, Journal of Chemical Physics, 49 (1968) 228-234.

[30] K.S. Spiegler, Transport processes in ionic membranes, Transactions of the Faraday Society, 54 (1958) 1408-1428.

[31] O. Kedem, A. Katchalsky, A physical interpretation of the phenomenological coefficients of membrane permeability, The Journal of general physiology, 45 (1961) 143-179.

[32] O. Kedem, A. Katchalsky, Permeability of composite membranes. Part 1.-Electric current, volume flow and flow of solute through membranes, Transactions of the Faraday Society, 59 (1963) 1918-1930.

[33] B. Auclair, V. Nikonenko, C. Larchet, M. Métayer, L. Dammak, Correlation between transport parameters of ion-exchange membranes, Journal of Membrane Science, 195 (2002) 89-102.

[34] I. Michaeli, O. Kedem, Description of the transport of solvent and ions through membranes in terms of differential coefficients. Part 1.—Phenomenological characterization of flows, Transactions of the Faraday Society, 57 (1961) 1185-1190.

[35] A. Katchalsky, O. Kedem, Thermodynamics of flow processes in biological systems, Biophysical Journal, 2 (1962) 53-78.

[36] T.G. Kaufmann, E.F. Leonard, Studies of intramembrane transport: A phenomenological approach, AIChE Journal, 14 (1968) 110-117.

[37] V.I. Zabolotsky, V.V. Nikonenko, Effect of structural membrane inhomogeneity on transport properties, Journal of Membrane Science, 79 (1993) 181-198.

[38] T. Teorell, An Attempt to Formulate a Quantitative Theory of Membrane Permeability Proc. Soc. Exp. Biol. Med., 33 (1935) 282-285.

[39] K.H. Meyer, J.F. Sievers, La perméabilité des membranes I. Théorie de la perméabilité ionique, Helvetica Chimica Acta, 19 (1936) 649-664.

[40] R. Schlögl, Stofftransport durch Membranen, Dr. Dietrich Steinkopff Verlag, Darmstadt, 1964.

[41] J.V. Leyendekkers, The chemical potentials of seawater components, Marine Chemistry, 1 (1973)

75-88.

[42] M. Whitfield, An improved specific interaction model for seawater at 25°C and 1 atmosphere total pressure, Marine Chemistry, 3 (1975) 197-213.

[43] M. Higa, A. Tanioka, K. Miyasaka, Simulation of the transport of ions against their concentration gradient across charged membranes, Journal of Membrane Science, 37 (1988) 251-266.

[44] T. Teorell, Studies on the "diffusion effect" upon ionic distribution. I. Some theoretical considerations, Proc. Natl. Acad. Sci. Wash., 21 (1935) 152-161.

[45] A.H. Galama, M. Saakes, H. Bruning, H.H.M. Rijnaarts, J.W. Post, Seawater Predesalination with Electrodialysis, Desalination, 342 (2013) 61-69.

[46] N. Lakshminarayanaiah, Transport phenomena in membranes, 1st ed., Academic Press, Philadelphia, 1969.

[47] S. Mafé, V.M. Aguilella, J. Pellicer, Film control and membrane control in charged membranes, Journal of Membrane Science, 36 (1988) 497-509.

[48] R. Schlögl, F.G. Helfferich, Zur Theorie des Potentials von Austascher-Membranen, Zeitschrift Fur Elektrochemie, 56 (1952) 644-647.

[49] T. Teorell, Transport processes and electrical phenomena in ionic membranes, in: J.A.V.a.R. Butler, J. T. (Ed.) Progress in Biophysics and Biophysical Chemistry Academic Press, New York, 1953, pp. 305-369.

[50] C. Marshall, The electrochemical properties of mineral membranes. VIII. The theory of selective membrane behavior, The Journal of Physical Chemistry, 52 (1948) 1284-1295.

[51] A. Einstein, Über die von der molekularkinetschen Theorie der Wärme geforderte Bewegung von in ruhenden Flüssigkeiten suspendierten Teilchen, Annalen der Physik, 322 (1905) 549-560.

[52] M. von Smoluchowski, Zur kinetischen Theorie der Brownschen Molekularbewegung und der Suspensionen, Annalen der Physik, 326 (1906) 756-780.

[53] W.E. Morf, Calculation of liquid-junction potentials and membrane potentials on the basis of the planck theory, Analytical Chemistry, 49 (1977) 810-813.

[54] D.E. Goldman, Potential, Impedance, and Rectification in Membranes, J. Gen. Physiol., 27 (1943) 37-60.

[55] W.F. Pickard, Generalizations of the Goldman-Hodgkin-Katz equation, Mathematical Biosciences, 30 (1976) 99-111.

[56] P. Moon, G. Sandí, D. Stevens, R. Kizilel, Computational modeling of ionic transport in continuous and batch electrodialysis, Separation Science and Technology, 39 (2004) 2531-2555.

[57] Y. Kim, W.S. Walker, D.F. Lawler, Competitive separation of di- vs. mono-valent cations in electrodialysis: Effects of the boundary layer properties, Water Research, 46 (2012) 2042-2056.

[58] Y. Tanaka, Concentration polarization in ion-exchange membrane electrodialysis—the events arising in a flowing solution in a desalting cell, Journal of Membrane Science, 216 (2003) 149-164.

[59] C. Forgacs, N. Ishibashi, J. Leibovitz, J. Sinkovic, K.S. Spiegler, Polarization at ion-exchange membranes in electrodialysis, Desalination, 10 (1972) 181-214.

[60] P.M. Biesheuvel, Two-fluid model for the simultaneous flow of colloids and fluids in porous media, Journal of Colloid and Interface Science, 355 (2011) 389-395.

[61] J. Manzanares, K. Kontturi, Encyclopedia of Electrochemistry. V. 2. Interfacial Kinetics and Mass Transport/Eds Bard AJ, Stratmann M., Calvo EJ VCH, in, Wiley, Weinheim, 2003.

[62] S.-T. Hwang, K. Kammermeyer, A. Weissberger, Membranes in separations, Wiley New York, 1975.

[63] V.V. Nikonenko, A.B. Yaroslavtsev, G. Pourcelly, Ion transfer in and through charged membranes, Structure, properties, theory., in: A. Ciferri, A. Perico (Eds.) Ionic Interactions in Natural and Synthetic Macromolecules, John Wiley & Sons, Inc, 2012, pp. 267-336.

[64] V.V. Nikonenko, A.V. Kovalenko, M.K. Urtenov, N.D. Pismenskaya, J. Han, P. Sistat, G. Pourcelly, Desalination at overlimiting currents: State-of-the-art and perspectives, Desalination, 342 (2014) 85-106.

[65] R.B. Gunn, P.F. Curran, Membrane potentials and ion permeability in a cation exchange membrane, Biophysical Journal, 11 (1971) 559-571.

[66] A.L. Hodgkin, B. Katz, The effect of sodium ions on the electrical activity of the giant axon of the squid, J. Physiol. , 108 (1949) 37-77.

[67] T. Sata, Ion Exchange Membranes; Preparation, Characterization, Modification and Application, The Royal Society of Chemistry, Cambridge UK, 2004.

[68] A.H. Galama, J.W. Post, M.A. Cohen Stuart, P.M. Biesheuvel, Validity of the Boltzmann equation to describe Donnan equilibrium at the membrane-solution interface, Journal of Membrane Science, 442 (2013) 131-139.

[69] H.P. Gregor, Gibbs-donnan equilibria in ion exchange resin systems, Journal of the American Chemical Society, 73 (1951) 642-650.

[70] E. Glueckauf, R.E. Watts, The Donnan law and its application to ion exchanger polymers, Proceedings of the Royal Society A, 269 (1962) 339-349.

[71] K. Kontturi, L. Murtomäki, J.A. Manzanares, Ionic Transport Processes : in Electrochemistry and Membrane Science: in Electrochemistry and Membrane Science, OUP Oxford, 2008.

[72] G.B. Westermann-Clark, C.C. Christoforou, The exclusion-diffusion potential in charged porous membranes, Journal of Electroanalytical Chemistry, 198 (1986) 213-231.

[73] Y. Oren, A. Litan, The state of the solution-membrane interface during ion transport across an ion-exchange membrane, Journal of Physical Chemistry, 78 (1974) 1805-1811.

[74] K.N. Mikhelson, A. Lewenstam, S.E. Didina, Contribution of the diffusion potential to the membrane potential and to the ion-selective electrode response, Electroanalysis, 11 (1999) 793-798.

[75] Y. Lanteri, A. Szymczyk, P. Fievet, Membrane potential in multi-ionic mixtures, Journal of Physical Chemistry B, 113 (2009) 9197-9204.

[76] Y. Lanteri, A. Szymczyk, P. Fievet, Influence of steric, electric, and dielectric effects on membrane potential, Langmuir, 24 (2008) 7955-7962.

[77] K. Asaka, Electrochemical properties of asymmetric cellulose acetate membranes, Journal of Membrane Science, 52 (1990) 57-76.

[78] M. Ersoz, The electrochemical properties of polysulfone ion-exchange membranes, Journal of Colloid and Interface Science, 243 (2001) 420-426.

[79] W.J. Shang, X.L. Wang, Y.X. Yu, Theoretical calculation on the membrane potential of charged porous membranes in 1-1, 1-2, 2-1 and 2-2 electrolyte solutions, Journal of Membrane Science, 285 (2006) 362-375.

[80] Y. Kobatake, N. Takeguchi, Y. Toyoshima, H. Fujita, Studies of membrane phenomena. I. Membrane potential, Journal of Physical Chemistry, 69 (1965) 3981-3988.

[81] M. Kawaguchi, T. Murata, A. Tanioka, Membrane potentials in charged membranes separating solutions of weak electrolytes, Journal of the Chemical Society - Faraday Transactions, 93 (1997) 1351-1356.

[82] M. Tasaka, N. Aoki, Y. Kondo, M. Nagasawa, Membrane potentials and electrolyte permeation velocities in charged membranes, The Journal of Physical Chemistry, 79 (1975) 1307-1314.

[83] A.H. Galama, G. Daubaras, O.S. Burheim, H.H.M. Rijnaarts, J.W. Post, Seawater electrodialysis with preferential removal of divalent ions, Journal of Membrane Science, 452 (2014) 219-228.

[84] W. Nernst, Theorie der Reaktionsgeschwindigkeit in heterogenen Systemen, Z. phys. Chem., 47 (1904) 52-55.

[85] B. Levich, The theory of concentration polarisation, Discussions of the Faraday Society, 1 (1947) 37-49.

[86] D. Mackay, P. Meares, On the correction for unstirred solution films in ion-exchange membrane cells, Kolloid-Zeitschrift, 167 (1959) 31-39.

[87] K.S. Spiegler, Polarization at ion exchange membrane-solution interfaces, Desalination, 9 (1971) 367-385.

[88] L. Dammak, C. Larchet, B. Auclair, Theoretical study of the bi-ionic potential and confrontation with experimental results, Journal of Membrane Science, 155 (1999) 193-207.

[89] L. Dammak, C. Larchet, B. Auclair, V. Nikonenko, V. Zabolotsky, From the multi-ionic to the bi-ionic potential, European polymer journal, 32 (1996) 1199-1205.

[90] E. Kumamoto, Effect of unstirred layers on the membrane potential in a concentration cell, Journal of Membrane Science, 9 (1981) 43-51.

[91] C. Larchet, S. Nouri, B. Auclair, L. Dammak, V. Nikonenko, Application of chronopotentiometry to determine the thickness of diffusion layer adjacent to an ion-exchange membrane under natural convection, Advances in Colloid and Interface Science, 139 (2008) 45-61.

[92] J.B. Jensen, T.S. Sørensen, B. Malmgren-Hansen, P. Sloth, Ion exchange and membrane potentials in cellulose acetate membranes separating solutions of mixed electrolytes, Journal of Colloid and Interface Science, 108 (1985) 18-30.

[93] V.M. Barragán, C. Ruíz-Bauzá, Membrane potentials and electrolyte permeation in a cation-ex-

change membrane, Journal of Membrane Science, 154 (1999) 261-272.

[94] M. Nagasawa, Y. Kobatake, The theory of membrane potential, Journal of Physical Chemistry, 56 (1952) 1017-1024.

[95] T.S. Sørensen, V. Compañ, Salt flux and electromotive force in concentration cells with asymmetric ion exchange membranes and ideal 2:1 Electrolytes, Journal of Physical Chemistry, 100 (1996) 15261-15273.

[96] Y. Lanteri, P. Fievet, A. Szymczyk, Evaluation of the steric, electric, and dielectric exclusion model on the basis of salt rejection rate and membrane potential measurements, Journal of Colloid and Interface Science, 331 (2009) 148-155.

[97] X. Lefebvre, J. Palmeri, Nanofiltration theory: Good Co-Ion exclusion approximation for single salts, Journal of Physical Chemistry B, 109 (2005) 5525-5540.

[98] D. Liu, Y. Zhang, Membrane potentials across the cation exchange membrane in aqueous mixed electrolyte solutions, in: W. Chen, Q. Li, Y. Chen, P. Dai, Z. Jiang (Eds.) Advanced Materials Research, 2012, pp. 1825-1828.

[99] C.A. Lewis, Ion-concentration dependence of the reversal potential and the single channel conductance of ion channels at the frog neuromuscular junction, Journal of Physiology, Vol. 286 (1979) 417-445.

[100] S.G. Spangler, Expansion of the constant field equation to include both divalent and monovalent ions, The Alabama journal of medical sciences, 9 (1972) 218-223.

[101] A. Mauro, A. Finkelstein, Realistic model of a fixed-charge membrane according to the theory of Teorell, Meyer, and Sievers, The Journal of general physiology, 42 (1958) 385-391.

[102] G.J. Hills, P.W.M. Jacobs, N. Lakshminarayanan, Membrane Potentials I. The Theory of the e.m.f. of cells containing ion- exchange membranes, Proc. Roy. Soc. A, 262 (1961) 246-256.

[103] J. Mackie, P. Meares, The diffusion of electrolytes in a cation-exchange resin membrane. I. Theoretical, Proceedings of the Royal Society of London. Series A. Mathematical and Physical Sciences, 232 (1955) 498-509.

[104] J. Cervera, V. García-Morales, J. Pellicer, Ion size effects on the electrokinetic flow in nanoporous membranes caused by concentration gradients, Journal of Physical Chemistry B, 107 (2003) 8300-8309.

[105] V.M. Barragán, J.P.G. Villaluenga, M.P. Godino, M.A. Izquierdo-Gil, C. Ruiz-Bauzá, B. Seoane, Experimental estimation of equilibrium and transport properties of sulfonated cation-exchange membranes with different morphologies, Journal of Colloid and Interface Science, 333 (2009) 497-502.

[106] V.M. Barragán, M.J. Pérez-Haro, Correlations between water uptake and effective fixed charge concentration at high univalent electrolyte concentrations in sulfonated polymer cation-exchange membranes with different morphology, Electrochimica Acta, 56 (2011) 8630-8637.

[107] E. Fetcher Jr, A Criticism of the Teorell–Meyer–Sievers Theory of Membrane Permeability, The Journal of Physical Chemistry, 46 (1942) 570-574.

[108] A. Sonin, Osmosis and Ion Transport in Charged Porous Membranes: A Macroscopic, Mechanistic Model, in: E. Sélégny, G. Boyd, H. Gregor (Eds.) Charged Gels and Membranes, Springer Netherlands, 1976, pp. 255-265.

[109] W. de Lint, P.M. Biesheuvel, H. Verweij, Application of the charge regulation model to transport of ions through hydrophilic membranes: one-dimensional transport model for narrow pores (nanofiltration), Journal of Colloid and Interface Science, 251 (2002) 131-142.

[110] R. Schlögl, The significance of convection in transport processes across porous membranes, Discussions of the Faraday Society, 21 (1956) 46-52.

[111] F.A. Morrison Jr, J.F. Osterle, Electrokinetic energy conversion in ultrafine capillaries, The Journal of Chemical Physics, 43 (1965) 2111-2115.

[112] J.C. Fair, J.F. Osterle, Reverse electrodialysis in charged capillary membranes, The Journal of Chemical Physics, 54 (1971) 3307-3316.

[113] G.B. Westermann-Clark, J.L. Anderson, Experimental verification of the space-charge model for electrokinetics in charged microporous membranes, Journal of the Electrochemical Society, 130 (1983) 839-847.

[114] L. Onsager, R.M. Fuoss, Irreversible processes in electrolytes. Diffusion, conductance, and viscous flow in arbitrary mixtures of strong electrolytes, Journal of Physical Chemistry, 36 (1932) 2689-2778.

[115] A. Mauro, Nature of solvent transfer in osmosis, Science, 126 (1957) 252-253.

[116] P.M. Ray, On the theory of osmotic water movement, Plant physiology, 35 (1960) 783-795.

[117] R. Schlögl, Theory of anomalous osmosis, Z. Phys. Chem. NF, 3 (1955) 73-102.

[118] J.L. Anderson, D.M. Malone, Mechanism of osmotic flow in porous membranes, Biophysical Journal, 14 (1974) 957-982.

[119] I. Medved, R. Černý, Osmosis in porous media: A review of recent studies, Microporous and Mesoporous Materials, 170 (2013) 299-317.

[120] A. Yaroshchuk, Osmosis and reverse osmosis in fine-porous charged diaphragms and membranes, Advances in Colloid and Interface Science, 60 (1995) 1-93.

[121] N. Lakshminarayanaiah, Electroosmosis in Ion-Exchange Membranes, Journal of the Electrochemical Society, 116 (1969) 338-343.

[122] N.P. Berezina, S.A. Shkirskaya, A.A.R. Sycheva, M.V. Krishtopa, The electric transport of proton-bound water in MF-4SK/PAni nanocomposite membranes, Colloid Journal, 70 (2008) 397-406.

[123] J. Barrett, Inorganic chemistry in aqueous solution, in: E.W. Abel (Ed.), Royal Society of Chemistry, Cambridge (UK), 2003.

[124] B. Tansel, J. Sager, T. Rector, J. Garland, R.F. Strayer, L. Levine, M. Roberts, M. Hummerick, J. Bauer, Significance of hydrated radius and hydration shells on ionic permeability during nanofiltration in dead end and cross flow modes, Separation and Purification Technology, 51 (2006) 40-47.

[125] V.I. Zabolotskii, O.A. Demina, K.V. Protasov, Capillary model of electroosmotic transport of the free solvent through ion-exchange membranes, Russian Journal of Electrochemistry, 50 (2014) 412-418.

[126] V.I. Zabolotskii, K.V. Protasov, M.V. Sharafan, Sodium chloride concentration by electrodialysis with hybrid organic-inorganic ion-exchange membranes: An investigation of the process, Russian Journal of Electrochemistry, 46 (2010) 979-986.

[127] N.P. Berezina, E.N. Komkova, A comparative study of the electric transport of ions and water in sulfonated cation-exchange polymeric membranes of the new generation, Kolloidnyj Zhurnal, 65 (2003) 5-15.

[128] Y. Kobatake, Y. Toyoshima, N. Takeguchi, Studies of membrane phenomena. II. Theoretical study of membrane potentials, Journal of Physical Chemistry, 70 (1966) 1187-1193.

[129] P.M. Biesheuvel, S. Porada, M. Levi, M. Bazant, Attractive forces in microporous carbon electrodes for capacitive deionization, Journal of solid state electrochemistry, 18 (2014) 1365-1376.

[130] A. Yaroshchuk, Current-induced concentration polarization of interfaces between non-ideally perm-selective ion-exchange media and electrolyte solutions, Journal of Membrane Science, 396 (2012) 43-49.

[131] J.A. Manzanares, S. Mafé, J. Bisquert, Electric Double Layer at the Membrane/Solution Interface: Distribution of Electric Potential and Estimation of the Charge Stored, Berichte der Bunsengesellschaft für physikalische Chemie, 96 (1992) 538-544.

[132] J. Kielland, Individual activity coefficients of ions in aqueous solutions, Journal of the American Chemical Society, 59 (1937) 1675-1678.

[133] A. Volkov, S. Paula, D. Deamer, Two mechanisms of permeation of small neutral molecules and hydrated ions across phospholipid bilayers, Bioelectrochemistry and bioenergetics, 42 (1997) 153-160.

[134] J. Cervera, P. Ramírez, J.A. Manzanares, S. Mafé, Incorporating ionic size in the transport equations for charged nanopores, Microfluidics and Nanofluidics, 9 (2010) 41-53.

[135] O. Stern, Zur Theorie der Elektrolytischen Doppelschicht, Zeitschrift für Elektrochemie und angewandte physikalische Chemie, 30 (1924) 508-516.

[136] L.L. Zhang, X.S. Zhao, Carbon-based materials as supercapacitor electrodes, Chemical Society Reviews, 38 (2009) 2520-2531.

[137] J.C. Eijkel, A. van den Berg, Nanofluidics and the chemical potential applied to solvent and solute transport, Chemical Society Reviews, 39 (2010) 957-973.

[138] S. Basu, M.M. Sharma, An improved Space-Charge model for flow through charged microporous membranes, Journal of Membrane Science, 124 (1997) 77-91.

[139] P. Długołęcki, K. Nymeijer, S. Metz, M. Wessling, Current status of ion exchange membranes for power generation from salinity gradients, Journal of Membrane Science, 319 (2008) 214-222.

[140] A.H. Galama, D.A. Vermaas, J. Veerman, M. Saakes, H.H.M. Rijnaarts, J.W. Post, K. Nijmeijer, Membrane resistance: The effect of salinity gradients over a cation exchange membrane, Journal of Membrane Science, 467 (2014) 279-291.

[141] Y. Kobatake, N. Kamo, Transport processes in charged membranes, Prog. Polymer Sci. Japan, 5 (1973) 257.

[142] CRC Handbook of Chemistry and Physics, 85th ed., Boca Raton (Florida, U.S.A.), 2004.

[143] C. Marshall, W. Bergman, The Electrochemical Properties of Mineral Membranes. I. The Estimation of Potassium Ion Activities*, Journal of the American Chemical Society, 63 (1941) 1911-1916.

[144] S. Mafé, P. Ramírez, J. Pellicer, Activity coefficients and Donnan coion exclusion in charged membranes with weak-acid fixed charge groups, Journal of Membrane Science, 138 (1998) 269-277.

[145] E.H. Cwirko, R.G. Carbonell, Ionic equilibria in ion-exchange membranes: a comparison of pore model predictions with experimental results, Journal of Membrane Science, 67 (1992) 211-226.

[146] E. Glueckauf, A New Approach to Ion Exchange Polymers Proceedings of the Royal Society A, 268 (1962) 350-370.

[147] J.H. Petropoulos, Membrane transport properties in relation to microscopic and macroscopic structural inhomogeneity, Journal of Membrane Science, 52 (1990) 305-323.

[148] J.A. Manzanares, S. Mafe, J. Pellicer, Transport phenomena and asymmetry effects in membranes with asymmetric fixed charge distributions, The Journal of Physical Chemistry, 95 (1991) 5620-5624.

[149] P. Ramírez, V. Gómez, J. Cervera, B. Schiedt, S. Mafé, Ion transport and selectivity in nanopores with spatially inhomogeneous fixed charge distributions, The Journal of Chemical Physics, 126 (2007) 194703.

[150] A. Genç, Membrane potentials for linearly varying fixed charges, Turkish Journal of Engineering and Environmental Sciences, 33 (2009) 73-81.

[151] S. Ohki, Electrical potential of an asymmetric membrane, Journal of Colloid and Interface Science, 37 (1971) 318-324.

[152] N. Kamo, Y. Kobatake, Interpretation of asymmetric membrane potential, Journal of Colloid and Interface Science, 46 (1974) 85-93.

[153] R. Takagi, M. Nakagaki, Facilitated and reverse transport of electrolytes through an asymmetric membrane, Journal of Membrane Science, 27 (1986) 285-299.

[154] A.V. Sokirko, J.A. Manzanares, J. Pellicer, The Permselectivity of Membrane Systems with an Inhomogeneous Distribution of Fixed Charge Groups, Journal of Colloid and Interface Science, 168 (1994) 32-39.

[155] M. Nishizawa, V.P. Menon, C.R. Martin, Metal Nanotubule Membranes with Electrochemically Switchable Ion-Transport Selectivity, Science, 268 (1995) 700-702.

[156] J. Mayer, K. Khairy, J. Howard, Drawing an elephant with four complex parameters, American Journal of Physics, 78 (2010) 648.

[157] R. Yamamoto, H. Matsumoto, A. Tanioka, Ionic transport behavior across charged membranes with low water content. I. Theoretical aspect of membrane potentials in membranes having inhomogeneously distributed fixed-charge groups, The Journal of Physical Chemistry B, 107 (2003) 10615-10622.

[158] A.A. Qaiser, M.M. Hyland, D.A. Patterson, Membrane potential and impedance studies of polyaniline composite membranes: Effects of membrane morphology, Journal of Membrane Science, 385 (2011) 67-75.

[159] I. Makra, G. Jágerszki, I. Bitter, R.E. Gyurcsányi, Nernst–Planck/Poisson model for the potential response of permselective gold nanopores, Electrochimica Acta, 73 (2012) 70-77.

[160] P. Bühlmann, S. Amemiya, S. Yajima, Y. Umezawa, Co-Ion Interference for Ion-Selective Electrodes Based on Charged and Neutral Ionophores: A Comparison, Analytical Chemistry, 70 (1998) 4291-4303.

[161] M. Tasaka, S. Morita, M. Nagasawa, Membrane potential in nonisothermal systems, The Journal of Physical Chemistry, 69 (1965) 4191-4197.

[162] M. Tasaka, T. Mizuta, O. Sekiguchi, Mass transfer through polymer membranes due to a temperature gradient, Journal of Membrane Science, 54 (1990) 191-204.

[163] S. Kim, M. Mench, Investigation of temperature-driven water transport in polymer electrolyte fuel cell: Thermo-osmosis in membranes, Journal of Membrane Science, 328 (2009) 113-120.

Appendix A

In this Appendix is shown how the TMS theory can be derived from the Nernst-Planck flux equation (eq. 9 in the main text and here given as eq. A1). In the main text it was shown that the membrane potential according to the TMS theory is given as the sum of the two Donnan potentials and a diffusion potential (eq. 16). These two terms will be derived in this Appendix.

A.1 Donnan interface potential

The Nernst-Planck flux equation describes ion movement as function of a concentration gradient and an electric field gradient. In the presented form (eq. A1) it assumes a stagnant fluid (solvent). The ion-solvent friction is reflected in the ion diffusion coefficient, D_i.

$$J_i = -D_i \left[\frac{dc_i(x)}{dx} + c_i(x)z_i \frac{d\psi}{dx} \right]$$ eq. A1

Where $\psi = \phi \cdot F/RT$. Now the equation is solved for the case that there is no ion flux ($J_i = 0$), which results in:

$$\frac{1}{c_i} \frac{\partial c_i}{\partial x} = -z_i \frac{\partial \psi}{\partial x}$$ eq. A2

Eq. A2 is integrated across the solution-membrane interface, from just outside to just inside the membrane. The voltage drop across the interface is the Donnan potential.

$$\int_{sol}^{mem} \partial \ln c_i = -z_i \int_{sol}^{mem} \partial \psi$$ eq. A3

$$\ln \frac{c_i^{mem}}{c_i^{sol}} = -z_i (\psi^{mem} - \psi^{sol}) = -z_i \Delta \psi_D$$ eq. A4

$$c_i^{mem} = c_i^{sol} \exp(-z_i \Delta \psi)$$ eq. A5

Both in the external solution (eq. A6) and in the membrane phase (eq. A7) electro neutrality is assumed, which is given for a 1:1 salt as:

$$c_+ - c_- = 0$$ eq. A6

$$\overline{c_+} - \overline{c_-} + \omega X = 0$$ eq. A7

Where the overbar refers to ion concentrations in the membrane. The fixed membrane

charge density, X, is defined as a positive number while the charge sign, ω, is either -1 (for CEM) or +1 (for AEM). Combining eqs. A5-A7 results in:

$$2c^{sol}\sinh(\Delta\psi_D) = \omega X \qquad \text{eq. A8}$$

To get an expression for the Donnan potential on either solution-membrane interphase the equation can be rewritten as:

$$\Delta\psi_D^{L,R} = \omega \cdot \ln\left[\frac{1}{c_{L,R}^{sol}}\left(X + \sqrt{X^2 + (2c_{L,R}^{sol})^2}\right)\right] \qquad \text{eq. A9}$$

As two Donnan potentials develop, one on left side (L) of the membrane and one on the right (R), the total Donnan potential is then given as:

$$\Delta\psi_D = \omega \cdot \ln\left[\frac{c_R^{sol}}{c_L^{sol}}\frac{\left(X + \sqrt{X^2 + (2c_L^{sol})^2}\right)}{\left(X + \sqrt{X^2 + (2c_R^{sol})^2}\right)}\right] \qquad \text{eq. A10}$$

A.2 Diffusion potential (membrane)

Due to the imperfect selectivity of the IEMs a small number of co-ions will diffuse through the membrane from the high concentration side to the low concentration side. For zero-current conditions, this co-ion flux is the same as the counterion flux. The current, being zero, is given by:

$$J_+ - J_- = -\overline{D_+}\left(\frac{\partial\overline{c_+}}{\partial x} + \overline{c_+}\frac{\partial\overline{\psi}}{\partial x}\right) + \overline{D_-}\left(\frac{\partial\overline{c_-}}{\partial x} - \overline{c_-}\frac{\partial\overline{\psi}}{\partial x}\right) = 0 \qquad \text{eq. A11}$$

For further simplification, we divide by the diffusion coefficient of the positive ion, so there is only one system parameter, α (-), and eq. A7 is used to relate the counterions to co-ions, to result in:

$$\alpha = \frac{\overline{D_-}}{\overline{D_+}} \qquad \text{eq. A12}$$

$$-\left(\frac{\partial\overline{c_+}}{\partial x} + \overline{c_+}\frac{\partial\overline{\psi}}{\partial x}\right) + \alpha\left(\frac{\partial\overline{(c_+ + \omega X)}}{\partial x} - \overline{(c_+ + \omega X)}\frac{\partial\overline{\psi}}{\partial x'}\right) = 0 \qquad \text{eq. A13}$$

The membrane charge is assumed to be homogenously distributed and therefore, X is independent of x, and the variables can be separated, resulting in:

$$\frac{\partial \psi}{\partial x} = \frac{(\alpha-1)}{\alpha \omega X + (\alpha+1)\overline{c_+}} \frac{\partial \overline{c_+}}{\partial x}$$

eq. A14

Now both sides can be integrated over the membrane, leading to:

$$\psi_{diff} = \frac{(\alpha-1)}{(\alpha+1)} \ln \frac{\alpha \omega X + (\alpha+1)\overline{c_+}^R}{\alpha \omega X + (\alpha+1)\overline{c_+}^L}$$

eq. A15

At the solution-membrane interfaces on the left hand and right hand side of the membrane, the expressions for the Donnan equilibrium can be used to relate the internal ion concentration with the external concentration and the fixed membrane charge, according to:

$$\overline{c_{L,R}} = \frac{1}{2}\sqrt{X^2 + (2c_{L,R})^2} - \frac{1}{2}\omega X$$

eq. A16

Inserting eq. A16 into eq. A15 leads to the following expression of the (dimensionless) diffusion potential:

$$\psi_{diff} = \frac{(\alpha-1)}{(\alpha+1)} \ln \left[\frac{\frac{(\alpha-1)}{(\alpha+1)}\omega X + \sqrt{X^2 + (2c_R)^2}}{\frac{(\alpha-1)}{(\alpha+1)}\omega X + \sqrt{X^2 + (2c_L)^2}} \right]$$

eq. A17

Now, the following replacement can be made:

$$\overline{U} = -\frac{(\alpha-1)}{(\alpha+1)} = \frac{\overline{D_+} - \overline{D_-}}{\overline{D_+} + \overline{D_-}}$$
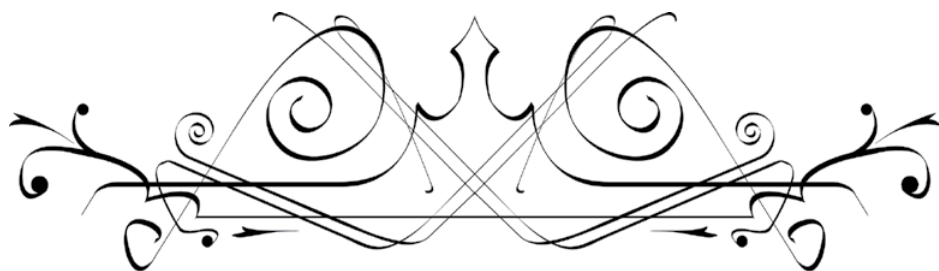
eq. A18

Eq. A18 can be inserted in eq. A17, which than can be rewritten to:

$$\psi_{diff} = \overline{U} \cdot \ln \left[\frac{-\overline{U}\omega X + \sqrt{X^2 + 4c_L}}{-\overline{U}\omega X + \sqrt{X^2 + 4c_R}} \right]$$

eq. A19

A.3 equation for the Teorell Meyer Sievers theory

Inserting eq. A10 and eq. A19 into eq. 16, will lead to the TMS equation:

$$\phi_m = \Delta\phi_D + \phi_{diff} = \frac{RT}{F}\left(\omega \ln \frac{c_R}{c_L}\left[\frac{X + \sqrt{X^2 + 4c_L}}{X + \sqrt{X^2 + 4c_R}} \right] + \overline{U}\ln\left[\frac{-\overline{U}\omega X + \sqrt{X^2 + 4c_L}}{-\overline{U}\omega X + \sqrt{X^2 + 4c_R}} \right] \right)$$

eq. A20

Chapter 8

General discussion and outlook

Nomenclature

A	=	area (m^2)
a	=	constant (Ω m^2)
b	=	constant (Ω m^2)
c	=	concentration (mol/m^3)
F	=	Faraday constant (C/mol)
I	=	current (A)
j	=	current density (A/m^2)
k	=	dimensionless concentration (-)
N	=	number of membrane pairs (-)
Q	=	charge (C)
R	=	resistance (Ω m^2)
R	=	gas constant (J/mol·K)
r	=	water recovery rate (-)
T	=	temperature (K)
V	=	volume (m^3)
z	=	valence (-)
δ	=	thickness (m)
Π	=	osmotic pressure (bar)
σ	=	conductivity (S/m)

This thesis is structured in two sections. Chapters 2-4 are focusing on the electrodialysis (ED) process and accompanying phenomena, while Chapters 5-7 address the ion exchange membranes (IEMs). In this final chapter the core findings presented in these two 'pillars' of the thesis will be discussed. In this discussion the suitability of ED as a seawater (pre)desalination technology will be evaluated as well as the application of IEMs in high salinities in general. Moreover, ED as single technology and in hybrid application is discussed and is compared with SWRO.

Paragraph **8.1** discusses that the main energetic losses in the ED process origin from the membrane stack resistance. Paragraph **8.2** explains how presence of a stagnant diffusion layer (SDL) adjacent to the membrane can negatively affect transport of divalent ions, may lead to reduced coulombic efficiency in the stack, and limits the maximum applied current density. Paragraph **8.3** addresses how the ion sorption is enhanced at increased ion concentration of the external solution, that enhanced ion sorption leads to better ion conductance, and that the internal ion concentration profile is very important in understanding membrane phenomena. Furthermore, it is discussed that formation of the membrane potential is still not fully understood. Paragraph **8.4** focusses on the (relative) importance of the membrane, SDL, and bulk resistance on the stack resistance. The difference between the membrane test cell (Chapter 6: Figure 1) and a practical ED stack are discussed. In this paragraph is shown that in practical application the size of the SDL resistance is small, but the effect of concentration polarization in this SDL on the membrane resistance may be large. Paragraph **8.5** treats the effect of divalent ions on the ED process and on the membrane resistance. An outlook is provided that addresses the selectivity of membranes and some hypothesis are formulated. Paragraph **8.6** provides some leads for future research based on questions that were raised in the present work. This section mainly focuses on research related to IEMs. Paragraph **8.7** discusses the economical perspective for ED used in waters with high salinity, and a comparison between the hybrid electrodialysis – brackish water reverse osmosis (ED-BWRO) and stand-alone seawater reverse osmosis (SWRO) is made. In this section is shown that the ED-BWRO becomes more attractive when high water recovery is required to lower pretreatment and concentrate treatment costs.

8.1 Electrodialysis process: large irreversible losses, especially due to stack resistance

In Chapter 2 is shown that from an energetic point of view the ED-BWRO process seems favorable over the application of ED as a stand-alone technology when the applied current density is larger than ~50 A/m². Typical SWRO energy consumption is around 3-4 kWh/m³, although also energy consumptions below 2 kWh/m³ were report-

ed [1, 2]. The energy consumption of an ED process is less easy to point down as it is largely depending on the applied current density. When the applied current density is very low (e.g. 10 A/m^2) an energy consumption lower than 2 kWh/m^3 can be reached. A drawback is that for such application a large (and expensive) membrane area is required. When a current density of 50 A/m^2 is applied the energy consumption will likely be ~3.5 kWh/m^3 and thus very comparable to state of the art SWRO. In Chapter 2 it is elaborated that at higher applied current density, energy consumption for seawater desalination can be much higher (>10 kWh/m^3). This high energy consumption was due to concentration polarization (CP) phenomena and stack resistance. The energy comparison should take into account that SWRO has a typical water recovery of about 30 – 40%, and as such the thermodynamic minimum required energy for desalination is lower compared to systems with higher water recovery.

In Chapter 2 only ED processes are considered with a constant applied current density, while in practice the ED process will be typically a multiple stage process (ED in series). In every stage the influent salt concentration is lower and, therefore, to avoid reaching the limiting current density (LCD) the applied current density is also lowered in every stage (typically to ~70% of the LCD [3]). LCD occurs due to CP, which can be minimized by optimization of the stack hydrodynamics. Therefore, in every stage the hydrodynamic conditions can also be changed [3]. Higher flow velocity through the stack reduces the energy losses acquainted to CP, but requires more pumping energy. When there is no recirculation, higher flow velocities lead to a requirement for more membrane area as the residence time is shorter and the amount of ions (or charge) that is removed is directly related to this time through the applied current density, as A/m^2 = C/(m^2·s). In this thesis, applied flow velocities are low (~0.5 cm/s), while in practice flow velocities around 6-12 cm/s and up to 20-40 cm/s [3, 4] are applied. Therefore CP effects are relatively important in this thesis.

In Chapter 2 is concluded that when the applied current density > 50 A/m^2, the stack resistance accounts for 80% of the energetic losses and this percentage is increasing with increasing applied current density. At a very low applied current density (10 A/m^2), the energetic losses resulting from water transport and 'back diffusion' are much more pronounced and are combined approximately the same as the losses related to the resistance of the membrane stack. When the applied current density will be even further decreased, the stack resistance will become marginal compared to diffusive ion transport and osmotic water transport. Although it might at first glance appear from the graphs in Chapter 2 that by further decreasing the applied current density, the energy consumption can be further decreased and the theoretical minimum energy consumption may be approached. However, this is not true as (diffusive) mass transport (water

from diluate to concentrate and ions from concentrate to diluate), causes relatively more energy losses at lower applied current densities. Therefore, energy consumption goes through a minimum when the applied current density is decreased. After this minimum, the increasing energy loss due to mass transport is limiting the process. At an applied current of 10 A/m^2 this minimum is already approached as the energetic loss caused by ion diffusion and water transport is already similar in size as the loss caused by the stack resistance.

The energy loss due to water transport and ion diffusion is related to the membrane selectivity and the water permeability. The membranes that are used in this thesis possess a permselectivity of ~93% (~98% according to manufacturer), therefore, the effect of back diffusion is rather limited. It also implies that improvement will be difficult as membranes with a permselectivity of a 100% will (most likely) never be produced. Concerning the water transport, it is a safe assumption that ions will be transported together with their primary hydration shell. For NaCl can be assumed that the average amount of water in the primary hydration shell is approximately 6 mol H$_2$O / mol NaCl [5-7]. In Chapter 2 we found a number of 6.4 mol H$_2$O / mol NaCl (as the ion valance = -/+ 1). That means that the amount of water transport through the membrane is already very small. The amount of osmotic water transport through these membranes can also be considered to be small. Some effect of ion diffusion and water transport is unavoidable as the membranes are designed for transport of dissolved ions and without water, ions cannot be transported through these membranes.

Sub conclusion 8.1

It can be concluded that efforts to further reduce the energy loss due to water transport and ion diffusion will only have limited effect as these losses are already small. Commercially available ED membranes are already close to optimized with respect to permselectivity and water transport. Moreover, these losses are only important at very low applied current densities. In practice, a current density of 10 A/m^2 will not be applied for seawater desalination, as the required membrane area would become too large for a feasible ED process (certainly at current membrane prices). In seawater application, applied current densities in the range of 100-600 A/m^2 [3, 8] is far more likely (considering the LCD value being in this order of magnitude). In this current range, the energetic losses due to ion diffusion and water transport with membranes as used in this work is very small. Therefore, the focus should be on the energetic losses due to the stack resistance. Minimization of the ionic membrane resistance and resistance of flow channels is the key to lower the energy consumption of seawater ED and to make it a feasible and competing seawater desalination technology.

8.2 Stagnant diffusion layer: reducing thickness, improving process

In this work we identified that for seawater ED the focus for improvement should be on reduction of the stack resistance. In an ED cell mass transport takes place due to convectional, migrational, and diffusional forces. However, as thoroughly described in this thesis (Chapter 3 and 7), the mass transport through the IEMs can be assumed as a result of migration and diffusion only. Adjacent to the membrane an SDL is present on either side of the membrane. It is in this layer that CP takes place. With respect to the energetic loss the SDL on the diluate side is of main importance, as here the ion concentration is lowered towards the membrane, leading to higher resistivity (i.e. reduced conductivity). On the concentrate side, the ion concentration will be higher in the SDL just outside the membrane than in the bulk solution.

CP is induced by the membrane selectivity, which largely prevents the migration of co-ions through a membrane (Chapter 7). Higher applied current density over an ED stack leads to a larger concentration gradient in the SDL and thus a higher resistivity. Presence of a relative thick SDL induces therefore a large transport resistance. Typical SDL thicknesses in ED are between 5-50 μm [9, 10], however an SDL thickness of 100 to several hundreds of μm's is possible at low applied flow velocity and large inter membrane distance [11-14]. When the applied current density is increased, the SDL thickness is somewhat reduced [11-13].

The SDL thickness of an ED stack described in Chapter 3 is estimated to be in the order of 150-200 μm on basis of the LCD and the data from [14, 15]. In Chapter 3 is shown that the SDL is not only adding resistance to the stack, but also influences the membrane selectivity with respect to mono- and divalent ions. Moreover, it is elaborated that most of the 'membrane selectivity' is actually due to the transport limitations of ions through the SDL. With respect to cations the study showed that at every applied current the ratio of monovalent cations over divalent cations is increasing in the diluate compartment during desalination. Only when the divalent ions were 'depleted' in the diluate, this ratio decreases again. This was only observed at an applied current density of 10 A/m^2 and when 90% of the salt was removed, which is beyond the predesalination range. For anions was found that irrespective of the applied current density the ratio of monovalent anions over divalent ions decreases during the first 60% of desalination. After that similar behavior as for cations was observed.

From a predesalination point of view it is beneficial to remove as much of the divalent ions as possible as these ions can cause scaling problems on the subsequent RO mem-

branes, and as such can limit the water recovery of this desalination step. In Chapter 3 of this thesis it is shown that these divalent ions are removed during the ED process. The amount of divalent ions compared to monovalent ions in seawater is relatively small, and therefore concentration polarization will initially have a larger effect on these ions. Chapter 4, discusses the transport of monovalent ions and divalent ions present in seawater in a 'fractioning ED stack'. The large role that the SDL's play in what appears to be the membrane selectivity was confirmed by the results presented there. LCD depends, amongst others, on the specific ion concentration in the bulk. When there is a mixture of several counterions and co-ions, it can happen that the concentration of one ion is already null at the diluate-membrane interface, but other ion concentrations are not [16-18]. The applied current density at which at least one of the ion concentrations becomes zero at the diluate-membrane interface is referred to as the critical current density of that ion [18].

Observations, presented in Chapter 4, show that the difference in obtained fractionation between an applied current density of 100 and 200 A/m^2 is very similar (especially for cations). This can be understood from the concept of critical current density. Given is the presence of a monovalent counterion in high concentration and a divalent counterion in lower concentration in an ED system, over which a constant current is applied. Assumed that for example the critical current density of the divalent counterion is 100 A/m^2 and the LCD is 300 A/m^2, the application of a current density > 100 A/m^2 will only lead to an increased transport of monovalent ions through the membrane. The coulombic efficiency of the fractioning stack will be in that case lower than when the applied current density = 100 A/m^2 (e.g. Chapter 4: Figure 2 and Figure 4 A). As stated before, a high removal rate of divalent ions is beneficial, therefore, the applied current density of a predesalinating ED stack, preferentially should not exceed the critical current density with respect to divalent ions.

Also in a normal ED stack CP will have a negative effect on the coulombic efficiency. Due to CP, the concentration difference adjacent the membrane can be several times higher than compared to the bulk concentration difference. As the external concentration is directly influencing the internal ion concentration, the chemical potential gradient in the membrane is enhanced resulting in a larger diffusion potential, what causes an increase of 'back diffusion' (Chapter 5, Chapter 7).

Sub conclusion 8.2

An increase in SDL thickness will reduce the amount of transported divalent ions through the membrane, as the ionic mobility and concentration of divalent ions is smaller than the mobility and concentration of monovalent ions in seawater. A lower

applied current density lowers the amount of concentration polarization and as such, 'the need' for diffusive transport through the SDL. Minimization of the SDL thickness is therefore beneficial in ED as predesalination technology, as it maximizes the 'removal' of divalent ions from the diluate. Other reasons why SDL thickness should be minimized (or CP minimized) are that back diffusion is than minimized and that thinner SDLs allows a higher applied current density, which is often beneficial from a commercial point of view (membranes are expensive).

8.3 Ion exchange membrane: direct interaction with the environment

Chapter 5 treats the ion partitioning or ion distribution described by the Donnan equilibrium. The fixed membrane charges are immobile, but do participate in the equilibrium like all dissolved ions (and other charged particles) in solution. The concentration of counterions in an IEM is often much higher than the ion concentration just outside the membrane. A large concentration gradient is present in just a few nanometers thick layer at the solution-membrane interface. As there is a slight excess of charge just outside the membrane an electrical double layer is formed. Chapter 5 illustrates how the membrane 'communicates with' (i.e. is influenced by) the surrounding solutions. When the ion concentration of the external solution increases, the amount of counterions and co-ions in the internal solution also increases. Due to an osmotic pressure difference, there is an uptake of water from the surrounding by the membrane. This membrane swelling depends on the size of the osmotic pressure difference, but is in commercial available ED membranes often limited due to membrane cross-linking. Nevertheless, swelling influences the ion concentration of the internal solution. Membrane pores have an estimated diameter of ~1 nm, ion volume is therefore significant and as shown in Chapter 5 influence the amount of ions in the pores. This size effect can be captured in the ion activity [19].

Ion activity can be seen as the effective ion concentration and is influenced by the ionic interactions. Changing for instance the ion concentration or the ionic composition will influence the ion activity. The ion activity will therefore be different in the membrane solution and the external solution. In Chapter 7 the membrane potential was investigated. This membrane potential is overestimated by the theory for highly charged membranes. It was shown that using the ion activity instead of the ion concentration of the external solutions leads to an improved prediction. In the presented work we did not investigate the ion activity within the membrane phase. The size of the activity coefficients in the internal membrane solution is unknown, but they will be smaller than in the external solution and are especially of importance at large concentration

difference between external and internal solution [20, 21]. IEMs with a fixed charge density around 5 M (mole fixed charge per liter of internal solution) usually have much higher internal concentration than their surrounding solutions. Using activity instead of concentration in the membrane would lead to somewhat lower 'effective concentrations' what lowers the potential jump at the solution-membrane interface and as such lowers the overall membrane potential. This might (almost) close the gap between theoretical and practical obtained potentials, but it would not enhance the insight into the functioning of membranes, as the activity coefficients will become some kind of fit parameter, that is different for each membrane. The term ion activity is then of course no longer entirely correct to use.

Chapter 6 explores the membrane resistance, which is described as the sum of two resistors placed in series. One resistor represents a gel-like phase associated to the fixed membrane charge density, which contains mainly counterions and a minority of co-ions. The second resistor represents an electrically neutral solution that is similar in concentration as the external solution concentration, when the external solutions are equal on either side of the membrane. These ions in free solution may also partly explain the difference between the number of co-ions found in the membrane and the theory as described in Chapter 5, but can not explain the observed plateau. In Chapter 6, it is described how the membrane resistance depends on the ion concentration in the membrane phase and thus is indirectly influenced by the external ion concentration (as described in Chapter 5). When the external solutions are unequal in concentration, the external solution with the lowest concentration largely determines the membrane resistance. When the NaCl concentration of the external solution with the lowest amount of ions is decreased below 0.1 M, the resistance increases very rapidly, irrespective of the ion concentration on the other side of the membrane.

Sub conclusion 8.3

The insight in the ion sorption, ion partitioning, membrane resistance, and formed membrane potential is enlarged in this thesis. A plausible explanation is given for the observed difference in ion sorption observed between established theory and experiments. The ions absorbed in the membrane play a crucial role in the membrane conductance as all current that is transported through the membrane is carried by these absorbed ions (ionic conductance). The internal concentration profile of absorbed ions in the membrane is very important with respect to the membrane resistance. The 'internal' ions also lead to the formation of the membrane potential, which can still not be entirely explained by the TMS theory and its expansions. Ion activity in the membrane phase may be helpful in this explanation, but the physical correctness should be considered.

8.4 Perspective on reducing stack resistance: reducing membrane thickness, the right way to go?

It was identified that stack resistance is the main factor determining the energy consumption of an ED stack, especially when the applied current densities is larger or equal to 50 A/m². In order to effectively reduce the energetic losses due to stack resistance it is required to identify the (relative) importance and size of i) the membrane resistance, ii) the SDL resistance, and iii) the flow channel (mainly diluate) resistance. To reduce IEM resistance, the membrane thickness can be reduced.
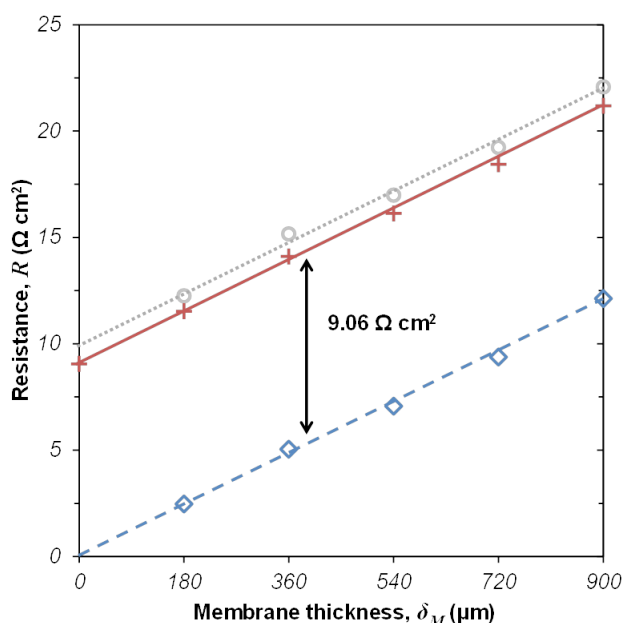

Figure 1. Relation between the membrane thickness, δ_M (µm), and the measured resistance, R (Ω cm²) at 0.5 M NaCl external solution. The resistance of the external water phase was determined as 9.06 Ω cm², measurements with alternating current are given by the crosses and solid line ($R_{M+water}$), measurements with a direct current include the membrane, stagnant diffusion layer (SDL), and water resistance ($R_{M+SDL+water}$) and are represented by the circles and the dotted line. The membrane resistance (R_M) is given by the diamonds and striped line.

Figure 1 displays how the membrane resistance increases linearly with the membrane thickness. Resistance measurements are done according to the methodology described in Chapter 6 and at an external solution concentration of 0.5 M. The membrane thickness was increased by piling membranes which were then pressed together in the measuring cell. Figure 1 shows that with a doubling of the membrane thickness the mem-

brane resistance is also doubled. When the membrane thickness is relative large, the SDL resistance is low compared to the membrane resistance. At a reduced membrane thickness the influence of the SDL resistance increases (~10-15% at δ_M = 180 μm, 0.5 M NaCl, based on data of Figure 1 and Chapter 6). A strategy to reduce stack resistance is to lower the membrane thickness, however, often these thinner membranes are (at the time being) less easy to produce and to handle and represent therefore additional costs. Furthermore, some mechanical strength of membranes is required for the use in ED stacks. A good question therefore is: *Is it an effective strategy to reduce the membrane thickness to reduce the stack resistance?* This question is answered in the next sections of this paragraph.

8.4.1 Membrane test cell used in this thesis: IEM resistance vs. SDL resistance

Based on the data in Appendix A of Chapter 6 (Table A2 and Table A3), the relative influence of the SDL and the membrane on their combined resistance was investigated.
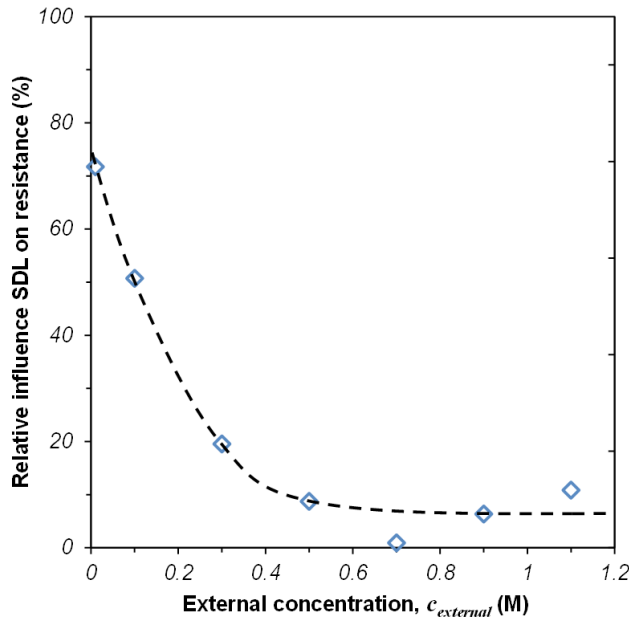

Figure 2. Relative influence of the stagnant diffusion layer (SDL) on the summed resistance of the SDL and membrane as a function of the external solution concentration. The striped line indicates the trend and has no further mathematical meaning.

Figure 2 shows that especially below 0.5 M the relative influence of the SDL increases with decreasing concentration. At an external solution concentration of 0.1 M, the measured resistance of the SDL is similar to the measured membrane resistance in the

membrane test cell. The membrane test cell used in Chapter 6 has a very low up flow velocity ($v_{average}$ = 0.07 cm/s) and no spacers or turbulence promoter are present in the stack. The SDL can therefore fully develop as gravitational convection is the dominant hydrodynamic process, and the SDL thickness may be >500 µm as can be derived from the work of Larchet *et al*. [12] and data for viscosity [22] and diffusion coefficients of Na$^+$ and Cl$^-$ [23] in NaCl solutions. This SDL thickness is larger than the inter membrane thickness of the ED stack used in Chapter 2,3 and 4 and therefore the effect of the SDL on the stack resistance will be there smaller than shown in Figure 2. Also the up flow velocity in those stacks was higher (~0.5 cm/s). In [24] a similar stack as in Chapter 6 has been used and the effect of flow velocity on the SDL resistance was investigated. From this work of Długołęcki *et al*. [24] it was derived that by increasing the average up flow velocity from ~0.04 cm/s to ~0.33 cm/s (100-800 ml/min) the SDL influence decreased by 73% (±2%) at 0.017 M external solution concentration, and by 21% (±6%) at 0.5 M external solution concentration. Thus, by increasing the flow velocity the resistance in the stack can be tremendously decreased. In practical application flow is at least ~20 time higher and spacers are presents, the size of the SDL resistance will therefore be small. In the next session, a more practical case is modeled. In this model also the resistance of the flow channel was included.

8.4.2 Typical ED stack used for practical application: IEM, SDL, and bulk resistance

In practice the influence of the SDLs will be much smaller as the flow velocity is larger. To get an impression of the relative contribution of the membrane, SDL, and bulk resistance (R_M, R_{SDL}, and R_{bulk}) a model is here introduced. In this model the resistance of the flow channel, SDL, and membrane is taken in account. Figure 3 shows a schematic model representation and an overview of the involved equations. In this model the SDL on the concentrate side is neglected and therefore the membrane is assumed to face the bulk concentration on the concentrate side.

In the model δ is the thickness (m), c is the NaCl concentration (M), N is the number of calculation planes in the SDL, σ is the conductivity (S/m), A_{eff} is the effective stack/membrane area (m^2), k is the dimensionless concentration (by dividing c with c_0 which is 1 M), and a and b are constants used to the calculate the membrane resistance according to equation 11 and 13 in Chapter 6. In the SDL k is taken as the average ($_{avg}$) of the plane. In the membrane phase, k is determined according to Equation 13 in Chapter 6, and is a function of the two solution-membrane interface concentrations. The conductivity of the solution is calculated by an empirical equation (R^2 = 0.9998) that is valid in the concentration range of 0.01-1.0 M NaCl (25°C), and that is based on the conductivity data from [22, 25].
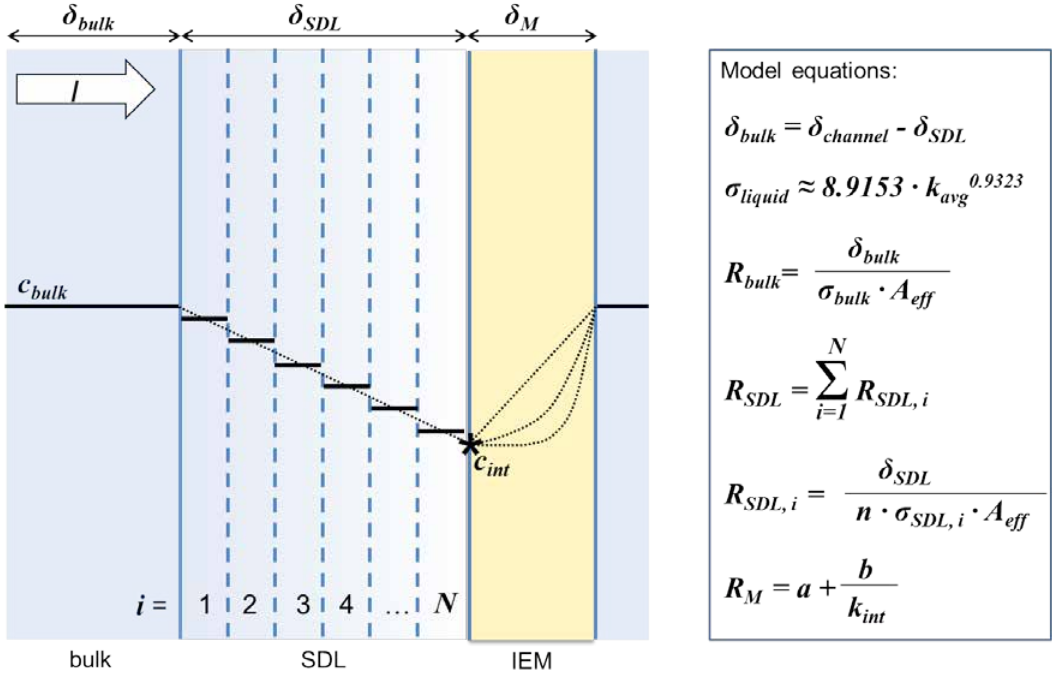
Figure 3. Schematic representation of the model parameters, the involved equations, and the schematic concentration profile in the bulk and stagnant diffusion layer (SDL). The concentration profile in the ion exchange membrane (IEM) depends on the interface concentration (c_{int}) as described by Equation 13 in Chapter 6.

The model was used to evaluate the situation where c_{bulk}, was fixed on either 0.5 or 0.1 M, while c_{int} was varied till a lowest concentration of 0.01 M. So, the model describes the resistances in situation with an under limiting applied current density. These modeled situations can be regarded as the first stage of seawater or brackish water desalination with ED. The SDL thickness was assumed to be constant and independent of the amount of concentration polarization (i.e. the applied current density). Resistance of the anion and cation exchange membranes is for now regarded as the same. Further details of the model parameters are given in Table A 1, in Appendix A at the end of this chapter.

Figure 4 shows the effect of concentration polarization on the relative importance of the modeled R_M, R_{SDL}, and R_{bulk} on the total resistance, and their modeled value when c_{bulk} = 0.5M (A), or c_{bulk} = 0.1M (B).
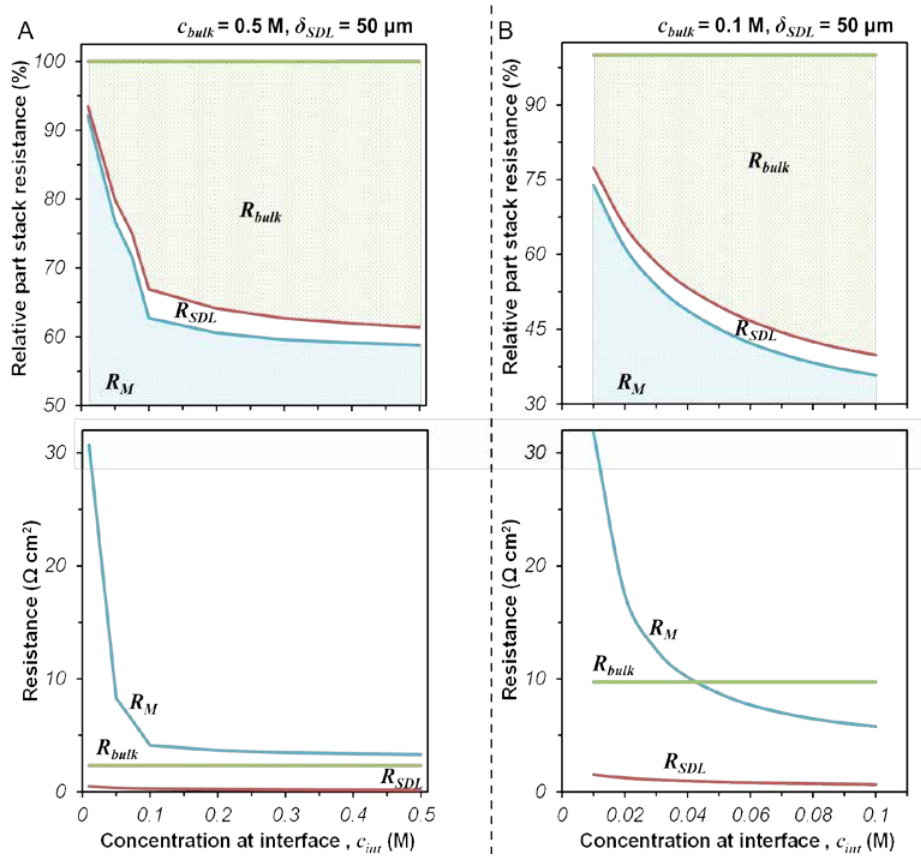
Figure 4. Relative influence of the membrane resistance (R_M), the stagnant diffusion layer resistance (R_{SDL}), and the flow channel resistance (R_{bulk}) on the total stack resistance as a function of the solution-membrane interface concentration c_{int}, when the bulk concentration is 0.5 (A) or 0.1 (B) M NaCl.

Figure 4A shows that the influence of R_M is always large when the bulk concentration is 0.5 M. At this concentration the bulk channels have a considerable influence on the total stack resistance, but R_{bulk} can be lowered by reducing the channel width ($\delta_{channel}$, which is here $\delta_{SDL} + \delta_{bulk}$), which had in this model a value of 800 μm, what is a typical number for ED applications in practice. Of course, there are limitations to the minimal intermembrane thickness as pumping energy increases at thinner channels and thinner channels are more sensitive to clogging. And because of the increase of pumping energy at reduced intermembrane distance, the energetical savings that can be achieved are less than may be assumed on basis of Figure 4.

The possibilities for reducing the intermembrane distance are currently especially investigated in the field of reversed electrodialysis (RED), where the presence of river

water in the stack leads to high 'diluate' channel resistance [26-28]. Furthermore is shown that the impact of the R_{SDL} is relative small. The maximum impact was 4.1%, when c_{int} = 0.1 M.

Figure 4B shows comparable results to Figure 4A, but due to lower bulk concentration, R_{bulk} has a larger influence on the total resistance, what justifies the investigations to reduce the channel width. The influence of R_{SDL} is at maximum 4.6%, when c_{int} = 0.04 M. Both figures show a rapid increase of the impact of R_M on the total resistance when the solution-membrane interface concentration is decreased below 0.1 M. This is an important finding for seawater desalination with ED as it implies that the applied current density should not only below the LCD, but rather chosen in such a way that the concentration polarization is limited and $c_{int} \geq 0.1$ M. Below this 'critical' concentration R_M increases much faster than R_{SDL}. The relative size of R_M compared to R_{SDL} is shown in Figure A 1 in Appendix A.

The model is also used to investigate a more technically improved stack (economy wise it may be very different) with reduced membrane, SDL and channel (bulk) thickness (δ_M = 25 µm, δ_{SDL} = 25 µm, δ_{bulk} = 200 µm). Results are shown in Appendix A: Figure A 2, and it can be concluded that R_M and R_{bulk} are the two most important stack resistances. R_M is the main resistance at low solution-membrane interface concentrations and R_{bulk} the main resistance when the bulk concentration is low and the degree of concentration polarization in the SDL is limited. It should be kept in mind that reducing the membrane thickness enhances the diffusional transport of ions and water through the membrane and as such has a negative effect on the coulombic efficiency and on the water recovery [29]. Production of thin membranes with very high selectivity is therefore more difficult. The model assumes perfect distribution of solution in the flow channels; something in practice usually not true, therefore in practice influence of the flow channel will be somewhat bigger.

In the special case when the LCD is reached, and the ion concentration at the membrane is ~0, the resistance of the membrane and the SDL becomes very high and a high voltage establishes over the membrane. When this voltage exceeds 1.23 V, water splitting is induced and H^+ / OH^- ions can continue charge transport through the SDL and membrane. H^+ and OH^- are relative fast (mobile) ions, when these ions enter the membrane (Chapter 5) it might very well be that the membrane resistance (Chapter 6) is lower than just before the ions were depleted in the SDL. It might be that in that occasion SDL is the main contributor to the stack resistance. This hypothetical case is, however, outside the scope of this work as ED is for desalination purposes operated at under limiting current density.

Sub conclusion 8.4

With respect to the question: '*Can reducing the membrane thickness be an effective approach to lower the stack resistance*', the answer is 'yes', especially in the case of high salinity feed waters, where the channel bulk and SDL possess relative high conductivity. At lower feed water salinity, reducing the channel thickness and thus R_{bulk} may be as important as reducing R_M. The SDL is in the modeled situations only of minor importance with respect to the resistance.

8.5 Divalent ions: higher stack resistance

Most of the experiments in this thesis are done with NaCl solutions in demineralized water. In Chapter 3 & 4, artificial seawater solutions with the main ions present in seawater, or ternary mixtures with divalent ions were used. As discussed in Chapter 5, all charged particles present in solution take part in the Donnan equilibrium and will be distributed over the membrane and external phase, in such way that the electrochemical potential is the same (eventually). Membrane affinity can affect the distribution of the ions, and as mentioned IEMs show under zero current conditions (i.e. no current is applied over the system / membrane), higher affinity towards divalent ions. Under applied current conditions, the ion partitioning in the membrane changes, and more mobile ions enter the membrane phase, whilst the less mobile divalent ions leave the membrane (Chapter 4). When doing experiments, it is often stated that the membranes should be brought in equilibrium with the solution it is going to be used in. However, it would be better to state that prior to experiments the membrane should be equilibrated under the conditions they are going to be used at.

Scaling problems arising with the presence of divalent ions are discussed in this work, the general conclusion is that the scaling tendency in ED(R) is low and can even be completely taken out by an inline (in the concentrate recycle stream) settler for supersaturated divalent ion solutions. However, this does not imply that the ED process is not affected by the presence of divalent ions. As the composition of the charged particle solution is changed, the conductivity of the membrane and external solutions will be affected. Divalent ions have in general somewhat lower ionic mobility (and higher viscosity) than monovalent ions, and therefore conductivity is reduced (Chapter 3). It is expected that, just as in solutions, the membrane resistance increases when divalent ions are present in solution compared to a solution only existing from monovalent ions (assuming a similar amount of charge present).

An experiment was performed to investigate the effect of composition of the feed water on the required desalination energy (see Appendix B). In this experiment four

different solutions were desalinated (compositions given in Table B 1, Appendix B). Each solution contained the same amount of charge. When divalent ions are present the conductivity is lower. SO_4^{2-} has a larger effect on the conductivity than Mg^{2+}, despite that the concentration of the latter is approximately two times larger in seawater (Table B 1). Results of the experiment are shown in Figure 5.
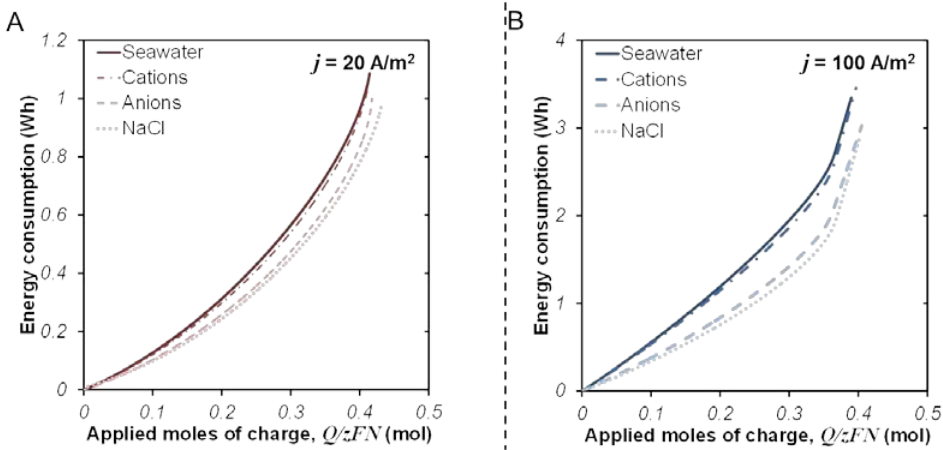

Figure 5. Energy consumption (Wh) of the membrane stack in a laboratory electrodialysis stack, as function of the applied moles of charge, Q/zFN (mol) at an applied current density, j of 20 A/m² (A) or 100 A/m² (B). Seawater, cations, anions, and NaCl, refers to the composition of the feed water, which is defined in Table B 1.

Figure 5A shows the results for experiments done at an applied current density of 20 A/m². On the x-axis is the applied moles of charge given, which is defined as Q/zFN, where, Q is the charge (C), z is the ion valence (-), F is the faraday constant (C/mol), and N is the number of cell pairs in the stack. On the y-axis the energy consumption (Wh) of the membrane stack ($N = 14$) was given as function of the cumulative applied moles of charge to the system. The amount of charge present in the diluate was ~ 0.38 C at the beginning of the experiment (diluate volume, $V_d = 0.6$ l). Figure 5B shows the results when the applied current density was 100 A/m². Both graphs show similar results, with of course higher energy consumption at larger applied current density. The required desalination energy of a seawater mixture is the largest, the energy consumption of a NaCl mixture the lowest. The additional energy consumption of a seawater composition is ~25%. Remarkable are however the results of the ternary mixtures. The effect of SO_4^{2-} presence on the energy consumption is rather small, whilst the effect of Mg^{2+} is large and energy consumption is almost as large as for seawater. From these graphs is concluded that the divalent cations (in this case Mg^{2+}) present in seawater cause the higher energy consumption of seawater desalination.

This finding is remarkable as the conductance of the ternary mixture with SO_4^{2-} is lower than the conductance of the ternary mixture with Mg^{2+}. Therefore, a higher stack resistance would be expected when SO_4^{2-} is present. Apparently, the effect of Mg^{2+} ions on the cation exchange membranes (CEM) resistance is larger than the effect of SO_4^{2-} ions on the anion exchange membrane (AEM) resistance. A larger effect of divalent ions on cation exchangers than on anion exchanges was also described by Helfferich (p. 304) [29]. In addition, Sata (p. 91) [30] has showed a large (2-3 time) increase of membrane resistance when the membrane is placed from a NaCl solution into a $MgCl_2$ or $CaCl_2$ solution. In [29] was discussed that interaction with the pore wall due to electrostatic attraction, or specific chemical interaction can explain larger retarding of cation than anions. Modeling of monovalent and divalent cation transport shows that the diffusion coefficients of monovalent and divalent cations were decreased by the same ratio in the CEM (Chapter 3: Table 4). Sulphate, however, was slowed down many times (~40 to ~115, depending on j) more than chloride ions. From that perspective, the higher energy consumption observed for seawater, is likely explained by the presence of divalent anions.

Outlook 8.5

At this stage it is not possible to give an explanation why the effect of divalent cations on the desalination energy consumption is relatively large. From the discussion in Chapter 3 it appears that divalent cations (Mg^{2+}, Ca^{2+}) are not extensively slowed down in the membrane compared to monovalent cations (Na^+, K^+), while the divalent SO_4^{2-} anion seems to be retarded more than Cl^- ions. It may be that an additional entrance resistance for divalent ions exists in CEMs. If that is the case, surface modifications might help to reduce the effect of divalent cations on the energy consumption. As discussed in Chapter 4, AEMs possess lower monovalent selectivity than CEMs, this also indicates that it is harder for divalent cations than divalent anions to be transported through a membrane. The detailed mechanisms require further underpinning by more experimental research. AEMs and CEMs probably have different characteristics. With respect to future membrane improvement it is interesting to study these differences as it may lead to a clue why sulphate can pass the membrane apparently very slowly, but without considerably affecting the membrane resistance. In [30], 19 different membrane characteristics that can be used for membrane characterization are identified. With respect to transport of divalent ions it would be interesting to investigate effects of ion exchange capacity, water content, membrane resistance, diffusion coefficients of electrolytes, adsorbed salts under equilibrium, and selectivity for different monovalent and divalent counterions at different external concentrations. In addition effects of surface modification on the ion transport and selectivity of the membrane can be studied.

8.6 Future research: directions to novel ED membranes and characterization

Chapter 6 describes the effect of two different external solutions on the measured membrane resistance. In this work was shown that the adjacent solution with the lowest ion concentration had a major effect on the membrane resistance. It is suggested that the internal concentration gradient is responsible for this influence and that this gradient is influenced by the applied current density, as has been suggested previously [31]. Further investigations should focus on the development of the internal concentration profile, and how this profile is influenced (e.g. by applied current density or osmosis). It is also unknown how reductions in membrane thickness affect the membrane resistance when the two solutions are unequal of concentration. If the absolute influence of the concentrate is the same (i.e. same 'penetration of high conductive solution') and the membrane thickness is much smaller, the concentration profile will be more 'linear-like' and the benefit of reducing the membrane thickness might be even larger than was discussed earlier this chapter (see paragraph 8.4).

In the present chapter, an entrance resistance for divalent cations was hypothesized. Further research is necessary on this topic. It could be that divalent cations need to 'loose' part of their hydration sphere before entering the membrane. This water dissociation requires energy (reversing the hydration energy), and forms the entrance resistance causing a higher 'apparent' membrane resistance. For sulphate ions dehydration involves about two times less energy than for magnesium ions [32]. The sulphate concentration is about twice lower than the magnesium concentration, so this could explain a higher energy consumption of the magnesium mixture compared to the sulphate mixture. On the membrane 'exit' the hydration sphere may be refilled, and energy is released as heat, which may be measured in the water temperature at the solution-membrane interface. Hydration enthalpy of Na^+ and Cl^- ions is very similar [32]. Membrane resistance measurements (see Chapter 6) were done in a six compartment stack at an applied AC current with a frequency of 1 kHz to avoid effects of CP. The correctness of this method was verified for the concentration range used in Chapter 6 (0.01-1.1 M). When resistance measurements without membrane are done, however, at higher or lower external solution concentrations, the results obtained through this method start to give deviation from the theoretical solution conductivity. Source of this error was not yet identified. The use of capillaries might make the method prone to errors, as exact positioning of these capillaries is difficult. Furthermore are the capillaries fragile, and flushing and changing solution in the capillaries is a time consuming process. In the six compartment stack are also 4 additional membranes present, through which the current has to be transported. This might affect the voltage response

to the current. Development of a more robust method that can be used in a broader concentration range would be interesting, as in literature many different approaches are described and there is not yet a satisfying standard method. An appealing method for investigation of the membrane conductance should be based on electrical impedance spectroscopy (EIS) [33, 34], which is already used by several researchers, as it can determine the membrane resistance in a broad frequency range.

As the membrane resistance is identified to be the one of the main factors determining the ED energy consumption it is justified to investigate the possibility to further enhance membrane conductance. Based on the results and discussion in Chapter 6, it is suggested that cross-linking induces spots with a concentration equal to the external concentration in the membrane. In these cross-linked spots or channels no fixed membrane charge is present at the walls. This leads to reduced selectivity and reduced membrane conductance. That cross-linking reduces the membrane conductance was also discussed in [29], where it is also mentioned that the membrane conductance increases with the increasing fixed charge density. Therefore an 'ideal membrane' would have cross-linking for stability, without local loss of fixed charge density. Very high fixed charge density throughout the membrane would lead to a very high counterion concentration, which induces a lot of ion-ion and ion-pore friction. To minimize friction, but still keep excellent selectivity, the membrane pore diameter should match the Debye length. This also implies that membranes are only 'perfect' at specific external concentration. Surface modification of membranes might lower the resistance for ions to enter the membrane and are therefore also an interesting direction to investigate.

So far this paragraph has discussed only future research for IEMs, as design of ED stacks was not in the focus of this work. Nevertheless, bulk resistance is shown to be very important, especially at lower bulk concentrations where it has large impact on the stack resistance. Engineering of flow channels is therefore very important, as reducing channel width, enhancing flow distribution, and increasing convective transport towards the membrane are very important with respect to reducing the overall stack resistance. Introducing turbulence promoters in the channel may therefore be an important engineering aspect of low resistant stacks.

8.7 Hybrid ED-BWRO versus SWRO: energy costs and brine treatment determine the winner

8.7.1 present situation

As discussed in this thesis, there are many factors influencing the overall real cost of a (hybrid) technology. In the work presented in this thesis the focus is mainly on understanding the processes and phenomena occurring in ED. From this understanding the system can be improved to lower the energy consumption and increase the process efficiency. At the end of the day, however, neither the energetic costs, nor the process sustainability, but the real costs (money) are determining the feasibility of the utilized technology. So, to return to the framework of this thesis, ED as pretreatment technology for seawater desalination succeeded by BRWO; *'how feasible is this approach?'* Would this hybrid technology be able to produce drinking water at a lower cost than stand-alone SWRO would do? In Chapter 2, it was shown that ED, from energetic perspective, can even be applied as a stand-alone technology. However, but as energy consumption (or membrane cost) of ED is high in the low salinity range and there is no physical barrier for uncharged particles, ED as stand-alone is not considered here. SWRO, has advanced from an energy consumption of about 15 kWh/m^3 in the 1970s to an energy consumption of already below 2.0 kWh/m^3 at present [35], with an minimum of ~1.5 kWh/m^3. Typical numbers from large scale plants are in the range of 2.2-3.0 kWh/m^3. The decrease in energy consumption in the past decades is due to better membranes and the application of energy recovery devices (ERD). Isobaric energy recovery devices can have an efficiency up to 97% [36], but can not be applied when the RO process contains several pressure stages (to increase pumping efficiency). Turbocharges, typically used in large scale SWRO plants as the ERD, operate at a maximum efficiency of ~81%, but in practical application this number is typically a bit lower (~75%). It is expected that developments in very high permeable membranes and more efficient ERDs leads to some additional energy savings, but that these will be marginal.

As mentioned in the introduction (Chapter 1), there are very highly permeable membranes in the developing stage (e.g. graphene or membranes with aquaporins), these membranes will, however, not lead to a substantial decrease of the energy consumption of the process. The membrane modules will still be operated at ~ 70 bars and the same amount of liquid is pumped through the system. However, the number of membrane modules can be decreased and as such will lead to decreasing footprint (referring to the plant size) and capital expenditures (capex). The new membranes are, however, likely to increase concentration polarization in the diffusion layer, leading to higher tendency for colloidal fouling (scaling) and biofouling. Therefore, it is likely that due

to a higher membrane price and higher maintenance costs per membrane module, the profit of highly permeable membranes is very limited.

Despite claims that mega scale SWRO plants are capable producing desalinated water at cost prices far below 1 $/m³ [37, 38], a typical number from the industry is currently 1.20 $/ m³ (4.55 $/kgal) [39], as also shown by the work of Ghaffour *et al.*[40]. (Note that all quoted costs here are in U.S. $.) For large SWRO facilities, costs can be roughly divided in, capex, energy costs, and operation and maintenance costs. The cost breakdown estimations show high variations [37, 39]: capex ≈ 14-60%, energy ≈ 26-52%, and operation and maintenance ≈ 15-33%. It was recognized that often the energy costs form the largest share at large scale facilities [37, 39] and that the operating expenses (opex: energy costs + operation and maintenance costs) are key factors determining the water costs of large scale facilities [40]. As the energy consumption of SWRO is very hard to reduce much further [35], it will be hard to achieve desalination costs below 1 $/m³. As indicated by [35, 41] the main improvement of seawater desalination using RO should not be achieved by enhancing the RO unit itself but should be realized by engineering the whole desalination process, where especially should be focused on the pretreatment and brine treatment steps.
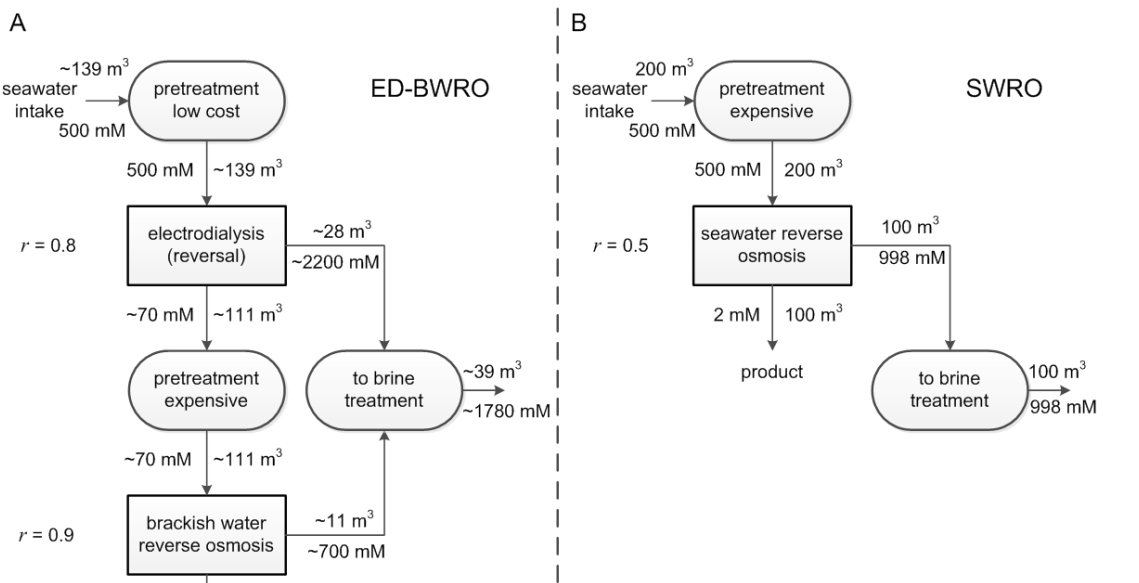

Figure 6. Schematic flow chart with volumes and concentrations of water streams in an ED-BWRO desalination process (A) and a SWRO desalination process (B), with r being the water recovery rate (-).

This total process approach is where the combination ED-BWRO would have an advantage over stand-alone SWRO. Figure 6 shows an estimation of the flow sizes in

an arbitrary 100 m³ (per certain time) producing desalination facility. In this scheme is assumed that no water is lost in the pretreatment and that the water quality of the product is similar for both processes. The water recovery rate (r, -) for the ED, BWRO, and SWRO are optimized in this scheme. The installation footprint of a hybrid system may be expected to be somewhat larger as two steps are required. However, the treated volume is ~30% less in scheme A and the footprint of individual ED and BWRO installations are usually quite smaller than SWRO installations, therefore, a similar footprint is considered for this evaluation.

8.7.2 Seawater intake

The large benefit of ED over pressure driven membranes makes it possible to achieve high water recovery. What directly comes forward from Figure 6 is that, due to this higher water recovery, the intake volume of an ED-BWRO is smaller than that of a stand-alone SWRO system. As intake water can be already for 15% responsible for the energy consumption, the first benefit of the hybrid system is made directly on the start.

Intake of seawater is mostly done with so called open intakes, located above the sea/ocean floor. Subsurface intakes, are located under the sea/ocean floor and water has to flow through wells or infiltration to the pipes, what usually limits the capacity, although large systems are present [42]. The location and design of the intake system determines the quality and quantity of the feed water and depends on the site conditions, technology options, permitting requirements, environmental impacts, stakeholder values, and utility constraints and interests [43-45]. A seawater intake facility may be expensive and can make up for 20% of the capex. However, a proper design of the intake system can decrease the opex of the desalination process by as much as 30% as the water quality increases [42]. Designing the seawater intake is, therefore, a trade-off between an increase of capex and reduction of the opex. Whether additional investment costs of an advanced intake system will or will not pay off is very case specific. Figure 6 shows that the required intake water is ~30% lower for scheme A than for scheme B, most likely this results in somewhat lower intake costs for A than B, but not the full 30%, because, e.g. construction of the intake system or installation and maintenance of intake pumps still needs to be done. Usually, the bigger the capacity of systems the lower are the costs per m³. Here it is assumed that the intake costs of system B are 10% lower per m³ water taken in. It assumed that the intake water costs are 0.05 \$/m³ feed water for scheme A and 0.045 \$/m³ feed water for scheme B. The total intake costs for producing 100 m³ fresh water are than in scheme A (139·0.05) ~ \$ 7.0, and in scheme B (200·0.05) ~ \$ 9.0. Which represents a saving of 0.02 \$/m³ of produced water of scheme A over B. An overview of the estimated costs of each step in the desalination process is shown in Table 1.

8.7.3 Pretreatment

The required pretreatment of the ED process is limited, a coarse filter is typically enough [3, 46] and therefore, the pretreatment cost can be low (~0.01 $/m³ [41]). However, more expensive pretreatment may be required with difficult feed waters, e.g. when iron and manganese are present [3, 47]. More extensive pretreatment is required for the pressure driven BWRO and SWRO process, as these membranes are sensitive to fouling and scaling [37, 48]. The pretreatment is therefore also expensive and for conventional pretreatment the costs of 0.07-0.14 $/m³ are reported [41, 49, 50]. For now, it can be assumed that the pretreatment cost for RO are ~0.10 $/m³ treated water. So, regarding Figure 6, this implies for scheme A total pretreatment costs of (139·0.01 + 111·0.10) ~12.5 $, and for scheme B (200·0.10) ~20.0 $. Which represents a saving of 0.075 $/m³ of produced water of scheme A over B.

8.7.4 Brine treatment

For most seawater desalination facilities it is common practice to discharge the concentrate back to the environment. These concentrate streams may have adverse effects on water and sediment quality, impair marine life and the functioning and intactness of coastal ecosystems [45, 51]. Concentrate streams do not only have a much higher salt concentration, also the temperature may be elevated (especially in distillation processes). Moreover, coagulants, a wide variety of cleaning, and anti-scaling/fouling/corrosion chemicals are present [45, 51-53]. Therefore, the concentrate is generally a mix of salt and pollutants, and their combination may have additive and adverse effects on marine life [45]. Therefore, it is very well possible that in the (near) future, discharge of concentrate streams back in the ocean will not be allowed anymore in many situations. Other options available for concentrate discharge are e.g. deep well injection, evaporation plants, mixing with waste water, and applying zero liquid discharge technologies (ZLD) [51, 53]. All methods have their limitations, costs, and impact on the environment, therefore ZLD is sometimes the only option left [54, 55]. In the ZLD process the concentrate stream is further treated and water and salts are produced. The water can be added to the product stream and salts (and nutrients) can be sold [51, 54, 56].

Typical options for handling concentrates are very energy intensive and expensive (0.40 - 1.78 $/m³ of brine [57]) . Therefore, there are two options in the desalination strategy; i) very low water recovery systems, where the brine has slightly increased salt concentrations compared to the feed water enabeling discharge without further treatment, or ii) very high water recovery systems, where the brine has a minimized volume enabling further processing towards ZLD. Option i), is not feasible as pretreatment and pumping costs would be too high and, cheap disposal of such 'mild concen-

trates' might not even be possible without treatment when it contains chemicals from the desalination industry. Furthermore, is the environmental impact likely to be increased when, a larger intake volume is required. For cases where no cheap treatment solutions can be developed to remove desalination associated organic chemicals from mild concentrates, option ii) will become the only alternative. From that perspective the ED-BWRO scheme shown in Figure 6 may be more attractive than the SWRO as the produced concentrate stream is reduced by ~60%.

Costs of brine handling are very case specific [51] and for that reason putting a number to this is very difficult. In any case, it can be assumed that in the future a substantial part of the desalination costs is due to concentrate handling. ZLD is an energy intensive process, but it might be the only truly sustainable solution for concentrate treatment on the long term [51]. Produced salts may add value, especially when individual salts can be recovered separately, which may reduce the ZLD costs. If schemes A and B from Figure 6 are considered, it is evident that, given the same situation, the brine handling cost for scheme B will be substantially higher than for scheme A. The amount of chemicals in the brine can also negatively influence the brine disposal costs, the amount of chemicals used in scheme A, is expected to be lower than in scheme B [3, 58]. An estimation of the costs of brine disposal is very difficult, here only the difference in costs is considered. It will be on the safe side to assume additional cost of 0.20 $/m³ produced water of scheme B compared to scheme A, but likely these costs will be higher.

8.7.5 Labor and chemicals

In the previous three sections it was assumed that scheme A will lead to cost reduction of the seawater intake, pretreatment, and brine treatment compared to scheme B (Figure 6). A difference in production costs of (0.02 + 0.075 + 0.20, see Table 1) ~0.30 $/m³ is at least expected. Cleaning chemical use will be somewhat higher in scheme B but it is roughly estimated that it will cancel out with the manual cleaning costs that may be more pronounced in scheme A. Labor costs can be somewhat higher for scheme A, but are typically < 5% [55], and as such will be of minor importance. For this case the labor and chemical costs are estimated to be 0.05 $/m³ for both schemes.

8.7.6 BWRO versus SWRO

As shown by [37, 38] the BWRO process is estimated as about 2-4 times cheaper as the SWRO process. In agreement to that in [41] the cost for the BWRO process, without energy consumption is estimated as ~0.125 $/m³ (0.10 €/m³) and the cost for the SWRO, without energy consumption is estimated as ~0.250 $/m³ (0.20 €/m³). Note that these cost estimation fit to optimized systems.

Energy consumption of an optimized SWRO system (50% recovery) is estimated as ~1.5 kWh/m³ (practical minimum), assuming an energy price of 0.1 $/kWh, this results in an RO energy cost of 0.15 $/m³ produced water. For the desalination is assumed that the salt rejection is 99.8%, what implies that the permeate has an ion concentration of ~2 mM (feed water 500 mM NaCl). The theoretical minimum energy requirement (see Chapter 2, eq. 1-3) for this is process is 0.934 kWh/m³ ($r = 0.5$, $T = 298$ K, $c_{feed} = 0.5$ M, $c_{product} = 2$ mM), which is only ~1.6 times less energy than the estimated practical minimum.

The maximum pressure applied on BWRO membrane is ~41.4 bar (600 psi) [59, 60]. In [41] was estimated that the irreversible losses of a BWRO were about 6 bar, this implies that that 35.4 bar pressure can be used usefully. When the salt rejection of the BWRO membrane is assumed to be 99.0% [59], slightly lower as SWRO membranes, and the maximum osmotic pressure drop is taken as 35 bar, the maximum concentrate concentration can be approximated by:

$$\Delta\Pi = \Pi_c - \Pi_d = 2RT(c_c - c_d) \cdot 10^{-5} \leq 35 \qquad \text{eq. 1}$$

Where Π is the osmotic pressure (bar), R is the gas constant (J/mol·K), T is the temperature (K), and c the concentration (mol/m³) of respectively the concentrate and diluate (or permeate). When the concentration of the product is as a first step taken as 2 mM, the maximum concentrate concentration is calculated as 708 mM. When in addition is assumed that $c_{c,\,BWRO} \approx 700$ mM and a water recovery of 90% is taken into account, the BWRO feed water concentration, $c_{feed,\,BWRO}$, is calculated as ~70 mM and the product water concentration $c_{product} \approx 0.8$ mM ($\Delta\Pi \approx 34.6$ bar). So the product water will have, an approximately 2.5 times, lower salt concentration than the SWRO product.

The minimum required energy for the described BWRO process is 0.238 kWh/m³ ($r = 0.9$, $T = 298$ K, $c_{feed} = 70$ mM, $c_{product} = 0.8$ mM). If it is estimated that, like in SWRO, the practical minimum energy requirement is 1.6 times larger, this results in a practical energy consumption of an optimized BWRO installation of ~0.38 kWh/m³. The energy cost in the BWRO system is estimated to be 0.04 $/kWh.

Table 1, shows that the BWRO costs are (0.125 + 0.04) ~0.17 $/m³ and that the SWRO costs are (0.250 + 0.15) ~ 0.40 $/m³. Together with the estimated costs from the seawater intake, pretreatment, and brine treatment step, the costs of scheme A without ED are so far 0.41 $/m³. The total estimated costs of scheme B are 0.94 $/m³. This implies that the ED step should not exceed 0.53 $/m³ in order to make ED-BWRO competitive

to SWRO. In the following section the attainability of desalination with ED, and with this 0.53 \$/m³ in mind, is discussed.

Table 1. Estimated costs of an electrodialysis – brackish water reverse osmosis scheme and a seawater reverse osmosis scheme (SWRO). The costs of brine treatment are indicated by '?' which depends on the brine stream concentration and volume.

Process step	ED-BWRO ($/m^3$)	SWRO ($/m^3$)
intake	0.07	0.09
pretreatment	0.125	0.20
brine treatment	? (c, V)	0.20+? (c, V)
labor, chemicals	0.05	0.05
equipment	0.125 + ED	0.250
energy	0.04 + ED	0.15
Total	*0.41+ED+?*	*0.94+?*

8.7.7 Electrodialysis

As mentioned in Chapter 1, ED costs are predominantly determined by the energy and membrane costs. At low applied current density, irreversible losses in the stack are low (Chapter 2), but required membrane area is high. At present state IEMs are still relatively expensive, that is why ED is operated close to limiting current density and thus energy consumption is high. However, with the application of IEMs in e.g. fuel cells technology and RED there is an increased interest in the development of high quality (i.e. high selectivity, low resistance, high mechanical strength etc.) membranes for a low price. Now heterogeneous membranes are available for < 5 \$/m² [61], but homogenous, low resistance, IEMs are still expensive and the current price is about the tenfold so ~ 50 \$/m². However, it is expected that with further developments of membranes and the membrane production process this price can be decreased to < 5 \$/m² as well. When taking into account the longer expected membrane lifetime of these membranes, compared to pressure membranes, this may result in quite lower equipment and membrane costs than for the SWRO installation. Additional costs like pumping and maintenance are currently of less importance in ED, but may gain importance [62, 63] when membrane prices are low and ED can be utilized at low applied current density (i.e. < 50 A/m²).

In the theoretical case sketched in this paragraph, in the ED predesalination process, the salt content should be lowered from 500 to 70 mM. The minimum required desalination energy for this process is 0.949 kWh/m³ (r = 0.8, T = 298 K, c_{feed} = 500 mM,

c_{product} = 70 mM). In practice ED is often operated in stages, in order to operate at low energy consumption (as it minimizes irreversible losses and allows operation close to LCD conditions at all time). For this case presence of multiple stages, high quality membranes and relatively low irreversible losses can be assumed. These assumptions should lead to a fair comparison as for both SWRO and BWRO, membranes, equipment, and process were assumed to be optimized. In Chapter 2 (Figure 9), is shown that with such high quality membranes, desalination of a 500 mM NaCl solution is possible at energy consumptions of ~ 2 - 6 times the minimum required energy, depending on the applied current density (10-100 A/m²). It can be reasonably assumed that desalination at an applied current density in the order of $50 - 100$ A/m² is feasible with low-cost membranes. This current range is presently only used for brackish water desalination with ED [63, 64].

In case there would be only one ED stage present for the desalination and the applied current density would be 100 A/m², the system energy consumption for desalination of a 500 mM NaCl solution with a product concentration of 70 mM would approximately cost (~6·0.949) 5.7 kWh/m³. But this factor 6, from Figure 9 in Chapter 2, is based on lab scale application and electrode losses (marginal for large scale) and pumping energy are not included in this number. Also no effect of divalent ions is included, but on the other hand the stack has a far from optimized flow design. Assuming that in a 'worst case' the ED process energy consumption is another 25% higher, this leads to an energy consumption of ~7.1 kWh/m³. This would imply a total energy cost of 0.71 $/m³.

As a second approach, an 'optimized' ED stack with multiple stages is considered. On basis of Figure 9 in Chapter 2, it is estimated that the desalination energy can be lowered to at least ~3 times the minimum thermodynamic energy which is (3·0.949) 2.85 kWh/m³, again a 25% safety margin can be assumed, resulting in an energy consumption of 3.6 kWh/m³, and a cost of 0.36 $/m³.

Considering systems with lower energy consumption does not seem realistic as water transport would limit the water recovery of the system and an 80% water recovery would most likely not be achieved. Therefore, for ED it is estimated that the energy cost are somewhere between 0.36-0.71 kWh/m³. The estimated 'available money' for ED `was 0.53 $/m³. The ED stacks may than have a material cost of (0.53 – 0.36) 0.17 $/m³ at best. According to Post *et al.* [41] the ED predesalination step, without energy costs, is ~0.18 $/m³ (0.14 €/m³). This implies that for the calculated cases scheme A is at best about as expensive as scheme B.

8.7.8 Perspective ED-BWRO

The in paragraph 8.7 discussed costs were shown in Table 1. Without any brine treatment costs, what can be approximated by discharge of brine into the sea, the estimated costs of an stand-alone SWRO are 0.74 $/m^3, what is comparable to cheap, large scale, state of the art SWRO plants [37, 38].

What comes forward from the previous section in this paragraph is that the energy costs of the ED-BWRO system are relatively high. These 'high' energy costs mainly stem from the ED process and effectively cancel out the benefits the hybrid approach has over SWRO due to its high water recovery. This high energy consumption is partly due to higher reversible energy losses in the ED-BWRO system compared to the SWRO system (1.19 and 0.93 kWh/m^3), but also due to higher irreversible losses of ED compared to SWRO. Other interesting costs are related to the brine / concentrate stream handling. These costs depend very much on the local situation and will also depend on the volume and concentration of the brine stream. Also the amount of chemicals in the brine stream may influence these costs. As discussed in the section 'brine treatment', the requirement of brine treatment will be increased in the (near) future and the price for brine treatment may press heavily on the total desalination costs. The brine treatment costs may even become larger than the total costs of the other steps in the desalination process together.

For now can be concluded that, at the present state of the art, SWRO is a cheaper technology than ED-BWRO for seawater desalination. When ED will become more developed for seawater desalination, the total cost of desalination with ED-BWRO may become very competitive. However, when advanced treatment of the brine stream is required, the ED-BWRO scheme will become more attractive. Increased demands for brine treatment will negatively affect the seawater desalination costs, and as such a large decrease in seawater desalination costs is not to be expected, even with further development of technologies.

8.8 Literature

[1] C. Fritzmann, J. Löwenberg, T. Wintgens, T. Melin, State-of-the-art of reverse osmosis desalination, Desalination, 216 (2007) 1-76.
[2] B. Peñate, L. García-Rodríguez, Current trends and future prospects in the design of seawater reverse osmosis desalination technology, Desalination, 284 (2012) 1-8.
[3] AmericanWaterWorksAssociation, Electrodialysis and Electrodialysis Reversal, manual of water supply practices M38, AWWA, Denver USA, 1999.
[4] V.D. Grebenyuk, O.V. Grebenyuk, Electrodialysis: From an Idea to Realization, Russian Journal of Electrochemistry, 38 (2002) 806-809.
[5] T. Kawai, Y.M. Lee, K. Nakajima, K. Ehara, Hydration of ions in aqueous electrolyte solutions studied by differential thermal analysis at low temperatures, Journal of Electroanalytical Chemistry, 422 (1997) 133-138.
[6] J.F. Hinton, E.S. Amis, Solvation numbers of ions, Chemical Reviews, 71 (1971) 627-674.
[7] E. Amis, Solvent Effects on Chemical Phenomena, Elsevier, 2012.
[8] M. Turek, Cost effective electrodialytic seawater desalination, Desalination, 153 (2003) 371-376.
[9] Y. Kim, W.S. Walker, D.F. Lawler, Electrodialysis with spacers: Effects of variation and correlation of boundary layer thickness, Desalination, 274 (2011) 54-63.
[10] M. Law, T. Wen, G.S. Solf, Thickness and concentration profile of the boundary layer in electrodialysis, Desalination, 109 (1997) 95-103.
[11] V.A. Shaposhnik, V.I. Vasil'eva, O.V. Grigorchuk, Diffusion boundary layers during electrodialysis, Russian Journal of Electrochemistry, 42 (2006) 1202-1207.
[12] C. Larchet, S. Nouri, B. Auclair, L. Dammak, V. Nikonenko, Application of chronopotentiometry to determine the thickness of diffusion layer adjacent to an ion-exchange membrane under natural convection, Advances in Colloid and Interface Science, 139 (2008) 45-61.
[13] A. Kozmai, V. Nikonenko, N. Pismenskaya, S. Mareev, E. Belova, P. Sistat, Use of electrochemical impedance spectroscopy for determining the diffusion layer thickness at the surface of ion-exchange membranes, Petroleum Chemistry, 52 (2012) 614-624.
[14] S. Pawlowski, P. Sistat, J.G. Crespo, S. Velizarov, Mass transfer in reverse electrodialysis: Flow entrance effects and diffusion boundary layer thickness, Journal of Membrane Science, 471 (2014) 72-83.
[15] A.H. Galama, G. Daubaras, O.S. Burheim, H.H.M. Rijnaarts, J.W. Post, Seawater electrodialysis with preferential removal of divalent ions, Journal of Membrane Science, 452 (2014) 219-228.
[16] V.I. Zabolotsky, J.A. Manzanares, V.V. Nikonenko, K.A. Lebedev, E.G. Lovtsov, Space charge effect on competitive ion transport through ion-exchange membranes, Desalination, 147 (2002) 387-392.
[17] M.A.-K. Urtenov, E.V. Kirillova, N.M. Seidova, V.V. Nikonenko, Decoupling of the Nernst-Planck and Poisson equations. Application to a membrane system at overlimiting currents, The Journal of Physical Chemistry B, 111 (2007) 14208-14222.
[18] V. Geraldes, M.D. Afonso, Limiting current density in the electrodialysis of multi-ionic solutions, Journal of Membrane Science, 360 (2010) 499-508.
[19] E. Glueckauf, A New Approach to Ion Exchange Polymers Proceedings of the Royal Society A, 268 (1962) 350-370.
[20] S. Mafé, P. Ramírez, J. Manzanares, Activity coefficients and coion exclusion in charged polymeric membranes with macroscopic inhomogeneities, Colloid and Polymer Science, 275 (1997) 599-603.
[21] S. Mafé, P. Ramírez, J. Pellicer, Activity coefficients and Donnan coion exclusion in charged membranes with weak-acid fixed charge groups, Journal of Membrane Science, 138 (1998) 269-277.
[22] CRC Handbook of Chemistry and Physics, 85th ed., Boca Raton (Florida, U.S.A.), 2004.
[23] J.A. Rard, D.G. Miller, The mutual diffusion coefficients of NaCl-H2O and CaCl2-H2O at 25°C from Rayleigh interferometry, Journal of Solution Chemistry, 8 (1979) 701-716.
[24] P. Długołęcki, P. Ogonowski, S.J. Metz, M. Saakes, K. Nijmeijer, M. Wessling, On the resistances of membrane, diffusion boundary layer and double layer in ion exchange membrane transport, Journal of Membrane Science, 349 (2010) 369-379.
[25] OLI_systems_Inc., OLIAnalyzer 3.1, in, Cedar Knolls, New Jersey (U.S.A.), 2010.
[26] D. Vermaas, M. Saakes, K. Nijmeijer, Power generation using profiled membranes in reverse electrodialysis, Journal of Membrane Science, 385-386 (2011) 234-242.
[27] D.A. Vermaas, M. Saakes, K. Nijmeijer, Doubled Power Density from Salinity Gradients at Reduced Intermembrane Distance, Environmental Science and Technology, 45 (2011) 7089-7095.

[28] J. Veerman, M. Saakes, S.J. Metz, G.J. Harmsen, Reverse electrodialysis: A validated process model for design and optimization, Chemical Engineering Journal, 166 (2011) 256-268.

[29] F.G. Helfferich, Ion Exchange, McGraw-Hill, New York, (1962).

[30] T. Sata, Ion Exchange Membranes; Preparation, Characterization, Modification and Application, The Royal Society of Chemistry, Cambridge UK, 2004.

[31] A. Moya, Electrochemical impedance of ion-exchange membranes in asymmetric arrangements, Journal of Electroanalytical Chemistry, 660 (2011) 153-162.

[32] D.W. Smith, Ionic hydration enthalpies, Journal of Chemical Education, 54 (1977) 540.

[33] E. Barsoukov, J. Ross Macdonald, Impedance Spectroscopy Theory, Experimental, and Applications, 2nd ed., Wiley-Interscience, New Jersey (U.S.A.), 2005.

[34] V.F. Lvovich, Impedance Spectroscopy, Applications to Elechtrochemical and Dielectric Phenomena, first ed., Wiley, Hoboken, New Jersey (U.S.A.), 2012.

[35] M. Elimelech, W.A. Phillip, The future of seawater desalination: energy, technology, and the environment, Science, 333 (2011) 712-717.

[36] R.L. Stover, Seawater reverse osmosis with isobaric energy recovery devices, Desalination, 203 (2007) 168-175.

[37] L.F. Greenlee, D.F. Lawler, B.D. Freeman, B. Marrot, P. Moulin, Reverse osmosis desalination: Water sources, technology, and today's challenges, Water Research, 43 (2009) 2317-2348.

[38] I.C. Karagiannis, P.G. Soldatos, Water desalination cost literature: review and assessment, Desalination, 223 (2008) 448-456.

[39] R.L. Stover, A Primer on Reverse Osmosis Technology, CHEMICAL ENGINEERING, 121 (2014) 38-44.

[40] N. Ghaffour, T.M. Missimer, G.L. Amy, Technical review and evaluation of the economics of water desalination: Current and future challenges for better water supply sustainability, Desalination, 309 (2013) 197-207.

[41] J.W. Post, H. Huiting, E.R. Cornelissen, H.V.M. Hamelers, Pre-desalination with electro-membranes for SWRO, Desalination and Water Treatment, 31 (2011) 296-304.

[42] T.M. Missimer, N. Ghaffour, A.H. Dehwah, R. Rachman, R.G. Maliva, G. Amy, Subsurface intakes for seawater reverse osmosis facilities: Capacity limitation, water quality improvement, and economics, Desalination, 322 (2013) 37-51.

[43] E.D. Mackey, N. Pozos, W. James, T. Seacord, H. Hunt, D.L. Mayer, Water Research Foundation, in: Assesing Seawater Intake Systems for Desalination plants, Denver, Colorado (U.S.A.), 2011.

[44] T. Pankratz, An overview of seawater intake facilities for seawater desalination, The Future of Desalination in Texas, 2 (2004).

[45] S. Lattemann, T. Höpner, Environmental impact and impact assessment of seawater desalination, Desalination, 220 (2008) 1-15.

[46] B. Pilat, Practice of water desalination by electrodialysis, Desalination, 139 (2001) 385-392.

[47] H. Strathmann, Electrodialysis, a mature technology with a multitude of new applications, Desalination, 264 (2010) 268-288.

[48] N. Voutchkov, Considerations for selection of seawater filtration pretreatment system, Desalination, 261 (2010) 354-364.

[49] P. Glueckstern, M. Priel, Comparative cost of UF vs conventional pretreatment for SWRO systems, International Desalination and Water Reuse Quarterly, 13 (2003) 34-39.

[50] F. Knops, S. van Hoof, H. Futselaar, L. Broens, Economic evaluation of a new ultrafiltration membrane for pretreatment of seawater reverse osmosis, Desalination, 203 (2007) 300-306.

[51] S.J. Khan, D. Murchland, M. Rhodes, T.D. Waite, Management of concentrated waste streams from high-pressure membrane water treatment systems, Critical reviews in environmental science and technology, 39 (2009) 367-415.

[52] T. Mezher, H. Fath, Z. Abbas, A. Khaled, Techno-economic assessment and environmental impacts of desalination technologies, Desalination, 266 (2011) 263-273.

[53] T. Younos, Environmental issues of desalination, Journal of Contemporary Water Research & Education, 132 (2005) 11-18.

[54] A. Neilly, V. Jegatheesan, L. Shu, Evaluating the potential for zero discharge from reverse osmosis desalination using integrated processes–A review, Desalination and Water Treatment, 11 (2009) 58-65.

[55] H. Cooley, P.H. Gleick, G. Wolff, Desalination: with a Grain of Salt, in, Pacific Institute, Oakland, California, 2006.

[56] M. Turek, Dual-purpose desalination-salt production electrodialysis, Desalination, 153 (2003) 377-381.

[57] B.C. McCool, A. Rahardianto, J.I. Faria, Y. Cohen, Evaluation of chemically-enhanced seeded precipitation of RO concentrate for high recovery desalting of high salinity brackish water, Desalination, 317 (2013) 116-126.

[58] E.R. Reahl, Half a century of desalination with electrodialysis, GE Water & Process Technologies, General Electric Company, (2006).

[59] Hydranautics, Brackish water RO membranes, in: http://www.membranes.com/pdf/HYDRABrochure.pdf, Oceanside, CA (U.S.A), 2014.

[60] Dow, Tech Manual Excerpt, Filmtech membranes, Form No. 609-02008-504, in: http://msds-search.dow.com/PublishedLiteratureDOWCOM/dh_0071/0901b803800710df.pdf?filepath=liquidseps/pdfs/noreg/609-02008.pdf&fromPage=GetDoc, Midland, MI (U.S.A), 2014.

[61] E. Guler, Y. Zhang, M. Saakes, K. Nijmeijer, Tailor Made Anion Exchange Membranes for Salinity Gradient Power Generation Using Reverse Electrodialysis, ChemSusChem, 5 (2012) 2262-2270.

[62] H. Strathmann, Assessment of electrodialysis water desalination process costs, in: Proceedings of the International Conference on Desalination Costing, Limassol, Cyprus, 2004, pp. 32-54.

[63] E.-Y. Choi, J.-H. Choi, S.-H. Moon, An electrodialysis model for determination of the optimal current density, Desalination, 153 (2003) 399-404.

[64] J. Ortiz, J. Sotoca, E. Exposito, F. Gallud, V. Garcia-Garcia, V. Montiel, A. Aldaz, Brackish water desalination by electrodialysis: batch recirculation operation modeling, Journal of Membrane Science, 252 (2005) 65-75.

Appendix A

In this appendix additional data of the model presented in Figure 3 is provided. In Table A 1 the size of the constants in the model are given in the bottom row. Where N, is the number of calculation planes in the stagnant diffusion layer (SDL), δ is the thickness of the SDL or channel, A_{eff} is the effective stack area (here is assumed 74%), a and b are constants used to the calculate the membrane resistance according to equation 11 and 13 in Chapter 6. The bulk resistances, R_{bulk} are constant for the situation of a bulk NaCl concentration 0.5 M or 0.1 M, and therefor also indicated in the bottom row. The table is split in two main columns, with each 4 sub columns. The first column indicates the input and results for a bulk concentration of 0.5 M, the second column indicates the input and results for a bulk concentration of 0.1 M.

Table A 1. Solution-membrane interface concentration (c_{int}), and the used n value for Equation 13 from Chapter 6, and calculated resistance of the membrane (R_M) and the stagnant diffusion layer (R_{SDL}).

c_{bulk} = 0.5 M				c_{bulk} = 0.1 M			
c_{int} (M)	n (-)	R_M (Ω cm^2)	R_{SDL} (Ω cm^2)	c_{int} (M)	n (-)	R_M (Ω cm^2)	R_{SDL} (Ω cm^2)
0.5	1	3.30	0.145	0.1	1.42	5.78	0.648
0.4	1	3.37	0.160	0.085	8.2	6.26	0.699
0.3	1	3.46	0.182	0.07	15	7	0.762
0.2	1.2	3.66	0.214	0.055	21.9	8.15	0.844
0.1	1.42	4.11	0.275	0.04	28.7	10.16	0.960
0.075	12.8	6.23	0.301	0.03	33.2	12.59	1.070
0.05	24.1	8.28	0.339	0.02	37.8	17.44	1.232
0.01	42.3	30.71	0.465	0.01	42.3	31.83	1.519

$N = 10$; $\delta_{SDL} = 50 \cdot 10^{-6}$, $\delta_{channel} = 800 \cdot 10^{-6}$ m; $A_{eff} = 0.347$ m^2; $a = 2.674$, $b = 0.311$; $R_{bulk\ 0.5} = 2.31$, $R_{bulk\ 0.1} = 9.73\ \Omega$ cm^2

Figure A 1 shows the relative size of the SDL and the membrane resistance when the bulk resistance is neglected for a 0.5 M (A) or 0.1 M (B) NaCl solution. In these figures R_M is represented by the shaded area under the blue curve, while R_{SDL} is represented as the unfilled area between the two curves. For both modeled situations, R_M is by far the largest resistance, and R_{SDL} has only a marginal influence.

Figure A 2, shows the effect of concentration polarization on the relative importance of the R_M, R_{SDL}, and $R_{membrane}$ on the total resistance when the c_{bulk} = 0.5M (A), or the c_{bulk} = 0.1M (B). In this figure, the membrane, SDL and bulk thickness are reduced (δ_M = 25 μm, δ_{SDL} = 25 μm, δ_{bulk} = 200 μm). Compared to the earlier calculations (shown in Figure 4), the influence of R_M is somewhat lowered, which is expected as the membrane

thickness is lowered relatively more than the SDL thickness and channel width. R_{SDL} forms maximally 11.3% (A) or 11.7% (B) of the total resistance.
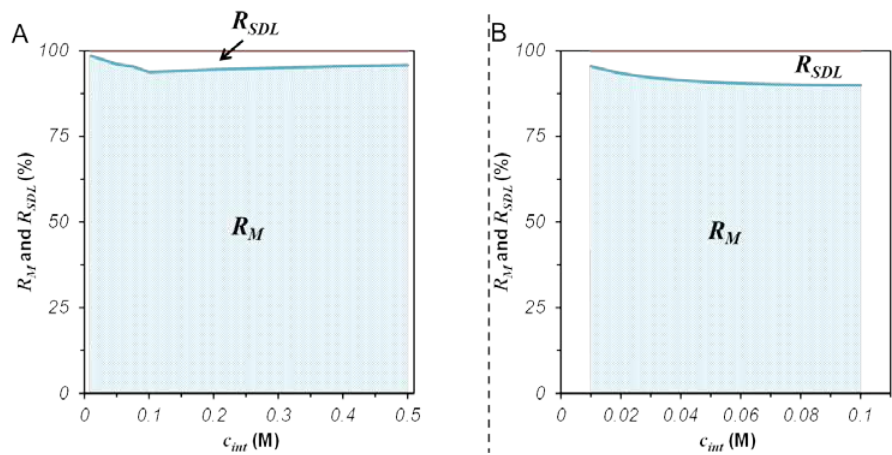

Figure A 1. Relative influence of the membrane resistance (R_M) compared to the stagnant diffusion layer resistance (R_{SDL}) as a function of the solution-membrane interface concentration when; A) the bulk solution concentration is 0.5 M NaCl and B) the bulk solution concentration is 0.1 M NaCl. Other parameters as defined as in Table A 1.
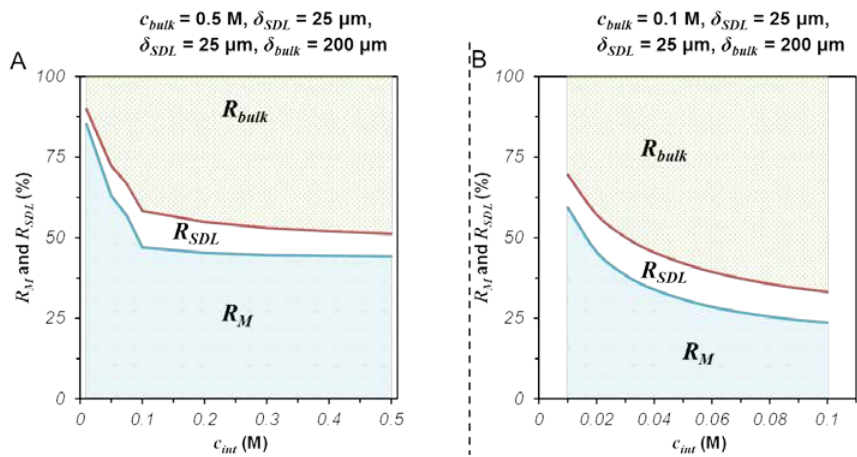

Figure A 2. Relative influence of the membrane resistance (R_M), stagnant diffusion layer resistance (R_{SDL}), and resistance of the flow channel (R_{bulk}) on the total stack resistance as a function of the solution-membrane interface concentration c_{int}. Where $c_{bulk} = 0.5$ M (A) / 0.1 M (B) and, $\delta_{SDL} = 25$ μm, $\delta_{SDL} = 25$ μm, $\delta_{bulk} = 200$ μm (A&B).
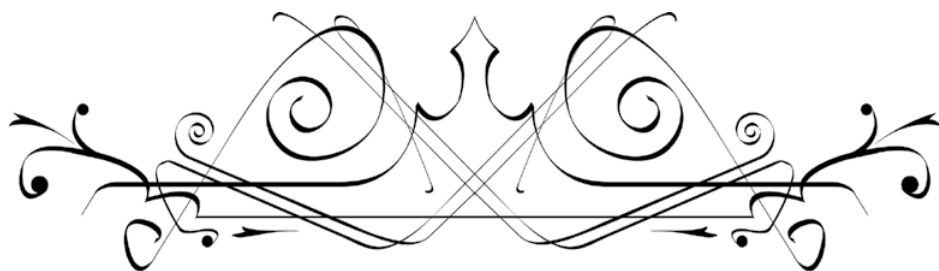
Appendix B

This appendix shortly describes an experiment for the investigation of the effect of divalent ions on the energy consumption of an electrodialysis (ED) stack. For this work a stack as described in Chapter 3, but with 14 membrane pairs was used. ED experiments were done with solutions that contained 0.63 C/l of charge. The composition of the used solutions is given by Table B 1. The binary solution contained only NaCl, the seawater solution contained ions in the concentration ratios as present in seawater (as given in Chapter 3). The ternary cation mixture contained besides NaCl only $MgCl_2$, as this divalent cation is the most present in seawater. The ternary anion mixture contained NaCl and Na_2SO_4. All experiments were performed at least 3 times and the results were repeatable. The experiments were performed at a temperature of 23°C (± 1 °C) and according to the methodology described in Chapter 3. Deviations of that method were that the applied current density was 20 and 100 A/m² and that no samples were taken.

Table B 1. Composition of the salt solutions used in the electrodialysis experiments

Salt	Binary (M)	Ternary Cat (M)	Ternary An (M)	Seawater (M)
NaCl	0.6312	0.5152	0.5729	0.4267
KCl	-	-	-	0.01074
$MgCl_2$	-	0.0580	-	0.0580
$CaCl_2$	-	-	-	0.00974
Na_2SO_4	-	-	0.02915	0.02915
Total charge	*0.6312*	*0.6312*	*0.6312*	*0.6312*
$\sigma_{solution}$ **(mS/cm)**	*57.05*	*55.54*	*54.81*	*53.23*

The solution conductivity, $\sigma_{solution}$ (mS/cm), was calculated for the defined mixture with the OLI analyzer 3.1 software [25]. The amount of charge that is applied to the system, $Q_{applied}$ (mol) was calculated according to:

$$Q_{applied} = \frac{\int_0^t I dt}{F \cdot N}$$

eq. B1

Summary

Ion exchange membranes in seawater applications

Processes and characteristics

Water is not a scarce resource as about 71% of the earth surface is covered with it. Fresh and drinkable water, however, may be scarce as sources are unequally distributed, are polluted, or are just not large enough to sustain the growing human population. Seawater desalination allows humans to tap from an apparently infinite water source. To make water really available, it should also be produced at low costs. Electrodialysis (ED) is a desalination technology that has potential to lower the costs of seawater desalination. In ED salt ions are transported through selective ion exchange membranes (IEMs) under the influence of an electric field. From saline feed water, a desalted stream (diluate) and a concentrated stream (concentrate / brine) are produced. ED is mainly used for brackish water desalination, but also used for further concentration of brine solutions, where utilization of pressure driven technologies are limited by the osmotic pressure and scaling. With ED higher water recovery can be achieved than with pressure driven seawater desalination technology and less pretreatment efforts are required as only salt (and a tiny fraction of water) are transported through the membrane. These benefits make ED attractive for application in seawater, although at the present state of art seawater ED cannot compete with seawater reverse osmosis (SWRO) due to large irreversible energy losses. A hybrid system of ED and brackish water reverse osmosis (ED-BWRO) is presented as an alternative for SWRO.

In **Chapter 2** reversible and irreversible energy losses in seawater desalination with ED are identified and quantified. It is shown how these losses are influenced by the applied current density. At very low applied current densities (~10 A/m^2), current efficiency and osmotic water transport are responsible for about 50% of the energetic losses. At higher applied current densities (>50 A/m^2), these losses cause less than 20% of the total energy loss. In all cases the internal resistance of the membrane stack is identified to be responsible for the largest energy loss. At applied current densities lower than 50 A/m^2, stand-alone ED can desalinate seawater at lower energy costs than RO.

Seawater contains besides the monovalent sodium, potassium, and chloride ions also considerable amounts of the divalent magnesium, calcium, and sulphate ions. These divalent ions may cause scaling, which limits the water recovery of BWRO systems. In **Chapter 3** the effect of the applied current density (10-300 A/m^2) on the composition of the diluate, which forms the feed water of the subsequent BWRO unit, is shown. At lower applied current densities a diluate stream with a lower amount of divalent ions relative to monovalent ions is produced, therefore, scaling potential is decreased. This influence of the applied current density is related to concentration polarization effects that occur in the stagnant diffusion layer (SDL) on the solution-membrane interface. The results are explained with a model based on the Nernst-Planck flux equation. Lower initial concentration of divalent ions compared to monovalent ions in seawater

lead to stronger depletion of these divalent ions in the SDL, especially at higher applied current densities, and as such the amount of divalent ions transported through the membrane decreases.

In **Chapter 4** a fractioning electrodialysis stack is presented and the proof of principle is given. By placing alternatingly monovalent selective IEMs and standard IEMs, which are exclusivly cation or anion selective, divalent and monovalent ions can be fractionated. Instead of a diluate and a concentrate stream now a stream with a low concentration of divalent ions and a stream with a high concentration of divalent ions are produced. Reversible losses in such a system are low as no actual desalination takes place. It is shown that ~90% of the divalent cations can be fractionated and ~60% of the anions from a typical seawater. At higher applied current densities, a higher extent of fractionation can be reached. Low coulombic efficiency of the seawater anion/cation fractioning stack leads to large volumetric energy consumption.

The principle of ED is based on selectivity of the IEMs, which stems from the charged groups that are fixed on to the polymer backbones of the membranes. These fixed charges play a role in the Donnan equilibrium, which describes that the electrochemical potential of each phase present in the electrochemical system is equal. To describe Donnan equilibrium, the simplest approach uses the classical Boltzmann equation, based on a mean-field description of ions as ideal point charges, in combination with the assumption of fully overlapping electrical double layers in the membrane pores. In **Chapter 5** the validity of this approach is tested by measurement of the counterion and co-ion concentration in densely charged membranes, after equilibration with various NaCl solutions (0.01-3 M). To obtain a good fit of data it was found necessary to express the membrane charge and ion concentrations per volume of aqueous solution phase in the membrane, and to include a small energetic term in the Boltzmann relation. A discrepancy between theory and experimental data is found at lower external NaCl concentrations. Similar deviations from the Donnan model are noted and reported for over half a century, but do not yet have a convincing explanation. Fairly well agreement of experiment data and theory at lower external NaCl concentrations is obtained when H^+ and OH^- ions as well as a postulated tiny amount of fixed groups with a charge opposite to overall fixed membrane charge, are taken into account in the model.
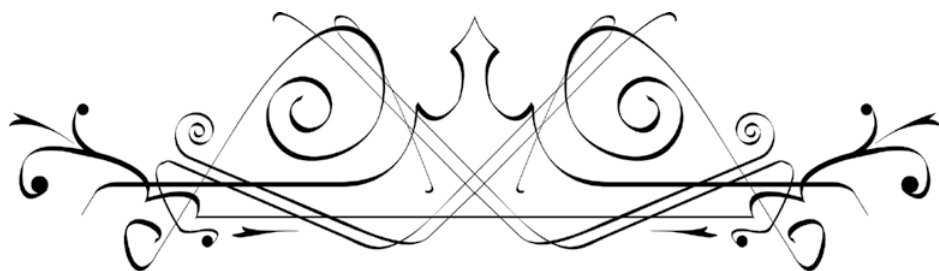
The amount of ions in the membrane phase is very determining for the ionic membrane resistance. In **Chapter 6** it is shown for the first time how resistance of an ion exchange membrane is influenced by the external salt concentrations, when these external salt concentrations are different (i.e. a concentration gradient is present). The NaCl solution concentrations are varied from 0.01-1.1 M. The results show that the

IEM resistance is mainly determined by the lowest external solution concentration. The membrane resistance can be considered as consisting from two resistors in series i.e. a gel phase (concentration independent) and an ionic solution phase (concentration dependent). The membrane conductivity is limited by the conductivity of the ionic solution when the external concentration is below 0.3 M. At higher concentrations the conductivity of the gel phase is limiting the membrane conductance. With a model based on this two parameter assumption a good approximation of the experimentally determined membrane resistance is obtained.

Membrane resistance is important in determining the irreversible losses in the stack. When stack resistances are further reduced, the reversible losses gain in importance. **Chapter 7** is about the (reversible) membrane potential (ϕ_m), which arises over an IEM when it is used to separate two solutions of different salt concentration, even without applied current. The focus of this chapter is on the origin of this potential and on the widely applied Teorell-Meyer-Sievers (TMS) theory. Deviations between theory and experiments are observed, especially at larger salt concentration differences across the membrane. At a certain salt concentration ratio, a maximum in ϕ_m is found, not predicted by the TMS theory. Before the maximum, the TMS theory can be used as a good estimate of ϕ_m though it overestimates the actual value. To improve the theory, various corrections to TMS theory were considered: A) Using ion activities instead of ionic concentration in the external solutions leads to an improved prediction; B) In-homogeneous distribution of the membrane fixed charge has no effect on ϕ_m; C) Consideration of stagnant diffusion layers on each side of the membrane can have a large effect on ϕ_m; D) Reducing the average value of the fixed membrane charge density can also largely affect ϕ_m; E) Allowing for water transport in the theory has a small effect; F) Considering differences in ionic mobility between co-ions and counterions in the membrane affects ϕ_m significantly. Modifications C) and F) may help to explain the observed maximum in ϕ_m.

In **Chapter 8** results from the previous chapters are combined and discussed. The (relative) influence of the membrane, SDL, and bulk resistance on the stack resistance is shown. In a modeled seawater ED stack the size of the SDL resistance is small, but the effect of concentration polarization in this SDL on the membrane resistance may be large, as the membrane resistance is largely depending on the solution-membrane interface ion concentration. The membrane resistance is for seawater desalination likely the main resistance of the system. An outlook on divalent ions and future experiments is also given in this final chapter, and it is expected that presence of these ions leads to increased stack resistance. In the final paragraph the feasibility of the ED-BWRO scheme is discussed and compared with a stand-alone SWRO process. At the present

state of the art, ED-BWRO can not compete with SWRO, as high quality IEMs are too expensive to allow low applied current densities. As such energy consumption of ED systems is too large. With development of high quality IEMs for low membrane price, the ED-BWRO scheme can become an attractive alternative for seawater desalination, especially when high water recovery is required to lower pretreatment and concentrate treatment costs.

Samenvatting

Ionwisselende membranen in zeewatertoepassingen

Processen en eigenschappen

Water is geen schaars goed, 71% van het aardoppervlak is overdekt met water. Zoet en drinkbaar water kunnen echter schaars zijn, omdat bronnen onevenredig zijn verdeeld, vervuild zijn geraakt, of simpelweg niet groot genoeg zijn om de alsmaar groeiende populatie van water te voorzien. Zeewaterontzouting stelt mensen in staat om drinkwater te maken uit een schijnbaar oneindige watervoorraad. Om water echt beschikbaar te maken is het een voorwaarde dat de kosten van het ontzoutingsproces laag zijn. Door gebruik van elektrodialyse (ED), een elektrochemische ontzoutingstechnologie, kunnen de kosten van het ontzoutingsproces mogelijk worden verlaagd. In ED worden ionen, onder invloed van een elektrisch veld, getransporteerd door ionwisselende membranen (verder kortweg membranen genoemd). Uit zoutwater worden met deze technologie een ontzoute waterstroom (diluaat) en een waterstroom met hoog zoutgehalte (concentraat) geproduceerd. ED wordt nu voornamelijk gebruikt voor het ontzouten van brakwater, maar ook voor het verder concentreren van oplossingen met een hoog zoutgehalte. Voor dit laatsgenoemde proces is het gebruik van bijvoorbeeld drukgedreven membraanprocessen gelimiteerd door de osmotische druk en de neerslagvorming van slecht oplosbare anorganische stoffen. Met ED kan een hogere waterefficiëntie worden behaald dan met drukgedreven zeewaterontzoutingsprocessen, ook zijn er minder voorbehandelingsinspanningen nodig omdat alleen zout (en een fractie water) door de membranen wordt getransporteerd. Deze voordelen maken ED aantrekkelijk voor de toepassing in zeewaterontzouting. ED kan echter, in de huidige staat van ontwikkeling, wat betreft zeewaterontzouting nog niet concurreren met 'reverse osmosis' (RO), omdat er nog grote onomkeerbare energieverliezen zijn. Een hybride systeem van ED en 'brakwater reverse osmosis' (ED-BWRO) wordt hier gepresenteerd als een alternatief voor zeewater omgekeerde osmose.

In **Hoofdstuk 2** zijn omkeerbare en onomkeerbare energieverliezen van het zeewaterontzoutingsprocess met ED geïdentificeerd en gekwantificeerd. Er wordt getoond hoe deze verliezen beïnvloed worden door de opgelegde stroomdichtheid. Bij een heel lage opgelegde stroomdichtheid ($\sim$10 A/m^2), zijn stroomefficiëntie en osmotisch watertransport verantwoordelijk voor ongeveer 50% van de energieverliezen. Bij hogere opgelegde stroomdichtheden (>50 A/m^2) vormen deze verliezen slechts tot 20% van het totale energieverlies. In elk geval is de interne weerstand van de membraanstack verantwoordelijk voor het grootste deel van het energieverlies. Wanneer de opgelegde stroomdichtheid lager is dan 50 A/m^2 kan ED met lagere energiekosten zeewater ontzouten dan RO.

Naast de monovalente natrium-, kalium-, en chloride-ionen zijn er ook aanmerkelijke hoeveelheden van de divalente magnesium-, calcium-, en sulfaat-ionen aanwezig in zeewater. Deze tweewaardig-geladen ionen kunnen neerslagproducten vormen, die de

watereﬃciëntie van de BWRO stap limiteren. In **Hoofdstuk 3** wordt het effect van de opgelegde stroomdichtheid (10-300 A/m^2) op de samenstelling van het diluaat getoond. Deze samenstelling is van belang omdat het diluaat vervolgens behandeld dient te worden in het BWRO proces. Bij lagere opgelegde stroomdichtheden wordt een diluaat geproduceerd met een, in verhouding tot de monovalente ionen, lagere hoeveelheid divalente ionen waardoor de kans op aanslagvorming lager is. Deze invloed van de opgelegde stroomdichtheid is gerelateerd aan concentratiepolarisatie-effecten die plaats hebben in de stilstaande diffusielaag (SDL) aan het grensvlak tussen het membraan en de oplossing. De resultaten worden uitgelegd aan de hand van een model dat is gebaseerd op de Nernst-Planck-fluxvergelijking. De lagere startconcentratie van divalente ionen in vergelijking met monovalente ionen in zeewater leidt tot een sterkere uitputting van deze divalente ionen in de SDL, vooral bij hogere opgelegde stroomdichtheden. Als gevolg hiervan wordt de getransporteerde hoeveelheid divalente ionen kleiner naarmate de opgelegde stroomdichtheid toeneemt.

In **Hoofdstuk 4** wordt een fractioneringselektrodialysestack gepresenteerd en de werking van dit concept wordt aangetoond. Door om en om monovalent selectieve membranen en standaard membranen, die enkel óf kation óf anion selectief zijn, te plaatsen kunnen divalente en monovalente ionen worden gefractioneerd. In plaats van een diluaat en concentraatoplossing ontstaan tijdens het ED proces nu een stroom met hoge en een stroom met lage concentratie van divalente ionen. Reversibele verliezen in een dergelijk systeem zijn laag, omdat er geen ontzouting plaatsvindt. Er wordt aangetoond dat op deze manier ~90% van de divalente kationen en ~60% van de divalente anionen gefractioneerd kunnen worden. Hogere opgelegde stroomdichtheden resulteren in een betere scheiding. Lage coulombische efficiëntie van de fractioneringsstack leidt echter tot een hoog energieverbruik per volume geproduceerd water.

ED is gebaseerd op selectiviteit van de membranen die voortkomt uit de geladen groepen die aanwezig zijn op de polymeerstructuur. Deze geladen groepen spelen een rol in het Donnan-evenwicht, dat stelt dat de elektrochemische potentiaal in elke fase van een elektrochemisch systeem gelijk moet zijn. De simpelste methode om dit Donnan-evenwicht te beschrijven maakt gebruik van de klassieke Boltzmann-vergelijking, welke gebaseerd is op een 'uitgemiddeld veld' beschrijving van ionen als ideale puntladingen, in combinatie met de aanname dat de elektrische dubbellagen in de porie elkaar volledig overlappen. In **Hoofdstuk 5** wordt de geldigheid van deze aanpak getest door middel van metingen van het aantal counterionen en co-ionen in membranen met een hoge ladingsdichtheid, nadat deze membranen in evenwicht zijn gebracht met verschillende NaCl oplossingen (0.01-3 M). Om een goede match tussen data en theorie te krijgen blijkt het nodig om de membraanlading uit te drukken als

concentratie per volume oplossing aanwezig in de membraanporiën en om een kleine energetische term mee te nemen in de Boltzman-vergelijking. Een kleine discrepantie werd gevonden tussen de theorie en de experimentele data bij lage externe NaCl concentraties. Deze verschillen ten opzichte van het Donnan-model zijn reeds opgemerkt en worden al een halve eeuw genoemd maar een overtuigende verklaring ontbreekt. Behoorlijk goede overeenstemming tussen de meetdata en theorie bij lage externe NaCl concentraties is verkregen wanneer de aanwezigheid van H^+- en OH^--ionen en een uiterst kleine hoeveelheid membraanlading met een tegenovergesteld ladingsteken worden meegenomen in het model.

Het aantal ionen in de membraanfase is erg bepalend voor de ionische geleiding (of weerstand) van het membraan. In **Hoofdstuk 6** wordt voor de eerste keer aangetoond hoe de weerstand van een membraan wordt beïnvloed door de externe zout concentraties, wanneer deze concentraties verschillend zijn aan beide kanten van het membraan (een concentratiegradiënt is aanwezig). De NaCl-concentraties worden gevarieerd van 0.01-1.1 M. De resultaten laten zien dat de membraanweerstand vooral beïnvloed wordt door de oplossing met de laagste zoutconcentratie. De membraanweerstand kan voorgesteld worden als bestaand uit twee weerstanden in serie. De een is een gel-fase (weerstand onafhankelijk van concentratie) en de andere is een ionische oplossing (weerstand afhankelijk van concentratie). De geleiding van het membraan wordt gelimiteerd door de geleiding van de ionische oplossing wanneer de concentratie van de externe oplossing lager is als 0.3 M. Bij hogere concentraties is de geleiding van de gel-fase limiterend. Met een model gebaseerd op deze serieschakeling kan een goede benadering van de experimentele membraanweerstand verkregen worden.

De membraanweerstand is van grote invloed op de onomkeerbare verliezen in de membraanstack. Wanneer de stackweerstand verder wordt verlaagd, worden omkeerbare verliezen belangrijker. **Hoofdstuk 7** gaat over de (omkeerbare) membraanpotentiaal (ϕ_m) die, onder stroomloze condities, aanwezig is over een membraan dat twee oplossingen met verschillende samenstelling van elkaar scheidt, zelfs zonder opgelegde stroom. Dit hoofdstuk richt zich op de oorsprong van deze potentiaal en op de veel gebruikte Teorell-Meyer-Sievers-theorie. Het is aangetoond dat deze theorie afwijkt (en een overschatting geeft) van de gemeten ϕ_m, vooral als er een groot concentratieverschil aanwezig is. Wanneer een groot concentratieverschil aanwezig is, kan een maximum in ϕ_m ontstaan. Dit maximum wordt niet voorspeld door de TMS-theorie. Alvorens dit maximum wordt bereikt kan de TMS-theorie gebruikt worden voor een goede schatting van ϕ_m, alhoewel de werkelijke potentiaal wordt overschat. Om de theorie te verbeteren worden verschillende correcties overwogen: A) gebruik van ionactiviteit in plaats van ionconcentratie geeft een verbeterde voorspelling; B) Inhomo-

gene distributie van de membraanlading heeft geen effect op ϕ_m; C) Meenemen van een SDL aan beide zijden van het membraan kan een groot effect hebben op ϕ_m; D) Verkleinen van de gemiddelde vaste membraanlading evenzo; E) Watertransport opnemen in de theorie heeft een klein effect; F) Inachtneming van verschillen in ionische mobiliteit van co-ionen en counterionen in het membraan heeft een significant effect op ϕ_m. Aanpassingen C) en F) kunnen helpen een maximum in ϕ_m te verklaren.

In **Hoofdstuk 8** worden de resultaten van de voorgaande hoofdstukken gecombineerd en bediscussieerd. De (relatieve) invloed van het membraan, de SDL en de zoutoplossing, aanwezig in de kanalen tussen de membranen, op de stackweerstand wordt gepresenteerd. De weerstand van de SDL is slechts klein in zeewaterontzouting, maar concentratiepolarisatie in deze laag kan indirect een groot effect hebben in de membraanweerstand, omdat deze direct afhankelijk is van de zoutconcentratie op het water-membraan grensvlak. Voor zeewaterontzouting is de membraanweerstand vaak de grootste weerstand. Verder leidt de aanwezigheid van divalente ionen tot een hogere stackweerstand. In de laatste paragraaf wordt de financiële haalbaarheid van de ED-BWRO combinatie bediscussieerd en vergeleken met een zeewater-RO ontzoutingsproces. Dit leidt tot de conclusie dat, op dit moment, de combinatie ED-BWRO niet kan concurreren met zeewater-RO, omdat goede membranen te duur zijn om een lage opgelegde stroomdichtheid te kunnen gebruiken. Hierdoor zijn de energiekosten van een ED-BWRO te hoog. Als er goede en goedkopere membranen kunnen worden gemaakt, kan er voor dezelfde prijs een groter membraanoppervlak worden ingezet en kan ED worden uitgevoerd met een lagere opgelegde stroomdichtheid wat leidt tot lagere energiekosten. In dat geval kan ED-BWRO een aantrekkelijk alternatief worden voor zeewaterontzouting, vooral wanneer een hoge waterefficiëntie nodig blijkt om voorontzoutingskosten en concentraatbehandelingskosten te verlagen.

Acknowledgments

At the start of a PhD project it is hard to imagine that after 4 years there will be a book, which contains your research, and bears your name as the author. Now I see that the book became reality, it was written, rewritten, edited, and printed. Although my initials and name are on the book, it is of course a product that can only be here if it was not for the decisions or the contributions of many others. And for this I would like to express my gratitude.

Autumn 2010, just after I obtained my MSc degree, I had a conversation with Jan Post about a project he had in mind about predesalination of seawater with electrodialysis. It was a good conversation and Jan invited me to consider doing a PhD on this topic. After, as I remember, a very familiar meeting with the Wetsus program director at that time, Gert-Jan Euverink. The intentions were there, and it was actually a matter of filling in the blanks of the project. I would like to thank Gert-Jan for this conversation and giving me the chance to work on this project. Furthermore I would like to thank the Wetsus directors Johannes Boonstra and Cees Buisman for accepting me to work at their company, which is truly an inspiring environment.

When the project was further defined, it became a project of Wetsus, KWR and the project was affiliated to the Wageningen University. After half a year the project was changed to a Wetsus and WUR project. Nevertheless, I would like to thank Jos Boere of KWR, for seeing the relevance of this project and allowing us to start this project at his department. From Wageningen University, I would like to thank Huub Rijnaarts for being my promoter. In the first year we did not have a lot of contact and we did not know each other too well. After the transfer of the project from KWR to Wageningen, you became more involved and we started to have regular meetings. As a promoter you were very interested in this project, although it might have been somewhat outside of your field of expertise. And maybe because of this you granted me a lot of freedom, and it is especially for this freedom and your confidence that I am very grateful. What I also appreciate in your approach as professor is that you are not only interested in the work of your students, but moreover, you also care about the well being of your students. When speaking of Wageningen I also like to thank Harry Bruning for his contribution to this project and for guiding this project through Wageningen. We worked together on our first paper and you stayed in touch during the whole project and you had usually some good advices in our meetings together with Huub.

My supervisor at Wetsus was Michel Saakes. Michel thanks for your help in the lab, I learned a lot from you about electric circuits and how to build a proper set-up. Al-

though sometimes I had some doubts, the system improved every time we worked on it. Later on when everything was up and running we had good contact and we had good conversations about our work and about our ideas. It was great to have you as a supervisor. Furthermore, I need to thank so many people from Wetsus as I cannot think of anyone of the analytical lab or technical staff with whom I did not have contact about my set-up, (use of) tools, or measurements. Thanks people for always being willing to help and for making life of researchers easy (although they do not always recognize you do it). Keep up the good work.

Another person to which I owe a big thank you is Maarten Biesheuvel. Initially Maarten was not officially involved in this project. I also do not exactly remember how he got involved. I think it was out of pure interest in the topic that we had our first conversations. Soon concrete ideas about some experiments were formed, an article was in progress, and Maarten got 'irreversibly' connected to the project. Maarten, you shared a lot of your knowledge and taught me many things. You also triggered me to work on what might be my best article, and to study the old school articles that are still so important for a more fundamental understanding. Names like: *Ostwald*, *Donnan*, *Teorell*, *Schlögl*, *Sonin*, *Probstein*, *Helfferich*, and *Lakshminarayanaiah* I first heard them from you. You are a good scientist and I thank you for your help and I am privileged to have you as a co-promoter.

Then I would like to thank my other co-promoter Jan Post. The idea of this project is Jan's and he should get all the credits for it. Jan, to start with, you are a very nice person to work with. It is possible to talk to you about any reserach concerns, but also about daily stuff, or about nice ideas for further projects. One of your great strengths is that you are always willing to look at things from different angles, even when it considers your own findings. Often you took the role of the devil's advocate, as you call it, so we were able to consider our research from a different perspective, which helped to substantially increase the quality of the project output. I also learned form you how to structure my articles and how to explain our research to a broader audience. Thank you very much for a very nice cooperation and for all the insights you shared with me.

Within this thesis you can find work which was published in six scientific articles, each article with their specific set of authors. Therefore, I would like to address these co-authors and thank them for their input. Michel, Harry, Gintaras Daubaras, Odne Burheim, Martien Cohen Stuart, David Vermaas, Joost Veerman, Kitty Nijmeijer, Bert Hamelers, Victor Nikonenko, Huub, Maarten, and Jan thank you very much for our cooperation and for your efforts to increase the quality of the output of this project. Although at first we might not always have had the same ideas about certain topics, we

shared the interest in this work and thanks to our discussions it was always possible to develop new insights. I also would like to acknowledge the students who worked on this project during their BSc or MSc studies: Marte Jarzembowska, Vadim Amirov, Gintaras Daubaras, Laura Braz Monteiro de Barros, and Małgorzata Nowak.

Besides the people that directly contributed to this research there are many other people that made my 4 years as PhD a great time. I would like to thank all Wetsus employees that keep this company running and which make it possible that 'we', the researchers, can focus on our work. Besides that, you are nice people to work with. I also need to thank my fellow PhD students and post-docs for the warm contacts. In person I thank my office mates Anna Casadella, Daniel Bergmair, Roel Meulepas, and Paweł Roman, thank you for our good times in the 'old building'. A special thanks to my two good friends and my paranimfs on the day of the defence of this work: Johannes Kuipers and Daniel Bergmair. Johannes, you are a warm and joyful person, a nice colleague, and since you left I miss our long lunches (with chocolonely) and our fun in the lab at Wetsus. One day perhaps we will work together again, but for sure we will stay friends. Daniel, you are one of a kind, you have many interests and good opinions, which makes you a good person for discussions (remember that the world is an everchanging vacuum of perspective). It was nice to train together for fierljeppen and to share some of our beloved Frisian culture and language with you, spitich dat it dy sa núver de bek útrôlet...

The final person I want to thank is my loving wife Renske. Tige tank datsto der foar my bist. Do joust my de romte mar tagelyk binne wy tegearre, dat is fantastysk.

About the author

Oane (Anne Haye) Galama was born, together with his twin brother, on the 10th of February 1985, in Sneek (The Netherlands). In 2003 he finished his pre-university education (VWO) at the Bogerman College in Sneek. From 2003-2007 he studied environmental sciences (BSc) at the Van Hall Instituut in Leeuwarden. In the period 2008-2010 he did his MSc Biotechnologie with specialization water technology at the Wetsus Academy (and affiliated to Wageningen University) in Leeuwarden. During the MSc he wrote a thesis about wastewater treatment plant effluent polishing with microalgae and another about hydrogen production in a microbial electrolysis cell using low cost electrode materials. After successfully completing this master track he started in 2011 his PhD research on electrodialysis and ion exchange membranes in seawater applications. This work was carried out at Wetsus, European centre of excellence for sustainable water technology.

**Netherlands Research School for the
Socio-Economic and Natural Sciences of the Environment**

D I P L O M A

For specialised PhD training

The Netherlands Research School for the
Socio-Economic and Natural Sciences of the Environment
(SENSE) declares that

Anne Haye Galama

born on 10 February 1985 in Sneek, The Netherlands

has successfully fulfilled all requirements of the
Educational Programme of SENSE.

Leeuwarden, 24 April 2015

the Chairman of the SENSE board

Prof. dr. Huub Rijnaarts

the SENSE Director of Education

Dr. Ad van Dommelen

The SENSE Research School declares that **Mr Anne Galama** has successfully fulfilled all requirements of the Educational PhD Programme of SENSE with a work load of 48.6 EC, including the following activities:

SENSE PhD Courses

o   Environmental Research in Context (2011)
o   Research in Context Activity: 'Co-organising the Wetsus Water Challenge Science and Technology', Wageningen (2013)

Other PhD Courses

o   Working Safely in Laboratories, Wetsus, The Netherlands (2011)
o   Summer School 'European Membrane Society', Warsaw University of Technology, Poland (2011)
o   Wetsus / Rabobank business Challenge, Wetsus, The Netherlands (2012)
o   Summer School 'Elechtrochemical Engineering', University of Zagreb, Croatia (2012)
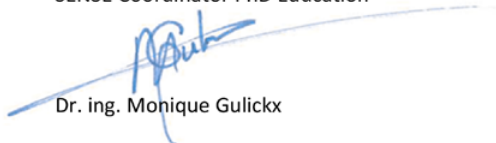o   Matlab course, Wageningen University/Wetsus, The Netherlands (2014)

Management and Didactic Skills Training

o   Supervision of two BSc students and four MSc student theses (2011-2014)
o   Co-organisation of the Interfaces in Water and Environmental Science, IAP 2014 congress, Leeuwarden, The Netherlands (2014)

Selection of Oral Presentations

o   *Membrane resistance at variable salt concentrations.* Wetsus Congress, 29 November 2012, Leeuwarden, The Netherlands
o   *Validity of the Boltzmann equation to describe the Donnan equilibrium.* International conference ion transport in organic and inorganic membranes, 2-7 June 2013, Tuapse, Russia
o   *Partitioning of ions in ion exchange membranes at different external salt concentrations.* The International Conference on Interfaces against Pollution (IAP) - 'Interfaces in Water and Environmental Science', 26-28 May 2014, Leeuwarden, The Netherlands
o   *Potential and constrains in desalination of feed waters with high salinity with electrodialysis.* FrieslandCampina Innovation Centre Research Meeting, 28 November 2014, Wageningen, The Netherlands

SENSE Coordinator PhD Education

Dr. ing. Monique Gulickx